Chemical and Biological Studies of Manganese Transferrin

A Thesis

Submitted for the Degree of Doctor of Philosophy

by

Kerry Emma Bunyan, *BSc (Hons), MSc*

School of Chemistry
Faculty of Science and Engineering
University of Edinburgh

December 2003

Declaration

The work presented in this thesis is to the best of my knowledge and belief, original except where acknowledged in the text. I hereby declare that I have not submitted this material, either in whole or in part, for a degree at this or any other institution.

Abstract

Oxidative stress is often seen as a result of ischaemic-reperfusion injury during liver transplant. A result of this is the dissipation of the mitochondrial transmembrane potential which can lead to cell death when the antioxidant defence system, including MnSOD found in mitochondria, becomes overwhelmed. If MnSOD can be up regulated in some way then this could potentially be averted.

Human serum transferrin (hTf) is a 80 kDa bilobal glycoprotein that transports iron around the body. It is typically loaded at only 30% saturation and has been shown to be capable of transporting other metal ions. This thesis is concerned with the loading of transferrin with manganese and some of its chemical and biological properties.

Manganese is bound to transferrin as Mn(III) with a characteristic ligand (Tyr) to metal (Mn(III)) charge-transfer band at a wavelength of 430 nm.

Caeruloplasmin is shown to enhance the uptake of manganese from $MnCl_2$ by apo-hTf. However binding is often incomplete and slow. A novel method of loading hTf with Mn using $KMnO_4$ is reported. This method leads to rapid uptake and inductively coupled plasma atomic emission spectroscopy (ICP-AES) determinations confirmed the binding of at least two Mn per hTf molecule. The possible oxidising effects of MnO_4^- on protein amino acid side chains was considered. In model systems MnO_4^- oxidises methionine to methione sulfoxide and methionine sulfone. Evidence of structural changes in apo-hTf induced by Mn(III) binding was obtained by studies using [ε-^{13}C]Met-hTf. Preliminary work suggests that Mn(III), like several other metals studied, preferentially binds to the C-lobe first, although this may result in an open domain conformation.

Fe(III) as $Fe(NTA)_2$ was found to displace Mn(III) from hTf but displacement was slower when hTf had been loaded using $KMnO_4$ rather than $MnCl_2$. $KMnO_4$ was not able to displace Fe(III) from Fe_2-hTf.

Attempts to crystallise Mn-hTf to characterise these structural changes proved difficult. Crystals grew but were of poor quality and did not diffract. Many large crystals were obtained from solutions of Fe_2-hTf. The crystals were red/orange and ellipsoidal in shape. Of the Fe_2-hTf crystals grown, one diffracted to 3.3 Å with the data being complete to 90%, but not enough information was gained for adequate molecular replacement and structural solution.

The effect of apo-, Fe- and Mn-hTf on human hepatocytes (WRL-68 cells) was studied. Fe and Mn was found to be taken up by these cells, as confirmed by ICP-AES. Cells grown in apo- and Fe-hTf maintained high cell numbers and viability. Mn-hTf treated cells resulted in decreased cell numbers and an increase in non-adherent cells, as determined by cell counting and MTT assays. This was not as a result of a cytotoxic effect and cell death, as confirmed by staining with Feulgans. A noticeable change in colour of the growth medium for cells incubated with 25 μM Mn-hTf, indicative of a fall in pH, suggested a metabolic effect on the cells. Further, there appeared to be a slight increase in mitotic activity in these cells and there was also a morphological effect. Dendritic-like processes grew from the cells. These processes, like the cells, contained mitochondria. The use of CMXRos dye showed that the mitochondrial transmembrane potential was maintained in these treated cells showing that the effect of Mn-hTf on WRL-68 cells was not on mitochondria. These novel findings suggest transferrin can

transport manganese, with the potential of carrying more than two manganese per protein molecule. Future work to investigate the effect of Mn-hTf on cells at varying concentrations and whether this leads to up-regulation of anti-oxidant defence mechanisms including namely Mn-SOD should be worthwhile.

Acknowledgements

School of Chemistry, University of Edinburgh

I would first of all like to thank Professor Peter Sadler for his supervision, ideas, advice and patience.

I would like to thank all members of the PJS group, past and present, particularly Dr. Hye-Seo Park for her help and expertise in the 2D NMR studies detailed in this thesis. Also, Drs Stephen Paisey and Vivienne Munk for all their help with NMR, general knowledge and their precious time given to me and my thesis. There is a special thank you to Alan Stewart (now Dr!) for his jokes, impressions, stupidity, singing etc.

Thank you to Dr. L. Yellowlees for her assistance with EPR and her support.

School of Medicine, University of Edinburgh

I would like to thank Professor David Harrison for his supervision, ideas, patience and advice. Also, everyone up at the Pathology department including Drs Sandrine Prost, Nick Wheelhouse, Chris McCulloch, Kate Henrikson and Gareth Clegg who were more than happy to give me help and advice when I asked. Thank you to Linda Wilson for her assistance using the confocal microscope. A special thank you to Ben Tura who luckily never tired of answering my questions and kept me amused.

Institute of Cell and Molecular Biology, University of Edinburgh

Professor Malcolm Walkinshaw, Paul Taylor and Stephen Robinson for X-ray crystal diffraction studies.

Cats

Thank you to all the cats and their owners who kindly donated whiskers to the crystallisation studies, these included Leeroy (owner: Stuart Johnstone), Sugar (owner: Simon Parsons) and JJ (owner: Sarah Hinchley).

Financial Support

I would like to thank BBSRC for financial support and to HSBC for its patience whilst I have been a student. Also, my parents who have also donated vast sums to my perpetual student status.

Finally, thank you to all my friends who have supported me during my studies.

Abbreviations:

AMU	Atomic mass units
Apo-hTf	Metal free human serum transferrin
ca.	*circa* (about)
D_2O	Deuterium oxide
DMSO	Dimethyl sulfoxide
DMT1	Divalent metal transporter 1
EDTA	Ethylene diaminetetraacetate
Fe-hTf	Iron transferrin
Hepes	4-(2-hydroxyehtyl)-1-piperazineethanesulfonic acid
His (H)	L-histidine
HSQC	Heteronuclear single quantum coherence
HTf	Human serum transferrin
ICP-AES	Inductively coupled plasma atomic emission spectroscopy
mClCCP	Mesoxalonitrile 3-chlorophenylhydrazone
Met (M)	L-methionine
NAc-met	N-acetyl-L-methionine
Mn-hTf	Manganese transferrin
MPT	Mitochondrial permeability transition
MTT	3-(4,5-dimethylthiazol-2-yl)-2,5-diphenyl tetrazolium bromide
NTA	Nitrilotriacetate

PAGE	Polyacrylamide gel electrophoresis
PDB	Protein data bank (http://www.rcsb.org/pdb/)
PEG	Poly (ethylene glycol)
pH^*	pH meter reading uncorrected for effects of deuterium
ROS	Reactive oxygen species
Tris	Tri[hydroxymethyl]aminomethane
Trp (W)	L-tryptophan
TSP	Sodium trimethylsilyl-d_4-propionate
Tyr (Y)	L-tyrosine
UV/Vis	Ultraviolet-visible spectroscopy

Contents

Declaration		i
Abstract		ii
Acknowledgements		v
Abbreviations		vii
Chapter 1	Introduction	1
1.1	Generation of Reactive Oxygen Species (ROS)	2
	1.1.1 Cellular Defence	4
	1.1.2 Oxidative Stress	6
	1.1.3 Mitochondrial-Induced Apoptosis	6
	1.1.3.1 Mitochondrial Permeability Transition	7
	1.1.4 Oxidative-Stress-Induced Apoptosis	8
	1.1.4.1 Target Tissues	10
1.2	Redox-Active Metal Ions	11
	1.2.1 Iron in Biological Systems	12
1.3	Metal Ion Transport	14
	1.3.1 Receptor-Mediated Endocytosis	17
	1.3.2 Transferrin as a Metal Ion Mediator	20
1.4	Caeruloplasmin	21
1.5	Manganese	24
	1.5.1 Manganese Chemistry	24
	1.5.2 Biology of Manganese	29
	1.5.3 Manganese Transport	30

1.5.4 Manganese Containing Proteins 32
1.5.4.1 Manganese Superoxide Dismutase 34
1.5.4.2 Mimics 36
1.5.4.3 Contrast Agents 37
1.6 Conclusion 38
1.7 Aims of Thesis 39
1.8 References 41

Chapter 2 Experimental Techniques 51
2.1 Source of Chemicals 51
2.1.1 Reagents 51
2.1.2 Transferrin 51
2.1.3 Water Purification 52
2.2 UV-Vis Spectroscopy 53
2.3 ICP-AES 54
2.3.1 Emission Properties 55
2.4 Gel Electrophoresis 56
2.5 Nuclear Magnetic Resonance Spectroscopy 57
2.5.1 Two-Dimensional NMR (2D NMR) 58
2.6 Electron Paramagnetic Resonance 59
2.7 pH Measurements 60
2.8 Ultrafiltration 60
2.9 Crystallisation of Transferrin 61
2.9.1 Screening Technique 61
2.9.2 Seeding Technique 62
2.10 Cell Culture 62
2.10.1 Standard Culture Conditions 62
2.10.2 Cell Viability Counts: Trypan Blue Exclusion 63
2.10.3 MTT Assay 63
2.10.4 Evaluation of Apoptosis and Mitosis 64

2.10.5 Induced Mitochondrial Depolarisation 65
2.10.6 Assessment of Mitochondrial Depolarisation 66
2.10.7 Analysis of Cellular Metal Content 66
2.11 References 68

Chapter 3 Manganese Binding by Transferrin and Its Characterisation 70
3.1 Introduction 70
3.1.1 Caeruloplasmin 72
3.1.2 Potassium Permanganate 72
3.1.2.1 Oxidation of Amino Acids 73
3.2 Materials and Methods 75
3.2.1 Purification and Characterisation of Apo-hTf 75
3.2.2 Preparation of Mn-hTf 75
3.2.2.1 Addition of an Oxidant 76
3.2.3 Preparation of Fe-hTf 76
3.2.4 UV/Vis Spectroscopy 77
3.2.5 Gel Electrophoresis 78
3.2.6 NMR Spectroscopy 78
3.2.6.1 Hepes Buffer 79
3.2.6.2 Amino Acids 79
3.2.6.3 HSQC NMR 80
3.2.7 EPR 80
3.3 Results and Discussion 81
3.3.1 Uptake of Mn(III) by Apo-hTf 81
3.3.1.1 Uptake of Mn(III) by Apo-hTf in the Presence of Caeruloplasmin 81
3.3.1.2 Uptake of Mn(III) from $KMnO_4$ by Apo-hTf 83
3.3.2 Reaction Between Hepes Buffer and $KMnO_4$ 87
3.3.3 Oxidation of Amino Acids by Permanganate 95
3.3.3.1 Tyrosine 96

3.3.3.2 Tryptophan 98
3.3.3.3 Histidine 99
3.3.3.4 N-Acetyl L-Methionine 101
3.3.3.5 Methionine Sulfoxide and Methionine Sulfone 102
3.3.4 Investigation into Oxidation of Methionine Residues of hTf 105
3.3.5 Order of Lobe Loading of Apo-hTf with Mn(III) 114
3.3.6 Fe(III) Displacement of Mn(III) from Mn_2-hTf 116
3.3.7 Mn(III) Displacement of Fe(III) from Fe_2-hTf 120
3.3.8 Mn(III) Release from Mn_2-hTf 122
3.4 Conclusions 125
3.5 References 128

Chapter 4 Crystallisation of Transferrin 132
4.1 Introduction 132
4.1.1 Crystallisation Theory 132
4.1.2 Previous Crystallisation of Transferrins 134
4.1.2.1 Structure of Transferrin 136
4.1.2.2 Metal Co-ordination 137
4.2 Materials and Methods 139
4.2.1 Crystallisation Techniques 140
4.2.1.1 Screening Technique 142
4.2.1.2 Seeding from Crystals 142
4.2.2 Data Collection 143
4.2.3 Freezing Solutions 143
4.3 Results and Discussion 144
4.3.1 Crystallisation of Fe-hTf 144
4.3.1.1 Data Collection and Processing 146
4.3.1.2 Model Building 149
4.3.1.3 Seeding of Crystals 151

4.3.2 Crystallisation of Mn-hTf 152
4.3.2.1 Screening Technique 154
4.4 Conclusions 155
4.5 References 158

Chapter 5 Effects of Manganese Transferrin on Hepatocytes 161
5.1 Introduction 161
5.1.1 Hepatocyte Iron Metabolism 162
5.1.2 Manganese Uptake 163
5.1.3 Manganese Toxicity 166
5.1.4 Mitochondrial Transmembrane Potential 167
5.1.5 Cell Adhesion and Divalent Cations 167
5.1.6 WRL-68 Cells 168
5.2 Materials and Methods 169
5.2.1 Cell Culture 169
5.2.2 Production of Fe-hTf and Mn-hTf 170
5.2.3 Analysis of Cellular Metal Content 170
5.2.3.1 Growth of Cells Under Standard Conditions 170
5.2.3.2 Growth of Cells in Transferrin 171
5.2.3.3 Determination of Cellular Metal Content Using ICP-AES 172
5.2.4 MTT Assay of Hepatocyte Viability Following Treatment with Transferrins 172
5.2.5 Evaluation of Apoptosis and Mitosis Following Treatment with Transferrins 173
5.2.6 Assessment of Mitochondrial Effect of Transferrins on Hepatocytes 174
5.2.6.1 Induction of Mitochondrial Depolarisation 174
5.3 Results and Discussion 175
5.3.1 Analysis of Cellular Metal Content 175

5.3.1.1 Cell Numbers Following Treatment 177
5.3.1.2 Iron Content 179
5.3.1.3 Manganese Content 181
5.3.1.4 Copper and Zinc Content 184
5.3.2 Analysis of Hepatocyte Viability 187
5.3.3 Analysis of Hepatocyte Mitosis and Apoptosis 192
5.3.4 Investigation into the Effect of Mn-hTf on Hepatocytes 194
5.3.4.1 Induction of Mitochondrial Depolarisation by mClCCP 195
5.3.4.2 Effect of Mn-hTf on Hepatocytes 197
5.4 Conclusions 200
5.5 References 203

Chapter 6 Conclusions and Future Work 206
6.1 Conclusions 206
6.2 Future Work 210
6.3 References 215

Appendix I-XIX

Chapter 1 Introduction – Cellular Redox Status, Transferrin and Manganese

Manganese is an important trace element that plays a role in mitochondrial protection from oxidant stress through its association with manganese superoxide dismutase (MnSOD). Manganese exists in a variety of redox states with most manganese bound within the mitochondrial matrix as Mn(II) and Mn(III). Dysregulation of manganese homeostasis suggests it has functions or effects beyond just association with MnSOD [1].

A major problem seen early in liver transplantation is injury related to ischaemia and reperfusion. The basis of this injury is at least in part the result of superoxide generation leading to apoptosis of liver cells. An alternative treatment strategy to SOD mimics is to deliver manganese to the cells in order to aid up-regulation of MnSOD that may be required to prevent oxidative stress. A feasible method of achieving this is by using the iron transport protein, transferrin. By loading transferrin with manganese, this may then result in delivery of manganese to cells and the effect of manganese on cells and mitochondria can then be studied. Further, chemical characterisation of the protein loaded with manganese may provide information on the protein and help elucidate the transport pathway of this metal in cell systems.

1.1 Generation of Reactive Oxygen Species (ROS)

Recent interest has arisen in oxidative stress and redox cycling of cells and their involvement in cell signalling and other mechanisms, including apoptosis.

Mitochondria are now known to be important in controlling cell life and death. Their role in cell death includes energy production, disruption of electron transport, oxidative phosphorylation, release of proteins that activate caspases and alteration of cellular redox cycling. Redox reactions have recently gained attention as being important chemical processes of the cell. Exchanging of reducing equivalents serves as an important element of signal transduction and other cellular mechanisms. However, as a result of this redox cycling, potentially damaging free radicals including reactive oxygen species (ROS), are often produced.

Aerobic organisms generate reactive oxygen species by the partial reduction of molecular oxygen to form superoxide ($O_2^{-\bullet}$), hydrogen peroxide (H_2O_2) and the hydroxyl radical ($OH^{\bullet}$). Superoxide is formed in the endoplasmic reticulum by the cytochrome P450 family [2] and in the cytoplasm by enzymes such as xanthine oxidase [3]. The activation of enzymes such as phospholipase A_2 and NAD(P)H oxidases can also produce superoxide in the plasma membrane of most cells [4]. It is suggested that NO and $O_2^{-\bullet}$ react rapidly to form the peroxynitrite anion which decomposes when protonated into the potent oxidants $OH^{\bullet}$ and $NO_2^{\bullet}$ [5]. However, most of the cellular superoxide is formed in the mitochondria as a result of respiration [6].

Mitochondria consume about 90% of inhaled oxygen and are a particularly rich source of ROS since about 1-2% of oxygen reduced in mitochondria is converted to superoxide during respiration by complexes I and III [7, 8]. A rat liver mitochondrion normally produces around $3x10^7$ superoxide radicals per day [7]. In respiring mitochondria, oxygen is reduced to water in four consecutive one-electron steps by the respiratory chain as shown in Figure 1.1.

Superoxide can act both as an oxidant and as a reductant and it can give rise to other dangerously reactive species. The standard redox potential of $O_2/O_2^{-\bullet}$ is –0.16 V [9].

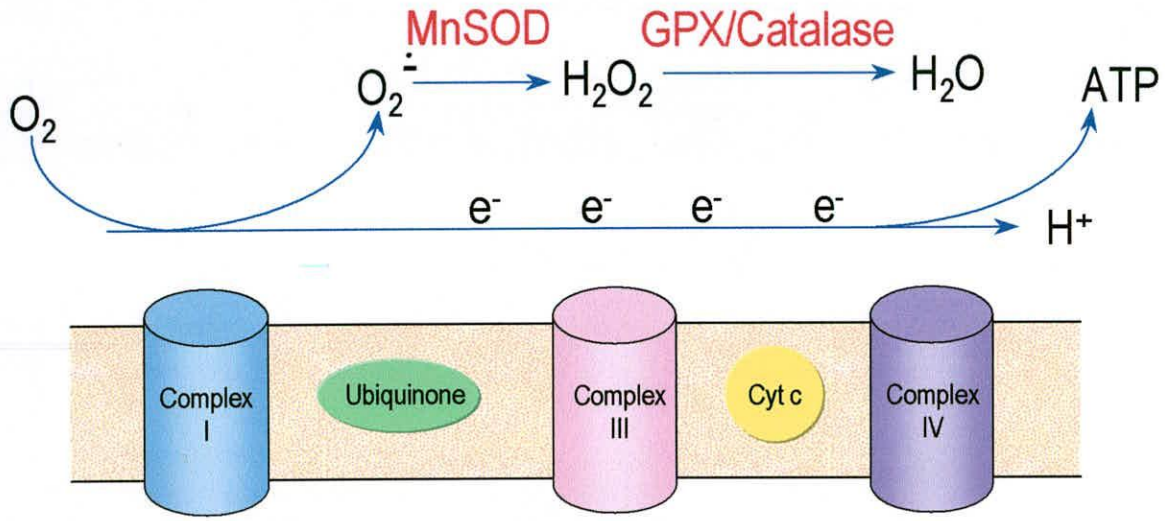

Figure 1.1 The Respiratory Chain and Production of Free Radicals. Energy production *via* the respiratory chain can also result in production of superoxide radicals by complexes I and III. In mitochondria these are converted by manganese superoxide dismutase (MnSOD) to dioxygen and hydrogen peroxide, which is further converted to water by glutathione peroxidase (GPX) or catalase.

1.1.1 Cellular Defence

Generation of superoxide is a continuous and physiological occurrence. Thus, cells have an efficient antioxidant system made up of enzymes such as superoxide dismutase (SOD), glutathione peroxidase (GPX), thiol peroxidases, glutathione reductase, and catalase. Other antioxidants are also involved, such as NAD(P) transhydrogenase, NADPH, glutathione, vitamins E and C, ubiquinol-10, lipoic acid, uric acid and mitochondrial respiration itself [7, 10-12]. SOD and catalase are metalloproteins that use efficient dismutation reactions in their mechanisms to detoxify ROS. A dismutation reaction involves a series of one or two electron transfers where the electrons are accepted from one $O_2^{-\bullet}$ or H_2O_2 and then donated to another (Equation 1.1, Equation 1.2) [13, 14]. These efficient reactions do not require reducing equivalents and so do not require energy from the cell in order to be carried out [13].

Two types of SOD have been found in mammalian liver; one enzyme contains manganese (MnSOD) and is found in the mitochondrial matrix. The other contains copper and zinc (Cu/ZnSOD) and is found primarily in the cytosol. Superoxide radicals produced in mitochondria readily undergo dismutation catalysed by MnSOD leading to the production of hydrogen peroxide (H_2O_2), which is further detoxified by glutathione peroxidase or catalase [8].

Equation 1.1 Superoxide dismutation reaction

$$O_2^{-\bullet} \longrightarrow O_2 + e^-$$

$$O_2^{-\bullet} + e^- + 2H^+ \longrightarrow H_2O_2$$

$$2O_2^{-\bullet} + 2H^+ \longrightarrow O_2 + H_2O_2$$

Equation 1.2 Hydrogen peroxide dismutation reaction

$$H_2O_2 \longrightarrow O_2 + 2e^- + 2H^+$$

$$H_2O_2 + 2e^- + 2H^+ \longrightarrow 2H_2O$$

$$2H_2O_2 \longrightarrow O_2 + 2H_2O$$

It has been hypothesised that in addition to their important role in respiration, mitochondria may also help in maintaining the cellular redox status by eliminating superoxide radicals from the cytosol [12, 15]. At the inner mitochondrial membrane, $O_2^{-\bullet}$ protonates to form the uncharged hydroperoxyl radical, $HO_2^{\bullet}$, that could diffuse into the mitochondrial matrix. This radical could then be dismutated by enzymatic action. Spontaneous dismutation reactions of $O_2^{-\bullet}$ and $HO_2^{\bullet}$ are most rapid at pH 4.7: the protonation/deprotonation equilibrium has a pKa of 4.69 [16]. As the pH increases, the rate of dismutation decreases. Thus, at pH 7.4 the effective rate constant for spontaneous dismutation is *ca.* 2×10^5 M^{-1} s^{-1} [17]. However, the reaction catalysed by superoxide dismutase is about 10^4 times faster having a rate constant of 2×10^9 M^{-1} s^{-1} [17].

1.1.2 Oxidative Stress

When ROS production is in excess or antioxidant defence systems become overwhelmed or dysfunctional, oxidative stress may occur. This can then go on to cause cellular damage and possibly even lead to cell death. A number of circumstances can lead to increased ROS production such as tumour necrosis factor-α (TNF-α), elevated Ca^{2+}, hypoxia and reperfusion. Reperfusion injury is a major problem during organ transplant. Following a period of anoxia, the sudden influx of oxygen into a hypoxic cell can lead to the increased formation of ROS [18, 19]. This increased level of ROS can actually cause more damage than the ischaemia itself [18]. Some key features of hypoxia/reperfusion injury seen after organ transplantation include a rise in cytosolic Ca^{2+}, an increased ROS production in mitochondria and cytosol, cellular ATP depletion and finally necrosis [7]. Cellular damage caused by ROS and oxidative stress can be seen as oxidative modification of cellular macromolecules such as lipids, carbohydrates, proteins and DNA, causing cell damage and hence tissue malfunction. As previously mentioned, mitochondria are major producers of ROS so they are particularly susceptible to ROS attack.

1.1.3 Mitochondrial Induced Apoptosis

There is an early and important mitochondrial involvement in the apoptotic cascade [19-21]. Cytochrome *c* is found in the inter-membrane space of the mitochondria and acts as a diffusable electron carrier used in the respiratory chain [22]. It was recently shown that caspase cascades can be activated or amplified after release of cytochrome *c* from the mitochondria into the cytosol during the early stages of apoptosis [23, 24]. Once cytochrome *c* is released from mitochondria it is involved

in a series of interactions leading to activation of caspases [25, 26]. This then leads to initiation of apoptosis. Overexpression of the protein Bcl-2, prevents TNF-α-induced apoptosis and increases mitochondrial membrane potential [15, 27, 28].

1.1.3.1 Mitochondrial Permeability Transition

Under normal physiological conditions the outer membrane of the mitochondria is permeable to all molecules <6,000 Da, whereas the inner mitochondrial membrane is seemingly impermeable resulting in the creation of a membrane potential and a pH gradient which are essential for mitochondrial function [28]. Zamzami *et al* [29] have previously shown that cells undergo a reduction of the mitochondrial transmembrane potential before they exhibit signs of nuclear apoptosis. The mechanism of membrane potential disruption is thought to involve the opening of the mitochondrial permeability transition (MPT) pore [28, 30, 31]. It has been shown that MPT causes uncoupling of the respiratory chain with collapse of the mitochondrial membrane potential, calcium (Ca^{2+}) release, hypergeneration of superoxide radicals and mitochondrial release of apoptotic proteins such as apoptosis-inducing factor (AIF). These events lead to apoptosis [15, 32-34].

Kroemer and co-workers [35] have shown in a series of experiments that induction of the MPT is sufficient to induce chromatin condensation and internucleosomal DNA fragmentation, these being well established signs of apoptosis. The result of MPT and pore formation may then go on to cause further membrane potential disruption and ROS generation. Thus MPT and the MPT pore may themselves cause a self-propagating mechanism.

The MPT pore is also thought to regulate the permeability of the outer membrane [36, 37]. Opening of the MPT pore will cause an increase in matrix volume leading to disruption of the outer membrane which has been described in several models of apoptosis [7, 38].

Bcl-2 and Bcl-X_L have been shown to prevent the opening of the MPT pore in isolated mitochondria and to prevent oxidant-mediated MPT [20, 28, 35, 37].

1.1.4 Oxidative Stress Induced Apoptosis

The role of ROS and oxidative stress in mitochondrial-induced apoptosis still remains somewhat controversial. A large amount of experimental data [7, 21, 23, 24, 37-41] indicates an involvement of oxidative stress and MPT in mitochondrial induced apoptosis. However, the exact mechanism still remains unclear.

It has been demonstrated that cells undergo apoptosis in very low levels of oxygen and that many antioxidants fail to protect cells against apoptosis suggesting that ROS are not involved in some apoptotic pathways [42]. However, this may be due to the antioxidants not reaching the specific part of the cell where they are needed. In many experimental models used to study the MPT pore, oxidative stress was involved in the mechanism of cell injury supporting a possible connection between oxidative stress and permeability transition, and hence also to cell injury and even cell death.

Apoptosis induced by oxidative stress appears to involve some of the same steps in the commitment and execution stages in other causes of apoptosis, i.e. cytochrome *c* release and caspase activation [21, 43]. However, oxidative stress may represent an early intrinsic component of an apoptotic cascade rather than being one of several

signals required to commit a cell to apoptosis. A possible fundamental step in apoptosis due to oxidative stress is the opening of the MPT pore leading to a fall of the mitochondrial membrane potential [21, 31, 35]. The correlation between MPT and mitochondria-mediated nuclear apoptosis suggests that MPT is a critical event in the regulation of apoptosis induction by mitochondria due to oxidative stress.

It also must be remembered that oxidative stress can lead to necrosis as well as apoptosis, as does MPT [44]. Loss of membrane potential associated with MPT and pore opening would result in collapse of mitochondrial respiration and thus stop production of ATP. Hence the cell would then undergo necrosis as opposed to apoptosis, which is an energy requiring process. What factors determine which path the cell takes? Energy in the form of ATP could possibly be one of these switches. In conditions with low ATP, necrotic cell death may occur instead of apoptosis. If MPT involves only a subpopulation of mitochondria, as seen at least initially during TNF-α-induced apoptosis in hepatocytes, then the remaining normal mitochondria may maintain membrane potential and thus produce enough ATP to allow apoptosis to proceed as the membrane potential is maintained [36].

It is possible that cells experiencing only slight assault from oxidative stress may undergo a transient opening of the MPT pore which then closes again, allowing re-establishment of vital ion gradients and ATP production. When this occurs there may be sufficient stimuli for the release of cytochrome *c* to initiate the apoptotic cascade. If insult is severe and prolonged MPT pore opening may stay open for longer periods or even permanently and so lead to necrosis. Hence necrosis is possibly more of a catastrophic event in response to severe oxidative stress.

1.1.4.1 Target Tissues

A major problem seen early in liver transplant is injury related to ischaemia and reperfusion; this is thought to be a consequence of oxidative stress. Other tissues may also be affected by oxidative stress from ischaemic or toxic damage. These include the heart, kidney and lungs which are all thought to be in danger from the action of free radicals. Ide *et al.* [45] provide evidence for the involvement of ROS, produced by the respiratory chain in the mitochondria, in the myocardium during heart failure. This and other work has lead to investigations into antioxidants and their use in organs. Metallothionein has recently been proposed as a useful antioxidant in the heart [46]. Red wine has also been implicated as containing antioxidants and may impart some protection against coronary heart disease. The cardio-protective effects of resveratrol, an ingredient of red wine, following ischaemia/reperfusion injury were recently investigated [47]. The results from this study suggest that the protective effects of red wine may be due to its free radical scavenging ability. Venditti *et al.* [48] have shown that vitamin E treatment gives some protective action against lipid peroxidation and cardiac dysfunction associated with ischaemia/reperfusion, possibly by acting as a scavenger of free radicals produced as a result of reperfusion.

Lungs are also affected by free radicals, and have their own antioxidant system including glutathione to deal with oxidative stress. This defence mechanism may be altered in inflammatory lung diseases such as chronic obstructive pulmonary disease and also in cigarette smoke-induced airway disease [49]. There is also evidence that asthma sufferers are subject to increased oxidative stress indicated by reduced levels of lung lining fluid ascorbic acid (vitamin C), α-tocopherol (vitamin E) and

increased amounts of oxidised glutathione in their airways [50]. ROS have also been implicated in other disorders and have even been suggested as mediators of the development of malformations in diabetic pregnancy [51]. As such, loss of control or dysregulation of ROS may have important roles in the pathogenesis of a variety of diseases in multiple tissues.

1.2 Redox-Active Metal Ions

The d-block elements are a family of metals with generally similar characteristics and represent the 'transition' between the highly electropositive s-block metals and the electronegative p-block. The first row is home to many biologically important metals: V, Cr, Mn, Fe, Co, Ni, Cu and Zn. Their behaviour as ions in solution mainly entails co-ordination and redox chemistry.

The transition elements show variable oxidation states and are usually present in biological systems as co-ordination complexes, with ligands ranging from cellular components such as water, small organic molecules and porphryins, to the side chains of amino acids. This group of cations can coordinate all types of donor atoms. The transition metals tend to hydrolyse at physiological pH values so to prevent this, the metal ions are chelated allowing transport in living systems. All first-row transition metals, except Zn, which exists invariably in the +2 state, have rich redox chemistry. The d-block metal ions can be associated with both small molecule binding and oxidoreductase enzyme activity. Alternatively the metal centre can act as a channel for electron transfer. One of the most important redox active metals is iron.

1.2.1 Iron in Biological Systems

The involvement of iron in biological systems is somewhat complicated. It has many functions including oxidation-reduction catalysis, bioenergetics and is connected to several control systems. Some iron containing proteins and enzymes are listed in Table 1.1.

Iron can exist in oxidation states 0, II, III, IV and VI, although the stability of each state varies. Iron (II) has the $3d^6$ electronic configuration. In octahedral complexes, the arrangement of the six *d* electrons can be in two dispositions (high spin and low spin) which plays an important role in iron-protein chemistry.

Table 1.1 Some iron proteins and enzymes [52].

Protein or enzyme	Localisation	Function
Haemoglobin	Cytoplasm	Transport of O_2
Transferrin	Plasma	Transport of Fe
Ferritin	Cytoplasm	Storage of Fe
Rubredoxin, ferrodoxin	Cytoplasm (prokaryotes) and membranes	Electron transfer
Hydroxylases	Cytoplasm and membranes	Hydroxylation
Peroxidases	Vesicles and extracellular	Utilisation of H_2O_2
Acid phosphatases	Vesicles and extracellular	Hydrolysis of phosphate groups
Superoxide dismutase	Mitochondria (prokaryotes)	Dismutation of $O_2^{-\bullet}$

Cytochromes are haem proteins and electron transfer is usually between the Fe(II) and Fe(III) forms. Electron transfer is facile since there is little structural change during the redox reaction. There are a large number of non-haem proteins containing an oxo-bridged unit, Fe-O-Fe, mononuclear iron proteins where the ligands are

nitrogen and oxygen donors and iron sulfur proteins displaying a variety of FeS clusters [52]. In these FeS clusters the high-spin iron is often co-ordinated to four sulfurs from inorganic sulfide and protein cysteines in an approximately tetrahedral arrangement around the metal ion. They make particularly effective redox centres.

Iron and the other transition metals have to be moved from ingestion to organs where they are needed. However, some of the ions precipitate at biological pH values and are often toxic. Therefore, carrier ligands are required for transport.

Iron homeostasis is maintained by the liver where it is the major site for iron storage and synthesis for the plasma iron transport protein, transferrin [53]. The hepatocyte synthesises and secretes transferrin into plasma where it can then be delivered to sites where iron is required. Alterations in storage depend on the balance between iron sequestration and the need for synthesis of haem [53].

A normal 70 kg adult man has a total body iron of *ca.* 4 or 5 g, most of this (60 – 65%) is located in haemoglobin in circulating erythrocytes. About 10% is in skeletal muscle as myoglobin and about 20 – 30% is present in the liver, spleen and bone marrow in the form of ferritin and haemosiderin [53]. A small (< 5%) but vital amount of tissue iron is associated with several metabolically important intracellular proteins such as the cytochromes and iron-sulfur proteins (ferredoxins) and about 7 mg is bound to transferrin. Approximately 80 – 85% of absorbed iron is transported by transferrin to the bone marrow where it is used in haemoglobin in developing red blood cells [53].

1.3 Metal Ion Transport

The transferrins are a class of iron binding proteins. Serum transferrin is an iron transport protein found in blood at a concentration of *ca.* 2.5 mg/mL (35 μM) [54]. Lactoferrin is found in a variety of secretory fluids such as saliva, milk and tears. Ovotransferrin is mainly present in egg whites. Melanotransferrin is a membrane-bound protein found at low levels on the surface of most cells [55]. Ferric-ion binding protein (FBP), also of the transferrin family of proteins, is found in several Gram-negative bacteria and is structurally similar to one half of the transferrin molecule [56-59].

Human serum transferrin (hTf) is a single chain glycoprotein with a molecular weight of about 80 000 Da made up of approximately 700 amino acids [60]. The structure of hTf has been determined using X-ray crystallography [61, 62]. It is a bilobal protein with two structurally similar lobes known as the N-lobe (the amino terminus) and the C-lobe (the carboxy terminus). In human serum transferrin there is *ca.* 40% homology between lobes [60]. Transferrins are glycoproteins, with the exception of some fish transferrins [63], with the glycan chains attached to the proteins by *N*-glycosidic linkages to asparagine residues. The glycan chains appear to play no direct role in the function of the protein. Human transferrin has two biantennary glycan chains both of which are attached to the C-lobe of the protein (Asn413 and Asn611) [60], whereas rabbit serum transferrin has only a single glycan chain bound to the C-lobe (Asn491) [64, 65]. There are two carbohydrate chains, one on each lobe, in human lactoferrin (Asn137 and Asn490, N- and C-lobe respectively) [66] The structure of the principal glycan chains is shown in Figure 1.2.

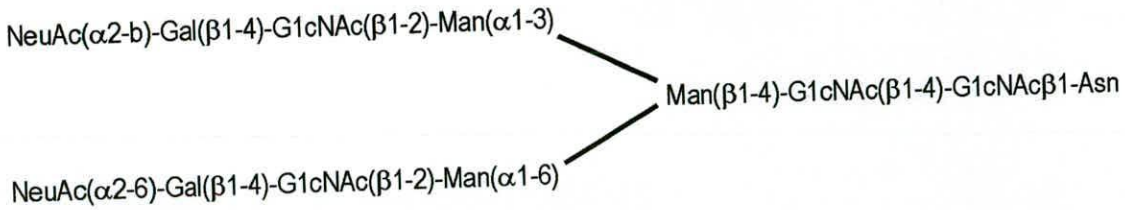

Figure 1.2 The sequence of the glycan chains of human serum transferrin [67].

The protein can bind two Fe^{3+} ions tightly but reversibly, with one ion in each lobe [54]. Figure 1.3 shows the crystal structure of Fe_c-hTf, where Fe(III) is bound to the C-lobe. This is the only structure of human transferrin which has been reported and then only in a thesis [62]. Each lobe is further divided into two domains (N1, N2, C1 and C2) which have alternating α-helical and β-sheet segments. A cleft that separates the two domains in each lobe contains the metal binding site of transferrin. Both lobes have similar folding patterns. The N-terminus of many helices is directed towards the central binding cleft which creates a positive charge to attract anions to the binding cleft. Two extended β-strands run anti-parallel to each other behind the metal binding site which form a hinge that allows the lobes to open and close to accommodate metal binding and release [61, 68-74].

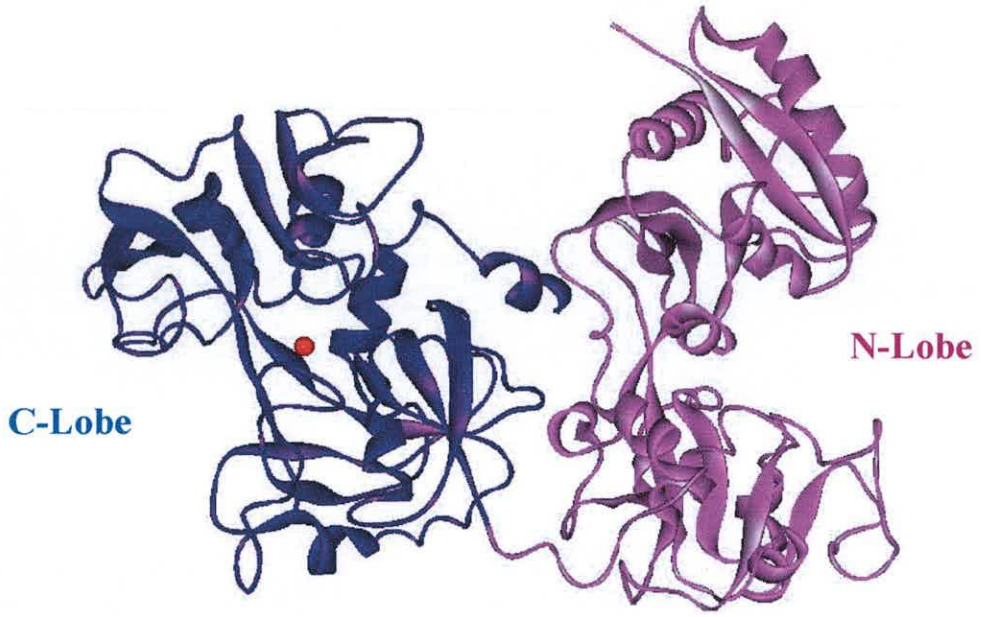

Figure 1.3 X-ray Crystal Structure of Fe_c-transferrin at 2.6 Å [62]. The C-lobe with Fe^{3+} bound is in the closed form and the N-lobe with no metal bound is in the open form.

Each metal binding site has a distorted octahedral geometry and consists of five oxygen donors: two from the phenolate groups on the tyrosine residues, one carboxylate from an aspartate residue and a bidentate carbonate anion, and one nitrogen donor from a histidine residue. The binding site can be seen in Figure 1.4. In order for Fe^{3+} to bind strongly to transferrin a suitable anion must be present, the synergistic anion. Physiologically this is carbonate [68, 75].

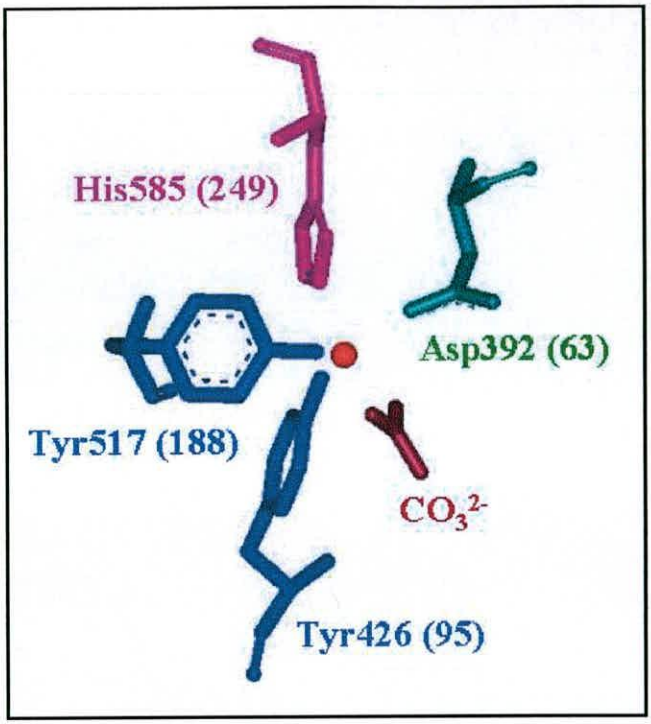

Figure 1.4 Metal Binding Site of Transferrin [62]. The binding site consists of five oxygen donors and one N donor. Fe^{3+} (shown as a red ball) can be seen in the binding site of the C lobe. Residue numbers are for the C-lobe site with N-lobe analogues in brackets.

1.3.1 Receptor Mediated Endocytosis

Receptor mediated endocytosis involves the binding of a substrate such as a protein, to a specific membrane bound receptor. The receptor and substrate are then internalised as the membrane invaginates to form a membrane bound vesicle which takes the receptor and substrate into the cell. Transferrin enters the cell by receptor mediated endocytosis, an ATP-dependent process [76] with the diferric form strongly bound to the receptor (TFR) [63]. The binding strength of apotransferrin for the receptor on the surface of human leukaemia K562 cells was found to be significantly

lower than that of diferric transferrin [77]. Each Fe_2-hTf binds to a monomer of the receptor. Iron-loaded transferrin binds to the receptor at neutral pH. After binding, diferric transferrin is internalised by endocytosis *via* clathrin-coated pits which bud from the plasma membrane as membrane-bound vesicles, the transferrin-TFR complex is routed into the endosomal compartment. Within 2 – 6 minutes [63], the diferric transferrin is inside the cell and retained in endosomes where upon maturation and loss of the clathrin coat, the endosomes become competent to pump protons in an ATP-requiring process so that the pH is lowered from that of cellular pH of 7.4 to about 5.5. This then leads to the release of Fe^{3+} where it is later found associated with cytosolic ferritin [63, 77, 78]. In cell studies, diferric transferrin was found to give up iron more readily than monoferric transferrin [79]. The acidification of endosomes is due to ATP-dependent proton pumps and protons are actively transported from the cytosol to the interior of the endosomes. The free Fe^{3+} released from transferrin into the endosome is reduced to Fe^{2+} on the *cis*-side of the endsomal membrane probably by oxidoreductase [80]. Free Fe^{2+} is then transported to late endosomes and lysosomes followed by transport into the cytoplasm by NRAMP2 (natural resistance-associated macrophage protein 2)/DMT1 (divalent metal transporter 1). The passage of iron from early to late endosomes is thought to occur by one of two mechanisms; vesicles pinch off from the early endosomes delivering the iron to late endosomes by specific carriers or the early endosomes and their contents mature into late endosomes with recruitment of late endosomal components [81].

NRAMP2 is a pH-dependent divalent metal transporter that shows a broad substrate range and mediates active proton-coupled transport [82]. Use of the microcytic

anaemia (*mk)* mouse and Belgrade *(b)* rat, both of which have autosomal recessive defects in iron metabolism [83-85] due to the same mutation of the *Nramp2* gene [86, 87], has shown that NRAMP2 is localised to the membrane of late endosomes and lysosomes and acts as an iron transporter in the transferrin cycle [81].

Once iron has been removed from the protein, apo-transferrin remains bound to the receptor at low pH and is taken back to the cell membrane in the endosome. Once at cellular pH the apotransferrin then dissociates from the receptor and is exocytosed (see Figure 1.5) [77, 88, 89]. At pH 5.4 apotransferrin binds to the receptors with the same affinity as diferric transferrin binds at pH 7.0. However, at pH 7.0 apotransferrin readily dissociates [78]. The free receptor is then available for another cycle of receptor mediated endocytosis. The half-life of apo-transferrin in humans is 7.6 days while that of Fe-hTf is 1.7 hours [90]. A molecule of transferrin will undergo approximately 100 cycles of iron binding and release. The major receptor recognition sites on hTf are thought to be localised to the C-lobe [91-95].

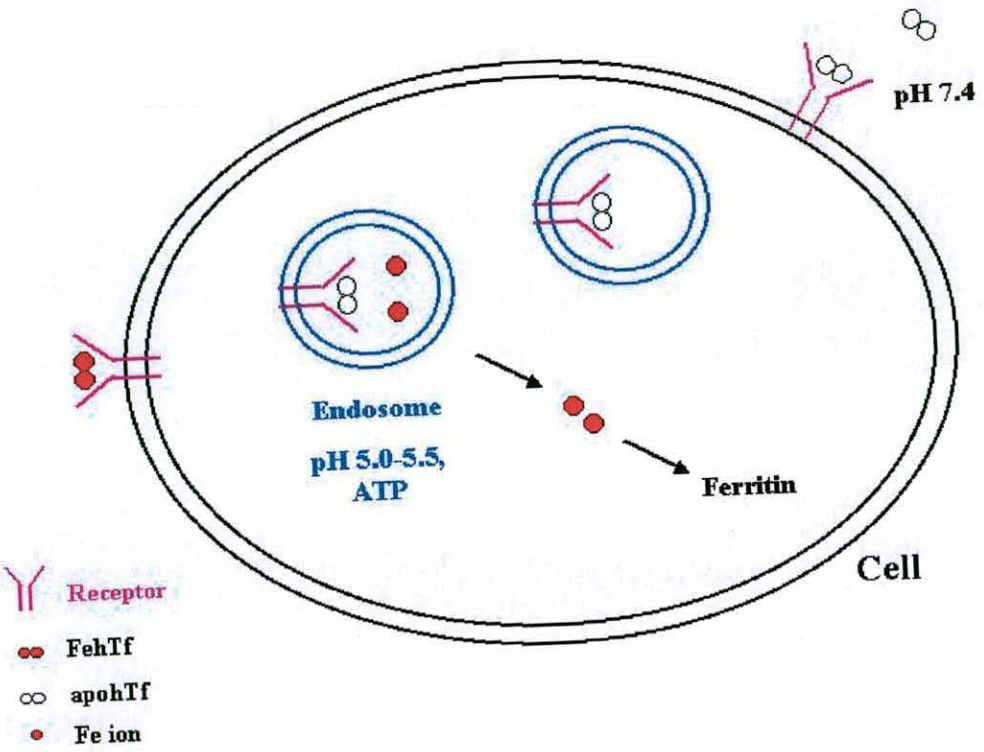

Figure 1.5 Receptor mediated endocytosis of transferrin. Fe-hTf binds to its receptor at neutral pH and is internalised inside vesicles. The transferrin-receptor complex then moves into acidic endosomes where Fe^{3+} is released and passed onto ferritin. The apotransferrin-receptor complex is then returned to the cell surface where the neutral pH allows the dissociation of transferrin from the receptor.

1.3.2 Transferrin as a Metal Ion Mediator

Transferrins are predominantly iron binding proteins, however, in human serum transferrin is only about 30% saturated with iron [54]. This suggests this protein may also transport other metals of importance. Of those metals studied so far, Fe^{3+} has the highest affinity for transferrin but other metals have been found to bind in the presence of a synergistic anion. Other main-group metal ions include Bi^{3+} [96], Ga^{3+} [97] and In^{3+} [98]. Transition-metal ions found to bind include Mn^{2+} [99] and Zn^{2+}

[100]. The determining factors for metal ion binding to transferrin are not clearly understood. There may be an optimum radius of the metal ion for secure binding into the cleft of the protein. However, Bi^{3+} (ionic radius of 0.103 nm) which is considerably larger than Fe^{3+} (0.065 nm), binds very tightly to serum transferrin [96]. It appears that the strength of metal ion binding is determined by the type of amino acid side-chain donors, mainly O donors, in transferrin rather than the size of the binding cleft [96]. Further, the most readily hydrolysed (most acidic) metal ions bind most strongly to transferrin. Hence, highly acidic trivalent metal ions such as Fe^{3+}, Bi^{3+} and Ti^{3+} bind more strongly than divalent metal ions [54].

1.4 Caeruloplasmin

Caeruloplasmin is found in serum and is a copper-containing glycoprotein with a molecular weight of *ca.* 132 kDa. Caeruloplasmin is synthesised in hepatocytes and secreted as a holoprotein and secreted locally within some non-hepatic tissues [101]. It belongs to a family of multi-nuclear 'blue' copper oxidases which includes ascorbate oxidase and laccase. At least four functions have been assigned to caeruloplasmin: copper transport, ferroxidase activity and amine oxidase activity, and it is an antioxidant in serum.

Caeruloplasmin is a plasma protein known for its oxidising activity. It is a multi-copper oxidase which contains most of the copper present in the plasma [102]. The precise physiological role of this enzyme is still unknown, but it is thought to have a multi-functional role including oxidising activity and is possibly a storage protein for copper. It has been suggested that caeruloplasmin has a distinct active site for glutathione-linked peroxidase activity apart from the copper complex giving it its

ferroxidase activity [101]. Anion binding studies have supported the theory that caeruloplasmin has multifunctional oxidase activity [103].

Caeruloplasmin is thought to be involved in the release of iron from cells, oxidation of the iron to Fe(III) and its subsequent incorporation onto apo-transferrin [104]. However, there is no firm evidence that transferrin interacts directly with caeruloplasmin or that caeruloplasmin oxidises Fe(II) to Fe(III) for uptake by transferrin. Since apo-transferrin has a high affinity for Fe(III), caeruloplasmin may act to prevent the release of harmful Fe(II) ions which might then participate in Fenton and Haber-Weiss-type reactions and hence production of $OH^{\bullet}$ [105]. In tissues where oxygen levels are low caeruloplasmin may be essential for ferroxidation.

The crystal structure of caeruloplasmin has been solved and can be seen in Figure 1.6 [106]. The structure comprises six domains arranged in a triangular array. Each of the domains contains a β-barrel with the strands organised in a manner typical of the small blue cupredoxin proteins. The barrels are orientated so that they are all the same way up but the even-numbered domains point inwards towards the pseudo-threefold axis, similar to the feet of a tripod, whereas the odd numbered domains point outward. There are six copper atoms present in the structure, three of these occupy mononuclear centres in domains 2, 4 and 6. The remaining three form a trinuclear cluster site at the interface between domains 1 and 6. The positioning of the trinuclear cluster and the nearest mononuclear copper in domain 6 is similar to that seen in ascorbate oxidase, suggesting that human serum caeruloplasmin may also exhibit an oxidase function [106]. Each of the mononuclear coppers is co-ordinated to a cysteine and two histidine residues and the coppers in domains 4 and 6

also coordinate to a methionine residue, in domain 2 the methionine is replaced by a leucine residue which may form van der Waal type bonding with the copper. Four pairs of histidine residues with Cu-N distances of approximately 2.1 Å, two pairs from domain 1 and the other two from domain 6, surround the trinuclear cluster.

Figure 1.6 X-ray crystal structure of human serum caeruloplasmin [106]. Structure solved to 3.1 Å. The six domains are displayed in different colours: red, blue, green, light blue, yellow, pink. The six copper atoms are shown as orange spheres, the two oxygen atoms as blue spheres.

The distances of around 18 Å between the mononuclear coppers is well within the range for effective electron transfer [104]. At the trinulcear cluster, oxygen is reduced to water. The extra distance between the coppers in domains 2 and 4 would lead to a slower oxidation rate than that involving the copper in domain 6, this may imply that the enzyme is able to oxidise more than one substrate molecule at a time

[104].

Upon further study of the crystal structure of caeruloplasmin, Lindley *et al* [104] proposed the presence of two copper labile sites in domains 4 and 6. The function of the sites is as yet unknown, however they could be used for copper transport.

1.5 Manganese

Manganese has the atomic number 25 and atomic weight of 54.938 atomic mass units. It is the fifth element of the first transition series in group 7. Manganese was recognised as an element in 1774 by Scheele, Bergman and others and isolated by Gahn in the same year by reduction of manganese dioxide with carbon. High purity manganese was only produced much later in the 1930s by electrolysis of Mn(II) solutions. Manganese minerals are widely dispersed with oxides, silicates and carbonates being the most common [107].

Manganese is relatively abundant making up about 0.085% of the earth's crust [108]. It is widely distributed as a number of substantial deposits which are mainly found as oxides, hydrous oxides or carbonate with large quantities also being found in seabeds of deep oceans as MnO_2. A large industrial use of Mn is in ferromanganese for steels.

1.5.1 Manganese Chemistry

Manganese can exist in eleven oxidation states from –3 to +7. The aqua Mn^{2+} ion is the most common and most stable as shown in Figure 1.7. Free Mn^{2+} can be present at high concentrations in neutral solutions as it does not begin to hydrolyze until pH

10 [108]. Divalent manganese (Mn^{2+}) is a d^5 ion and typically forms high-spin complexes lacking crystal field stabilisation energies. These properties and the rather large ionic radius and small charge/radius ratio lead to manganese forming relatively weak complexes with many ligands [109].

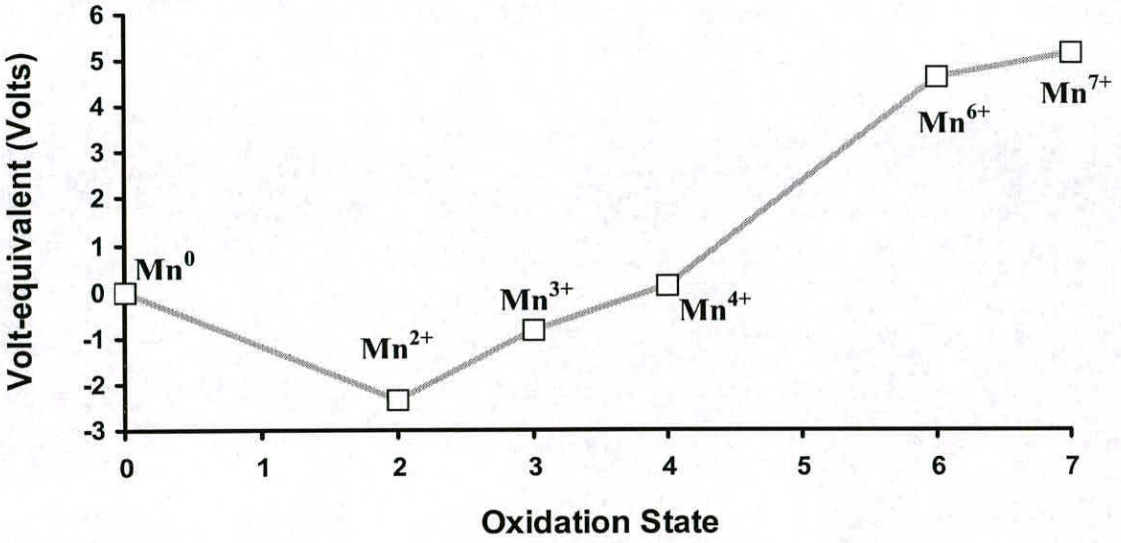

Figure 1.7 Plot of volt-equivalent versus oxidation state for Mn in aqueous, acidic solutions [110].

As seen with Ti, V and Cr, the highest oxidation state of Mn, Mn(VII), corresponds to the total number of 3*d* and 4*s* electrons. This state occurs only in the oxo compounds MnO^-_4 (permanganate), Mn_2O_7 (manganese oxide) and MnO_3F (manganese trioxide fluoride).

A summary of the co-ordination numbers and geometries of some of the most common oxidation states of Mn is shown in Table 1.2.

Table 1.2 Common Oxidation States and Stereochemistry of Manganese [108]

Oxidation state	Co-ordination number	Geometry	Examples
Mn(II), d^5	2	Linear	$Mn[C(SiMe_3)_2]_2$
	4	Tetrahedral	$MnCl_4^{2-}$, $MnBr_2(OPR)$
	4	Square planar	$[Mn(H_2O)_4SO_4.H_2O]$
	5	Trigonal bipyramidal	$[Mn(trenMe_6)Br]Br$
	5	Distorted trigonal bipyramidal	$MnBr_2[(MeHN)_2CO]_3$
	6	Octahedral	$[Mn(H_2O)_6]^{2+}$, $[Mn(NCS)_6]^{4-}$
Mn(III), d^4	4	Square planar	$[Mn(S_2C_6H_3Me)_2]^-$
	5	Square pyramidal	MnX sal_2en, $[bipyH_2]MnCl_5$
	5	Trigonal bipyramidal	$MnI_3(PMe_3)_2$
	6	Octahedral	$Mn(acac)_3$, $[Mn(ox)_3]^{3-}$, MnF_3(distorted)
Mn(IV), d^3	4	Tetrahedral	Mn(1-norbonyl)$_4$
	6	Octahedral	MnO_2, $MnCl_6^{2-}$
Mn(VII), d^0	3	Planar	MnO_3^+
	4	Tetrahedral	MnO_4^-, MnO_3F

Mn(VII) is a powerful oxidising agent usually being reduced to Mn(II). Only a few intermediate Mn(V) species have been identified in the reduction of permanganates [108]. Although Mn(II) is the most stable state, it is quite readily oxidized in alkaline solution. In neutral or acid aqueous solutions the very pale pink hexaaqua ion $[Mn(H_2O)_6]^{2+}$ forms which is resistant to oxidation as shown in Figure 1.8 [108].

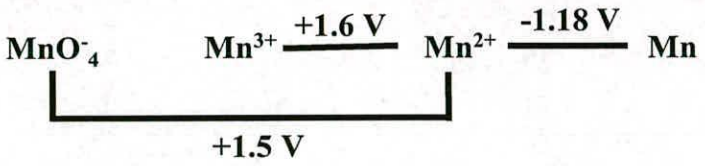

Figure 1.8 Oxidation potentials of Mn in neutral or acid aqueous solution

In basic media the hydroxide $Mn(OH)_2$ is easily oxidised by air as shown in Figure 1.9 [108].

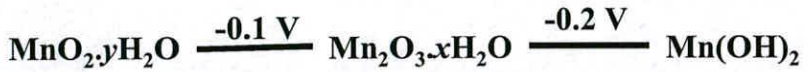

Figure 1.9 Oxidation potentials of Mn in basic aqueous solution

Mn(II) forms a large number of salts with all common anions. Most are soluble in water with the exception of phosphate and carbonate salts, which are only marginally soluble. Most of the salts crystallise from water as hydrates. Mn(III) exists naturally as salts of acetate, phosphate or trioxide, none of which are readily water soluble. The Mn(III) ion is important in the complex redox reactions of the higher oxidation states of manganese in aqueous solutions. It is most stable in acid solutions as it is easily hydrolysed with the initial monomer slowly polymerising [111].

$$Mn^{3+} + H_2O = Mn(OH)^{2+} + H^+ \qquad K=0.93$$

Under suitable conditions the Mn^{3+}-Mn^{2+} couple is reversible (E^0 = 1.559 V in 3 M $LiClO_4$). The Mn^{3+} ion is slowly reduced by water:

$$2Mn^{3+} + H_2O = 2Mn^{2+} + 2H^+ + \tfrac{1}{2}O_2$$

Complexing ions can stabilise the Mn(III) state in aqueous solution, however even the most stable species $[Mn(EDTA)(H_2O)]^-$ undergoes slow oxidation of the ligand leading to decomposition.

In many Mn(III) octahedral compounds a Jahn-Teller distortion in the form of elongation of two trans bonds with little difference in lengths of the other four, is often observed.

The Mn(III)/Mn(II) redox potential is highly dependent on the co-ordination sphere of the metal ion. Binding of nitrogen ligands to Mn(III) lowers the reduction potential of the Mn(III) complex and carboxylate ligands have the same although smaller effect. Five- and seven-coordinate Mn(II) complexes are more difficult to oxidise to Mn(III) than octahedral complexes. The behaviour of Mn bound proteins is consistent with the behaviour of the simple complexes; Mn(III) in enzymes such as catalase and superoxide dismutase is bound to two or more histidines although the conformation is not always octahedral. The Mn(II) ion in manganese-dependent peroxidases, which is oxidised to Mn(III), has a co-ordination sphere of two water molecules, a propionate from the haem group and three carboxylate residues.

The best known compounds of Mn(VII) are salts of the permanganate ion MnO_4^-, particularly sodium and potassium, with the latter being used as a common oxidising agent in the production of saccharin and benzoic acid and medically as a disinfectant.

In acid solution:

$$\mathbf{MnO_4^-} + \mathbf{8H^+} + \mathbf{5e^-} \rightleftharpoons \mathbf{Mn^{2+}} + \mathbf{4H_2O}$$

$$E^\theta = +1.51 \text{ V}$$

In alkali solution:

$$\mathbf{MnO_4^-} + \mathbf{2H_2O} + \mathbf{3e^-} \rightleftharpoons \mathbf{MnO_2} + \mathbf{4OH^-}$$

$$E^\theta = +1.23 \text{ V}$$

Permanganate is also being used in water purification having the advantage over chlorine in that the taste is not affected and the MnO_2 produced acts as a coagulant for colloidal impurities.

The MnO_4^- ion has no unpaired electrons, but it does have a small temperature independent paramagnetism [110].

1.5.2 Biology of Manganese

The average human body contains between 200 and 400 μmol of manganese with serum concentrations being typically less than 10 nM while tissue concentrations are generally less than 4 μM [112]. It is an essential metal which is particularly critical during development, however much is still unknown concerning basic aspects of manganese bioavailability, cellular uptake, processing and release. The estimated safe and adequate daily dietary intake (ESADDI) of manganese for adults is given as 2 – 5 mg Mn/day [113].

The valence state of Mn appears to have a critical role in the metals plasma-binding characteristics. This may have relevance to the toxicology and pharmacology of Mn and the degree to which it exerts its cytotoxicity [114]. Manganese in oxidation state +3 might have a significantly different profile to Mn(II) in terms of its uptake, distribution, accumulation and excretion.

Mitochondria have a higher concentration of manganese than the cytoplasm so tissues with high levels of mitochondria such as liver, bone, pancreas and kidney generally have high manganese concentrations.

1.5.3 Manganese Transport

Albumin, transferrin and 'transmanganin' have all been suggested as possible transport agents for Mn in plasma [115]. In studies using radio-labelled metals, Mn(II) was found to bind poorly to albumin compared with Cd(II), Zn(II) and Fe(III). However, the amount of Mn found to bind to transferrin increased as incubation time was increased, probably due to oxidation of Mn(II) to Mn(III), but not as readily as Fe(III). Further, saturation with Fe(III) prevented Mn(II) binding supporting the suggestion of Mn binding to the Fe-binding sites on the protein [115]. The mechanism of manganese transportation to and from extra-hepatic tissue has still not been identified. However, transferrin is thought to be the major transport protein [116, 117]. Gibbons *et al* [118] have shown that injected Mn(II) is cleared from the blood within 5 minutes whereas injected Mn(III)-hTf has a clearance of approximately 3 hours, which is comparable to clearance rates of ferric transferrin. Manganese and iron are taken up into cells *via* transferrin-dependent and -independent pathways requiring the divalent metal transporter 1 (DMT1) [119]. Currently it is thought that manganese is absorbed from the gastrointestinal tract and enters the portal blood where it remains either as free manganese or binds to α_2-macroglobulin which is then taken up by the liver [118]. A small amount, up to 10%, enters the systemic circulation where it can be oxidised to Mn(III) and bound to transferrin [116, 117]. Once manganese has entered the liver it can be transferred to the bile canaliculus *via* lysosomes. Some manganese is taken up by the mitochondria where it may be used to produce MnSOD. Uptake and release is thought to occur *via* the transport protein DMT1 and also through calcium channels [119]. Some manganese is thought to be retained by the nucleus although its function remains

unresolved. Alternatively, manganese can be incorporated into or is associated with newly synthesised manganese proteins [109]. Accumulation of manganese is tightly regulated due to metal toxicity so uptake is generally regulated by the bioavailability of the metal. As well as uptake into the cell, manganese must also be transported across the cell lumen to organelles where it can then be utilised.

Microorganisms also require manganese for survival in trace amounts. Certain oxygen-consuming organisms use manganese as the cofactor for antioxidant defence systems. Photosynthetic bacteria use manganese for oxygen evolution and metabolic processes such as DNA synthesis, sugar metabolism and protein modification.

The mechanism of manganese transport in *Bacillus* is not completely understood. A putative regulator of manganese, MntR, that responds to changes in manganese bioavailability has recently been discovered [112]. Possible targets for regulation by MntR include a member of the natural-resistance-associated macrophage protein (Nramp) family of metal transporters and putative ATP-binding-cassette (ABC) metal transport protein. Nramp is localised in the phagosomes of macrophages. Mammalian Nramp1 is believed to deprive mycobacteria of the redox-active metals iron and manganese as part of the oxygen radical defence against pathogens.

The unicellular cyanobacterium *Synechocystis* 6803 uses a tetramanganese cluster to produce molecular oxygen during photosynthetic growth [112].

The manganese transporter MntABC complex shows significant homology to polypeptide components of the ABC superfamily of transporter proteins. MntA appears to represent the ATP-binding cytoplasmic protein; MntB is a possible integral membrane protein and MntC may be the periplasmic component that captures the metal. Together these three subunits form the manganese permease at

the cell surface.

As is the case with bacteria, yeast also rely on manganese for growth. The acquisition of manganese in yeast cells involves the action of Smf1p, a member of the Nramp family. Smf1p, like other members of the Nramp family contains 12 transmembrane spanning domains. Smf1p, like Nramp2, is not specific for manganese, and transports other essential ions [112].

Multiple genes involved in the transport of manganese ions have been identified for yeast, however it is still to be understood how the ion is moved in a compartmentalised eukaryotic cell. For example, how is manganese transported to the mitochondria inside a cell for activation of proteins such as MnSOD?

1.5.4 Manganese-Containing Proteins

Manganese functions as a constituent of metalloenzymes and as an enzyme activator. Examples of some of these can be found in Table 1.3.

Table 1.3 Examples of some Mn-containing proteins[112]

Protein	O.S.	Function of protein	Examples
Phosphatases	II	Phosphate removal from proteins and sugars	Mn-activated phosphatases, inositol monophosphatase
Oxidoreductases	II/III	Oxidation/reduction	MnSOD, amine oxidase, cytochrome c oxidase
Dehydrogenases	II	Catalyse reduction with NAD^+	Isocitrate dehydrogenase
Peroxidases	II	Catalysis	Mn-dependent peroxidase, chloroperoxidase
Transferases	II	Transferase reactions including glycosyl and phosphate groups	Kinases, DNA and RNA polymerises, sugar transferases
Isomerase	II	Isomerisation reactions	Xylose isomerase, keto-aldose isomerases

O.S. = Oxidation State

Manganese-containing enzymes include MnSOD, arginase and pyruvate carboxylase. Arginase is a cytosolic enzyme responsible for the formation of urea and L-ornithine by the hydrolysis of L-arginine. It contains 4 mol Mn^{2+} per mol of enzyme and is most concentrated in mammalian liver. Manganese binding is critical for the pH sensing of arginase in the ornithine cycle. Hence, manganese may be involved in pH regulation [112]. Pyruvate carboxylase catalyses the first step of carbohydrate synthesis from pyruvate and also contains 4 mol Mn^{2+} per mol of enzyme [112].

There are a large number of manganese activated enzymes where the metal can act by binding the substrate directly such as ATP and/or by binding to the protein resulting in a conformational change. Manganese-activated proteins include

glycosyltransferases, phosphoenolpyruvate carboxykinase and glutamine synthetase [112].

1.5.4.1 Manganese Superoxide Dismutase

The role of MnSOD in defence against free radicals can be clearly shown in MnSOD knockout models. Knockout mice for MnSOD die within the first few weeks of life and mice that are heterozygous for MnSOD show a 50% decrease in liver MnSOD activity and severe oxidative damage to tissue [120]. Over-expression of MnSOD is characterised by improved resistance to various stresses [121].

MnSOD catalyses the disproportionation of $O_2^{-\bullet}$ to H_2O_2 and O_2 by using a reaction mechanism that involves cyclic oxidation and reduction of the active metal site coupled to the protonation of the co-ordinated anion [122]:

$$M^{n+1} + O_2^{-\bullet} \longrightarrow M^{n+} + O_2$$

$$M^{n+} + O_2^{-\bullet} + 2H^+ \longrightarrow M^{n+1} + H_2O_2$$

The enzyme works by way of a 'ping-pong' mechanism, which follows a relatively low-energy pathway. The first $O_2^{-\bullet}$ binds to the oxidative Mn(III) centre, transfers an electron and releases a molecule of O_2. The second $O_2^{-\bullet}$ attaches to the reduced Mn(II) and an electron is transferred and coupled with proton transfer, forming HO_2^- [16]. The actual reaction pathway is more complicated. For example, an inactive form of MnSOD has been observed which results from the oxidative addition of $O_2^{-\bullet}$ to a Mn(II) centre which slowly inter-converts back to the active form [123].

Borgstahl *et al* [124] have determined the crystal structure of MnSOD from

Escherichia coli (Figure 1.10).

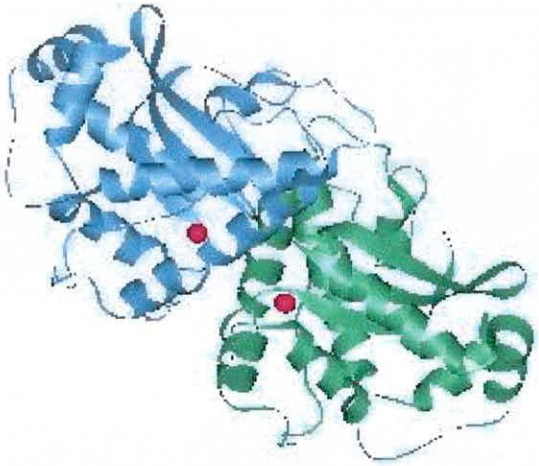

Figure 1.10 Crystal Structure of MnSOD [124]. *E. coli* MnSOD crystals were grown at pH 8.5 and cryocooled to 100 K. Resolution of 1.55 Å was achieved. Monomers are coloured blue and green. Manganese atoms are shown as red spheres.

This MnSOD is a homodimer with the active manganese sites separated by 18.3 Å. Each monomer is made up of a N-terminal α-helical domain and a C-terminal α/β domain. The active site is between the two domains with each contributing ligands to the active site co-ordination. The manganese in the active site is ligated by three histidine nitrogens (His26, His81, His171), one aspartate carboxylate oxygen(Asp167) and a water molecule (or a hydroxide group depending on the metal oxidation state) in a trigonal bipyramidal arrangement [112, 125]. The active site is shown in Figure 1.11.

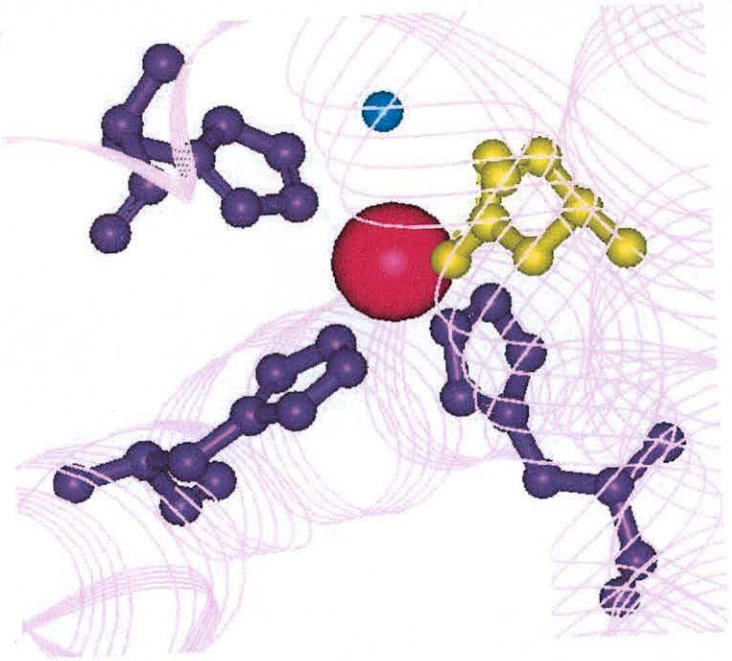

Figure 1.11 Active site of Mn superoxide dismutase [125]. Mn is bound to three histidines (purple), an aspartate (yellow) and a molecule of co-ordinated solvent (water or hydroxide, shown as blue sphere). Manganese is shown as a red sphere.

1.5.4.2 Mimics

The recent interest in oxidative stress and its involvement in disease and cell death has lead to the possible development of antioxidants as therapeutics. Many groups are currently working on the metalloproteins catalase and SOD. Most catalytic SOD mimics are designed with a redox-reactive metal centre that catalyses the dismutation reaction with superoxide in a manner similar to that found naturally in mammalian SODs. An ideal mimetic should be stable with high specificity for interaction with $O_2^{-\bullet}$ and a high rate constant. Metalloporphyrins are a relatively new class of metal containing SOD mimetics. Others include salen and macrocyclic SOD mimetics [13, 126]. A functional mimic being investigated is a manganese(II) complex with a bis (cyclohexyloyridine)-substituted macrocyclic ligand (M40403). M40403 has a high

catalytic SOD activity and is chemically and biologically stable in vivo [127]. However, these new products are not without their drawbacks in terms of expense, antigenicity and size. Further, if effective mimics are produced they must be targeted to the correct part of the tissue and act in the correct sequence of events when required. A general problem for SOD mimics is that they can react with most ROS; hence targeting to areas such as the mitochondria to deal with superoxide only may prove to be difficult.

1.5.4.3 Contrast Agents

Magnetic resonance imaging has proved to be a useful medical tool for looking at abnormal tissue. Differences between the ^{1}H NMR resonances of normal and abnormal tissue can be detected by the use of contrast agents. Useful contrast agents are paramagnetic metal ions such as Mn(II) ($3d^5$, 5 unpaired electrons) [128]. Toxicity is associated with the free metal ions therefore chelation of Mn(II) is necessary. The design of the ligand allows paramagnetic ions to be targeted to a particular organ, e.g. the liver, thereby increasing the signal intensity of the tissue containing the agent.

MnDPDP (manganese(II) *N,N'*-dipyridoxyl-ethylenediamine-*N,N'*-diacetate-5,5', bis(phosphate)) is the active ingredient of mangafodipir trisodium injection (Teslascan®) used as a contrast agent for MRI of the liver and hepatobiliary system [129].

1.6 Conclusion

The natural transferrin cycle for the delivery of iron to cells offers a potential strategy for metallo-drug targeting to hepatocytes undergoing oxidative stress.

It is known that hepatocytes have a high requirement for manganese due to its use in the mitochondrial matrix *i.e.* for incorporation into MnSOD. Hepatocytes are known to express high levels of the transferrin receptor due to the liver being a major site of haem/red blood cell synthesis [53, 130].

Although Fe(III) is the natural metal bound by transferrin, many other metal ions can also bind at the same specific sites [131]. In blood plasma, less than 30% of the iron sites in human transferrin are occupied by iron and the vacant sites could be used to transport other metal ions as well.

Investigation of transferrin as a potential carrier of manganese to hepatocytes may therefore aid understanding of the mechanisms of uptake, action and toxicity.

Since Mn(III) can bind transferrin, it is of interest to investigate the methods available for loading the protein and how this may effect the biological and chemical characteristics of the protein such as alteration to the binding site and/or protein conformation. More specifically, successful crystallisation of the protein with iron and manganese bound will allow direct comparisons between the two metal forms.

1.7 Aims of Thesis

i) To develop an efficient method of loading human serum transferrin with manganese with possible use of Mn(II) and the serum oxidant caeruloplasmin, or Mn(VII).

This may then help us to understand the possible mechanism(s) used by the body to transport manganese from ingestion to cells.

ii) To investigate the reaction of apo-transferrin with potassium permanganate, including studies of the possible oxidation of the protein and of insertion using labelled transferrin and NMR techniques.

Potassium permanganate is a well known oxidant so any reaction with the protein could lead to oxidation of the protein and possibly altered protein conformation.

iii) To grow crystals of transferrin with iron and manganese bound to one or both lobes.

If this can be achieved then a direct comparison can be made between the two different loaded proteins in terms of protein conformation and metal binding site. This may then provide further information on the behaviour of transferrin when metals other than iron are loaded with respect to receptor binding.

iv) To determine whether the highly efficient transferrin endocytosis pathway can be exploited for the targeted delivery of manganese to hepatocytes.

This could then lead onto further work as to what signalling systems are affected and if MnSOD can be up-regulated when a cell is experiencing oxidative stress.

v) To investigate if manganese transferrin has an effect on the mitochondria of hepatocytes.

As most of hepatocytes' manganese content is found in the mitochondria any excess manganese transported to the cell is likely to take effect here. Primarily it needs to be established if excess manganese alters mitochondrial function in terms of alteration of the transmembrane potential.

1.8 References

1. C.E. Gavin, K.K. Gunter, and T.E. Gunter, *Neurotoxicol.,* **1999**, 20: 445-454.

2. J. Rashba-Step, N.J. Turro, and A.I. Cederbaum, *Arch. Biochem. Biophys.,* **1993**, 300: 401-408.

3. I. Fridovich, *J. Biol. Chem.,* **1970**, 245: 4053-4057.

4. B.S. Robinson, C.S. Hii, and A. Ferrante, *Biochem. J.,* **1998**, 336: 611-617.

5. J.S. Beckman, T.S. Beckman, J.C. Chen, P.A. Marshall, and B.A. Freeman, *Proc. Natl. Acad. Sci. USA,* **1990**, 87: 1620-1624.

6. J.F. Turrens, B.A. Freeman, J.G. Levitt, and J.D. Crapo, *Arch. Biochem. Biophys.,* **1982**, 217: 401-410.

7. C. Richter, V. Gogvadze, R. Laffranchi, R. Schlapbach, M. Schweizer, M. Suter, P. Walter, and M. Yaffee, *Biochim. Biophys. Acta,* **1995**, 1271: 67-74.

8. B. Chance, H. Sies, and A. Boveris, *Phys. Rev.,* **1979**, 59: 527-605.

9. P.M. Wood, *Biochem. J.,* **1988**, 253: 287-289.

10. A.J. Kowaltowski and A.E. Vercesi, *Free Rad. Biol. Med.,* **1999**, 26: 463-471.

11. H.C. Sutton and C.C. Winterbourne, *Free. Rad. Biol. Med.,* **1989**, 6: 53-60.

12. D.M. Guidot, J.E. Repine, A.D. Kitlowski, S.C. Floes, S.K. Nelson, R.M. Wright, and J.M. McCord, *J. Clin. Invest.,* **1995**, 96: 1131-1136.

13. M. Patel and B.J. Day, *TiPS,* **1999**, 20: 359-364.

14. G.S. Waldo and J.E. Penner-Hahn, *Biochemistry,* **1995**, 34: 1507-1512.

15. H.J. Majima, T.D. Oberley, K. Furukawa, M.P. Mattson, H. Yen, L.I. Szweda, and D.K. St. Clair, *J. Biol. Chem.,* **1998**, 273: 8217-8224.

16. D.T. Sawyer and J.S. Valentine, *Acc. Chem. Res.,* **1981**, 14: 393-400.

17. I. Fridovich, *Ann. Rev. Biochem.,* **1975**, 44: 147-159.

18. A.P. Halestrap, P.M. Kerr, S. Javadov, and K.-Y. Woodfield, *Biochim. Biophys. Acta,* **1998**, 1366: 79-94.

19. G. Lenaz, *Biochim. Biophys. Acta,* **1998**, 53-67.

20. G. Kroemer, *Nature Med.,* **1997**, 3: 614-620.

21. P.X. Petit, S.-A. Susin, N. Zamzami, B. Mignotte, and G. Kroemer, *FEBS Letters,* **1996**, 396: 7-13.

22. J.D. Cortese and C.R. Hackenbrock, *Biochim. Biophys. Acta,* **1993**, 1142: 194-202.

23. R.M. Kluck, E. Bossy-Wetzel, D.R. Green, and D.D. Newmeyer, *Science,* **1997**, 275: 1132-1136.

24. J. Yang, X. Liu, K. Bhalla, C.N. Kim, A.M. Ibrado, J. Cai, T.-I. Peng, D.P. Jones, and X. Wang, *Science,* **1997**, 275: 1129-1132.

25. A. Samali, H. Nordgren, B. Zhivotovsky, E. Peterson, and S. Orrenius, *Biochem. Biophys. Res. Comm.,* **1999**, 255: 6-11.

26. P. Li, D. Nijhawan, I. Budihardjo, S.M. Srinivasula, M. Ahmad, E.S. Alnemri, and X. Wang, *Cell,* **1997**, 91: 479-489.

27. S. Krajewski, S. Tanaka, S. Takayama, M.J. Schibler, W. Fenton, and J.C. Reed, *Cancer Res.,* **1993**, 53: 4701-4714.

28. N. Zamzami, S.A. Susin, P. Marchetti, T. Hirsch, I. Gómez-Monterry, M. Castedo, and G. Kroemer, *J. Exp. Med.,* **1996**, 183: 1533-1544.

29. N. Zamzami, P. Marchetti, M. Castedo, D. Decaudin, A. Macho, T. Hirsch, A.A. Susin, P.X. Petit, B. Mignotte, and G. Kroemer, *J. Exp. Med.,* **1995**, 182: 367-377.

30. A.E. Vercesi, A.J. Kowaltowski, M.T. Grijalba, A.R. Meinicke, and R.F. Castilho, *Biosc. Rep.,* **1997**, 17: 43-52.

31. Zoratti and Szabo, *Biochim. Biophys. Acta,* **1995**, 1241: 139-176.

32. Y.A. Lazebnik, S.H. Kaugmann, S. Desnoyers, G.G. Poirier, and W.C. Earnshaw, *Nature,* **1997**, 371: 346-347.

33. S.J. Martin and D.R. Green, *Cell,* **1995**, 82: 349-352.

34. S.A. Susin, *J. Exp. Med.,* **1996**, 184: 1331-1341.

35. G. Kroemer, P. Petit, N. Zamzami, J.L. Vayssiere, and B. Mignotte, *FASEB,* **1995**, 9: 1277-1287.

36. J.J. Lemasters, A. Nieminan, T. Qian, L.C. Trost, S.P. Elmore, Y. Nishimura, R.A. Crowe, W.E. Cascio, C.A. Bradham, D.A. Brenner, and B. Herman, *Biochim. Biophys. Acta,* **1998**, 1366: 177-196.

37. R.S. Sohal and A. Dubey, *Free. Rad. Biol. Med.,* **1994**, 16: 621-626.

38. S. Moncada, R.M.J. Palmer, and E.A. Higgs, *Pharm. Rev.,* **1991**, 43: 109-141.

39. E.J. Griffiths and A.P. Halestrap, *Biochem. J.,* **1995**, 307: 93-98.

40. S.A. Susin, N. Zamzami, M. Castedo, E. Daugas, H.-G. Wang, S. Geley, F. Fassy, J.C. Reed, and G. Kroemer, *J. Exp. Med.,* **1997**, 186: 25-37.

41. M.G. Vander Heiden, N.S. Chandel, E.K. Williamson, P.T. Schumaker, and C.B. Thompson, *Cell,* **1997**, 91: 627-637.

42. M.D. Jacobson and M.C. Raff, *Nature,* **1995**, 374: 814-816.

43. M. Yoneda, K. Katsumata, M. Hayakawa, M. Tanaka, and T. Ozawa, *Biochem. Biophys. Res. Comm.*, **1995**, 209: 723-729.

44. B. Mignotte and J.L. Vayssiere, *Eur. J. Biochem.*, **1998**, 252: 1-15.

45. T. Ide, H. Tsutsui, S. Kinugawa, H. Utsumi, D. Kang, N. Hattori, K. Uchida, K.-I. Arimura, K. Egashira, and A. Takeshita, *Circ. Res.*, **1999**, 85: 357-363.

46. Y.J. Kang, *Proc. Soc. Exp. Biol. Med.*, **1999**, 222: 263-273.

47. P.S. Ray, G. Maulik, G.A. Cordis, A.A. Bertelli, A. Bertelli, and D.K. Das, *Free. Rad. Biol. Med.*, **1999**, 27: 160-169.

48. P. Venditti, P. Masullo, S. Di Meo, and C. Agnisola, *Arch. Physiol. Biochem,* **1999**, 107: 27-34.

49. I. Rahman and W. MacNee, *Am. J. Phys.*, **1999**, 277: L1067-1088.

50. F.J. Kelly, I. Mudway, A. Blomberg, A. Frew, and T. Sandstrom, *Lancet,* **1999**, 354: 482-483.

51. J. Cederberg, J. Galli, H. Luthman, and U.J. Eriksson, *Diabetes,* **2000**, 49: 101-107.

52. J.J.R. Frausto da Silva and R.J.P. Williams, *The Biological Chemistry of the Elements: The Inorganic Chemistry of Life*. Clarendon Press, Oxford, **1993**.

53. B.R. Bacon and A.S. Tavill, *Sem. Liv. Dis.*, **1984**, 4: 181-192.

54. H. Sun, H. Li, and P.J. Sadler, *Chem. Rev.*, **1999**, 99: 2817-2842.

55. T.M. Rose, G.D. Plowman, D.B. Teplow, W.J. Dreyer, K.E. Hellstrom, and J.P. Brown, *Proc. Natl. Acad. Sci. USA,* **1986**, 83: 1261-1265.

56. J.H. Crosa, *Ann. Rev. Micro.*, **1984**, 38: 69-89.

57. T.A. Mietzner, S.B. Tencza, P. Adhikari, K.G. Vaughan, and A.J. Nowalk, *Curr. Top. Microbiol. Immunol.*, **1998**, 225: 113-135.

58. A.J. Nowalk, S.B. Tencza, and T.A. Mietzner, *Biochemistry,* **1994**, 33: 12769-12775.

59. C.M. Bruns, A.J. Nowalk, A.S. Arvai, M.A. McTigue, K.G. Vaughan, T.A. Mietzner, and D.E. McRee, *Nature Stuct. Biol.,* **1997**, 4: 919-924.

60. R.T.A. MacGillivray, E. Mendez, S.K. Sinha, M.R. Sutton, J. Lineback-Zins, and K. Brew, *Proc. Natl. Acad. Sci. USA,* **1982**, 79: 2504-2508.

61. R.T.A. MacGillivray, S.A. Moore, J.C. Chen, B.F. Anderson, H. Baker, Y. Luo, M. Bewley, C.A. Smith, M.E.P. Murphy, Y. Wang, A.B. Mason, R.C. Woodworth, G.D. Brayer, and E.N. Baker, *Biochemistry,* **1998**, 37: 7919-7928.

62. H.J. Zuccola, PhD Thesis, 1992, Georgia Institute of Technology, Atlanta.

63. A. Dautry-Varsat, *Biochimie,* **1986**, 68: 375-381.

64. B. Gorinsky, C. Horsburgh, P.F. Lindley, D.S. Moss, M. Parkar, and J.L. Watson, *Nature,* **1979**, 281: 157-158.

65. R. Sarra, R. Garratt, B. Gorinsky, H. Jhoti, and P.F. Lindley, *Acta Crsytallogr.,* **1990**, B46: 763-771.

66. M.H. Metz-Boutigue, J. Jolles, J. Mazurier, F. Schoentgen, D. Legrand, G. Spik, and P. Jolles, *Eur. J. Biochem.,* **1984**, 145: 659-676.

67. G. Spik, B. Bayard, B. Fournet, G. Strecker, S. Bouquelet, and J. Montreuil, *FEBS Letters,* **1975**, 50: 296-299.

68. B.F. Anderson, H.M. Baker, E.J. Dodson, G.E. Norris, S.V. Rumball, J.M. Waters, and E.N. Baker, *Proc. Natl. Acad. Sci. USA,* **1987**, 84: 1769-1773.

69. B.F. Anderson, H.M. Baker, G.E. Norris, D.W. Rice, and E.N. Baker, *J. Mol. Biol.,* **1989**, 209: 711-734.

70. B.F. Anderson, H.M. Baker, G.E. Norris, S.V. Rumball, and E.N. Baker,

Nature, **1990**, 344: 784-787.

71. A. Rawas, H. Muirhead, and J. Williams, *Acta Crsytallogr.,* **1996**, D52: 631-640.

72. H. Kurokawa, B. Mikami, and J. Hirose, *J. Mol. Biol.,* **1995**, 254: 196-207.

73. M. Gerstein, B.F. Anderson, G.E. Norris, E.N. Baker, A.M. Lesk, and C. Chothia, *J. Mol. Biol.,* **1993**, 234: 357-372.

74. P.D. Jeffrey, M.C. Bewley, R.T.A. MacGillivray, A.B. Mason, R.C. Woodworth, and E.N. Baker, *Biochemistry,* **1998**, 37: 13978-13986.

75. A.L. Schade, R.W. Reinhart, and H. Levy, *Arch. Biochem. Biophys.,* **1949**, 20: 170-172.

76. S.L. Schmid and L.L. Carter, *J. Cell. Biol.,* **1990**, 111: 2307-2318.

77. R.D. Klausner, G. Ashwell, J. Van Renswoude, J.B. Harford, and K.R. Bridges, *Proc. Natl. Acad. Sci. USA,* **1983**, 80: 2263-2266.

78. A. Dautry-Varsat, A. Ciechanover, and H.F. Lodish, *Proc. Natl. Acad. Aci. USA,* **1983**, 80: 2258-2262.

79. H. Huebers, B. Josephson, E. Huebers, E. Csiba, and C. Finch, *Proc. Natl. Acad. Sci. USA,* **1981**, 78: 2572-2576.

80. M.-T. Nunez, V. Gaete, J.A. Watkins, and J. Glass, *J. Biol. Chem.,* **1990**, 265: 6688-6692.

81. M. Tabuchi, T. Yoshimori, K. Yamaguchi, T. Yoshida, and F. Kishi, *J. Biol. Chem.,* **2000**, 275: 22220-22228.

82. H. Gunshin, B. Mackenzie, U.V. Berger, Y. Gunshin, M.F. Romero, W.F. Boron, S. Nussberger, J.L. Gollan, and M.A. Hediger, *Nature,* **1997**, 388: 482-488.

83. E.S. Russel, D.J. Nash, S.E. Bernstein, E.L. Kent, E.C. McFarland, S.M.

Matthews, and M.S. Norwood, *Blood,* **1970**, 35.

84. J.A. Edwards and J.E. Hoke, *Proc. Soc. Exp. Biol. Med.,* **1972**, 141: 81-84.

85. J.A. Edwards and J.E. Hoke, *Blood,* **1975**, 46: 381-388.

86. M.D. Fleming, C.C. Trenor III, M.A. Su, D. Foernzler, D.R. Beier, W.F. Deitrich, and N.C. Andrews, *Nat. Genet.,* **1997**, 16: 383-386.

87. M.D. Fleming, M.A. Romano, M.A. Su, L.M. Garrick, M.D. Garrick, and N.C. Andrews, *Proc. Natl. Acad. Sci. USA,* **1998**, 95: 1148-1153.

88. P. Aisen, A. Leibman, and J. Zweier, *J. Biol. Chem.,* **1978**, 253: 1930-1937.

89. J.-N. Octave, Y.-J. Schneider, A. Trouet, and R.R. Crichton, *TIBS,* **1983**, 8: 217-220.

90. P. Aisen, in *Metal Ions in Biological Systems*, A. Sigel and H. Sigel Ed, Marcel Dekker Inc., New York, **1998**, 35: 585-631

91. P.K. Bali and P. Aisen, *Biochemistry,* **1991**, 30: 9947-9952.

92. O. Zak, D. Trinder, and P. Aisen, *J. Biol. Chem.,* **1994**, 269: 7110-7114.

93. A.B. Mason, B.M. Tam, R.C. Woodworth, R.W. Oliver, B.N. Green, L.N. Lin, J.F. Brandts, K.J. Savage, J.A. Lineback, and R.T.A. MacGillivray, *Biochem. J.,* **1997**, 326: 77-85.

94. C.M. Lawrence, S. Ray, M. Babyonyshev, R. Galluser, D.W. Borhani, and S.C. Harrison, *Science,* **1999**, 286: 779-782.

95. E. Wagner, D. Curiel, and M. Cotton, *Adv. Drug Del. Rev.,* **1994**, 14: 113-135.

96. H. Li, P.J. Sadler, and H. Sun, *J. Biol. Chem.,* **1996**, 271: 9483-9489.

97. W.R. Harris and V.L. Pecoraro, *Biochemistry,* **1983**, 22: 292-299.

98. R.W. Evans and W. Ogwang, *Biochem. Soc. Trans.,* **1988**, 16: 833-834.

99. W.R. Harris and A. Chen, *J. Inorg. Biochem.,* **1994**, 54: 1-19.

100. W.R. Harris, *Biochemistry,* **1983**, 22: 3920-3926.

101. M.K. Cha and I.H. Kim, *Biochemistry,* **1999**, 38: 12104-12110.

102. V.N. Zaitsev, I. Zaitseva, M. Papiz, and P.F. Lindley, *J. Biol. Chem.,* **1999**, 4: 579-587.

103. G. Musci, G.C. Bellenchi, and L. Calabrese, *Eur. J. Biochem.,* **1999**, 265: 589-597.

104. P.F. Lindley, G. Card, I. Zaitsev, V.N. Zaitsev, B. Reinhammar, E. Selin-Lindgren, and K. Yoshida, *J. Biol. Inorg. Chem.,* **1997**, 2: 454-463.

105. B.A. Freeman and J.D. Crapo, *Lab. Invest.,* **1982**, 47: 412-426.

106. I. Zaitsev, V.N. Zaitsev, G. Card, K. Moshkov, B. Bax, A. Ralph, and P.F. Lindley, *J. Biol. Inorg. Chem.,* **1996**, 1: 15-23.

107. http://www.speclab.com/elements/manganese.htm.

108. F.A. Cotton and G. Wilkinson, *Advanced Organic Chemistry*, 5th Ed. ed. John Wiley and Sons, Inc., New York, **1980**.

109. C.L. Keen, J.L. Ensunsa, and M.S. Clegg, in *Metal ions in Biological Systems: Manganese and its Role in Biological Processes*, A.S. Sigel, H. Ed, Marcel Dekker Inc, New York, **2000**, 37: 89-121

110. N.N. Greenwood and A. Earnshaw, *Chemistry of the Elements*, 1st Ed. ed. Pergamon Press Ltd., Oxford, **1984**.

111. P.A. Siskos, N.C. Peterson, and R.E. Huie, *Inorg. Chem.,* **1984**, 23: 1134-1137.

112. A. Sigel and H. Sigel, *Manganese and its role in biological processes*, Metal Ions in Biological Systems. Marcel Dekker Inc.37 **2000**.

113. J.L. Greger, *Neruotoxicology,* **1999**, 20: 205-212.

114. J.-Y. Chen, G.C. Tsao, Q. Zhao, and W. Zheng, *Tox. App. Pharm.,* **2001**, 175: 160-168.

115. A.M. Scheuhammer and M.G. Cherian, *Biochim. Biophys. Acta,* **1985**, 840: 163-169.

116. L. Davidsson, B. Lönnerdal, B. Sandstrom, K. Kunz, and C.L. Keen, *Journal of Nutrition,* **1989**, 119: 1087-1092.

117. J.W. Critchfield and C.L. Keen, *Metabolism,* **1992**, 41: 1087-1092.

118. R.A. Gibbons, S.N. Dixon, K. Hallis, A.M. Russel, B.F. Sanson, and H.W. Symonds, *Biochim. Biophys. Acta,* **1976**, 444: 1-10.

119. J.A. Roth and M.D. Garrick, *Biochem. Pharm.,* **2003**, 66: 1-13.

120. M.D. Williams, H. Van Remmen, C.C. Conrad, T.T. Huang, C.J. Epstein, and A. Richardson, *J. Biol. Chem.,* **1998**, 273: 28510-28515.

121. H. Yen, T.D. Oberley, C.G. Gairola, L.I. Szweda, and D.K. St. Clair, *Arch. Biochem. Biophys.,* **1999**, 362: 59-66.

122. R.K. Holm, P. Kenepol, and E.I. Solomon, *Chem. Rev,* **1996**, 96: 2239-2314.

123. C. Bull, E.C. Niederhoffer, T. Yoshida, and J.A. Fee, *J. Am. Chem. Soc.,* **1991**, 113: 4069-4076.

124. G.E.O. Borgstahl, M. Pokross, R. Chehab, A. Sekher, and E.H. Snell, *J. Mol. Biol.,* **2000**, 296: 951-959.

125. J. Li, C.L. Fisher, R. Konecny, D. Bashford, and L. Noodleman, *Inorg. Chem.,* **1999**, 38: 929-939.

126. D.P. Riley, *Chem. Rev.,* **1999**, 99: 2573-2587.

127. D. Salvemini, Z.-Q. Wang, J.L. Zweier, A. Samouilov, H. Macarthur, T.P.

Misko, M.G. Currie, S. Cuzzocrea, J.A. Sikorski, and D.P. Riley, *Science,* **1999**, 286: 304-306.

128. B.E. Van Beers, B. Gallez, and J. Pringot, *Radiol.,* **1997**, 203: 297-306.

129. K.G. Toft, G.M. Kindberg, and T. Skotland, *J. Pharm. Biomed. Anal.,* **1997**, 15: 983-988.

130. P. Aisen, *Sem. Liv. Dis.,* **1984**, 4: 193-206.

131. C.A. Smith, A.J. Sutherland-Smith, B.K. Keppler, F. Kratz, and E.N. Baker, *J. Biol. Inorg. Chem.,* **1996**, 1: 424-431.

Chapter 2 Experimental Techniques

In this Chapter, some specific techniques used in this study are briefly described.

2.1 Source of Chemicals

2.1.1 Reagents

Some common reagents used in this work and their sources are shown in Table 2.1. Other reagents and their sources are listed in the text.

2.1.2 Transferrin

All transferrins used in this work were from human serum and were of a high grade. Holo-transferrin was obtained from Sigma, catalogue number T-4778, lot 13H9315. Apo-transferrin catalogue number T-4382, lot 50K7608.

For cell studies, the highest quality of apo-transferrin suitable for cell culture was purchased, catalogue number T1147, lot 101K024825. This was then used to produce Mn_2-hTf and Fe_2-hTf.

Table 2.1 Reagents and sources

Reagent	Source
Apo- and holo- transferrin, human serum	Sigma
$MnCl_2.4H_2O$	Sigma
Sodium bicarbonate	Aldrich
Hepes Buffer (USP grade, powder)	Sigma
$KMnO_4$ (USP grade)	Sigma
Caeruloplasmin, human serum	ICN Biomedical
Tris-Borate EDTA buffer (x10)	Bio-Rad
Amido Black 10B	Acros
Sodium cacodylate buffer	Sigma
N-Acetyl L- methionine	Aldrich
L-Histidine	Sigma
L-Tryptophan	Aldrich
L-Tyrosine	Sigma
Methionine sulfoxide	Sigma
Methionine sulfone	Fluka
mClCCP	Sigma
Dulbeccos modified eagles medium DMEM	Invitrogen
Tryspin/EDTA (liquid, x1)	Sigma
DMSO	Sigma

2.1.3 Water Purification

All water used in this work was purified using a Millipore Elix 5 system, followed by an Elgastat UHQ PS deioniser to give 18.2 MΩ-cm at 298 K. The purified water obtained by this procedure is referred to herein as ultrapure water.

2.2 UV-Vis Spectroscopy

Determination of the concentration of an aqueous sample of a protein is most simply done by measuring its absorbance in the near-ultraviolet region. However, this requires a prior knowledge of the protein's specific extinction coefficient at a given wavelength.

The near UV (250-350 nm) absorbance spectrum of a protein is almost entirely generated from its aromatic amino acid residues. These include tryptophan (ε_{280} 5559 $M^{-1}cm^{-1}$), tyrosine (ε_{280} 1197 $M^{-1}cm^{-1}$) and phenylalanine (ε_{280} 0.7 $M^{-1}cm^{-1}$, ε_{257} *ca.* 195 $M^{-1}cm^{-1}$) [1], with a small contribution from disulfide bonds. This results in a unique UV spectrum for each protein due to its particular aromatic acid content. Protein concentrations can then be calculated using the spectral absorbance at 280 nm by the Beer Lambert law:

$$\mathbf{A_{280} = \varepsilon c l}$$

Where **c** is the protein concentration (M), **ε** is the molar extinction coefficient of the protein ($M^{-1}cm^{-1}$) at 280 nm and **l** is the path length (cm).

For a protein with a known amino acid sequence, **ε** can be calculated using the numbers of Trp (N_{Trp}), Tyr (N_{Tyr}) and disulfide bonds ($N_{S\text{-}S}$) [2]:

$$\varepsilon_{280} = 5540N_{Trp} + 1480N_{Tyr} + 134N_{S\text{-}S}$$

As well as absorption in the UV region, many metalloproteins show *d-d* transitions from the metal centre and charge-transfer absorption in the visible region. Most of the charge-transfer transitions involve a metal ion which acts as an electron acceptor

and side chains from the protein which act as electron donors. This can be seen in Fe_2-transferrin which shows a ligand-to-metal-charge-transfer (LCMT) band at *ca.* 465 nm. This is from the charge transfer from Tyr to Fe(III) [3]. LMCT bands of transferrin vary depending on the metal bound hence, this provides a convenient and effective way for determining metal binding and release from the protein.

UV-Vis spectra were recorded on a Shimadzu UV-2501PC UV/Vis spectrophotometer using 1 cm path length quartz cuvettes. The measurements were made at ambient temperature (unless described otherwise when the temperature was controlled using a Linkam Peltier stage controller PE60).

2.3 ICP-AES

Inductively coupled plasma atomic emission spectroscopy (ICP-AES) is a spectroscopic method used for quantitative and qualitative elemental analysis. A more detailed description of the theory of ICP-AES can be found in a number of textbooks [4-6].

ICP-AES was used for determination of metal concentration. A Thermal Jarrell Ash IRIS spectrometer equipped with a concentric Meinhard nebulizer and a CID camera detector was used. Aqueous samples were introduced into a cyclonic spray chamber by a peristaltic pump. The R.F. power was 1150 watts, the nebulizer flow was 30 psi, the pump rate was 100 rpm and the purge time was 90 s. Iron, manganese, copper and zinc atomic absorption standard solutions (Aldrich and BDH Laboratories) at *ca.*1000 ppm were diluted and used to calibrate the ICP-AES spectrophotometer. All samples were diluted with ultrapure water and metal content measured without further digestion. All data were interpreted using thermospec/CID

IRIS software.

2.3.1 Emission Properties

The elements studied in this thesis and their emission properties are given in Table 2.2. The emission intensity at a characteristic wavelength of an element is proportional to the concentration of the element in the sample.

Table 2.2 Emission properties of metals used

Element	Sensitivity (ppb)	Emission Wavelength/λ (nm)	Relative Intensity
Manganese	0.4	257.610	100
		257.610*	101
		260.569	101
		293.306	89
Iron	1	238.204	109
		239.562	108
		259.940*	100
		271.441	95
		271.441	96
Copper	0.9	224.700	115
		324.754*	80
		327.396	79
Zinc	1	202.548	128
		206.200	126
		213.856*	121
		213.856	122
		334.502	77
		334.502	78
		481.053	54

* Emission wavelengths used

2.4 Gel Electrophoresis

Polyacrylamide-gel electrophoresis was carried out in 6 M urea, as described by Makey and Seal [7].

Gels were either purchased or prepared from reagents obtained from Bio-rad (Bio-

Rad, Hemel Hempstead UK) and run using a Bio-rad Mini Protean II system with a Bio-rad Powerpac 200 according to the manufacturer's instructions. Where cast by hand, 6 M urea polyacrylamide gels were prepared using clean glass plates and 10-well tooth combs. No stacking gel was used. Samples were diluted with ultrapure water and loaded into the gel either with Laemmeli sample buffer (Sigma) to aid visualisation of progression down the gel or with glycerol to help the sample sink to the bottom of the well of the gel.

Electrophoresis was carried out at 100 V for 5-7 hours and run in 1x Tris-Borate EDTA (TBE) buffer (Bio-rad) (pH 8.4). The electrophoresis apparatus was disassembled and the plates separated. The gel was removed from the glass plates and a corner of the gel marked uniquely for future orientation. The protein in the gel was stained for 5 min in 1% amido black 10B in a solvent of methanol/water/acetic acid (4:4:1) followed by de-staining in the same solvent with glycerol added to the final de-stain in order to help maintain gel integrity.

2.5 Nuclear Magnetic Resonance Spectroscopy

Nuclear magnetic resonance (NMR) spectroscopy is a very powerful tool that can be used to study the structure and dynamics of a molecule. The physical basis of NMR spectroscopy is nuclear magnetisation. A number of textbooks have been published describing the theory and applications of NMR spectroscopy [8-10]. NMR signals can be detected with relative ease for many magnetic nuclei and most elements have at least one naturally occurring magnetic isotope. The magnetic properties of the nuclei used in this thesis are given in Table 2.3.

Table 2.3 Selected NMR properties of nuclei used in this study

Nucleus	Nuclear Spin	Natural Abundance (%)	Frequency (MHz) at 11.74 T	Relative Sensitivity‡
^{1}H	½	99.985	500.0	1.000
^{13}C	½	1.108	125.7	0.016

‡ versus ^{1}H at constant field

NMR spectra for biomolecules are normally recorded in aqueous media such as 100% D_2O or H_2O/D_2O (90%/10% v/v) and referenced to a known standard. The large H_2O signal often has to be suppressed for the NMR spectrum to be interpreted. NMR data interpretation was by multipulse sequences such as Shaka [11] or presaturation.

2.5.1 Two-Dimensional NMR (2D NMR)

2D NMR can often provide much more information about a sample compared with 1D NMR. By use of a suitable pulse sequence and processing a 2D plot can be obtained. This is seen as a contour map with two axes, one of which is the conventional 1D axis. Shift-correlated 2D spectra allow the establishment of which nuclei are coupled, either through bonds, through space or even by chemical exchange processes. The coupling can be either homonuclear or heteronuclear. Heteronuclear single quantum correlation (HSQC) is a useful technique used to study proteins labelled with ^{13}C or ^{15}N. It is possible to run samples at very low concentrations.

NMR data were acquired on a Bruker DMX500 spectrometer using 5 mm tubes operating at 500.13 MHz for ^{1}H and 125.66 MHz for ^{13}C. Standard Bruker pulse

sequences were used for 1D ^{1}H and ^{13}C and 2D [^{1}H, ^{13}C] HSQC experiments. Typically data were recorded using 10 or 20 mM solutions for 1D ^{1}H NMR and 100 mM solutions for 1D ^{13}C at 298 K and *ca.* 0.3 mM solutions at 310 K for 2D NMR. All solutions used for NMR were made up in 100% D_2O (actual 99.9 atom % D, herein referred to as 100%). The ^{1}H and ^{13}C chemical shifts for 1D spectra were internally referenced to sodium 3-trimethylsilylpropionic acid (TSP, 0 ppm). For 2D spectra ^{1}H and ^{13}C chemical shifts were referenced to TSP (external). The water signal was suppressed using excitation sculpting [11]. Data were converted to XWinNMR (Version 2.0, Bruker U.K., Ltd.) prior to Fourier transform.

2.6 Electron Paramagnetic Resonance

Electron paramagnetic resonance (EPR) spectroscopy, also known as electron spin resonance, can be used to investigate paramagnetic molecules.

An X-band (ca. 9.25 GHz) Bruker ER200D-SRC electron spin resonance spectrometer was used with flat cells made of high purity fused quartz to minimise the absorption of microwave radiation by aqueous solutions.

Mn(II) commonly has a high-spin d^5 electron configuration with five unpaired electrons giving rise to a S = 5/2 ground state. This often produces a well resolved 6-line EPR spectra at ambient temperature due to a hyperfine interaction with ^{55}Mn (I = 5/2).

Mn(III) commonly has a high-spin d^4 electron configuration with four unpaired electrons resulting in a spin ground state of S=2. Mn(III) complexes often display large zero-field splitting due to the low symmetry as a result of Jahn-Teller distortions of octahedral geometry. This, plus unfavourable (fast) spin relaxation

effects, makes the observation of EPR spectra at conventional microwave frequencies (X-band: ~9 GHz; Q band: ~35 GHz) of S = 2 systems relatively rare.

2.7 pH Measurements

All pH measurements were made using either a Corning 240 pH meter or a Corning 145 pH meter, equipped with an Aldrich glass/calomel combination pH electrode and calibrated with reference standard pH buffer solutions of 4.00, 7.00 and 10.00, purchased from either Sigma Chemical Company or Aldrich Chemical Company. Adjustments of pH were made using HCl or NaOH.

The pH-meter readings for D_2O solutions are recorded as pH^* values, *i.e.* uncorrected for the effects of deuterium on the glass electrodes. Adjustments of pH for samples in D_2O were made with DCl or NaOD.

2.8 Ultrafiltration

All protein samples were ultrafiltered using Amicon Centricon® centrifugal filter tubes (Millipore) that have a regenerated cellulose membrane with a 30 kDa molecular weight cut off. These were then centrifuged using a Beckman GS-15R centrifuge with temperature control. All tubes were thoroughly washed by centrifugation of ultrapure water prior to their use to remove any trace impurities from the membrane. The hydrophilic membranes allow low molecular weight solutes and solvents to pass through while retaining the high molecular weight protein above the membrane. The centricon tubes can then be inverted to collect the sample for further use.

2.9 Crystallisation of Transferrin

The most successful method to induce protein crystal formation is to force the protein out of a supersaturated solution. The rate with which the protein precipitates out of solution determines whether suitable crystals will form. The hanging drop vapour diffusion method was used to crystallise apo-hTf, Fe-hTf and Mn-hTf (more detail is given in Chapter 4). Purified, concentrated protein samples (*ca.* 1 mM, 5 μl) and precipitant well solution (5 μl) (20-26% PEG 400, 100 mM Na cacodylate buffer, pH 5.4 – 5.6) were placed on a siliconised cover-slip (Molecular Dimensions Ltd.) which was then placed upside down over a vacuum grease coated well lip (24 flat bottomed multiwell plates, ICN Biomedicals) in a dropwise fashion. The droplets were incubated against 995 μl of the precipitant solution in the well at 277 K.

2.9.1 Screening Technique

By carrying out the crystallisation in 24 well plates, the screening technique could be utilised to establish specific growth conditions which may give rise to optimum crystal growth. Each well solution can be made up of differing ingredients and the plate left and observations taken of crystal growth or other activity, such as precipitation or aggregation. This can then help in future crystallisation and is also a useful tool for crystallising novel compounds. More details of the screening technique and conditions used can be found in Chapter 4.

2.9.2 Seeding Technique

If crystals do appear as a result of one of the above techniques but are not of the highest quality further steps can be taken on these pre-formed crystals in order to achieve better resolution. This involves seeding from a previously grown crystal (more detail is given in Chapter 4). Briefly, plates are set up using the same conditions in the well solution as found in the well of the sample which produced crystals. However, differing protein concentrations may be used in the drop. The crystals of low quality are then stroked with a cat's whisker and the new drop is streaked with the whisker.

2.10 Cell Culture

2.10.1 Standard Culture Conditions

WRL-68 cells were cultured in DMEM (Dulbecco's modified eagles medium) supplemented with 10% NCS (newborn calf serum), Penicillin and streptomycin and x 1 concentrate NEAA (Non-essential amino acids). Cells were grown in 20 cm^2, 80 cm^2 or 175 cm^2 tissue culture grade flasks, 24 or 96 well tissue culture plates or 4 well chamber slides at 37°C, in 5% CO_2 in an incubator. Cells were supplemented with fresh medium every 2-3 days or as required by monitoring the colour indicator (phenol red) in the medium, with a yellow colour indicating supplementation was necessary. Once the cells grown in flasks became confluent they were harvested using trypsin/EDTA and PBS. The cell suspension was centrifuged at 1000 rpm for 10 minutes in a MSE Mistral 1000 centrifuge until a pellet was formed. The supernatant was removed and the pellet of cells resuspended in medium and used as

required.

2.10.2 Cell Viability Counts: Trypan Blue Exclusion

Trypan blue is used to estimate the proportion of viable cells in a population. The reactivity of the stain is based on the fact that the chromophore is negatively charged and does not react with the cell unless the membrane is damaged [12]. Live (viable) cells do not take up the dye and only dead (non-viable) cells do.

To estimate the concentration of viable cells or total cell numbers in cultures, 200 µl of a well-mixed sample of cultured cells, 300 µl PBS and 500 µl of 0.4% trypan blue (Sigma) solution were mixed and left at room temperature for a 2-3 minutes. The cell suspension was transferred to a haemocytometer, viewed using an Olympus inverted phase-contrast light microscope and the number of dead (blue) and live (colourless) cells were counted within the 4 x 4 square grid. Counting was made using 10 square grids in total. These cell counts were used to estimate the concentration of cells to be used further or number of live cells (viability) according to the following equations:

cells/ml = average cell count x 5 (dilution factor) x $1x10^4$ (haemocytometer chamber factor)

cell viability (%) = (total viable/total viable and nonviable) x 100

2.10.3 MTT Assay

MTT (3-(4,5-dimethylthiazol-2-yl)-2,5-diphenyl tetrazolium bromide) is a water-

soluble tetrazolium salt that gives a yellow solution when prepared in phenol red free media or salt solutions. The MTT assay depends upon the reduction of the exogenous yellow MTT tetrazolium salt (Sigma) to a purple formazan by mitochondrial succinate dehydrogenase in living cells [13, 14]. This water-insoluble formazan can then be solubilised using organic solvents such as DMSO. The resulting purple solution is measured spectrophotometrically to give absorbance as a function of concentration of converted dye.

Cells used for the MTT assay were cultured on 24- or 96- well plates and incubated with MTT made up in PBS at a final concentration of 1 mg/ml in the medium at 310 K for 3 hours. Cells were then washed twice with PBS after removal of medium/MTT and left to dry completely. DMSO was added to dissolve the formazen dye and the absorbance was read at 490 nm by a MR 5000 Dynatech plate reader. Where cells were grown on 24-well plates, DMSO was added and 100 μl was transferred to a 96-well plate and the absorbance was read.

2.10.4 Evaluation of Apoptosis and Mitosis

Apoptosis and mitosis were assessed morphologically by Feulgan staining of DNA. Cells used were cultured on 96-well plates and 4-well chamber slides. After removal of culture medium, plates and slides were fixed and stored in Bouin's fixative (85% methanol, 4% formaldehyde, 5% glacial acetic acid) at 277 K. When required, plates and slides were allowed to thaw and were denatured in 5 M HCl for 45 minutes at room temperature. Slides were then stained in Schiff's reagent (Sigma, see Appendix B, diluted in water) for 1 hour at room temperature. Schiff's reagent was removed by washing three times in water and then held under running tap water for 5

minutes until a pink colour developed. The cell cytoplasm was then counterstained with 1% Light Green stain. Slides were cover-slipped using mowiol as a mountant (see Appendix C). Mowiol 4-88 is a high quality mounting medium with good anti-fade characteristics. It hardens to match the refraction index of immersion oil and so is particularly suitable when using high magnification. Additional anti-fade (DABCO) is added to reduce photo-bleaching further. Apoptotic cells are recognisable by their distinct morphology, including condensed and fragmented DNA which is stained pink by the Schiff's reagent. Mitotic cells can easily be seen by their stained chromatin and alignment prior to cell division. Cells were then counted and percentage of apoptotic and mitotic cells determined.

2.10.5 Induced Mitochondrial Depolarisation

To induce mitochondrial depolarisation, cells were seeded at *ca.* 4 x 10^4 cells/ml onto 4-well chamber slides and left overnight in medium. Mesoxalonitrile 3-chlorophenylhydrazone (mClCCP) was then added to the medium at a concentration of 30, 40 and 50 mM simultaneously with chloromethyl-X-Rosamine (CMX Ros, Molecular Probes) to give a concentration of 100 nM (see below, 2.10.6) and incubated in the dark at 310 K for 45 minutes. From this stage onwards cells were protected from light. The medium was then aspirated and the cells washed twice with PBS. Slides were then fixed in 4% paraformaldehyde for 10 minutes and washed again in PBS and allowed to dry before being cover-slipped using mowiol as a mountant. Cells were then assessed morphologically – see below (section 2.10.6).

2.10.6 Assessment of Mitochondrial Depolarisation

Cells to be assessed for mitochondrial depolarisation were cultured on 4-well chamber slides. Where possible the procedure was carried out in minimum light to prevent fading of the dye. CMX was added to the medium to give a concentration of 100 nM and slides were incubated in the dark at 310 K for 45 minutes. From this stage onwards cells were protected from light. Following incubation the medium and CMX was aspirated off and cells were washed with PBS. Cells were then fixed for 10 minutes in 4% paraformaldehyde which was then removed and the slides were allowed to dry before cover-slipping using mowiol. Slides were then viewed using a Leica upright TCS-NT confocal microscope with the kind help of Linda Wilson (Pathology Department, University of Edinburgh). CMX Ros dye is a mitochondria-selective dye that is sequestered by intact mitochondria but not a de-energised organelle [15]. The dye remains in the organelle following fixing and has been used to study mitochondrial membrane permeability transitions in rodent hepatocytes [16]. CMX is linked with a rhodamine fluorescent dye which appears as a red stain under green light. It is a charge-sensitive fluorochrome that binds to the inner mitochondrial membrane. The fluorescence decreases due to apoptotic-mediated loss of mitochondrial transmembrane potential. Cells can then be assessed morphologically for mitochondrial depolarisation.

2.10.7 Analysis of Cellular Metal Content

Using ICP-AES, Mn can be detected at levels as low as 0.01 ppm. For analysis 5 ml of sample was required. Preliminary studies were carried out on untreated cells in order to determine the number of cells required to give an accurate reading of metal

content using ICP-AES.

Cells were typically cultured at an initial concentration of *ca.* 10^6 cells/ml in large flasks until confluent. Medium that had been removed during cell growth was retained for metal analysis. All cells analysed in parallel were cultured in the same batch of supplemented DMEM medium. When the cultures were set up, samples of the medium used to culture the cells were taken for analysis to ensure that the media had uniform concentrations of the metals analysed. Samples of trypsin-EDTA were also analysed for metal content.

Cells to be analysed were removed from the flasks using trypsin-EDTA and PBS. The cell suspension was transferred to sterile universal tubes (Rosslabs, Cheshire UK) and pelleted at 1000 rpm for 10 minutes. The supernatant was removed and the pellet was resuspended and counted for viability and total cell number as previously described in section 2.10.2. The cell suspension was then centrifuged again. The remaining pellet was then frozen and kept at 253 K until needed. The pellet was removed from the freezer and a known volume of ultrapure water added to ensure rupture of the cells. The cells and medium were then analysed for metal content using ICP-AES (section 2.3).

2.11 References

1. G.D. Fasman, *Practical Handbook of Biochemistry and Molecular Biology*. CRC Press, Boca Raton, Fla.. **1989**.

2. H. Mach, C.R. Middlaugh, and R.V. Lewis, *Anal. Biochem.*, **1992**, 200: 74-80.

3. E.N. Baker, *Adv. Inorg. Chem.*, **1994**, 41: 389-463, and references therein.

4. C. Vandecasteele and C.B. Block, *Modern Methods for Trace Element Determination*. John Wiley and Sons Ltd., Chichester, **1993**.

5. L. Ebdon, E.H. Evans, A.S. Fisher, and S.J. Hill, *An Introduction to Analytical Atomic Spectrometry*, ed, E.H. Evans. John Wiley and Sons, Chichester, **1998**.

6. L.H.J. Lajunen, *Spectrochemical Analysis by Atomic Absorption and Emission*. The Royal Society of Chemistry, Cambridge, **1992**.

7. D.G. Makey and U.S. Seal, *Biochim. Biophys. Acta,* **1976**, 453: 250-256.

8. W. Kemp, *NMR in Chemistry: A Multinuclear Introduction*. MacMillan Press Ltd., London, **1986**.

9. P.J. Hore, *Nuclear Magnetic Resonance*. Oxford University Press Inc., New York, **1995**.

10. H. Friebolin, *Basic One- and Two-Dimensional NMR Spectroscopy*. VCH Publishers, Cambridge, **1991**.

11. T.-L. Hwang and A.J. Shaka, *J. Mag. Res. Ser. A,* **1995**, 112: 275-279.

12. H.J. Phillips and J.E. Terryberry, *Exp. Cell. Res.*, **1957**, 13: 341-347.

13. T. Mossman, *J. Immunol. Met.*, **1983**, 65: 55-63.

14. J. Carmichael, W.G. DeGraff, A.F. Gazdar, J.D. Minna, and J.B. Mitchell, *Cancer Res.*, **1987**, 47: 936-942.

15. R.C. Scadutao and L.W. Grotyohann, *Biophys. J.*, **1999**, 76: 469-477.

16. J.S. Isenberg and J.E. Klaunig, *Toxicol. Sci.*, **2000**, 53: 340-351.

Chapter 3 Manganese Binding by Transferrin and Its Characterisation

3.1 Introduction

Manganese is an essential trace element however, the mechanisms involved in manganese transport are poorly understood [1].

As described in Section 1.3.2, transferrin is an 80 kDa protein found in blood serum at concentrations of *ca.* 35 μM and transports iron [2]. It has two Fe(III) binding sites, one in the C-lobe and one in the N-lobe, each providing an approximately octahedral co-ordination from His, Asp, two Tyr and a bidentate carbonate anion as ligands. The major receptor recognition sites of transferrin are on the C-lobe, supported by the recent X-ray crystal structure of the human transferrin receptor [3-7]. Initially, Fe(III) binds to apo-transferrin and induces a major conformational change of the protein from a lobe-opened to lobe-closed form [8-10]. Then the iron-saturated holo-transferrin binds to the specific transferrin receptors on the cell surface and is internalised by clathrin-coated vesicles into endosomes where the acidic pH (pH *ca* 5.0-5.5) leads to the release of Fe(III) from transferrin [11, 12].

Serum transferrin is only 30% saturated with iron in blood. Previous work in this laboratory has shown that metals other than iron such as Bi^{3+}, Cu^{2+} and Gd^{3+} can bind strongly to transferrin [13-16]. Therefore, if other metals are able to bind to transferrin, could manganese be loaded onto the protein and be transported to sites where it may be useful against oxidative stress in the form of MnSOD and so act as a carrier mechanism for manganese?

Electronic absorption spectroscopy is often used to study metal binding to the specific iron sites of transferrins. The apo form of the protein is colourless with an intense ultraviolet absorption near 280 nm which is used to determine the concentration of the protein. When metals are bound to transferrin the resulting complexes often have colour, for example when Fe^{3+} is bound to the protein a characteristic red/orange colour develops. The complexation of metal ions to the phenolic groups of two tyrosine residues at each of the two transferrin specific metal-binding sites perturbs the electronic transitions in the phenolic ring system, causing small shifts in the ultraviolet spectrum of the protein [17]. This allows the uptake of metals to be followed by UV/Vis spectroscopy. For some metal ions intense tyrosine-to-metal charge-transfer bands can be seen in the visible region of the spectrum (400 nm to 500 nm). The Mn(III)-HCO_3-Tf complex has been reasonably well characterised by UV-Vis spectroscopy [18, 19].

When complexed with transferrin, Mn is expected to be present in the +3 oxidation state, with two metal ions tightly bound to each transferrin [19]. Since the characteristic deep brown colour of Mn(III)-Tf develops much slower under anaerobic conditions [19] this suggests that carbonate from the air is required for faster loading of Mn onto transferrin. Harris and Chen [20] have shown that air oxidation of Mn(II) in the presence of apo-hTf at pH 7.4 is a very slow process, however, oxidation of Mn(II) in serum is considerably faster [21-23]. Hence, the loading of Mn onto transferrin is most probably a redox process which is likely to involve participation from a serum oxidant to oxidise Mn(II) to Mn(III).

3.1.1 Caeruloplasmin

Caeruloplasmin is a plasma protein known for its oxidising activity. It is a multi-copper oxidase which contains most of the copper present in the plasma [24]. The precise physiological role of this enzyme is still as yet largely unknown but it is thought to have a multi-functional role including oxidising activity, and possibly as a pool for copper. It has been suggested that caeruloplasmin has a distinct active site for glutathione-linked peroxidase activity as well as the copper giving it its ferroxidase activity [25]. Anion binding studies have supported the theory of caeruloplasmin having multifunctional oxidase activity [26]. Caeruloplasmin may be the oxidising enzyme responsible for the loading of hTf with Mn(III) in serum. However, Critchfield and Keen [23] found that caeruloplasmin deficient plasma from rats that had been restricted with regard to dietary copper and exposed to a copper chelator showed no impairment of the kinetics of ^{54}Mn appearance in hTf suggesting that caeruloplasmin plays no role in the loading of Mn onto hTf.

An alternative route to using caeruloplasmin to oxidise Mn(II) to Mn(III) for binding to transferrin was employed in this study. This involved using potassium permanganate as a source of manganese and thus reducing Mn(VII) to Mn(III) for binding to transferrin.

3.1.2 Potassium Permanganate

The highest oxidation state of manganese corresponds to the total number of $3d$ and $4s$ electrons and occurs only in the oxo compounds MnO_4^-, Mn_2O_7 and MnO_3F. The best known Mn(VII) compounds are sodium and potassium permanganates which are made industrially on a large scale by electrolytic oxidation of basic solutions of

MnO_4^{2-}.

Potassium permanganate is known for its characteristic intense purple colour. This is a result of the absorption corresponding to the charge-transfer between O^{2-} and Mn(VII) in the visible region of the spectrum.

Potassium permanganate is used in the water industry primarily to control taste, odours and biological growth in treatment plants as an alternative to chlorine.

Manganese (VII) is a powerful oxidising agent which is often reduced in reactions to Mn(II). Mn(V) species are thought to be intermediates in the reduction of permanganates. For the purposes of this study it is hoped that the reduction of Mn(VII) will result in the production of Mn(III) that will then bind to transferrin. However, whilst Mn(VII) is being reduced some other species must be oxidised.

3.1.2.1 Oxidation of Amino Acids

Pandey *et al* [27] suggest that oxidation of some amino acids in acidic conditions by MnO_4^- proceeds with oxidative decarboxylation and deamination. They suggest that five molecules of substrate require two molecules of permanganate for complete oxidation of each of the amino acids. The overall reaction proposed for their experiments is shown in Equation 3.1.

$$5R.CH.NH_2.COOH + 2MnO_4^- + 6H^+ \rightarrow 5RCHO + 3H_2O + 2Mn^{2+} + 5CO_2 + 5NH_3$$

Equation 3.1 Oxidation of amino acids

Brillas *et al* [28] carried out kinetic studies using UV/Vis spectroscopy on the oxidation of L-leucine by permanganate in neutral solutions. At the end of each

experiment the solutions were transparent but yellow/brown in colour. The spectra suggested the presence of a soluble form of colloidal manganese dioxide which gradually precipitated out of solution as brown manganese dioxide.

Sahu *et al* [29] suggest that the addition of Mn(II) in a sulphuric acid medium to a reaction catalyses oxidation of L-amino acids by permanganate and does so by two possible mechanisms: either Mn(II) forms a complex with amino acids which may then be oxidised by permanganate or initially Mn(II) may react with Mn(VII) to give Mn(III) which may accelerate the rate of the reaction. Under similar conditions, however, Mn(III) does not oxidise the amino acids directly hence the catalytic effect of Mn(II) may be due to complex formation between Mn(II) and substrate.

Although Mn(III) has been reported to bind to transferrin [19], there has been little direct structural characterisation of the bound Mn ion. Since aquated Mn(III) ions are unstable in aqueous solution Mn(III) transferrins are difficult to prepare by methods usually available for other metal ions.

In this chapter, routes for introduction of Mn(III) via oxidation of weakly bound Mn(II) were employed with the addition of a serum oxidant. As an alternative the strong oxidant potassium permanganate was also used to load transferrin by reducing Mn(VII) to Mn(III). UV/Vis spectroscopy was used to follow reactions between transferrins and metals. The effects of the use of $KMnO_4$ were also investigated by use of NMR techniques. In order to assess whether Mn(III) could dissociate from transferrin in a manner similar to that seen with iron in the endosomes, pH studies were conducted. Attempts were also made into investigating the order of lobe loading of metals onto transferrin.

3.2 Materials and Methods

3.2.1 Purification and Characterisation of Apo-hTf

Iron-free human apo-hTf was purchased from Sigma and weighed into a sample vial. It was then fully dissolved in 0.1 M KCl and transferred to a 'Centricon 30' ultrafilter and washed three times using 0.1 M KCl to remove low molecular weight impurities. The centricon tube was then inverted and the purified apo-hTf collected for further use. Concentrations of apo-hTf and other hTfs were determined by UV/Vis spectroscopy using ε_{280} 93, 000 $M^{-1}cm^{-1}$ [30].

Iron was removed from recombinant (non-glycosylated) ε-[^{13}C]Met-hTf (kindly supplied by Professor R. C. Woodworth and Dr. A. B. Mason, University of Vermont) [31] by treatment with NTA and EDTA (both 1 mM) in 0.5 M sodium acetate at pH 4.9 as previously described [32, 33] and centrifuged in 'Centricon 30' tubes until a colourless solution was obtained and the resulting solution was then concentrated down in the 'Centricon' tubes. The concentration of the apo-protein was then determined using UV/Vis spectroscopy as mentioned above.

3.2.2 Preparation of Mn-hTf

Mn-hTf was prepared by the addition of one or two molar equivalents of Mn to apo-hTf. Initially this was done by addition of 100 mM Mn(II) chloride solution to a solution of purified apo-hTf in 20 mM Hepes buffer, pH 7.4 with the addition of 10 mM bicarbonate. Preliminary studies involved daily oxidation of the solution using O_2(g) from a standard cylinder: oxygen was allowed to blow over the surface of the solution (direct bubbling would result in the solution foaming) for approximately 10

minutes daily for up to two weeks. The solution was kept at 310 K until the solution was brown in colour. Mn-hTf was washed using centricon tubes with 0.1 M KCl and concentrated down and then collected as described previously for purification of apo-hTf in section 3.2.1. Once Mn-hTf had been prepared its concentration was determined by UV/Vis and ICP-AES.

3.2.2.1 Addition of an Oxidant

Human caeruloplasmin was added to the reaction of apo-hTf, bicarbonate and $MnCl_2$ to act as an oxidant. The caeruloplasmin was made up into buffer at 1 mg/ml (Appendix A) and frozen in aliquots, each of known oxidant activity, and defrosted as required. Units of activity of caeruloplasmin are determined by the oxidation of *p*-phenylenediamine [34] and were given with receipt of the protein from the supplier. The solution of Hepes buffer containing apo-hTf, bicarbonate, $MnCl_2$ and caeruloplasmin was kept at 310 K until it was brown in colour.

Potassium permanganate, a well known oxidant, was used as a source of Mn. Molar equivalents were added to a solution Hepes buffer containing apo-hTf and bicarbonate and the solution was kept at 310 K until brown in colour.

3.2.3 Preparation of Fe-hTf

Fe_2-hTf was prepared by the addition of $Fe(NTA)_2$ to holo-transferrin that had been purchased from Sigma, to ensure full saturation with Fe(III). A solution of $[Fe(NTA)_2]^{3-}$ was prepared from the iron atomic absorption standard solution and 2 mol euiv of H_3NTA. The pH was slowly raised to 5.5 with microlitre amounts of NaOH (1 M). This solution was then diluted to 4 mM. Holo-transferrin was

weighed and transferred to a 'Centricon' tube and washed using 0.1 M KCl as described earlier for apo-transferrin in Section 3.2.1. Two molar equivalents $Fe(NTA)_2$ were then reacted with holo-hTf in Hepes buffer, pH 7.4 with the addition of 10 mM bicarbonate. The solution was kept at 310 K for *ca.* 1 hour. Fe_1-hTf was prepared by the addition of one mol equivalent $Fe(NTA)_2$ to a solution of apo-hTf in Hepes buffer, pH 7.4 with 10 mM bicarbonate at 310 K.

The reaction of apo-hTf with $Fe(NTA)_2$ over a range of pH 6 – 8.5 results in the preferential binding of Fe(III) to the C-lobe of transferrin [2, 35]. Fe_C-hTf was prepared by reacting one mole equivalent $Fe(NTA)_2$ with apo-hTf that had been purified as described earlier in Section 3.2.1 in 20 mM Hepes buffer, pH 7.4 with 10 mM bicarbonate at 310 K.

The Fe-hTfs were washed using centricon tubes and 0.1 KCl as previously mentioned. UV/Vis spectroscopy and ICP-AES was then carried out to establish concentrations of protein and metals.

3.2.4 UV/Vis Spectroscopy

Solutions were prepared by dilution with 20 mM Hepes buffer (pH 7.4). UV difference spectra after addition of $MnCl_2$, $KMnO_4$ or $Fe(NTA)_2$ to apo-hTf, Mn-hTf or Fe-hTf were recorded immediately and at regular time intervals. For titration experiments aliquots of Mn were added and the solution was left to equilibrate at 310 K for 30 min.

For pH experiments, the pH of a solution containing Mn-hTf in 20 mM Hepes buffer was lowered using 1 M HCl. Readings of pH were taken immediately and following 30 min equilibrium time at 310 K when UV/Vis spectra were recorded.

The binding or release of Mn(III) was monitored by the increase or decrease in absorbance at 430 nm. The binding or release of Fe(III) was monitored by the increase or decrease in absorbance at 465 nm.

Solutions of *ca.* 20 mM Hepes buffer, TRIS buffer and phosphate buffer were each reacted with molar equivalents of $KMnO_4$ and the reactions followed spectrophotometrically.

All UV/Vis experiments were performed in 1 cm quartz cuvettes on a computer controlled Shimadzu UV-1000 spectrometer with temperature control at 310 K using a Linkam Peltier stage controller PE60 (except where stated otherwise).

3.2.5 Gel Electrophoresis

Gels were purchased or cast and run as described in Section 2.4. Protein in the form of apo-hTf, Fe-hTf and Mn-hTf was loaded at concentrations typically ranging from 1-100 μM. Electrophoresis was then carried out at 100 V for 5-7 hours in TBE tank buffer (ph 8.4) until the samples were nearing the bottom of the gel (this was observed by adding Laemelli sample buffer to one of the samples in an end well). Once gels had been stained with 1% amido black 10B and destained using methanol/water/acetic acid (4:4:1), images were taken by placing the gel on a flatbed scanner attached to a PC. Gels were then scanned and saved as picture files for future examination.

3.2.6 NMR Spectroscopy

All NMR experiments were carried out on a Bruker 500 MHz spectrometer using 5-mm tubes operating at 500.13 MHz for ^{1}H and 125.66 MHz for ^{13}C. Standard

Bruker pulse sequences were used for 1D [^{1}H] and [^{13}C] and 2D [^{1}H, ^{13}C] HSQC experiments as described in Section 2.5. Data were converted using XWinNMR (version 2.0, Bruker U.K. Ltd.) prior to Fourier transform. The pH-meter readings for D_2O solutions were recorded as pH* values, *i.e.* uncorrected for the effects of deuterium on the glass electrode. Adjustments of pH* for samples in D_2O were made with DCl or NaOD. All solutions used for NMR experiments were made up in 99.9% D_2O, herein referred to as 100% D_2O.

3.2.6.1 Hepes Buffer

^{1}H NMR spectra of *ca.* 20 mM Hepes buffer in D_2O were recorded and following the addition of 0.2 molar equivalents of 20 mM $KMnO_4$ in D_2O and referenced internally to TSP (0 ppm).

3.2.6.2 Amino Acids

^{1}H NMR spectra of amino acids N-acetyl L-methionine, L-histidine, L-tyrosine, L-tryptophan, L-methionine sulfone and L-methionine sulfoxide were carried out in D_2O at 298 K and referenced internally to TSP (0 ppm). Solutions were made up at *ca.* 10 mM in eppendorf tubes. One molar equivalent of $KMnO_4$ (using microlitre aliquots of a 99 mM stock solution of in D_2O) was added to amino acid solutions and spectra recorded at various time intervals. In some instances solutions were filtered using a syringe filter prior to spectral acquisition.

For ^{13}C NMR, spectra were collected for N-acetyl L-methionine, L-methionine sulfoxide and L-methionine sulfone at 298 K. Solutions were made up at *ca.* 100 mM in 100% D_2O and referenced internally to TSP (0 ppm). One molar equivalent

$KMnO_4$ (using microlitre aliquots of a 1.02 M stock solution of in D_2O) was added to a solution of 100 mM N-acetyl L-methionine and filtered prior to spectral acquisition. The spectrum was collected over night.

3.2.6.3 HSQC NMR

A NMR sample of ε-[^{13}C]Met-hTf (*ca.* 0.3 mM) was prepared in 0.1M KCl in D_2O, and pH* values were adjusted to 7.4 ± 0.1 using NaOD or DCl. Sodium bicarbonate in D_2O (0.25 M) was added to give a concentration of 10 mM. After addition of microlitre aliquots of $KMnO_4$ in D_2O (*ca.* 17 mM) to give molar equivalents, the pH* was readjusted using NaOD or DCl to pH 7.4 ± 0.1 if required and the samples were left at 310 K for 30 minutes for equilibration. 2D [^{1}H, ^{13}C] HSQC spectra were acquired at 310 K. ^{1}H and ^{13}C chemical shifts were referenced to TSP (external). The water signal was suppressed using excitation sculpting [36]. Spectra were collected with the kind help of Dr. H-S. Park.

3.2.7 EPR

EPR spectra were obtained for Hepes buffer (20 mM) at ambient temperature following addition of 1/30 molar equivalent $KMnO_4$ (using microlitre aliquots of a 40 mM stock solution). Spectra were acquired using flat cells in a Bruker ER200D-SRC X-band electron spin resonance spectrometer with the help of Dr. L. J. Yellowlees (University of Edinburgh). Reactions were followed at 298 K and spectra recorded at regular time intervals.

3.3 Results and Discussion

3.3.1 Uptake of Mn(III) by apo-hTf

Uptake of Mn(III) by apo-hTf from $MnCl_2$ in the presence of the serum oxidant caeruloplasmin and from $KMnO_4$ were studied by UV/Vis spectroscopy and ICP-AES. Apo-hTf gives a colourless solution with an absorbance band at 280 nm in UV/Vis spectra. Mn-hTf is brown in colour and shows two extra absorbance bands at 430 and 330 nm.

3.3.1.1 Uptake of Mn(III) by Apo-hTf in the Presence of Caeruloplasmin

The uptake of Mn(III) by apo-hTf was initially studied by reacting $MnCl_2$ in 20 mM Hepes buffer with 10 mM bicarbonate. Oxygen was added on a daily basis from a standard cylinder and the solution turned from colourless to yellow/brown suggesting Mn-hTf had been formed. However, the process was slow (typically about 2 weeks) and UV/Vis and ICP-AES showed that uptake of Mn(III) was incomplete. In an effort to speed up the process and improve lobe loading, the blood serum oxidant caeruloplasmin was introduced. Caeruloplasmin was added to the reaction to give 4 units of oxidase activity. When 1 mol equivalent of $MnCl_2$ was added to an aqueous solution of apo-hTf (7.6×10^{-5} M) at 310 K, two new bands emerged at 430 nm and 330 nm which increased in intensity over time as shown in Figure 3.1. The resulting protein was stable at 277 K for several months.

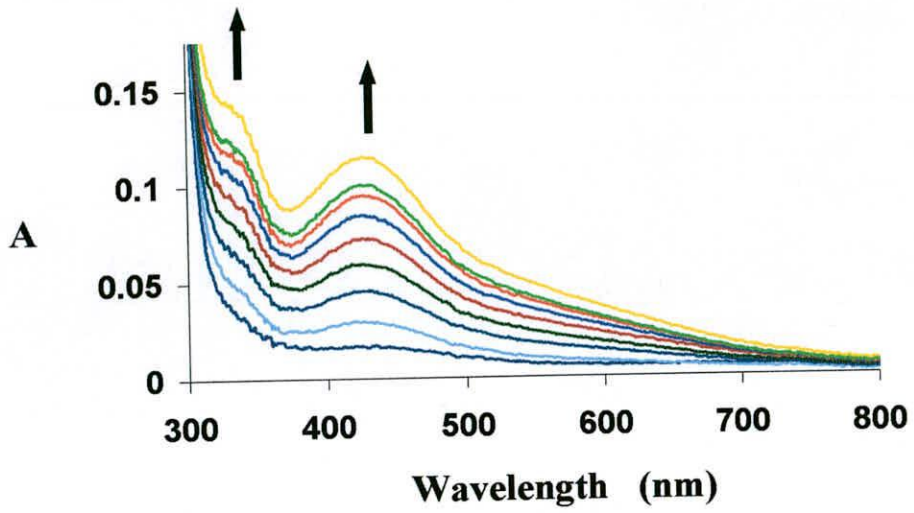

Figure 3.1 UV/Vis timecourse of reaction of apo-hTf with 1 mol equivalent $MnCl_2$ in the presence of caeruloplasmin (100 µl of 1 mg/ml, *ca.* 4 units of activity). Time intervals shown are every 12 hours. Final reading taken at 96 hours. Appearance of the LMCT bands at 430 and 330 nm confirms the formation of Mn-hTf and increases with time. Conditions: 20 mM Hepes buffer, pH 7.4, 10 mM $NaHCO_3$, 7.6×10^{-5} M apo-hTf, 310 K.

UV/Vis and ICP-AES confirmed that Mn had been loaded onto the protein however, the protein was only partially loaded with a ratio of only 0.55 Mn : 1 protein. Although the process was faster when compared with loading transferrin with manganese in the absence of caeruloplasmin, it is still quite slow. Something that must be considered when using this system is the loss of bicarbonate from the solution to air. This would result in the increase in pH of the solution, which may be beyond the buffering capacity of the buffer under these conditions. As Mn(III) favours more acidic conditions and more acidic metal ions are known to bind to transferrin [13, 14], it seems plausible that any increase in pH could result in

decreased binding of Mn to transferrin. Further, any increase in pH could also inhibit the oxidase activity of caeruloplasmin.

Due to these initial experiments giving slow and incomplete loading of manganese onto transferrin, an alternative method was investigated; rather than starting with Mn(II) and oxidising it to Mn(III) a higher oxidation state of Mn was used and reduced to Mn(III). For this reason $KMnO_4$ was introduced as a new source of manganese. Potassium permanganate is a well-known oxidising agent so this may also aid the loading of transferrin resulting in a faster reaction time.

3.3.1.2 Uptake of Mn(III) from $KMnO_4$ by Apo-hTf

$KMnO_4$ was used in future experiments as a source of loading apo-hTf with Mn(III). On addition of $KMnO_4$ to a solution of apo-hTf in Hepes buffer containing bicarbonate the solution turned immediately from colourless to yellow/brown, suggesting the formation of Mn-hTf. The process was much quicker compared with loading using $MnCl_2$ and caeruloplasmin as shown in Figure 3.2. The resulting protein was stable at 277 K for several months allowing further experiments to be carried out.

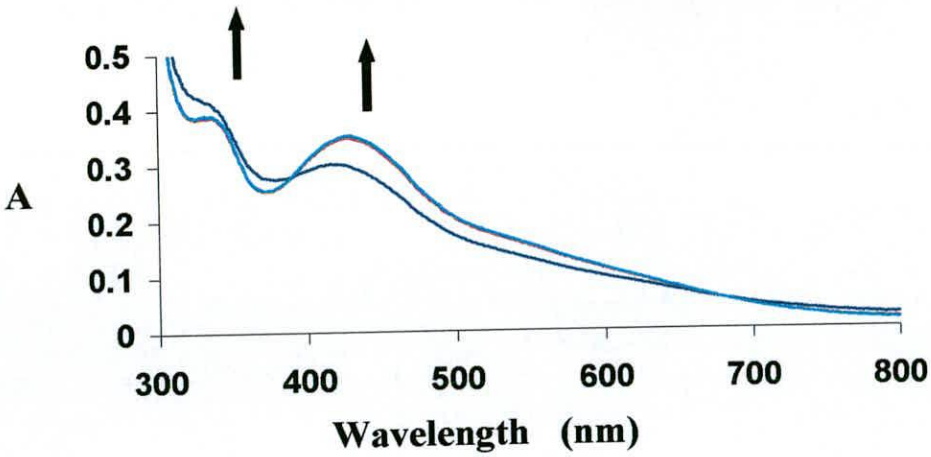

Figure 3.2 UV/Vis timecourse of apo-hTf and one mol equivalent $KMnO_4$. Time intervals are initial reading and then every 30 minutes, final reading after 120 minutes. Appearance of the LMCT bands at 430 and 330 nm confirms the formation of Mn-hTf. The reaction is complete after 60 min. Conditions: 20 mM Hepes buffer, pH 7.4, 10 mM $NaHCO_3$, 310 K, 7.5 x 10^{-5} M apo-hTf.

The spectrum clearly shows that the reaction is very rapid, being complete by 60 minutes. Traces taken after 60 minutes are overlapped with that taken at 60 minutes so are not visible. There was no further change in the spectrum over a period of 24 hours. As well as being a much quicker reaction, ICP-AES analysis of the protein formed confirmed improved loading with 0.77 Mn : 1 protein, suggesting that maybe both lobes are loaded when two or more molar equivalents of Mn are provided by this method. To study this, molar equivalents of $KMnO_4$ were added to apo-hTf and the reaction followed again by UV/Vis. A plot of ΔA_{430} against molar ratio (r) of $KMnO_4$ to apo-hTf is shown in Figure 3.3. It can be seen that with the increase of r, the band at 430 nm increases in intensity.

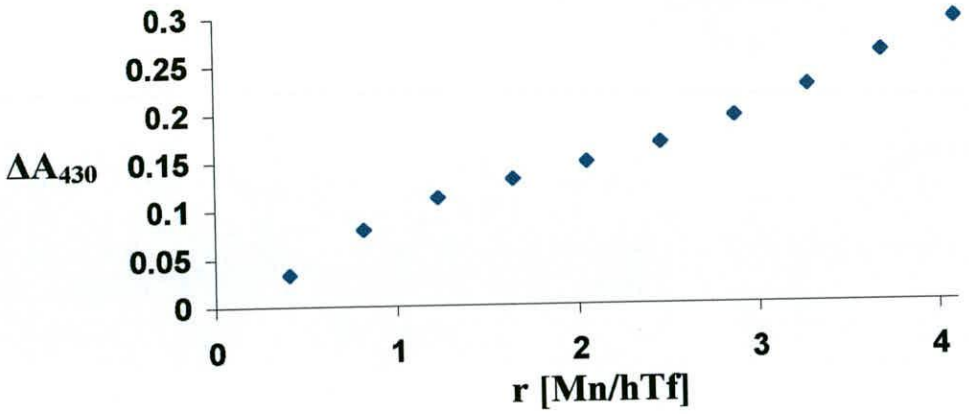

Figure 3.3 Variation in the absorbance at 430 nm (for Mn(III) transferrin) in addition of various molar equivalents of $KMnO_4$ to apo-hTf. There appears to be a biphasic response during the reaction. Conditions: 20 mM Hepes buffer, pH 7.4, 310 K, 10 mM $NaHCO_3$, 24.8 μM apo-hTf, $KMnO_4$ was added in 0.41 increments.

However, a plateau at r=2 is expected due to transferrin having two lobes available for metal binding but this is not seen. Rather, the intensity of the band at 430 nm continues to increase after addition of 0.41 - 4 molar equivalents MnO_4^- with evidence of a biphasic response occurring at two equivalents. This suggests that either more than two Mn(III) ions bind to transferrin or that a side reaction occurs so that not all of the Mn that is added to the reaction is taken up by the protein as Mn(III).

To investigate further the loading of Mn onto hTf, apo-hTf was reacted with 1, 2, 3 and 4 mol equivalents of $KMnO_4$ in 20 mM Hepes buffer with 10 mM bicarbonate present, pH 7.4. The reactions were left at 310 K and the ratio of metal-to-protein was determined using ICP-AES (Mn) and UV/Vis spectroscopy (protein). The molar extinction coefficient for the LMCT band at 430 nm was also calculated for each reaction. The results are shown in Table 3.1.

Table 3.1 Extent of loading hTf with Mn by reaction of apo-hTf with $KMnO_4$

No. of $KMnO_4$ equivalents added	Ratio (Mn : hTf) determined by ICP-AES and UV/Vis	% loaded of equivalents added	Molar extinction coefficient at 430 nm ($M^{-1}cm^{-1}$)
1	0.76 : 1	76	6228
2	1.17 : 1	59	8533
3	2.18 : 1	73	8651
4	2.8 : 1	70	10776

These results suggest that the expected stoichiometric loading of the protein with 2 mol equivalents of Mn using $KMnO_4$ is quite difficult to achieve, as when reacted at 1:1 ratio this is not achieved. Further when more than two molar equivalents of $KMnO_4$ are added to the protein, again only partial loading is achieved, usually in the region of 70% of the equivalents added. It seems interesting that when two equivalents $KMnO_4$ are added loading drops considerably to only 59% of the manganese added binding to transferrin. Further, the calculated molar extinction coefficient for the LMCT band at 430 nm increases with additions of $KMnO_4$ although there is only a slight increase following additions of two and three equivalents. This suggests that extra $KMnO_4$ is required to achieve full loading of transferrin and that more than two manganese ions can bind to transferrin. The observed molar extinction coefficient of Mn_2-hTf at 430 nm (*ca.* 8600 M^{-1} cm^{-1}) is somewhat higher than that found for Fe_2-hTf ($\Delta\varepsilon_{465}$ = 4950 M^{-1} cm^{-1}) [37] and Ti_2-hTf ($\Delta\varepsilon_{321}$ = 4830 M^{-1} cm^{-1} [38]. However a value of $\Delta\varepsilon_{429}$ = 8700 M^{-1} cm^{-1} has been cited previously in calculating Mn(III) binding to transferrin [39] supporting the values found here. These results support the possibility that more

than two Mn ions can bind to transferrin. Recent work on ferric binding protein (FBP), a bacterial protein similar to the two lobes of transferrin, has been shown to bind hafnium as a metal cluster whereby the protein remains in an open form. Human serum apo-transferrin was also treated with an excess of $[Hf(NTA)_2]^{2-}$ which was found to result in a metal-to-protein ratio of 3.5: 1 [40]. The N-lobe of apo-transferrin is thought to be wide open and capable of binding metal clusters whereas the C-lobe is not thought to be able to open wide enough for this. Open lobe transferrin conformations are known with a single Fe(III) ion bound [41-43]. Therefore, manganese may bind to transferrin as a cluster when added as the MnO_4^- ion.

If $KMnO_4$ is reacting so that Mn(VII) is being reduced to Mn(III) for loading onto the protein then something is being oxidised. Typically if Mn(VII) is reduced to Mn(II), then five electrons are gained. If we look at what compounds in the reaction are available, Hepes buffer might be a good candidate to act as a reductant. Possible reactions between Hepes buffer and $KMnO_4$ were therefore investigated.

3.3.2 Reaction Between Hepes Buffer and $KMnO_4$

To further investigate the course of the reactions between $KMnO_4$ and transferrin in Hepes buffer, reactions between Hepes and $KMnO_4$ were studied. When small amounts of $KMnO_4$ were added to Hepes e.g. to achieve a ratio of 220: 1 Hepes: $KMnO_4$ as used for the reactions involving transferrin (Hepes buffer 20 mM and $KMnO_4$ *ca.* 9×10^{-5} mM, at pH 7.4 and 310 K) the solution immediately turned yellow/brown and then became colourless with time. This suggests that Mn(VII) was being reduced to Mn(II) resulting in the colourless solution with intermediate

oxidation states of manganese appearing giving the yellow/brown colour. When high concentrations were used to give a 2:1 mol ratio of $KMnO_4$ (40 mM) to Hepes (20 mM), a brown precipitate developed which was filtered off and dried leaving a colourless clear solution. The brown precipitate was likely to be MnO_2. The higher concentration of permanganate to Hepes may have resulted in Mn(VII) being reduced only as far as Mn(IV) rather than completely to the colourless Mn(II) seen previously when small ratios of $KMnO_4$ were reacted with Hepes. The reaction of Hepes buffer and $KMnO_4$ was followed by UV/Vis spectroscopy. Similar conditions were used as for reactions of apo-hTf and $KMnO_4$ except that the protein was omitted. The results are shown in Figure 3.4.

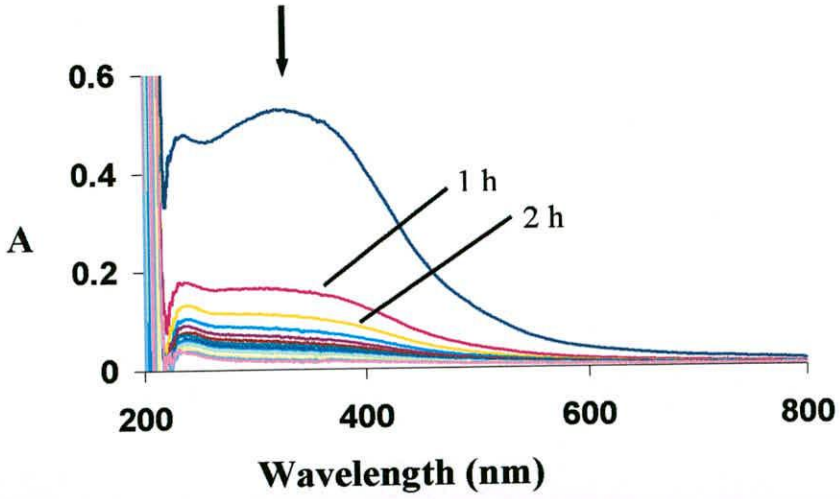

Figure 3.4 Reaction of Hepes buffer and $KMnO_4$ monitored by UV/Vis spectroscopy. The intense pink colour (indicated by arrow) of the permanganate disappears leaving a colourless solution. Conditions: 20 mM Hepes buffer, pH 7.4, 8.96×10^{-5} M $KMnO_4$, 310 K. Readings shown immediate (*ca.* 2 min mixing time) and every hour until 10 hours, then after 15, 20 and 30 hours.

The reaction between Hepes buffer and $KMnO_4$ may be a necessary part of the

reaction, allowing Hepes buffer to be oxidised while Mn(VII) is reduced to Mn(II) *via* Mn(III) which is taken up by transferrin. To investigate a possible role in the uptake of Mn(III) by transferrin, Hepes buffer and $KMnO_4$ were reacted prior to introduction of apo-hTf. If there was a necessary reaction between Hepes buffer and $KMnO_4$ that leads to the production of Mn(III) during reduction of Mn(VII) to Mn(II), then addition of the protein after this reaction finished should lead to little or no loading of Mn onto the protein. The uptake of Mn by apo-hTf following the reaction of Hepes and $KMnO_4$ was monitored by UV/Vis and is shown in Figure 3.5. Hepes buffer (20 mM) was reacted with $KMnO_4$ (7.9×10^{-5}) at pH 7.4, 310 K. After 8 hours bicarbonate (10 mM) and apo-hTf (7.9×10^{-5}) were added to the reaction.

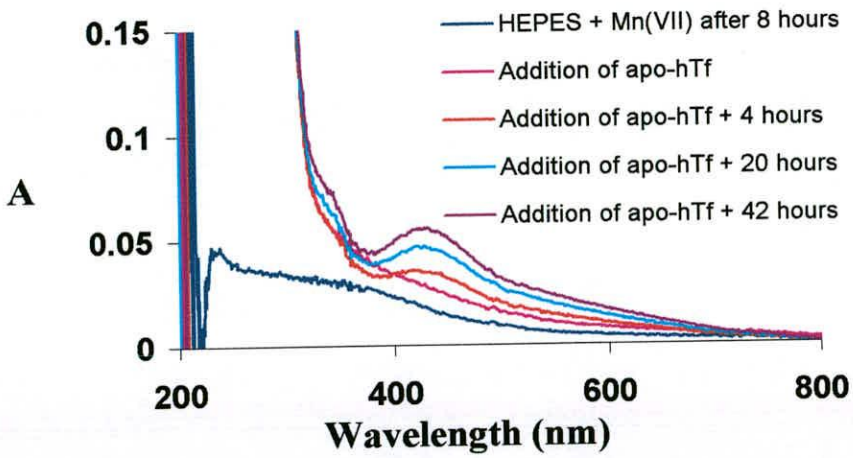

Figure 3.5 Reaction of Hepes buffer and $KMnO_4$ for 8 hours, followed by the addition of apo-hTf. Appearance of the LMCT band at 430 nm confirms the formation of Mn-hTf although the intensity is lower than that seen previously. Conditions: 20 mM Hepes buffer, pH 7.4, 7.9×10^{-5} M $KMnO_4$, 7.9×10^{-5} M apo-hTf, 10 mM $NaHCO_3$, 310 K.

As can be seen from Figure 3.5 by the appearance of the LMCT band at 430 nm some Mn-hTf is being formed. However, when compared with previous experiments in which similar concentrations have been used, the reaction is much slower and the absorbance band at 430 nm is of much lower intensity suggesting a lower concentration of Mn-hTf has been formed. UV/Vis and ICP-AES confirmed poor loading of the protein with a final ratio of 0.11 Mn : 1 protein. This further suggests an intermediate during the reaction is active in inserting Mn(III) into the protein, otherwise the reaction is completed when Mn(II) is formed which has been shown to be slow to insert. To investigate the possible reduction of Mn(VII) to a lower oxidation state of manganese with the involvement of Hepes buffer EPR experiments were carried out. Once again, small ratios of $KMnO_4$ to Hepes were used to replicate conditions used when loading transferrin. The resulting EPR spectrum is shown in Figure 3.6.

A g value of 2.01 with the hyperfine splitting into 6 lines typical of coupling to ^{55}Mn (I = 5/2) was determined which is indicative of the Mn(II) ion being present. The signal generated by EPR increases in amplitude with time. Presumably this strong signal must mean that most of the manganese ends up as the Mn(II) ion under these conditions. Due to the unusual relaxation properties of the paramagnetic Mn(III) ion it is difficult to detect it on the equipment used, therefore the production of Mn(III) during the reaction cannot be completely ruled out.

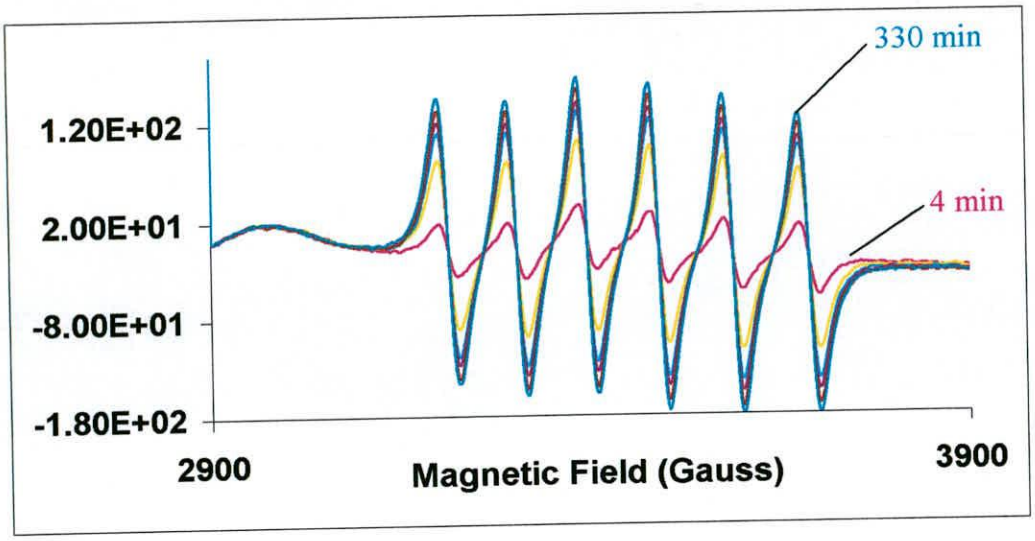

Figure 3.6 EPR Spectrum of Hepes buffer and $KMnO_4$. The trace is typical of that observed in the presence of Mn^{2+}. Conditions: 20 mM Hepes buffer, pH 7.4, 6.56 x 10^{-4} M $KMnO_4$, room temperature (*ca.* 298 K). Initial spectrum was recorded *ca.* 4 mins after mixing and further spectra after 10, 20 60, 150, 240 and 330 min. The signal increases with time.

The EPR spectrum shows the formation of Mn(II) therefore it is possible that Mn(III) is being formed during the reduction of Mn(VII) to Mn(II) and this is then being loaded onto transferrin. The reaction requires the oxidation of Hepes buffer (for structure of Hepes see Figure 3.7). In an attempt to determine which part of the Hepes molecule was being oxidised by $KMnO_4$, ^1H NMR was carried out on a solution of Hepes buffer and $KMnO_4$ to help to establish structural changes of Hepes which might be taking place due to oxidation.

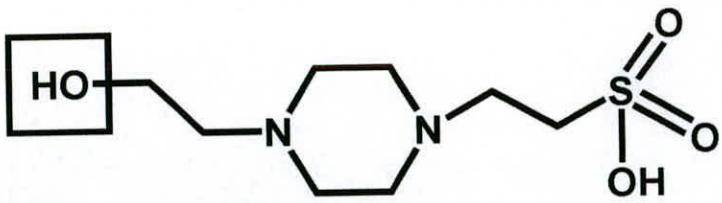

Figure 3.7 Structure of Hepes. The hydroxy terminus (boxed) is the likely target for oxidation by permanganate during the reaction.

Hepes buffer (20 mM) was reacted with 0.2 molar equivalents of $KMnO_4$ in D_2O and spectra were recorded. ^1H NMR spectra are sensitive to the presence of paramagnetic species such Mn(II), however some information can still be obtained from the spectra. ^1H NMR showed a broadening of the spectra when 0.2 molar equivalents of $KMnO_4$ were added to Hepes buffer, along with the production of a brown precipitate (for NMR spectra see Appendix D, Figure D.1). With time the brown precipitate settled on the bottom and a clear yellow solution remained which gave a NMR spectrum still showing some broadening. Unfortunately no new peaks were detected in the resulting spectrum only a broadening of the original peaks, but this result and the information gathered from the EPR spectra, suggest that Mn(VII) is reduced to Mn(II) in Hepes.

To further support the theory that Hepes is a necessary part of the reaction which leads to the loading of transferrin with Mn(III) from MnO_4^-, reactions of apo-hTf and $KMnO_4$ were carried out in other buffer types including Tris and phosphate buffer.

Once again the reactions were followed by UV/Vis spectroscopy and the results are shown in Figure 3.8. If Hepes was important to the reaction then there might be no formation of Mn-hTf in the other buffers. However, Mn-hTf was formed in both buffer types as indicated by the appearance of the LMCT band at 430 nm.

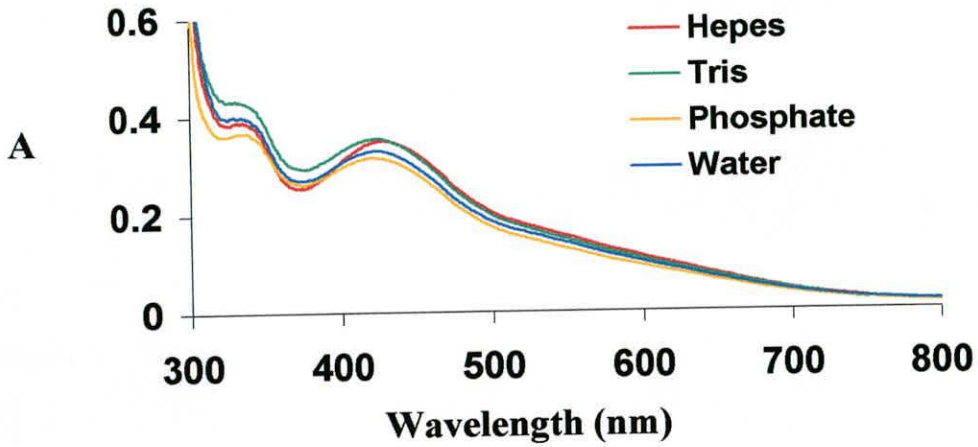

Figure 3.8 UV/Vis spectra 60 min after reaction between $KMnO_4$ and apo-hTf in Hepes buffer, Tris buffer, Phosphate buffer and water. Appearance of the LMCT bands at 430 and 330 nm confirms the formation of Mn-hTf. Conditions: All buffers at 20 mM, pH 7.4, 310 K, 7.5 x 10^{-5} M apo-hTf, 7.5 x 10^{-5} M $KMnO_4$, 10 mM $NaHCO_3$.

On examination of the structure of Tris (shown in Figure 3.9) it can be seen there are groups that could be oxidised by $KMnO_4$. However Mn-hTf was also found to be formed from MnO_4^- in phosphate buffer (see Figure 3.8), as shown by the appearance of the LMCT band at 430 nm. Phosphate buffer has no group which could be oxidised during the reaction, thus questioning the role of Hepes in the reaction. To explore this further, experiments between apo-hTf and $KMnO_4$ in water were set up.

Somewhat surprisingly, reacting apo-hTf with $KMnO_4$ in water also led to the formation of Mn-hTf (also shown on Figure 3.8) as shown by the characteristic peak at 430 nm.

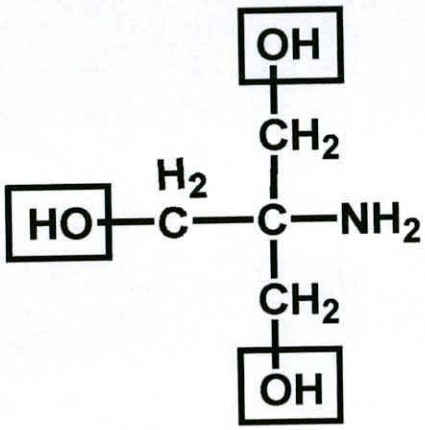

Figure 3.9 Structure of Tris Buffer. Groups which may be oxidised by permanganate are boxed.

This implies that some part of the transferrin molecule itself may be undergoing oxidation by the permanganate, possibly one or several amino acids of the transferrin molecule or even the glycan chains. However, all conditions were the same for these experiments but a slightly higher absorbance at 430 nm is reached when the reaction was carried out in Hepes and Tris buffers. It may be that Tris and Hepes both provide some form of protection against oxidation of the protein by permanganate by being oxidised themselves. To investigate this further, experiments were carried out on reactions of MnO_4^- with selected amino acids.

3.3.3 Oxidation of Amino Acids by Permanganate

The amino acids studied for possible oxidation by permanganate during loading of Mn(III) onto transferrin were tyrosine, tryptophan, histidine and methionine (see Figure 3.10 for their structures). Solutions of the amino acids were made up at *ca.* 10 mM in D_2O and reacted with one mol equivalent $KMnO_4$. Initial observations were made and ^1H NMR spectra were acquired. Where necessary, solutions were filtered using a syringe filter that had been washed through with D_2O. Solutions were left to react over time and again observations made and spectra run. In most of the spectra, peaks appeared that were attributable to acetic acid (CH_3 singlet at *ca.* 1.2 ppm), formic acid (*ca.* 8.22 ppm) and in some cases glycerol (*ca.* 3.5 ppm). The glycerol is thought to originate from the plastic Eppendorf tubes, syringes and filters. These were washed through before use with D_2O in order to try and keep this to a minimum.

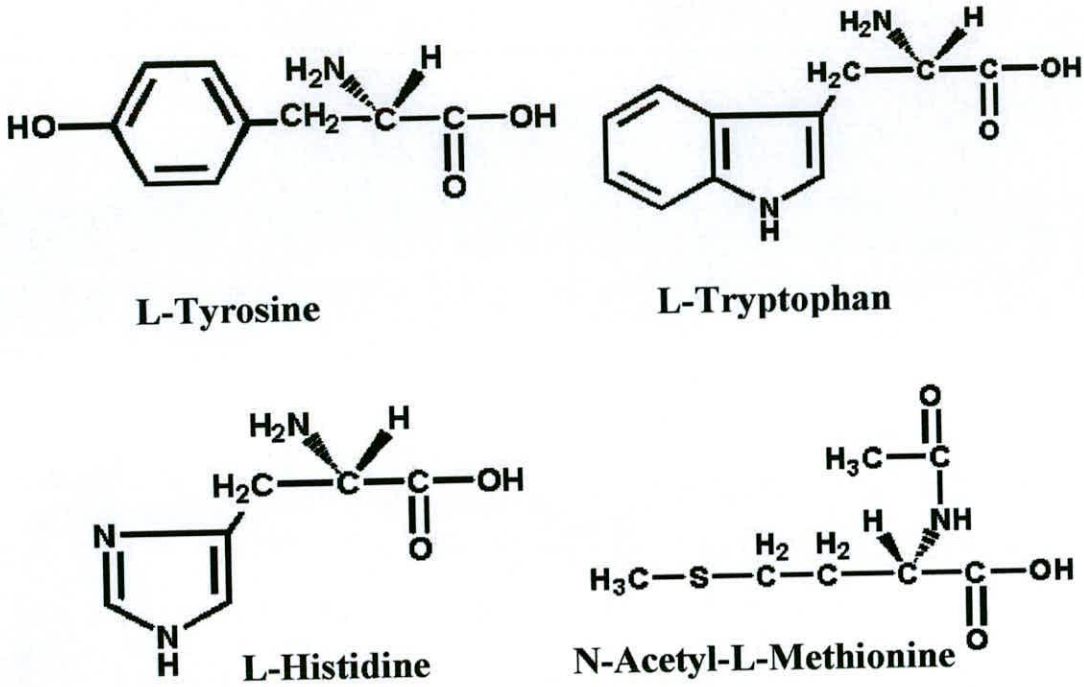

Figure 3.10 The amino acids used for NMR analysis: L-tyrosine, L-tryptophan, L-histidine and N-acetyl-L-methionine. Solutions of amino acids were made up at *ca.* 10 mM in D_2O. One mol equiv of 99 mM $KMnO_4$ (in D_2O) was added to the amino acids and ^1H NMR spectra run immediately and after several hours. Initial observations were made such as colour change of solutions and formation of any precipitate.

3.3.3.1 Tyrosine

Tyrosine was found to be only slightly soluble in D_2O so was filtered prior to spectrum acquisition to give a clear colourless solution. The lower spectrum in Figure 3.11 shows tyrosine alone. Upon addition of $KMnO_4$ to tyrosine, the solution immediately turned brown in colour with the slight formation of a brown precipitate.

The solution was filtered prior to spectrum acquisition. Figure 3.11 shows that the immediate spectrum following addition of $KMnO_4$ contains a broadening, most probably due to the presence of a paramagnetic species. This paramagnetic species could be either the Mn(II) or Mn(III) ion. After 18 hours the solution was brown in colour with a brown precipitate. This was again filtered to give a clear brown solution. The resulting NMR spectrum of the brown clear solution shows there is still some broadening of the peaks, however resolution appears to be returning.

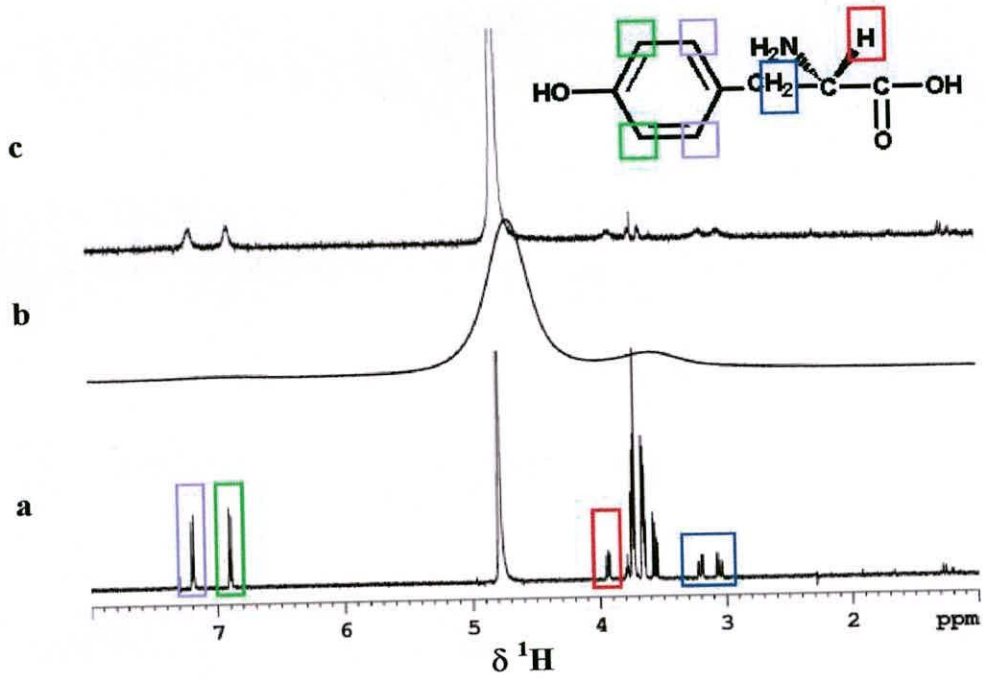

Figure 3.11 1D ^1H NMR spectra for reaction of tyrosine with $KMnO_4$. **(a)** Tyrosine alone, **(b)** tyrosine and $KMnO_4$ upon immediate mixing, **(c)** tyrosine and $KMnO_4$ after 18 hours. Conditions: 9.25 mM tyrosine, 1 mol equivalent $KMnO_4$ added, reactions at room temperature.

The brown precipitate seen after addition of permanganate to the solution of tyrosine is most likely to be due to the formation of manganese dioxide, $Mn(IV)O_2$. This

being the case then some part of the tyrosine molecule is being oxidised. The most likely part of the tyrosine molecule to be oxidised by permanganate is the amine group. There is a slight shift upfield of the peaks representing the α and β protons which could be as a result of the amine group being oxidised causing a slight change in the spectrum. However, the fact that there is still some tyrosine left following 18 hours suggests that this oxidation may take time or that all the permanganate has reacted leaving a residual amount of tyrosine.

3.3.3.2 Tryptophan

Tryptophan was found to be poorly soluble in D_2O so again was filtered prior to spectrum acquisition to give a clear colourless solution. The NMR spectrum of tryptophan alone is the lower spectrum, **a**, in Figure 3.12. Upon addition of $KMnO_4$ the solution immediately turned brown in colour but with no formation of a precipitate. The solution was filtered prior to spectral acquisition and gave the middle spectrum, **b**, in Figure 3.12. This spectrum again shows broadening, as was seen previously with tyrosine. After 18 hours, some brown precipitate had formed. Precipitates often lead to spectrum broadening due to the sample no longer being homogenous. The solution was filtered and the precipitate removed leaving a clear yellow/brown solution which gave rise to the upper spectrum, **c**, in Figure 3.12 where the peak intensities began to return, with no obvious change to the spectrum. It is likely the situation with tryptophan is similar to that seen with tyrosine in that the amine group is being oxidised by permanganate resulting in the formation of manganese dioxide as seen by a brown precipitate. On closer inspection of the spectrum acquired after 18 hours there is a small shift upfield in the peaks

representing the α and β protons which would support the notion of oxidation of the amine group occurring, however this could be due to a change in pH upon mixing permanganate with the amino acids.

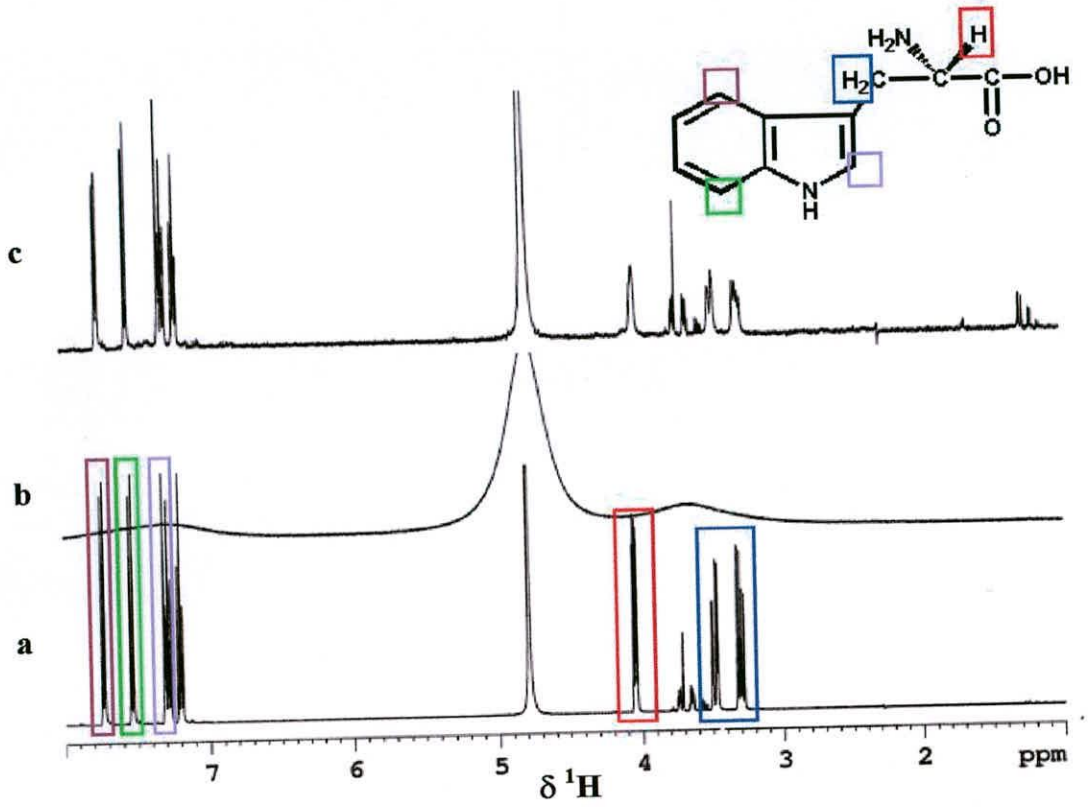

Figure 3.12 1D ^{1}H NMR spectra of tryptophan. (**a**) Tryptophan alone, (**b**) tryptophan and $KMnO_4$ upon immediate mixing, (**c**) tryptophan and $KMnO_4$ after 18 hours. Conditions: 9.76 mM tryptophan, 1 mol equivalent $KMnO_4$ added, reactions at room temperature.

3.3.3.3 Histidine

Histidine was found to be readily soluble in D_2O and dissolved to give a clear colourless solution. The NMR spectrum of histidine alone is the lower spectrum, **a**, in Figure 3.13.

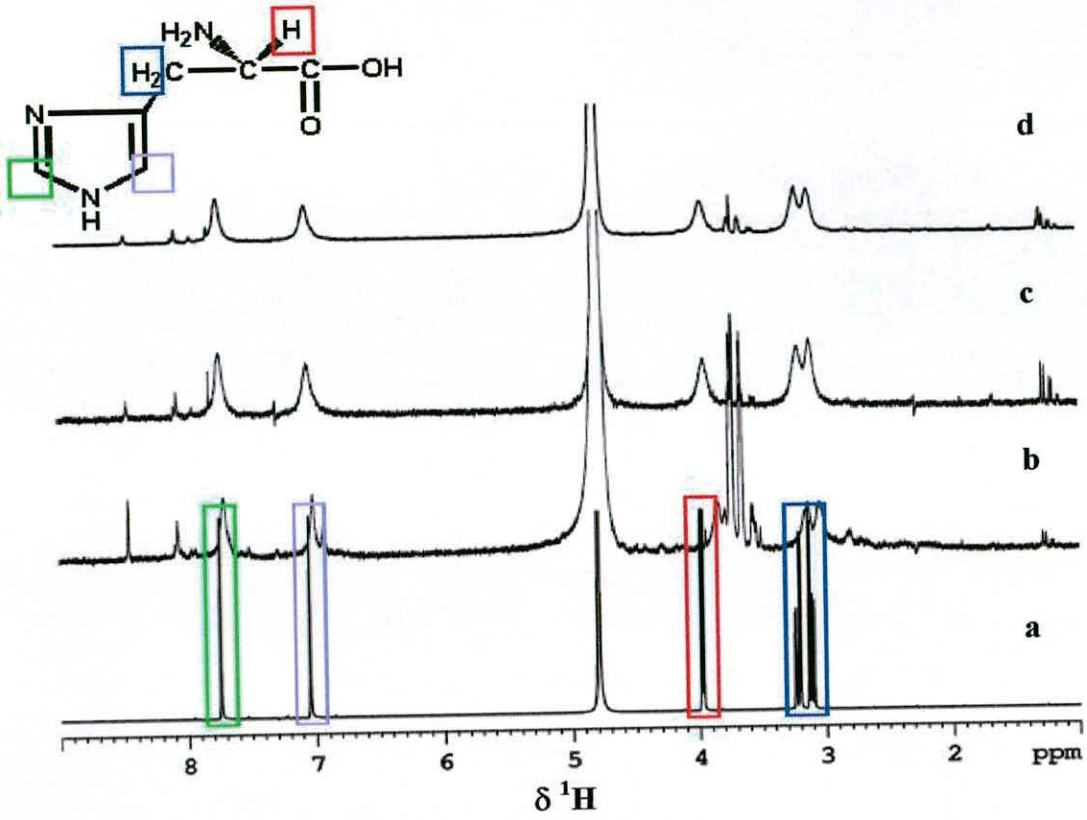

Figure 3.13 1D ^{1}H NMR spectra of histidine. **(a)** Histidine alone, **(b)** histidine and $KMnO_4$ upon immediate mixing, **(c)** histidine and $KMnO_4$ after 18 hours, **(d)** histidine and $KMnO_4$ after 24 hours. Conditions: 10.09 mM histidine, 1 mol equivalent $KMnO_4$ added, reactions at room temperature.

Upon addition of $KMnO_4$ the solution immediately turned a pink/purple colour with no formation of a precipitate. The solution was filtered prior to spectrum acquisition, which is spectrum **b** in Figure 3.13. This spectrum again shows some broadening as seen previously. New peaks have emerged at *ca.* 8.1 and 8.5 ppm. These new peaks could be due to oxidation of the amino acid or the presence of formic acid. After 18 hours, brown precipitate had formed.

The solution was filtered and the precipitate removed leaving a clear yellow/brown solution which gave rise to spectrum **c** in Figure 3.13 with some changes to the

spectrum suggesting oxidation of histidine by permanganate. The new peaks first seen in spectrum **b** at *ca.* 8.1 and 8.5 ppm are still present. Spectrum **d** is after 24 hours reaction time. Brown precipitate had again formed and the resulting filtered solution was yellow/brown in colour. There is still some broadening of the spectrum but no new peaks compared with spectra **b** and **c**. The slight change of the original peaks seen in the spectrum after addition of permanganate may result from oxidation of histidine or could be due to the paramagnetic broadening by Mn(II).

3.3.3.4 N-Acetyl L-Methionine

N-acetyl L-methionine (NAc-met) was found to be readily soluble in D_2O and dissolved to give a clear colourless solution. The NMR spectrum of NAc-met alone is the lower spectrum, **a**, in Figure 3.14. Upon addition of $KMnO_4$ a brown precipitate formed immediately. The solution was filtered to give a clear colourless solution, prior to spectral acquisition, which is spectrum **b** in Figure 3.14. This spectrum again shows some broadening as seen previously with the emergence of new peaks at *ca.* 2.7 ppm and 3.1 ppm. After 18 hours, some brown precipitate had again formed which was removed by filtering to give a clear colourless solution. The resulting spectrum is shown as **c** in Figure 3.14 with the same new peaks as seen in **b**, as indicated by green arrows. This suggests that NAc-met is being oxidised by permanganate. The most likely part of the amino acid to be oxidised is the sulfur group, which markedly changes the chemical shift of the ε-CH_3 group. A peak at *ca.* 2.1 ppm is assigned to the ε-CH_3 group of NAc-met, the two new peaks at 2.7 ppm and 3.1 ppm have shifted downfield by *ca.* 0.7 and 1.1 respectively. The sulfur group is probably being oxidised to produce methionine sulfoxide initially and then

to methionine sulfone shortly afterwards. To investigate this, NMR experiments were carried out on methionine sulfone and methionine sulfoxide.

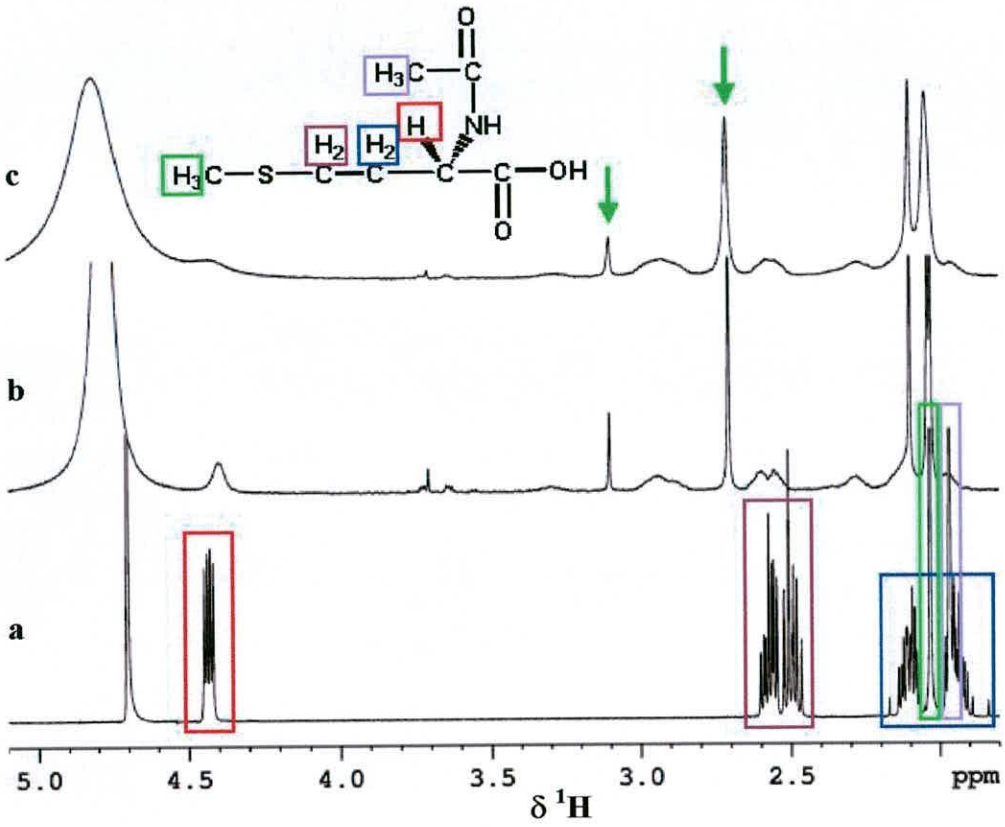

Figure 3.14 1D ^{1}H NMR spectra of NAc-met. (**a**) NAc-met alone, (**b**) NAc-met and $KMnO_4$ upon immediate mixing, (**c**) NAc-met and $KMnO_4$ after 18 hours. Conditions: 9.85 mM NAc-met, 1 mol equivalent $KMnO_4$ added, reactions at room temperature.

3.3.3.5 Methionine Sulfoxide and Methionine Sulfone

The structures of methionine sulfoxide and methionine sulfone are shown in Figure 3.15. These amino acids were reacted with $KMnO_4$ following the same method as used previously with other amino acids and 1D NMR spectra obtained. Methionine

sulfoxide and sulfone were both readily soluble in D_2O.

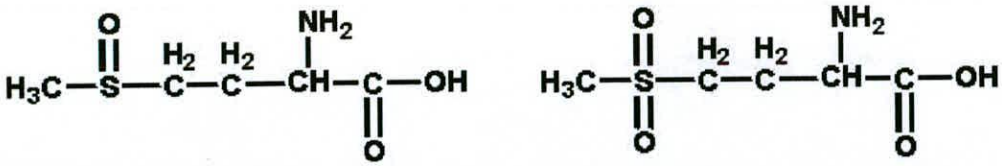

L-methionine sulfoxide **L-methionine sulfone**

Figure 3.15 Structures of met-sulfoxide and met-sulfone

Upon immediate mixing of methionine sulfoxide with one mol equivalent permanganate, the solution changed from colourless to brown but with no obvious precipitate. Prior to NMR analysis, the solution was filtered, resulting in a clear light brown solution. The spectrum for methionine sulfoxide alone is the lower spectrum in Figure 3.16 with the upper spectrum showing the reaction following mixing with permanganate. Arrows indicate the emergence of two new peaks. The ε-CH_3 group of methionine sulfoxide gives a peak at *ca.* 2.75 ppm. This is probably a similar peak as that at 2.7 ppm in the spectrum of NAc-met following reaction with permanganate (see Figure 3.14, spectra **b** and **c**) confirming the oxidation of methionine to methionine sulfoxide. The green arrow on the upper spectrum of Figure 3.16, where methionine sulfoxide has been reacted with permanganate, shows a shift downfield of the ε-CH_3 peak to *ca.* 3.1 ppm. This shift was also seen previously with methionine upon addition of permanganate, again confirming that the same reaction has taken place. The blue arrow shows a shift downfield of the protons attached to the β carbon. Both these shifts suggest a change in the structure of the amino acid. Some of the methionine sulfoxide has possibly been oxidised to

methionine sulfone, however some of the original amino acid remains (as indicated by the presence of peaks for the original amino acid).

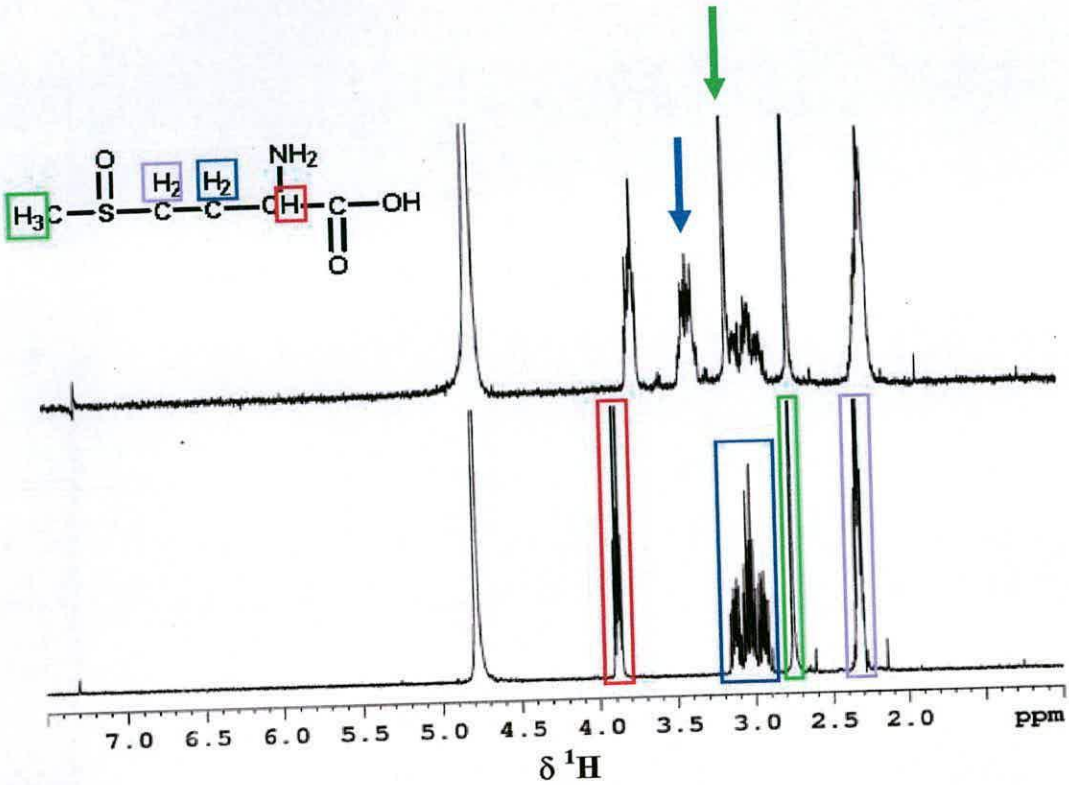

Figure 3.16 1D ^{1}H NMR spectra of L-methionine sulfoxide (lower spectrum) and following immediate reaction with 1 mol equivalent permanganate (upper spectrum). Conditions: 10.08 mM L-met sulfoxide, 1 equivalent $KMnO_4$ added, reactions at room temperature.

Methionine sulfone was also reacted with one mol equivalent of permanganate. Upon immediate mixing the clear colourless solution turned pink/purple with no formation of a precipitate. The lower spectrum in Figure 3.17 shows methionine sulfone alone, the upper spectrum is following addition of permanganate. As can be seen there is no obvious difference between spectra suggesting that no immediate

oxidation of methionine sulfone has taken place. The terminal methyl group shows a peak at *ca.* 3.1 ppm. This is the same peak as seen in the spectrum showing methionine reacted with permanganate (Figure 3.14, spectra **b** and **c**) and methionine sulfoxide reacted with permanganate (Figure 3.16, upper spectrum). This confirms the oxidation of methionine and methionine sulfoxide to methionine sulfone following addition of permanganate.

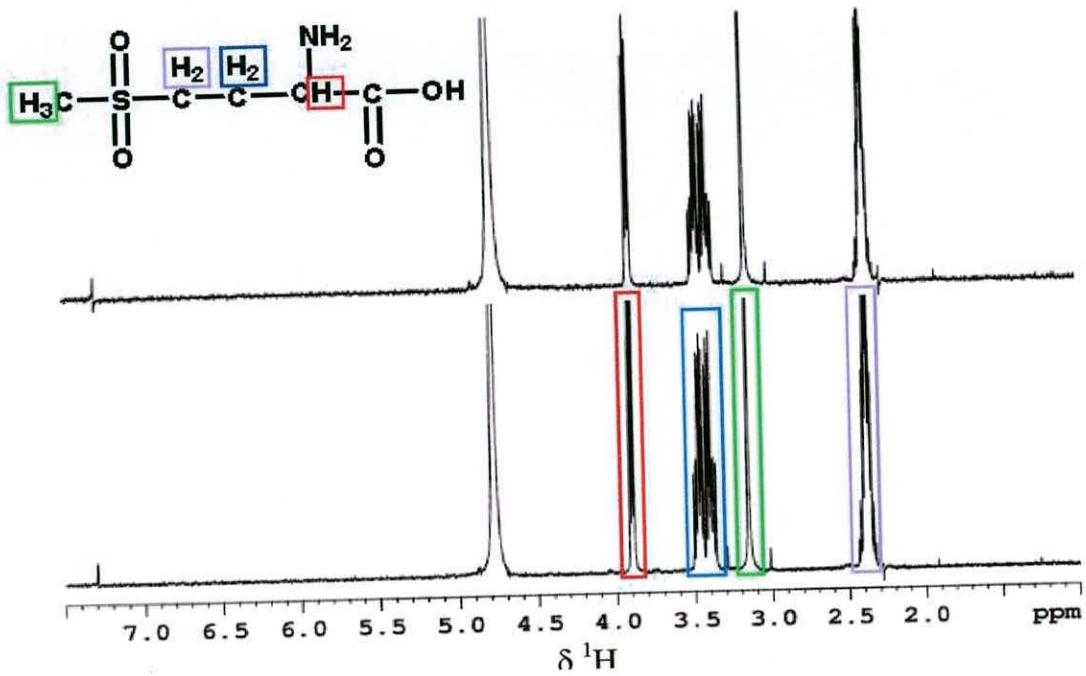

Figure 3.17 1D ^{1}H NMR spectra of L-methionine sulfone and following reaction of permanganate. Lower spectrum shows met sulfone alone. Upper spectrum is following immediate reaction with permanganate. Conditions: 9.97 mM L-met sulfone, 1 mol equivalent $KMnO_4$ added, reactions at room temperature.

3.3.4 Investigation into Oxidation of Methionine Residues of hTf

These results suggest that of the amino acids looked at, methionine is the most likely

to be oxidised by permanganate as it is readily oxidised to the sulfoxide and sulfone. To investigate further the possibility that permanganate oxidises methionine residues of transferrin, 2D [^{1}H, ^{13}C] NMR spectra of recombinant non-glycosylated human transferrin with > 95% ε-$^{13}CH_3$ enrichment at all nine Met residues (for locations see Figure 3.18) were obtained using inverse detection [33, 44]. It is possible to detect peaks at micromolar concentrations. Further, the protein can be de-metallated and recycled as it was for this study. The recombinant hTf is non-glycosylated but there is no evidence that glycosylation interferes with metal uptake [31]. The SCH_3 NMR peaks appear as singlets. Also the Met residues are well dispersed throughout the protein and provide information on several different types of environment such as different lobes.

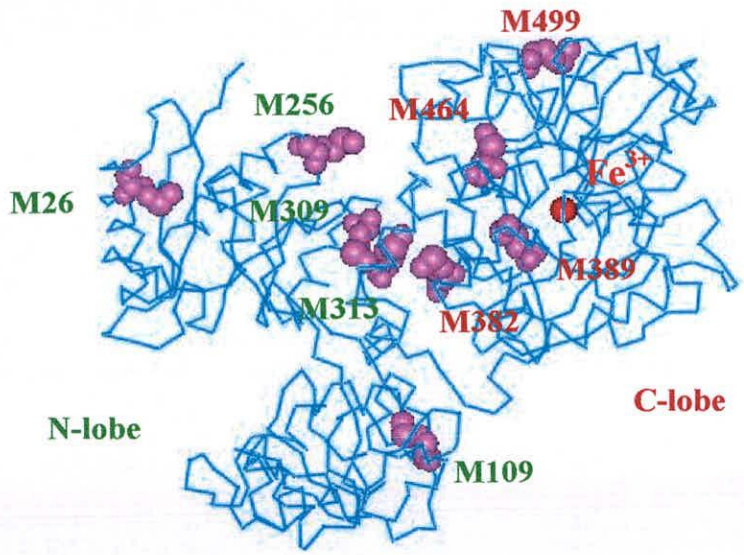

Figure 3.18 The locations of the nine Met residues in hTf (coordinates from the crystal structure of hTf with Fe(III) in C-lobe and no metal in N-lobe [45].

Cross-peaks for Met residues were assigned using work previously carried out by Beatty *et al* [32]. The protein had been used in previous experiments where it had

been loaded with various metals and stripped. Prior to this work all metal was removed from the protein. The continuous loading and stripping of metal from the protein had gradually lowered the concentration and so the signals were relatively weak in these experiments. Although not all nine cross-peaks were initially visible (Figure 3.19) and some were slightly different to those reported previously, those matching most closely were assigned. As already mentioned the protein was recycled and had been stored for some time which may be why the peaks were different to those found previously [33, 38].

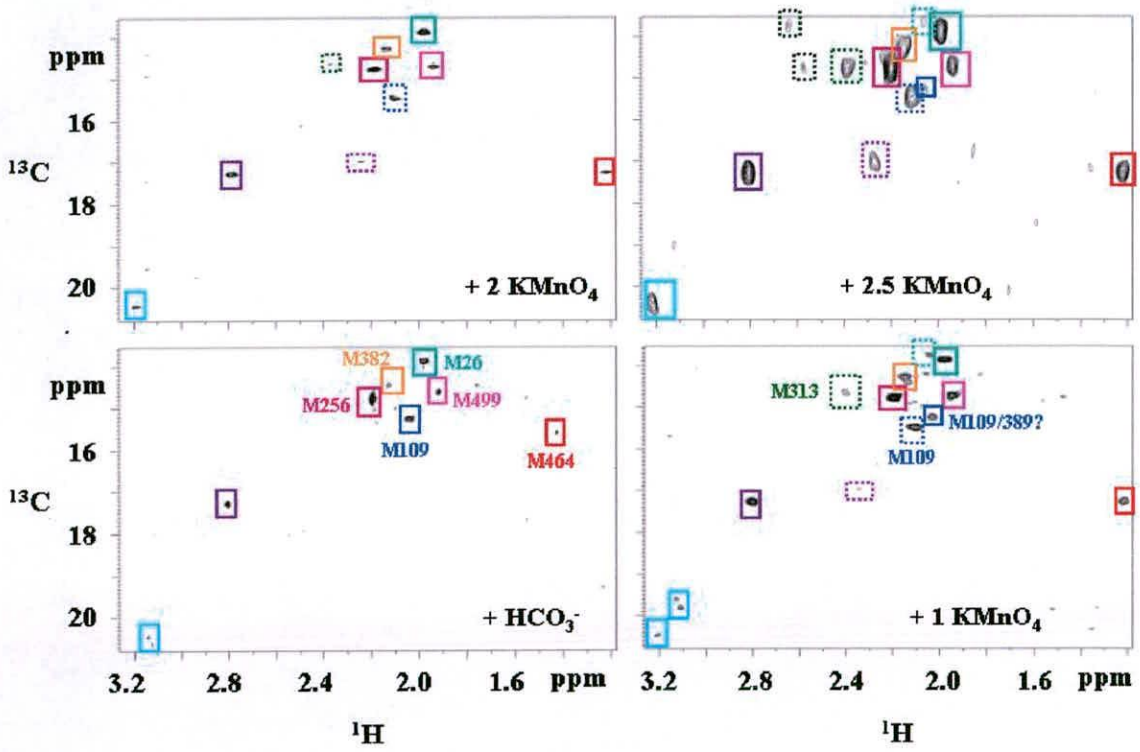

Figure 3.19 2D [^{1}H, ^{13}C] HSQC spectra of ε-$^{13}CH_3$-Met-hTf (0.3 mM in 0.1 KCl, 10 mM bicarbonate, pH* 7.4) and after addition of 1.0, 2.0 and 2.5 mol equiv of $KMnO_4$. The assignments are based on refs [32, 38, 44]. The solid boxes indicate initial peaks and possible shifts of those peaks. Dotted boxes indicate new peaks.

Table 3.2 ^{1}H and ^{13}C NMR chemical shifts of ε-$^{13}CH_3$-Met residues for apo-form and after reaction with 1-2.5 mol equiv $KMnO_4$

		δ ($^{1}H/^{13}C$) (ppm)					
Residue	**Location**	**Beatty *et al*[a]**	**+ HCO_3^-**	**+ 1 $KMnO_4$**	**+ 2 $KMnO_4$**	**+ 2.5 $KMnO_4$**	**+2.5 $KMnO_4$ + time[c]**
Met464	Trp460 hydrophobic patch of helix 5	1.38/16.3	1.43/15.6	1.22/17.3	1.22/17.25	1.22/17.26	1.21/17.25
Met499	C2, mostly exposed	1.86/15.41	1.92/14.6	1.94/14.72	1.94/14.7	1.94/14.7	1.94/14.7
Met109	N2, partially buried	1.98/14.55	2.04/15.3	2.03/15.2 2.11/15.49	2.11/15.5	2.05/15.3 2.11/15.49	2.10/15.5
Met26	N1, helix 1, buried	1.98/16.02	1.97/13.9 1.99/13.9	1.98/13.9 2.04/13.8	1.98/13.8	1.98/13.8 2.04/13.7	1.98/23.9
Met382	C1, hinge region, partially exposed	2.08/15.22	2.14/14.5	2.15/14.3	2.14/14.3	2.15/14.3	2.14/14.3
Met389	C1, completely buried	2.02/15.49[b]		2.11/15.49		2.11/15.49	
Met256	N1, completely exposed	2.13/15.53	2.20/14.8	2.20/14.8	2.20/14.8	2.20/14.8	2.19/14.8
Met313	N1, hinge region, partially exposed	2.29/15.18		2.35/14.7	2.39/14.8	2.39/14.8	
Met309	N1, hinge region, moslty buried	2.27/17.52		2.27/17.0	2.27/17.0	2.27/17.0	2.25/17.0
						2.55/14.7	
						2.65/13.8	
Met ?			2.80/17.3	2.80/17.28	2.80/17.27	2.80/17.27	2.80/37.2
				3.1/19.8			
Met ?			3.14/20.4	3.20/20.4	3.20/20.4	3.22/20.4	3.20/40.4

[a] Apo-hTf used, pH 7.1, 310 K. [b] Data collected at 318 K. [c] Data collected with ^{13}C spectral width altered to 40 ppm

The chemical shifts of the peaks observed following addition of HCO_3^- and $KMnO_4$ and their assignments are given in Table 3.2 and the shift changes of peaks are given in Table 3.3. When the spectrum for apo-hTf with bicarbonate was collected eight cross peaks were observed. Of these eight peaks, six were assigned to possible Met residues. Assignment was initially based on peaks that most closely matched those found previously in terms of the pattern of the spectrum and position of peaks.

Table 3.3 ^1H and ^{13}C NMR chemical shifts of apo-hTf , Mn(III)-induced shifts for the Met-(ε)-$^{13}CH_3$ residues of hTf at 310 K.

Residue	Location	Apo-hTf	2.5 $KMnO_4$	Δδ ($^1H/^{13}C$) (ppm)
Met464	Trp460 hydrophobic patch of helix 5	1.43/15.6	1.22/17.26	-0.21/1.66
Met499	C2, mostly exposed	1.92/14.6	1.94/14.7	0.04/0.1
Met109	N2, partially buried	2.04/15.3	2.05/15.3 2.11/15.49	0.01/0 0.7/0.19
Met26	N1, helix 1, buried	1.97/13.9 1.99/13.9	1.98/13.8 2.04/13.7	0.01/0.1 0.05/-0.2
Met382	C1, hinge region, partially exposed	2.14/14.5	2.15/14.3	0.01/-0.2
Met389	C1, completely buried	2.03/15.2[a]	2.05/15.3	0.02/0.1
Met256	N1, completely exposed	2.20/14.8	2.20/14.8	0/0
Met313	N1, hinge region, partially exposed	2.35/14.7[a]	2.39/14.8	0.04/0.1
Met309	N1, hinge region, moslty buried	2.80/17.3 2.27/17.0[a]	2.80/17.27 2.27/17.0	0/0 0/0 (-0.53/-0.27)
			2.55/14.7	
			2.65/13.8	
		3.14/20.4	3.22/20.4	

[a] Chemical shift data taken from hTf + 1 $KMnO_4$ as peak not present with apo-hTf

Upon addition of the first mol equiv of $KMnO_4$ the cross-peak assigned to Met464 instantly disappeared (Figure 3.19). A new peak appeared at a shift of *ca.* 1.7 ppm to

low field in the ^{13}C dimension and *ca.* 0.2 ppm to high field in the ^{1}H dimension (Table 3.3). Although the peak assignment is somewhat ambiguous the shift is comparable to that seen by previous workers on addition of a metal to apo-hTf [32, 33, 38, 46]. There was no apparent further shift of this peak upon addition of more $KMnO_4$ or with time. This suggests a conformational change in the C-lobe upon binding the first equivalent of manganese. The Met464 residue is situated in the hydrophobic patch of helix 5 which backs onto the metal binding site and H-bonds to the synergistic anion [45, 47] which is disturbed by the loading of metal ions in the C-lobe.

The cross-peak assigned to Met499 also disappeared and a new peak appeared which shifted slightly to low field (Figure 3.19, Table 3.2 and Table 3.3). When further molar equivalents of permanganate were added only slight additional shifts were seen for Met499. Again, this is similar to that seen previously following addition of metals.

The peak assigned to Met26 (Figure 3.19) looks as if it is split into two upon addition of one equivalent of permanganate. The new peak is shifted slightly with the initial peak still visible (Table 3.2 and Table 3.3). The new peak then disappeared when two mol equivalents were added. However, the new peak then reappeared to a small extent when two and a half equivalents were added and the spectrum collected overnight. When the ^{1}H spectral width was altered for collection of the spectrum following addition of 2.5 mol equivalents overnight, the peak now appeared at 1.98/23.9 ppm (see Table 3.2). Met26 is buried in the N-lobe so would not thought to be a target for oxidation by permanganate. However, there may be a small conformational change which is only seen when one equivalent manganese binds to

the C-lobe. The second equivalent results in a further conformational change so that the new cross peak representing Met26 is no longer visible but this returns following addition of 2.5 mol equivalents $KMnO_4$.

No shift was seen for the cross peak assigned to Met256. This is consistent with previous work where no change was observed on addition of metals suggesting no conformational change. However, if the methionines were being oxidised by permanganate then this residue would be a particularly susceptible target due to its position: it is completely exposed.

The peak assigned to Met313 was not visible for the apo protein, only upon addition of permanganate. A small additional shift was seen when more permanganate was added. Shifts were only seen for this residue in previous work after the second mol equivalent of metal was added [33, 38, 46]. This peak then disappeared after addition of 2.5 molar equivalents and time with the spectrum collected overnight.

The peak assigned to Met382 had a slight shift following addition of one molar equivalent $KMnO_4$ (Table 3.3) which remained following further additions of permanganate.

There is some ambiguity in the assignments of peaks for Met109 and 389. Met109 was assigned to the peak appearing at 2.04/15.3 ppm (Table 3.2). Upon addition of $KMnO_4$ this peak remains, with the exception of the spectrum collected following the addition of 2 molar equivalents, with a new peak appearing at 2.11/15.49 ppm (Table 3.2). This could be due to a conformational change or due to oxidation of the protein by permanganate. Alternatively, this new peak could be due to the appearance of Met389. Previously this residue had proved difficult to detect, only appearing on addition of oxalate [32], addition of one equivalent metal [38] or the

raising of the temperature [33].

In previous work on metal binding, only a small shift was seen for Met109, however, no strong oxidant such as permanganate was used. This may have an influence on some of the peak shifts if in fact the shifts are due to oxidation and/or conformational change.

The peaks visible at low field have in some cases been assigned (see Figure 3.19 and Table 3.2). For example a peak for Met309 has been assigned although this is tentative as the peak is outside the expected range. It is difficult to assign these extra peaks. They could be due to already oxidised methionines or a conformational change from the continuous recycling and storage of the protein.

There are a few additional peaks that appeared in the spectrum following addition of two and a half molar equivalents permanganate. These could be due to oxidation of the methionines. The change in chemical shifts seen in the 1D [^{1}H] NMR spectrum (Figure 3.14) of NAc-met following addition of one mol equivalent $KMnO_4$ of *ca.* 0.7 and 1.1 ppm downfield were attributed to the oxidation of methionine to the sulfoxide and sulfone by permanganate. To establish the chemical shift for ^{13}C for comparison with the 2D NMR, 1D [^{13}C] experiments were carried out on NAc-met, methionine sulfoxide, methionine sulfone and NAc-met following reaction with one mol equivalent permanganate. The results are given in Appendix E. A shift of 10 ppm downfield is seen for the ε-CH_3 group following oxidation of methionine with permanganate which corresponds to the ε-CH_3 peak assigned to methionine sulfoxide and sulfone. The only instance where a 10 ppm chemical shift is seen in the HSQC data is for the peak representing Met26 where the spectral width of ^{13}C had been expanded (see Table 3.2). However, this residue is found in the N-lobe so would not

be an obvious target for oxidation by permanganate. It is possible that any methionine residues that have been oxidised by permanganate do not generate a strong enough signal to be detected during these experiments.

Any paramagnetic effects from Mn(III) are probably not seen due to the binding site being some distance from the methionine residues. However, if manganese is binding to areas of the protein other than the two binding sites this may have effects on peaks for other residues.

These experiments show that a conformational change is observed when permanganate is added to apo-transferrin which is of a similar nature to that observed for other metal binding to transferrin. However, it is important to consider the reaction occurring when Mn(VII) from permanganate is being reduced to Mn(III) for binding to transferrin. During this reaction a redox process is occurring; Mn(VII) is gaining four electrons in order to be reduced to Mn(III) for transferrin binding. Permanganate has already been shown in section 3.3.3.4 and section 3.3.3.5 to oxidise N-acetyl methionine to the corresponding sulfoxide and sulfone. The sulfur of N-acetyl methionine is losing two electrons to be oxidised to the sulfoxide and then a further two to be oxidised to the sulfone. This then accounts for the four electrons required for the reduction of Mn(VII) to Mn(III). Further, the one methionine residue (Met26) on the protein that is seen to shift in a similar manner to oxidation of N-acetyl methioine in 1D spectra ($[H^1]$, $[C^{13}]$) could be due to this reaction mechanism. The remaining eight methionine residues then shift in accordance to metal binding and change in protein conformation as seen previously with other metal binding to transferrin [33, 44, 46]

These experiments need to be repeated with a batch of new protein although the

labelling is an expensive process.

3.3.5 *Order of lobe loading of apo-hTf with Mn(III)*

Previously work has been carried out on transferrin to investigate the order of lobe-loading by metal ions. It is of interest to determine which lobe is loaded preferentially by Mn^{3+}. Owing to the paramagnetism of Mn^{3+}, alternative techniques were investigated to determine the order of lobe loading of transferrin by manganese. It had not been possible to examine the two monoferric transferrins (Fe_C-hTf and Fe_N-hTf) until Mackey and Seal described their technique of urea gel electrophoresis [48]. In this procedure a 6 M urea gel is used to separate the different forms of transferrin resulting in the production of four visible bands on the gel representing, from top (the well end of the gel) to bottom, apo-hTf, Fe_C-hTf, Fe_N-hTf and Fe_2-hTf. This separation appears to be related to the increase in protein stability as iron is bound to transferrin, the net negative charge of the protein increases with each iron atom bound and the asymmetrical distribution of amino acids in the transferrin molecule [49]. There are more disulfide bridges in the C-terminal domain than in the N-terminal domain which may explain the separation of the two mono-ferric forms of Fe-hTf. In the absence of bound metal, 6 M urea causes a partial unfolding of the protein and consequent reduction in electrophoretic mobility. The unfolding of the N-terminal domain causes a greater decrease in mobility than does the unfolding of the C-terminal domain and this may be due to the greater number of disulfide bridges in the latter.

This technique has been adopted by others with slight modifications to identify lobe loading of iron by transferrin [49, 50] and ovotransferrin [51]. In an attempt to

separate and distinguish the different forms of Mn-hTf, this method was used. Initially however, Fe-hTf was run on gels to determine the correct conditions, unfortunately with limited success. An example of this is shown in Figure 3.20. Apo-hTf and Fe-hTf of varying concentrations, ranging from *ca.* 1 x 10^{-6} M to 2.5 x 10^{-5} M, were run on 6 M urea gels.

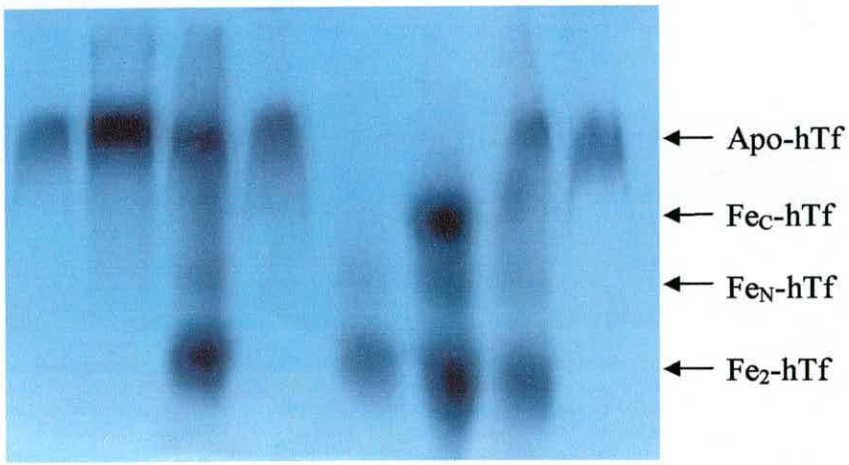

Figure 3.20 6 M Urea gel electrophoresis of apo-hTf, monoferric hTf and diferric hTf. Lanes run from 1 (left) to 8 (right). Lanes 1,2 and 8 loaded with apo-hTf, lanes 3, 5 and 7 loaded with Fe-hTf, lanes 4 and 6 loaded with mixture of apo-hTf and Fe-hTf. Appearance of bands identifies the different forms of transferrin. Gel run for 5 hours at 100 V.

As can be seen in Figure 3.20, four distinct bands appeared indicating the presence of the four different forms of transferrin in the samples. However, some bands are missing when they would be expected to appear, such as a band representing apo-hTf when mixtures of apo- and Fe-hTf are loaded. Slight modifications were made to the method such as length of time the gel was run, up to 7 hours, but with no improvement. Problems of missing bands may include faulty gel composition when

gels were cast manually, however pre-cast gels seemed to give no improvement, the use of chelates in the buffer that could mediate iron exchange among iron-binding sites, technical problems with the electrophoreses procedure such as heating up of the equipment during the process or possibly iron contamination in the gel or buffer.

The technique was applied to Mn-hTf with the aim of characterising Mn_C-hTf, Mn_N-hTf and Mn_2-hTf but no distinct bands appeared. Samples of Mn-hTf that had been prepared by reaction of apo-hTf with $MnCl_2$ or $KMnO_4$ were both used. The method was modified slightly by altering the pH of the tank buffer using HCl and NaOH but this gave no improvement. The lack of success of separating Mn-hTf by this method of electrophoresis may be due to the difference in binding of Mn(III) to transferrin compared to Fe(III). The harsh conditions of a 6 M urea gel may lead to the manganese dissociating from the protein during the separation.

3.3.6 Fe(III) displacement of Mn(III) from Mn_2-hTf

Experiments were carried out to determine the ability of iron to displace manganese from transferrin (Figure 3.21).

A

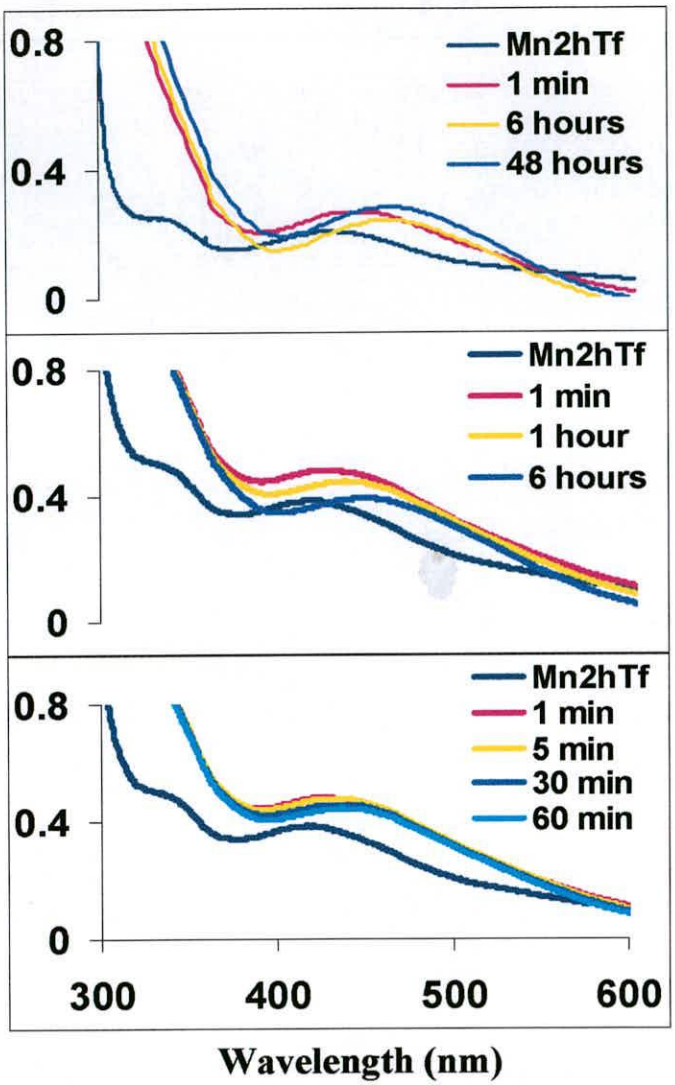

Figure 3.21 UV/Vis absorption spectrum of Mn_2hTf following addition of 3 mol equivalents of $Fe(NTA)_2$. Conditions: Mn_2hTf prepared using $MnCl_2$ and caeruloplasmin, 20 mM Hepes buffer, 10 mM $NaHCO_3$, pH 7.4, 310 K, 50 μM Mn_2hTf (upper spectrum), 65 μM Mn_2hTf (middle and lower spectra). Immediate reading shown as 1 minute to allow for mixing time. Shifts of LMCT bands indicates displacement of Mn(III) by Fe(III).

When 3 mol equivalents of $Fe(NTA)_2$ was added to a solution of Mn_2-hTf (20 mM

Hepes buffer, 10 mM bicarbonate, pH 7.4, 310 K), which had been prepared by reacting $MnCl_2$ in the presence of caeruloplasmin, a new broad band in the visible region appeared immediately (mixing time of *ca.* 1 minute) at *ca.* 440 nm (see lower spectrum in Figure 3.21). This band then appeared to decrease in intensity and moved to a longer wavelength until centred at *ca.* 465 nm after about 6 hours (see middle spectrum Figure 3.21) and then gradually increased in intensity again over a period of 48 hours (see upper spectrum Figure 3.21). There appears to be an initial and immediate reaction, which is seen as the LMCT band of Mn-hTf at 430 nm shifts towards the position associated with the LMCT band of Fe-hTf at 465 nm. Once this initial reaction, which is most likely to be the displacement of manganese from transferrin, is complete, the band seen at 465 nm then increases in intensity representing binding of iron to transferrin.

ICP-AES analysis of the Mn_2-hTf used gave a metal-to-protein ratio of 2.1 Mn: 1 hTf. On completion of the reaction (total reaction time of 48 hours) of Mn_2-hTf with $Fe(NTA)_2$, the protein was found to have a very small amount of Mn bound (4.7×10^{-3} Mn: 1 hTf) but some Fe had bound to the protein to give a ratio of 1.4 Fe : 1 hTf. This suggests that the majority of the Mn has been removed and Fe has taken its place on the protein but has not achieved full loading.

The experiment was repeated using Mn_2-hTf that had been produced using $KMnO_4$ to load the protein to investigate if there were any differences in displacement of Mn from Mn_2-hTf when permanganate was used to see if this supported any theory of the nature of the protein being altered by this method of loading. The UV/Vis spectra collected are shown in Figure 3.22.

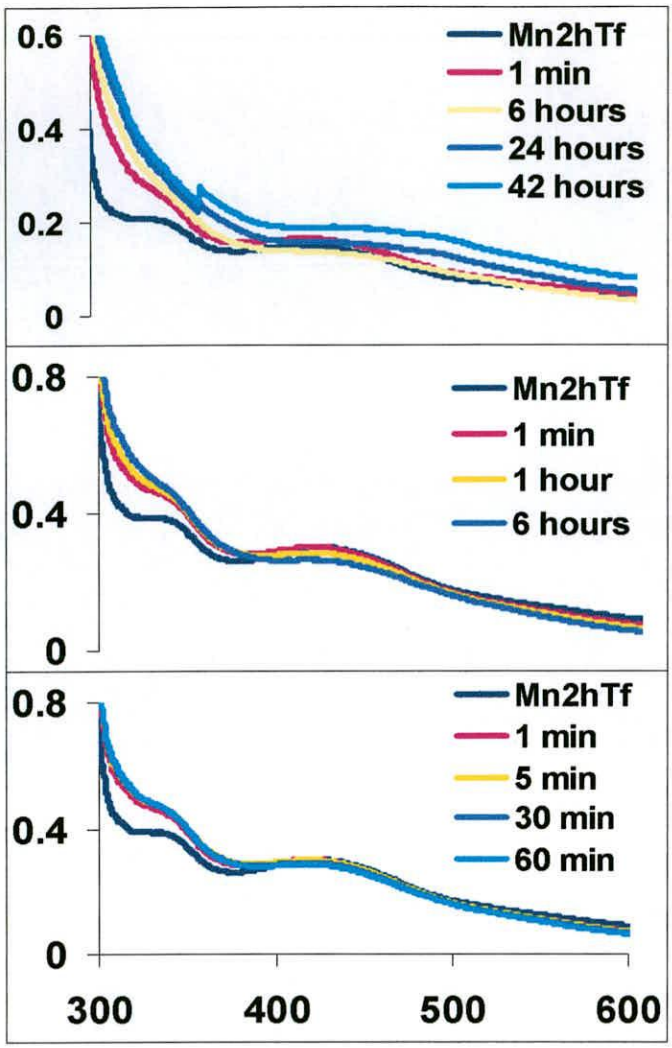

Figure 3.22 UV/Vis absorption spectrum of Mn_2hTf following addition of $Fe(NTA)_2$. Conditions: Mn_2hTf prepared using $KMnO_4$, 20 mM Hepes buffer, 10 mM $NaHCO_3$, pH 7.4, 310 K, 24 μM Mn_2hTf (upper spectrum), 40 μM (middle and lower spectra). Immediate reading shown as 1 minute to allow for mixing time. Shifts of LMCT bands indicates displacement of Mn(III) by Fe(III).

Compared with the previous experiment the nature of the displacement of Mn appears to have altered. The reaction appears to proceed more slowly with the

immediate change being very slight. There is a change over a period of 42 hours although this is much more gradual when compared with the change seen in the upper spectrum of Figure 3.21. This gradual change is more obvious during the first six hours (see middle and lower spectra of Figure 3.22). What is apparent is not only the much slower change in peak at 430 nm but also the persistence of a peak at 330 nm, characteristic of Mn_2-hTf.

This supports the theory that the loading of hTf with Mn by $KMnO_4$ does induce different changes to the protein compared with loading by $MnCl_2$. ICP-AES analysis showed the protein to have a metal: protein ratio of 2 Fe: 1 hTf but surprisingly some Mn was still found to be bound to the protein at a ratio of 0.7 Mn: 1 hTf. This supports previous experiments carried out on hTf loaded with Mn by $KMnO_4$ in that a greater ratio of 2 metals per protein molecule can be achieved. This may be due to some extra or alternative binding sites for Mn on hTf. The fact that Mn is not so readily displaced from Mn_2-hTf when $KMnO_4$ is used to load the protein also supports the theory that in some way the protein and its binding capability is altered.

3.3.7 Mn(III) displacement of Fe(III) from Fe_2-hTf

To try to establish whether the binding of Mn(III) to hTf using $KMnO_4$ was strong and comparable to binding of Fe(III) to hTf, $KMnO_4$ was reacted with Fe_2-hTf to see if manganese could displace iron. Fully loaded Fe_2-hTf as determined by ICP-AES was reacted with 2.5 molar equivalents of $KMnO_4$ and the reaction followed by UV/Vis spectroscopy. The results are shown in Figure 3.23.

A

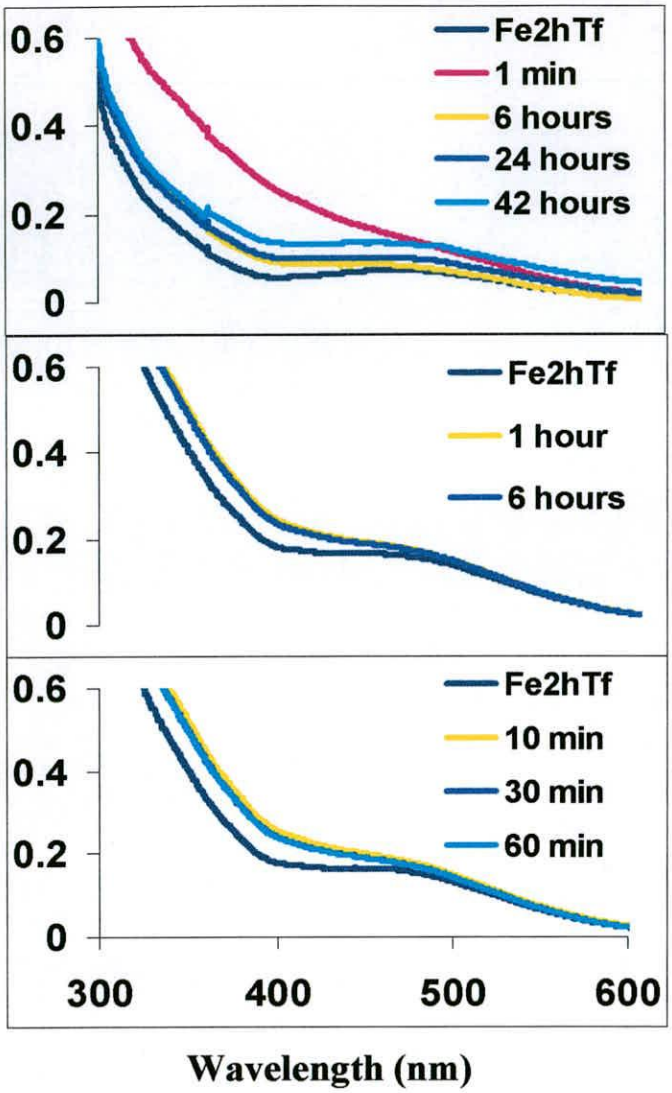

Figure 3.23 UV/Vis absorption spectrum of Fe_2-hTf following addition of $KMnO_4$. Conditions: 20 mM Hepes buffer, 10 mM $NaHCO_3$, pH 7.4, 310 K, 24 μM Fe_2-hTf (upper spectrum), 40 μM Fe_2-hTf (middle and lower spectra). Immediate reading shown as 1 minute to allow for mixing time. Strong band of Fe_2-hTf remains following addition of $KMnO_4$.

As can be seen in the upper spectrum, when $KMnO_4$ is initially added the strong pink colour of the permanganate hides any immediate shifts in peaks. However, this soon

subsides as can be seen in the lower spectrum of Figure 3.23. This change in the spectrum may be due to the reaction between Hepes buffer and permanganate already discussed (section 3.3.2) or as a result of the permanganate reacting with the Fe_2-hTf.

There is a slight change in the spectrum of Fe_2-hTf following addition of $KMnO_4$ in the first 6 hours although this is probably due to any residual colour of the permanganate as there is no emergence of new peaks or change in wavelength of the original peak. ICP-AES and UV/Vis results confirmed that Mn had not displaced Fe from Fe_2-hTf. However, UV/Vis spectroscopy does not show any structural changes that may have occurred therefore further work would be necessary in order to establish if $KMnO_4$ had any effect on Fe_2-hTf.

ICP-AES found no manganese bound to Fe_2-hTf even though it appears that MnO_4^- may bind to transferrin in sites other than the usual metal binding sites. It may be that once a metal is bound to both lobes of the protein it prevents further addition of manganese. This may be due to both lobes being fully closed when occupied by Fe(III).

3.3.8 Mn(III) Release from Mn_2-hTf

As described in Section 1.3.1 transferrin takes up Fe(III) at pH 7.4 and delivers it to cells *via* receptor-mediated endocytosis. Once inside the mildly acidic endosomes (pH 5.0 – 5.5) Fe(III) is released [11, 12, 52, 53]. Release of Mn(III) from Mn_2-hTf following a fall in pH was investigated using UV/Vis spectroscopy.

Fully loaded Mn_2-hTf with a ratio of 2.17 Mn: 1 hTf (as determined by ICP-AES) was used and the pH lowered by 0.5 (± 0.05) increments using 1 M HCl. UV/Vis

spectra were collected after equilibrium for 30 min at 310 K at each pH using a Cary 300 scan spectrophotometer. The results are shown in Figure 3.24.

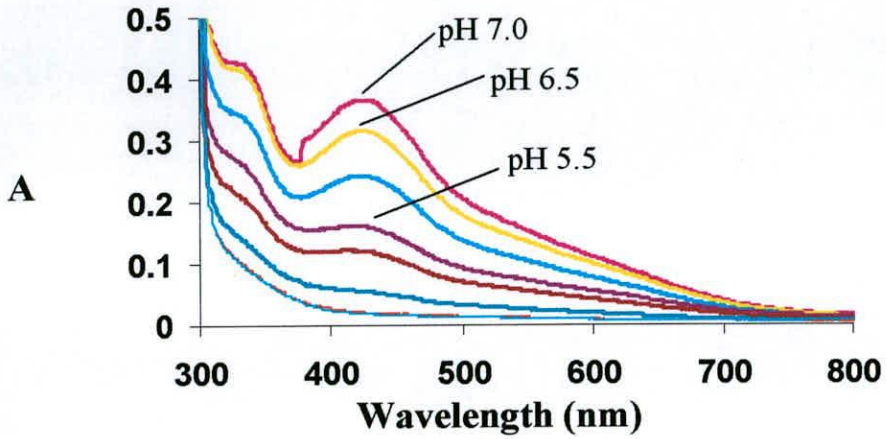

Figure 3.24 UV/Vis spectra showing release of Mn(III) from Mn_2-hTf following reduction in pH. The disappearance of the LMCT band at 430 nm of Mn_2-hTf suggests Mn(III) dissociates from transferrin with a fall in pH. Conditions: 20 mM Hepes buffer, 54.24 μM Mn_2-hTf. Initial reading at pH 7.0 (±0.05), pH then reduced in 0.5 increments to pH 3.0 (±0.05).

The results show that following a reduction in pH, Mn(III) is released from Mn-hTf as indicated by a fall in intensity of the LMCT associated with Mn-hTf (430 nm). The decrease in intensity is consistent until a pH of 3.5. The calculated molar extinction coefficients are 6747 M^{-1} cm^{-1} at pH 7.0 and 415 M^{-1} cm^{-1} at pH 3.0. This is most probably indicative of virtually all of the Mn(III) no longer being bound to transferrin. During the course of the experiment the solution changed colour from brown to colourless. These results are consistent with those seen with Fe_2-hTf where in the absence of chelators Fe(III) is released over the pH range 6.0 to 4.0. One site loses Fe(III) at a pH near 6.0 (N-lobe) the other nearer 5.0 (C-lobe) [53, 54]. The

results found here suggest a higher pH of 6.5 leads to the initial dissociation of Mn(III) from transferrin and that a lower pH is required before full dissociation of Mn(III) is reached as indicated by the continuous fall in intensity of the LMCT band at 430 nm until pH 3.5. However, this slightly wider pH range may arise from experimental conditions. The dependence of A_{430} on pH is shown in Figure 3.25.

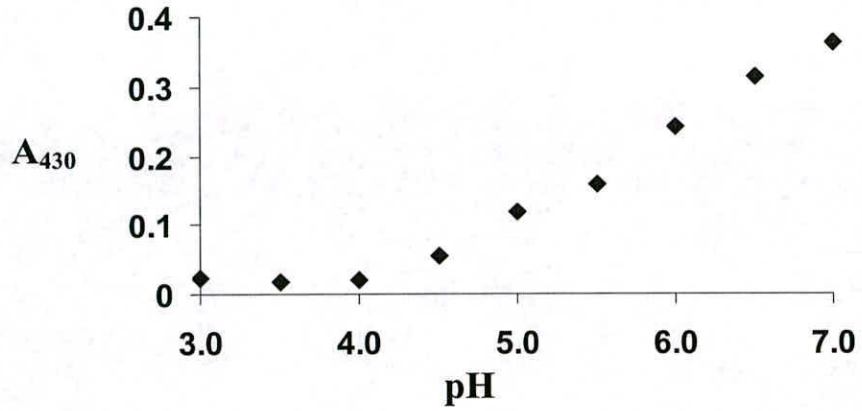

Figure 3.25 Variation in absorbance at 430 nm (Tyr to Mn(III) LMCT band) of a Mn_2-hTf solution with pH. For conditions see Figure 3.24. Dissociation appears to be a two-stage process.

There is a plateau reached at a pH of *ca.* 5.5 which suggests that one Mn(III) ion has been released between pH 7 and 5.5. This would suggest that the dissociation occurs in two stages whereby one lobe is vacated preferentially. It is most likely that the N-lobe is vacated first followed by dissociation from the more acid-stable C-lobe at a pH below 5.5. These results support the hypothesis that Mn(III) release from transferrin could occur in the endosomes in the same manner as it does for Fe(III).

3.4 Conclusions

The natural cycle of delivery of iron to cells by transferrin offers a great potential for targeting metals to target tissues. In particular to tissues where there is a high level of transferrin for example, the liver. This potential is vastly increased by the ability of transferrin to carry other metals [13, 14, 19, 38, 46, 52, 53, 55]. In blood serum, transferrin is only 30% fully loaded with iron, therefore the vacant sites of apo-transferrin could be used to act as a transport mechanism for other metals such as manganese.

Binding of metal ions to the phenolic oxygen of the tyrosine residues in the specific metal binding sites of apo-hTf perturbs the π-π^* transitions of the aromatic rings and leads to the production of two new absorption bands near 241 and 295 nm [14, 53]. These new bands can be seen in the UV spectra of apo-hTf and metal-hTf. Specific binding by certain metals such as Fe(III), Ti(IV) and Cu(II) also give rise to LMCT bands in the visible region of the spectrum. This can provide a convenient way to detect metal binding to transferrin, specific metal binding and also its release.

This work has shown that manganese can be loaded onto transferrin. The serum oxidant caeruloplasmin has been found to speed up the process. However, by using potassium permanganate as a source of manganese, transferrin can be loaded quickly and efficiently. However, this may be of some consequence to the protein due to the strong oxidising nature of potassium permanganate. NMR studies have shown that methionine is readily oxidised to methionine sulfoxide and sulfone following addition of permanganate.

2D [^{1}H, ^{13}C] NMR provides a method of determining the order of lobe loading of transferrin with various metal ions using ε-[^{13}C]Met-labelled recombinant transferrin.

Under the conditions used here, Mn(III) appears to preferentially load the C-lobe when introduced as permanganate. This is in agreement with previous work which has shown that NTA complexes of Fe(III) and Bi(III) both preferentially bind the C-lobe [33]. The conformational changes seen by shift changes of Met464 induced by Fe(III), Bi(III), Al(III), Ti(IV) and Ga(III) are all similar [33, 38]. A similar shift was seen with Mn(III). The slight discrepancies between the shifts seen for methionine residues in this work compared with previous work may support the theory of MnO_4^- loading transferrin in a different manner. If the C-lobe remains open following binding of Mn(III) or due to a cluster binding then this may result in a slight modification in chemical shifts of the peaks representing the methionine residues.

The methionine residues of hTf are well distributed throughout the protein and the changes in their ^1H and ^{13}C NMR resonances can provide a useful tool for determining the conformational changes of transferrin that occur during metal binding. This can then be useful to compare various metals. However, new protein would enable more definitive results to be obtained.

Although apo-hTf can sometimes be separated from mono- and di-ferric transferrin by electrophoresis, harsh conditions are required and these could not be used to separate Mn-hTf suggesting that only tightly bound metals can be separated. This is supported by the fact that iron is able to displace manganese from transferrin, whether loaded by $MnCl_2$ or $KMnO_4$, but manganese (added as MnO_4^-) is unable to displace iron from the protein. Mn(III) dissociates from Mn_2-hTf following a reduction of pH in a manner similar to that observed for Fe_2-hTf. The results suggest that Mn(III) dissociates from one lobe first, probably the N-lobe which is more

facile, followed by the C-lobe at pH < 5.5. This is consistent with the pH dependence of Fe(III) release observed for Fe_2-hTf [53] suggesting that once inside the cell Mn(III) will dissociate from Mn_2-hTf in a similar fashion to that seen with Fe(III) under the acidic conditions found in endosomes.

3.5 References

1. A. Sigel and H. Sigel, *Manganese and its role in biological processes*, Metal Ions in Biological Systems. Marcel Dekker Inc.37 **2000**.

2. D.C. Harris and P. Aisen, in *Iron Carriers and Iron Proteins*, T.M. Loehr Ed, VCH Publishers, Inc., New York, **1989**, 239-351

3. P.K. Bali and P. Aisen, *Biochemistry,* **1991**, 30: 9947-9952.

4. O. Zak, D. Trinder, and P. Aisen, *J. Biol. Chem.,* **1994**, 269: 7110-7114.

5. A.B. Mason, B.M. Tam, R.C. Woodworth, R.W. Oliver, B.N. Green, L.N. Lin, J.F. Brandts, K.J. Savage, J.A. Lineback, and R.T.A. MacGillivray, *Biochem. J.,* **1997**, 326: 77-85.

6. C.M. Lawrence, S. Ray, M. Babyonyshev, R. Galluser, D.W. Borhani, and S.C. Harrison, *Science,* **1999**, 286: 779-782.

7. E. Wagner, D. Curiel, and M. Cotton, *Adv. Drug Del. Rev.,* **1994**, 14: 113-135.

8. B.F. Anderson, H.M. Baker, E.J. Dodson, G.E. Norris, S.V. Rumball, J.M. Waters, and E.N. Baker, *Proc. Natl. Acad. Sci. USA,* **1987**, 84: 1769-1773.

9. M. Gerstein, B.F. Anderson, G.E. Norris, E.N. Baker, A.M. Lesk, and C. Chothia, *J. Mol. Biol.,* **1993**, 234: 357-372.

10. P.D. Jeffrey, M.C. Bewley, R.T.A. MacGillivray, A.B. Mason, R.C. Woodworth, and E.N. Baker, *Biochemistry,* **1998**, 37: 13978-13986.

11. A. Dautry-Varsat, A. Ciechanover, and H.F. Lodish, *Proc. Natl. Acad. Aci. USA,* **1983**, 80: 2258-2262.

12. A. Dautry-Varsat, *Biochimie,* **1986**, 68: 375-381.

13. H. Sun, M.C. Cox, H. Li, and P.J. Sadler, *Struc. Bond.*, **1997**, 88: 1-102.

14. H. Sun, H. Li, and P.J. Sadler, *Chem. Rev.*, **1999**, 99: 2817-2842.

15. H. Li, P.J. Sadler, and H. Sun, *J. Biol. Chem.*, **1996**, 271: 9483-9489.

16. H. Li, P.J. Sadler, and H. Sun, *Eur. J. Biochem.*, **1996**, 242: 387-393.

17. M.H. Gelb and D.C. Harris, *Arch. Biochem. Biophys.*, **1980**, 200: 93-98.

18. Y. Tomimatsu, S. Kint, and J.R. Scherer, *Biochemistry,* **1976**, 15: 4918-4924.

19. P. Aisen, R. Aasa, and A.G. Redfield, *J. Biol. Chem.*, **1969**, 244: 4628-4633.

20. W.R. Harris and A. Chen, *J. Inorg. Biochem.*, **1994**, 54: 1-19.

21. R.A. Gibbons, S.N. Dixon, K. Hallis, A.M. Russel, B.F. Sanson, and H.W. Symonds, *Biochim. Biophys. Acta,* **1976**, 444: 1-10.

22. A.M. Scheuhammer and M.G. Cherian, *Biochim. Biophys. Acta,* **1985**, 840: 163-169.

23. J.W. Critchfield and C.L. Keen, *Metabolism,* **1992**, 41: 1087-1092.

24. V.N. Zaitsev, I. Zaitseva, M. Papiz, and P.F. Lindley, *J. Biol. Chem.*, **1999**, 4: 579-587.

25. M.K. Cha and I.H. Kim, *Biochemistry,* **1999**, 38: 12104-12110.

26. G. Musci, G.C. Bellenchi, and L. Calabrese, *Eur. J. Biochem.*, **1999**, 265: 589-597.

27. S. Pandey, V.R. Chourey, L.V. Shastry, and V.R. Shastry, *Oxidation Comm.*, **2000**, 23: 138-144.

28. E. Brillas, J.A. Garrido, J. Perez-Benito, R.M. Rodriguez, and J. de Andres, *Coll. Czech. Chem. Comm.*, **1988**, 53: 479-486.

29. B.R. Sahu, V.R. Chourey, S. Pandey, and V.R. Shastry, *Asian. J. Chem.*, **1998**, 10: 320-323.

30. N.D. Chasteen, *Coord. Chem. Rev.*, **1977**, 22: 1-36.

31. A.B. Mason, M.K. Miller, W.D. Funk, D.K. Banfield, K.L. Savage, R.W.A. Oliver, B.N. Green, R.T.A. MacGillivray, and R.C. Woodworth, *Biochemistry,* **1993**, 32: 5472-5479.

32. E.J. Beatty, M.C. Cox, T.A. Frenkeil, B.M. Tam, A.B. Mason, R.T.A. MacGillivray, P.J. Sadler, and R.C. Woodworth, *Biochemistry,* **1996**, 35: 7635-7642.

33. H. Sun, M.C. Cox, H. Li, A.B. Mason, R.C. Woodworth, and P.J. Sadler, *FEBS Letters,* **1998**, 422: 315-320.

34. G. Curzon and L. Vallet, *Biochem. J.,* **1960**, 74: 279-287.

35. N. Suarez and H. Eriksson, *J. Neurochem.,* **1993**, 61: 127-131.

36. T.-L. Hwang and A.J. Shaka, *J. Mag. Res. Ser. A,* **1995**, 112: 275-279.

37. P.K. Bali and W.R. Harris, *Arch. Biochem. Biophys.,* **1990**, 281: 251-256.

38. M. Guo, H. Sun, H.J. McArdle, L. Gambling, and P.J. Sadler, *Biochemistry,* **2000**, 39: 10023-10033.

39. P. O'Hara, S.M. Yeh, C.F. Meares, and R. Bersohn, *Biochemistry,* **1981**, 20: 4704-4708.

40. D. Alexeev, H. Zhu, M. Guo, W. Zhong, D.J.B. Hunter, W. Yang, D.J. Campopiano, and P.J. Sadler, *Nature Stuct. Biol.,* **2003**, 10: 297-302.

41. K. Mizutani, H. Yamashita, H. Kurokawa, B. Mikami, and M. Hirose, *J. Biol. Chem.,* **1999**, 274: 10190-10194.

42. J.A. Khan, P. Kumar, A. Srinivasan, and T.P. Singh, *J. Biol. Chem.,* **2001**, 276: 36817-36823.

43. P. Kuser, D.R. Hall, M.L. Haw, M. Neu, R.W. Evans, and P.F. Lindley, *Acta Crsytallogr.,* **2002**, D58: 777-783.

44. Q.-Y. He, A.B. Mason, B.M. Tam, R.T.A. MacGillivray, and R.C. Woodworth, *Biochem. J.,* **1999**, 344: 881-887.

45. H.J. Zuccola, PhD Thesis, 1992, Georgia Institute of Technology, Atlanta.

46. W. Zhong, J.A. Parkinson, M. Guo, and P.J. Sadler, *J. Biol. Inorg. Chem.,* **2002**, 7: 589-599.

47. S. Bailey, R.W. Evans, R.C. Garratt, B. Gorinsky, S. Hasnain, C. Horsburgh, H. Jhoti, P.F. Lindley, A. Mydin, R. Sarra, and J.L. Watson, *Biochemistry,* **1988**, 27: 5804-5812.

48. D.G. Makey and U.S. Seal, *Biochim. Biophys. Acta,* **1976**, 453: 250-256.

49. P. Aisen, A. Leibman, and J. Zweier, *J. Biol. Chem.,* **1978**, 253: 1930-1937.

50. R.W. Evans and J. Williams, *Biochem. J.,* **1978**, 173: 543-552.

51. J. Williams, R.W. Evans, and K. Moreton, *Biochem. J.,* **1978**, 173: 535-542.

52. P. Aisen, in *Metal Ions in Biological Systems*, A. Sigel and H. Sigel Ed, Marcel Dekker Inc., New York, **1998**, 35: 585-631

53. E.N. Baker, *Adv. Inorg. Chem.,* **1994**, 41: 389-463, and references therein.

54. C.A. Smith, E.W. Ainscough, H.M. Baker, A.M. Brodie, and E.N. Baker, *J. Am. Chem. Soc.,* **1994**, 116: 7889-7890.

55. R.W. Evans and W. Ogwang, *Biochem. Soc. Trans.,* **1988**, 16: 833-834.

Chapter 4 Crystallisation of Transferrin

4.1 Introduction

One of the best methods of investigating the structures of proteins is by X-ray crystallography. This allows similarities between families of proteins and structural changes when metals are bound to proteins to be studied. The main aim of this chapter was to develop a method of crystallisation of transferrin with iron or manganese bound in order to investigate structural changes induced by these metals.

4.1.1 Crystallisation Theory

Crystals packed into a regular lattice of repeating subunits, or unit cells, diffract X-ray wavelength light at certain angles depending on their size and composition and this provides structural information on the protein [1].

The formation of ordered crystals is thermodynamically unfavourable due to a drive towards maximum entropy. However, under the right conditions that include exact kinetic rate and thermodynamic change in enthalpy and entropy, crystals do form. The most successful way to control these is to force the compound, in this case protein, out of a supersaturated solution. As moisture is lost from the solution, the protein concentration is gradually increased until the protein cannot maintain its supersaturation. At this point the protein begins to precipitate out of solution. The rate of this precipitation determines whether it will randomly nucleate or crystallise correctly. Nucleation is the process where molecules or non-crystalline aggregates free in solution come together to form a stable aggregate with a repeating lattice. Formation of this lattice does not necessarily lead to crystal growth. The aggregate

must reach a critical size for further growth of the nucleus to take place. The extent of supersaturation and hence degree of nucleation is determined by the solubility of the protein. A phase diagram can be used to show protein solubility and saturation (Figure 4.1). Higher solubility increases the chances of stable nuclei being formed.

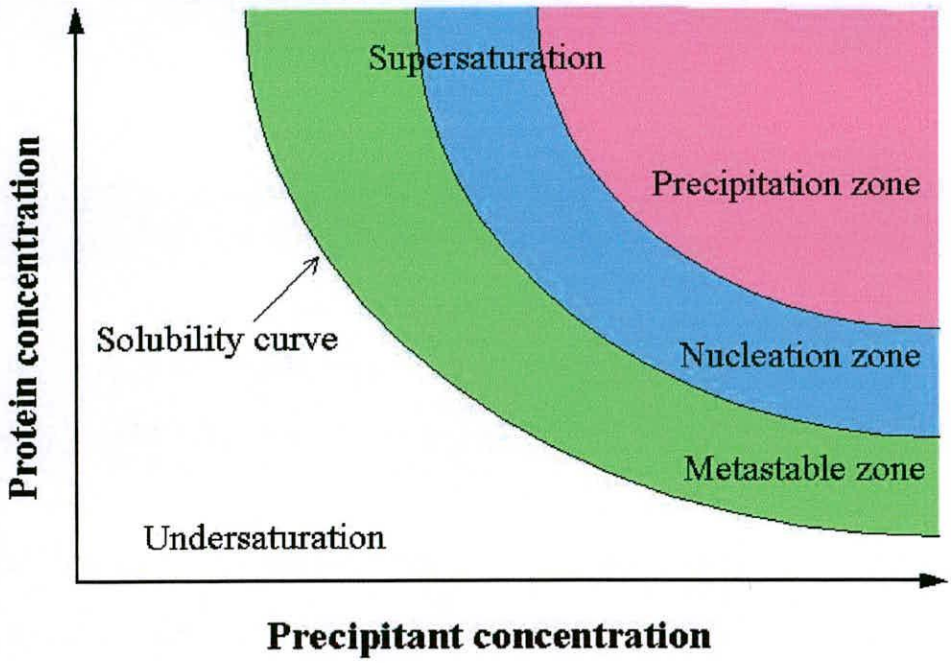

Figure 4.1 Phase diagram for crystallisation of proteins. Proteins are in equilibrium between solution and crystal on the curve. Crystals will not grow in the undersaturation area. Supersaturation is further divided. In the metastable zone nucleation may not occur for some time but growth is sustained, seeding may be successful here. In the nucleation zone protein crystals will grow. Protein will precipitate out of solution in the precipitation zone (adapted from [2]).

Protein purity can be an influencing factor in the crystallisation process as impurities can lead to poor diffraction.

4.1.2 Previous Crystallisation of Transferrins

The first crystallographic studies on transferrins were carried out in 1970 [3] with limited success, as was the case in 1978 also [4]. Crystals of various transferrins have since been reported (see Table 4.1) although as yet there is no published structure of intact human serum transferrrin.

Table 4.1 X-Ray crystal structures of Transferrins

Transferrin	Residues	Geometry	Resolution (Å)
Fe_C-hTf [5][a]	679	Distorted Octahedral	2.6
Fe-hTf/2N [6]	337 (N-lobe)	Distorted Octahedral	1.6
Fe-hTf/2N [6]	337 (N-lobe)	Distorted Octahedral	1.8
Apo-hTf/2N [7]	337 (N-lobe)	Distorted Octahedral	2.2, 3.2
Fe_2-rTf [8][b]	676	Distorted Octahedral	3.3
Fe_2-oTf (chicken) [9]	686	Distorted Octahedral	2.4
Fe_2-oTf (duck) [10]	686	Distorted Octahedral	2.35

hTf: human serum transferrin, 2N: N-lobe only, rTf: rabbit transferrin, oTf: ovotransferrin

[a] Terminal sialic acid residues removed. [b] Glycan chains not defined.

However, the crystals are often difficult to handle and the X-ray analysis somewhat challenging. Numerous attempts to alter the crystallisation conditions to try and improve upon the quality of diffraction patterns have been met with only partial success. A low resolution analysis of rabbit serum transferrin in 1979 showed the bilobal structure of the molecule [11] but more complete details of the structure emerged with the publication of the structure of human lactoferrin in 1987 [12]. The structure of rabbit serum transferrin soon followed at a resolution of 3.3 Å [8],

confirming information already gained. More recently the crystal structure of diferric porcine transferrin at a resolution of 2.15 Å has been published [13]. It has been shown by many workers that transferrins can be proteolytically cleaved to give half-molecular-weight fragments corresponding to individual lobes with each containing a single iron-binding site [7]. As the glycan chains are on the C-lobe of human serum transferrin, and the N-lobe fragments are not glycosylated, this eliminates any problems during crystallisation that may be due to glycosylation. In some cases further cleavage can occur to produce stable quarter-sized fragments (half lobe, single domain) which can bind iron [14, 15]. It was therefore believed that crystallisation of these fragments might give rise to better-ordered, more closely packed crystals which would then give higher resolution diffraction patterns and hence finer details of protein structure. In some cases mutants of transferrins and transferrin fragments have been crystallised providing information on the binding of metals to the protein [16, 17].

The structure of an iron-containing half N-lobe fragment (39 kDa) of rabbit transferrin [18] was not found to be significantly altered by proteolysis and it is thought that this may be due to the fragment being a stable structural unit which can fold in an independent manner. The environment and hydrogen bonding of the anion to Fe^{3+} confirmed that the anion bound is carbonate and not bicarbonate. Further, the residues surrounding the anion (Asp63, Gly65, Tyr95, Thr120, Arg124, Ser125, Ala126, Gly127, Tyr188 and His249) are conserved in all transferrins [19, 20] and the attachment of the carbonate anion is a general feature in all members of the transferrin family. An exception to this, however, is the C-lobe of melanotransferrin (a membrane bound protein) [21], where Thr120 and Arg124 have been replaced by

Ala and Ser respectively, and also Asp63 has been substituted by a Ser residue.

4.1.2.1 Structure of Transferrin

All the transferrins with the exception of fish transferrin are glycoproteins [22, 23]. The polypeptide folding is very similar for all proteins of the transferrin family. The polypeptide chain is folded into two globular lobes representing the N-terminal and the C-terminal halves which are known as the N- and C-lobe respectively. Human serum transferrin has two bi-antennary carbohydrate chains, both on the C-lobe attached to asparagine residues (Asn413 and Asn611) [23, 24]. The structure of these are shown in Figure 1.2, Chapter 1. The polypeptide chain of human transferrin contains 678 amino acids, with two glycan chains each of a molecular weight of 2207 Da, giving an overall molecular weight of 79, 550 Da [25]. When residues 1-336 are aligned with residues 337-678 the two sequences are 40% identical and those residues that are not identical are similar in chemical nature. These similar regions form the two Fe-binding lobes of the protein [25]. When the nature of the amino acids conserved between the two domains is analysed, a large portion appears to be of potential structural significance such as cystines, glycines and hydrophobic residues. This could reflect the preservation of a similar three dimensional structure in two domains. Some conserved residues are likely to have a functional significance.

There are some differences between the NH_2-terminal (N) and COOH-terminal (C) lobe. The N-lobe contains fewer disulfide bonds than the C-lobe (8 compared to 11), whereas the C domain is home to both glycosylation sites of human transferrin [25]. Within each lobe there is a further subdivision into two separately folded domains.

The cleft separating the two domains of each lobe contains the metal binding site. Each domain is made up of a mixed β-sheet overlaid with α-helices. This is important since the N-termini of many helices are directed toward the central binding cleft and the partial positive charges they carry may help to attract anions to the binding cleft. Two extended β-strands run behind the iron site to act as a backbone which is vital to the conformational change during metal ion binding [24].

4.1.2.2 Metal Co-ordination

The iron co-ordination is distorted octahedral with ligands provided by four amino acid side chains from the protein, 2 Tyr, 1 His and 1 Asp with a synergistically bound bicarbonate anion. Metal-ligand bond lengths are all around 2.0 – 2.2 Å. The bond angles show larger deviations from ideal because of the small chelate 'bite' angle of the bicarbonate anion of *ca.* 65° [23]. The involvement of tyrosine ligands is expected as indicated by the absorption band seen at 465 nm in the visible spectrum, typical of iron-phenolate interaction [26, 27]. It is this that gives rise to the orange-red colour of iron transferrin. EPR [28, 29] and NMR [30] studies have suggested metal-histidine co-ordination.

Extended X-ray absorption fine structure (EXAFS) spectroscopy can provide relatively accurate information on the metal environment. Average metal-ligand bond lengths and co-ordination numbers can be determined but oxygen cannot be distinguished from nitrogen as a ligand. The two metal sites in doubly-loaded transferrin cannot be distinguished either. However, EXAFS can provide useful information on proteins where crystallisation is very difficult as is the case with

transferrin, particularly when loaded with various metals such as manganese. Previous work in this laboratory by S. Bihari [31] on Mn-hTf has given the bond lengths shown in Table 4.2. These values suggest small differences between the bonding of iron and manganese to transferrin. Both manganese and iron have a distorted octahedral geometry but whereas with Fe(III) the co-ordination sphere is more nearly regular octahedral, Mn(III) shows a reverse Jahn-Teller distortion with two short axial bonds and four long equatorial bonds.

Table 4.2 Metal-ligand bond lengths for the N-lobe of hTf with Mn(III) or Fe(III) bound determined by EXAFS and X-ray crystallography respectively.

Mn Bond	Length (Å) [31]	Fe Bond	Length (Å) [6]
2 Mn-O/N	1.937	5 Fe-O	1.99, 1.90 (Tyr) 2.02 (Asp) 2.06, 2.24 (CO_3^{2-})
4 Mn-O/N	2.204	1 Fe-N	2.10 (His)

Further information on the geometry of metal-ligand interactions in proteins can be gained by comparing structures of metalloproteins deposited in the Protein Data Bank (PDB) and from information on small molecule complexes in the Cambridge Structural Database (CSD). Predications can then aid refinement of structures when resolution is poor. An example of predicted metal-donor distances for manganese and iron is shown in Table 4.3. If these values are compared with those shown in Table 4.2, it can be seen that the distances for Fe(III) in transferrin are quite similar to those predicted whereas the distances found with Mn(III) by EXAFS are quite different. This may be in part due to averages being used where more than one

oxidation state of the metal is given.

Table 4.3 Metal-donor distances [32]. Metal-donor target distances (Å). These values are based on distances found in the CSD.

	O water	O Asp or Glu, monodentate	O Ser or Thr	O Tyr	N His	S Cys
Mn	2.21	2.21[b]	2.25	1.88	2.19	2.35
Fe	2.09	2.01	2.13	1.93	2.08	2.27

[a] In bidentate carboxylates these values are increased by 0.11 Å. [b] Values derived from the PDB. Distances found in CSD with the use of weighted averages where distances given for more than one oxidation state or co-ordination number

Ideally the best way to investigate the binding of manganese to transferrin would be to obtain a crystal structure and then to compare this to the structures previously found for members of the transferrin family with and without iron bound.

4.2 Materials and Methods

A number of factors can affect the solubility of a protein and the rate of precipitation. These include temperature, original concentration of the protein, purity of the protein, type and concentration of additives used in the crystallisation process. The most difficult part of protein crystallography is determining the correct conditions for crystallisation of the protein being studied. A number of texts including *Practical Protein Crystallography* [1] give information and techniques for crystallisation of proteins.

4.2.1 Crystallisation Techniques

As already mentioned, crystallisation of a protein is achieved by the gradual removal of solvent from a solution containing the protein. A common method of crystallisation is by vapour diffusion whereby a droplet of protein solution containing precipitant is equilibrated with a reservoir solution containing a higher concentration of precipitant so that water preferentially evaporates from the drop. In the correct conditions, this will allow a few crystals to develop as protein and precipitant concentrations are gradually increased. Conditions can be achieved using the hanging drop and sitting-drop methods as shown in Figure 4.2. The coverslip is sealed with vacuum grease so as to create a closed system with the drop of the well. The concentrations of the precipitants in the drop are half of what they are in the well and this results in a vapour equilibration from the drop to the well. As the drop evaporates the protein becomes further concentrated until it is forced out of solution. The sitting drop technique is similar to the hanging drop except that the drop is placed on a pedestal above the well solution; this is often used for larger drops, perhaps to obtain larger crystals.

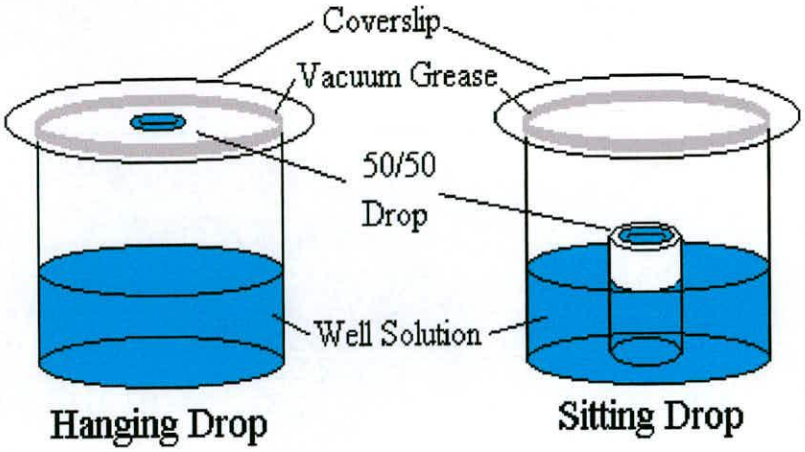

Figure 4.2 Vapour diffusion methods used for crystallisation of proteins. Both methods have a well solution containing buffered precipitate solution. The drop contains well solution and the protein to be crystallised.

Iron transferrin was prepared as described in Chapter 3, section *3.2.3*. Briefly, holo-hTf was reacted with 2 mol equivalents $Fe(NTA)_2$ to ensure full saturation of the metal binding sites. The Fe_2-hTf was set up on 24 well plates as hanging drops using similar conditions to those used previously by Zuccola [5]. Protein samples of *ca.* 1 mM (5 µl) and precipitant well solution (5 µl) made up of 20-26% PEG 400, 100 mM Na cacodylate buffer, pH 5.4 – 5.6 was used. Exact conditions can be found in Appendix G. Plates were then kept at 277 K and checked on a regular basis for signs of crystal formation. Plates were set up with similar conditions using Mn-hTf. Mn-hTf was prepared as described in Chapter 3, section *3.2.2*. Briefly, apo-hTf was reacted with $MnCl_2$ in the presence of caeruloplasmin or alternatively with $KMnO_4$. Mn-hTf with differing ratios of metal to protein were used for crystallisation experiments and details are given in the text where appropriate.

4.2.1.1 Screening Technique

Screening techniques can often be employed in order to help determine suitable conditions for crystal growth. The screening solutions are of a varying range of pH and precipitants. They take the form of a number of solutions selected from previously published works in which crystallisation of a protein has been achieved. Two 24 well plates were used to screen for conditions of Mn-hTf crystallisation. A set of solutions were obtained from Structure Screen 1, Molecular Dimensions Ltd. The conditions used can be found in Appendix H. The hanging drop method was used as in previous experiments and the drop consisted of the reservoir liquid and Mn-hTf to give protein concentrations in the drop of *ca.* 175 μM. The Mn-hTf used for screening experiments had been made by reacting molar equivalents of $KMnO_4$ with apo-hTf to produce singly and doubly loaded Mn-hTf. Plates were kept at 277 K and monitored for any signs of crystal formation or precipitation.

4.2.1.2 Seeding from Crystals

Crystals may form but may not be of a high enough quality to collect data. In this case the poor quality crystals can be used to seed better ones. Cat's whiskers provide a good tool for seeding from grown crystals. Whiskers were kindly supplied by cat owners from members of the School of Chemistry, Edinburgh University. The whiskers were cut at 1 cm intervals using a sharp sterile scalpel so that pieces of whisker of varying thickness were obtained. These were then glued onto the ends of disposable pipette tips to act as a handle. The whiskers were labelled so that later identification could be made if necessary. The whiskers were then washed in ultrapure water and 70% ethanol and allowed to air dry before use. Seeding was

done from Fe-hTf crystals that had formed but were of poor diffraction quality. Plates were set up using conditions similar to those in plates where crystals were found except that the protein concentration in the drop was reduced to approximately half or a quarter of that used previously, i.e. 0.25 and 0.125 mM Fe-hTf. The plates were then allowed to equilibrate overnight after which time the coverslips were removed ensuring that the drop was not disturbed. The cat's whisker was then used to gently stroke the already-formed crystal. The whisker was then dragged through the drop on the new plate. This procedure was repeated for each drop. Plates were then incubated at 277 K as before.

4.2.2 Data Collection

Once crystals were grown data collections were kindly carried out by Stephen Robinson and Malcolm Walkinshaw (Department of Structural Biochemistry, Edinburgh University) and using the synchrotron (SRS, Daresbury). To increase lifetime, it is often necessary to freeze the crystals. Cryo-preserved crystals often ensure longer data collection before crystal degradation. However, there are problems in ensuring the correct freezing conditions are achieved so that the crystal is not destroyed during the freezing process [33].

4.2.3 Freezing Solutions

One approach to establish freezing conditions is to use the mother liquor as the freezing solution. This can be frozen without the crystal initially to determine if the solution is suitable. If ice-rings form in the mother liquor then glycerol can be added at 10% (v/v) to see if this improves conditions. The amount of glycerol can be

increased until optimum freezing solutions are obtained. Crystals can then be picked out using an appropriately sized cryoloop (Hampton Research, UK), dipped in the freezing solution for 1-5 seconds and then immediately submerged in liquid nitrogen in a cryovial (Hampton Research, UK).

4.3 Results and Discussion

4.3.1 Crystallisation of Fe-hTf

Fe_2-hTf was prepared as described earlier. Crystallisation was carried out following the method of Zuccola [5]. Zuccola managed to crystallise monoferric transferrin with iron bound in the C-lobe; the N-lobe remained open. The transferrin used by Zuccola had been treated with neuraminidase to remove all terminal sialic acid residues. These conditions were repeated in this current work but without treatment of transferrin with neuraminidase. Reservoir conditions were set up as shown in Appendix G, plates G.1 – G4. A 5 μL volume of drop of *ca.* 1 mM Fe_2-hTf (approximately 78 mg/ml) was mixed with 5 μl drop of reservoir solution. These mixtures formed the drops which were spotted on silicanised coverslips. These were then placed over the tops of the wells and sealed with vacuum grease as shown in Figure 4.2. The plates were then incubated at 277 K. The plates were checked for appearance of crystals. After approximately six weeks ellipsoidal crystals were observed in the precipitant of wells on plate G.2. The crystals were red in colour and were visible to the naked eye. Further crystals were found on plates G.3 and G.4. All Fe-hTf crystals were red in colour with the same ellipsoidal shape. An example of the crystals formed can be seen in Figure 4.3. The crystals were quite large,

around 0.8 – 1 mm across with the absence of any flat surfaces which are normally expected for crystals. Although crystals appeared after approx six weeks on plate G.2, others formed after only two weeks on plate G.3. Some crystals appeared after several months. An example of these can be seen in Figure 4.4. Unfortunately these were found to give no better resolution.

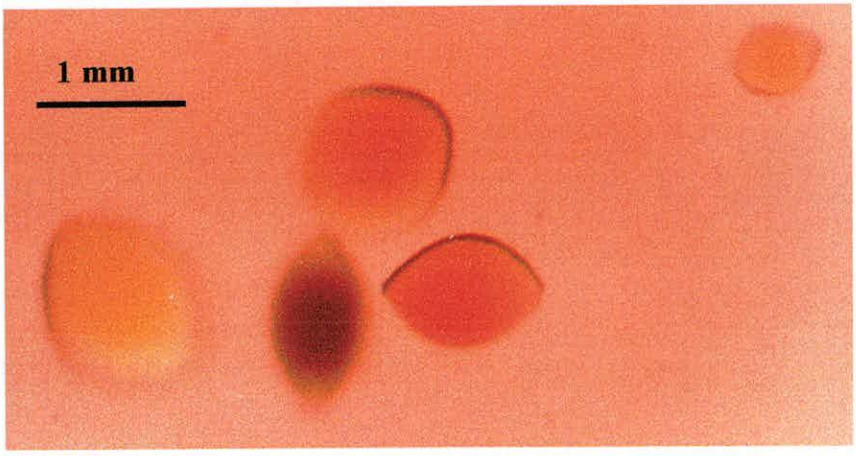

Figure 4.3 Crystals obtained from a solution of Fe_2-hTf. Crystals found in wells where there is some precipitate giving a tinted background. Approximate scale bar shown. Crystals shown were grown in 100 mM Na cacodylate, pH 5.43, 24% PEG 400 at 277 K.

Freezing conditions for these crystals were found to be the mother liquor with 30% added glycerol. Crystals were picked out using a cryoloop and transferred to a cryovial.

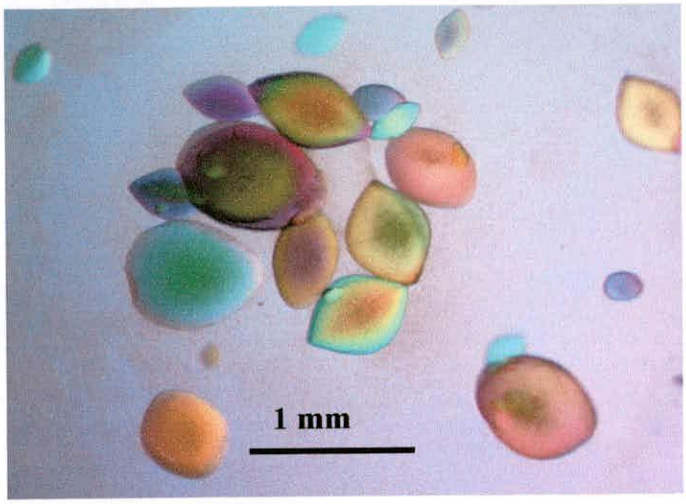

Figure 4.4 Crystals obtained from a solution of Fe_2-hTf. Crystals shown were grown in 100 mM Na cacodylate, pH 5.6, 26% PEG 400 at 277 K. Approximate scale bar shown.

4.3.1.1 Data collection and Processing

This was kindly carried out by Stephen Robinson and Prof. M. Walkinshaw of the Institute of Cell and Molecular Biology. The crystal was mounted on a Monnius 571 rotating anode X-ray generator. The X-ray source was a copper anode, wavelength of 1.542 Å. A test exposure was taken over 15 minutes with the image plate at 250 mm and with an oscillation angle of 1.5° traversed once. A repeat exposure with the image plate at 240 mm for 20 minutes showed diffraction spots to approximately 2.9 Å resolution. An example of the diffraction image of an intact Fe_2-hTf crystal collected on the home source is shown in Figure 4.5.

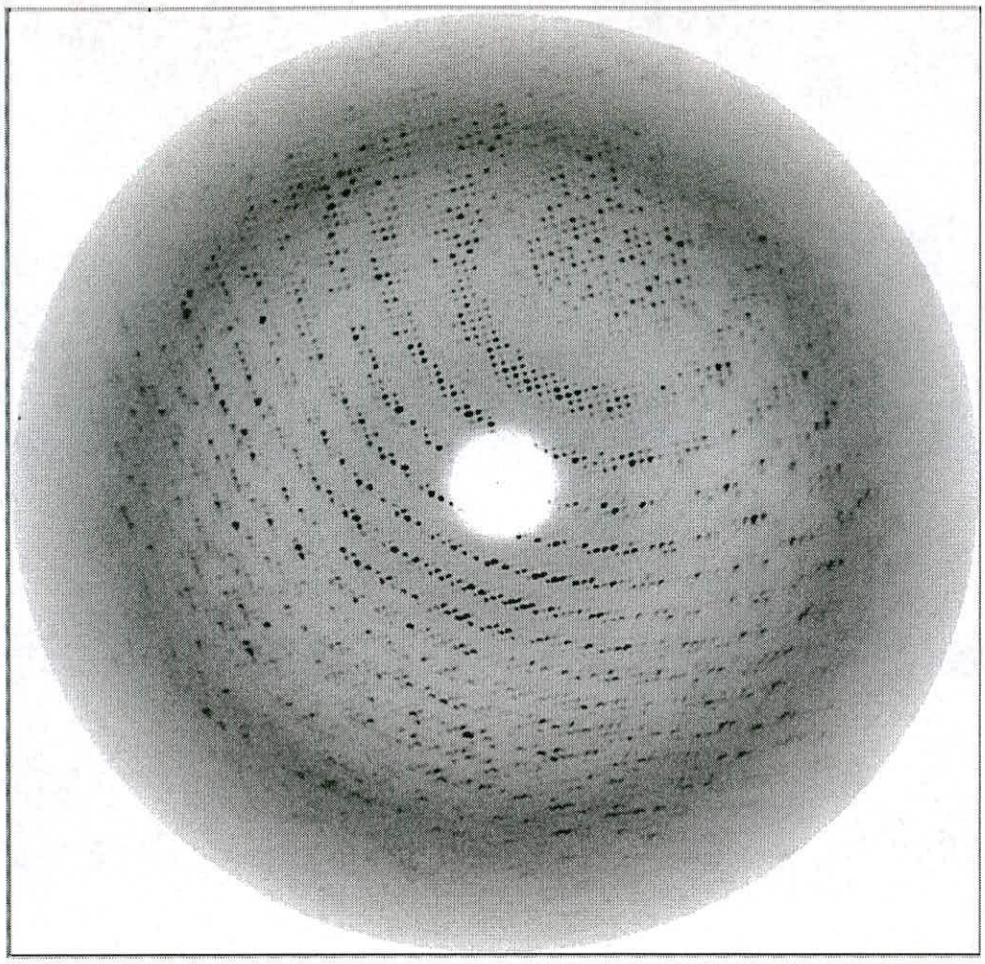

Figure 4.5 Diffraction image of Fe_2-hTf crystal taken at Edinburgh. Diffracted X-rays are seen as black spots on the film.

This image was indexed using DENZO to give the parameters shown in Table 4.4 along with the values obtained from Zuccola's crystal structure [5]. Measurements **a**, **b** and **c** are the lengths of the three axes of the parallelipiped making up the unit cell. The angle α is that made by the axis **b** and **c** around **a**. The measurements for the crystal grown here are similar to those gained by Zuccola except for **a,** which may be an indication of a different crystal packing. However, the terminal sialic acid had been removed from the transferrin Zuccola used to crystallise but no such treatment was applied to the Fe-hTf crystal used here. Further, only one iron was

bound to the transferrin that had been crystallised by Zuccola [5]. The transferrin used in this work was confirmed to be diferric in solution (by ICP-AES) but at the low pH (*ca.* 5.5) of the buffer used for crystallisation, it is likely that one Fe(III) ion has dissociated from transferrin, probably the N-lobe. Fe(III) is known to dissociate from transferrin under acidic conditions, with the C-lobe being more acid-stable [23, 34].

Table 4.4 Initial crystal parameters obtained from Fe-hTf diffraction image

Parameter	a (Å)	b (Å)	c (Å)	α (°)	β (°)	γ (°)
This Thesis	82.61	133.35	147.73	90.00	90.00	90.00
Zuccola's Thesis [5]	127.19	127.19	144.85	90.00	90.00	90.00

The diffraction patterns proved to be too close together and incomplete so data were not collected. This was largely because the diffraction spots appeared to be composed of multiple overlaying spots suggesting a split crystal. The intensity of the diffraction spots was insufficient beyond 2.9 Å so a dataset could not be collected. The crystals were taken to the SRS station 14.2 at Daresbury Laboratory for further screening. This confirmed that most crystals were split to some extent. However, the crystal was cleaved and a fragment mounted which gave reasonably good quality diffraction. An image taken at Daresbury laboratory is shown in Figure 4.6. Diffraction extended to 2.2 Å resolution and a dataset was collected and processed using *DENZO* [35] and *Scalepak* [35] to give fully scaled data 90% complete to 3.3 Å in space group $P2_12_12_1$ with 30024 unique reflections.

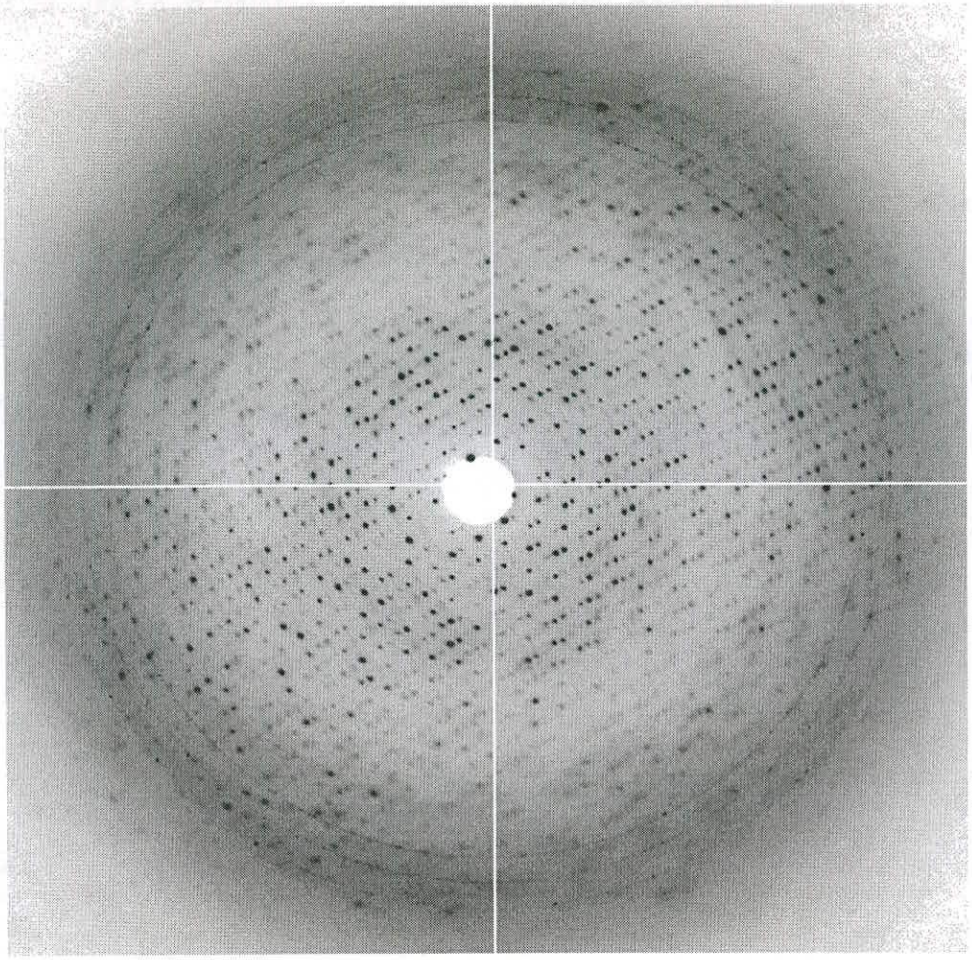

Figure 4.6 Diffraction image of Fe_2-hTf taken at the SRS, Daresbury Laboratories. A fragment of the original crystal was mounted to give good quality single crystal diffraction.

4.3.1.2 Model Building

Attempts were made by Stephen Robinson to solve the structure using molecular replacement. Full details of the procedure and computer software packages used can be found in his thesis [36]. A variety of search models were used for molecular replacement including the previously solved N-terminal half-molecule of human transferrin (PDB ID 1A8E) [6] and rabbit transferrin (PDB 1TFD) [18]. It was concluded that two molecules per unit cell were present. The main statistics from

collection and processing of data from the iron transferrin crystal are shown in Table 4.5.

Table 4.5 Statistics for Fe-hTf data collection and processing

Parameter	Value
Wavelength (Å)	0.978
Space Group (Å)	$P2_12_12_1$
Unit Cell Vector Lengths (Å)	$a = 82.77$, $b = 132.14$, $c = 146.68$
Unit Cell Angles (°)	$\alpha = \beta = \gamma = 90$
Unit Cell Volume ($Å^3$)	1604430.375
Estimated Water Content (%)	50.5
Resolution Range (Å)	100 – 2.988
No. of Measurements	550967
No. of Unique Deflections	33320
Completeness (%)	90
R_{merge}	14.9
Average I/σ	4.6

Further modelling was carried out using a previous human transferrin model kindly made available by Dr H. J. Zuccola, Harvard University Medical School. However, the structure was for a singly loaded Fe-hTf molecule with Fe^{3+} bound in the C-lobe. Unfortunately the deficiencies in the dataset due to poor crystal quality resulted in no solution of the crystal structure.

The rather odd shape and lack of flat surfaces suggests disorder of the crystals and helps explain the relatively low resolution.

Glycoslylation levels may differ between molecules within a sample, potentially promoting disorder in crystal packing. This may be overcome by treatment with

neuraminidase as was used by Zuccola [5] to remove the terminal sialic acid from the protein.

The unusual ellipsoidal shape of the Fe-hTf crystals suggests a disordered growth phase following initial nucleation and resulting in poorly ordered crystals. The transferrin supplied by Sigma was washed with KCl to remove low molecular weight impurities prior to use, as described in Chapter 3, section *3.2*. However, the mixture may not be entirely homogenous. Prior to further crystallisation studies it may be necessary to develop an HPLC technique to ensure a homogenous mixture. It is possible that some of the iron may be released from the protein during the crystallisation process thus contributing to the lack of homogeneity. The dissociation of Fe(III) is due to the acidic pH of the crystallisation process, as discussed earlier. Further, lack of bicarbonate in the crystallisation process may result in lobe opening and hence release of the iron.

4.3.1.3 Seeding of Crystals

Seeding of crystals was carried out using Fe-hTf crystals already obtained. A plate was set up using the conditions shown in Appendix G, plate G.5. Briefly Fe-hTf was used to give a concentration of 0.26 or 0.128 mM in the drop. The reservoir solution contained PEG 400 at 20 – 26 % with 100 mM sodium cacodylate buffer at pH values of 5.4, 5.5 and 5.6. These were a repeat of the conditions used to grow crystals previously (see Section 4.2.1) but using a lower concentration of Fe-hTf. The plate was kept at 277 K and checked for crystal growth. Unfortunately no crystals formed over a period of eight weeks. This may be due to the lower protein

concentration. Crystals may have required a longer time period to form.

4.3.2 Crystallisation of Mn-hTf

Mn-hTf was prepared as described previously in Chapter 3, Section *3.2.2.* Attempted crystallisation of Mn-hTf was carried out using Mn-hTf produced by loading of apo-transferrin using $MnCl_2$ in the presence of caeruloplasmin or by using $KMnO_4$. Similar conditions were used to those for Fe-hTf in the first attempt to crystallise Mn-hTf, as described in Appendix G, plate G.1. A 5 µl volume of drop of *ca.* 1 mM Mn_2-hTf (approximately 78 mg/ml, which had been prepared using $MnCl_2$) was mixed with 5 µl drop of reservoir solution. The reservoir solution was made up of PEG 400 at 20 – 26 % and 100 mM sodium cacodylate at pH 5.6. These mixtures formed drops which were spotted onto silicanised coverslips. These were then placed over the tops of the wells and sealed with vacuum grease as shown in Figure 4.2. The plates were then incubated at 277 K and were checked for appearance of crystals over a period of 3 months. Unfortunately no crystals formed just a precipitate within 3 weeks. Another plate was set up using the same conditions except with a range of pH values of 5.4 – 5.6. The conditions can be found in Appendix G, plate G.6. The Mn-hTf used had been prepared using $KMnO_4$. Precipitate formed in most of the wells but some crystals had formed after a period of *ca.* eight weeks. They were of similar shape to those seen for Fe-hTf but were pale brown in colour rather than red. An image of the crystals is shown in Figure 4.7 where the high level of precipitate is clearly visible.

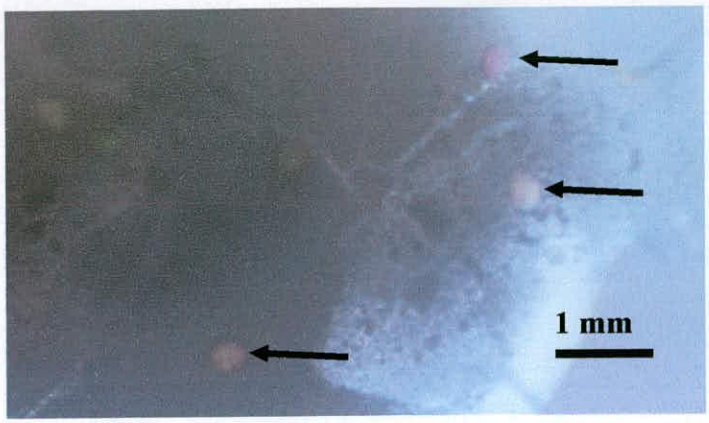

Figure 4.7 Crystals of Mn-hTf. Crystals found in wells where there is much precipitate. Crystals shown grown in 100 mM Na cacodylate, pH 5.6, 26 % PEG 400 at 277 K. Arrows indicate crystals. Approximate scale bar shown.

These crystals took much longer to appear and were much smaller than the Fe-hTf crystals found being approximately 0.3 mm in length. A diffraction pattern for one of these crystals found is shown in Figure 4.8. The Mn-hTf crystals did not diffract so no further work could be carried out on them. The Mn-hTf that had been used was found to have a ratio of 3 Mn: 1 hTf by UV/Vis spectroscopy and ICP-AES. The possibility of more than two manganese ions being bound to a transferrin molecule is discussed in Chapter 3 where experiments showed that this could be achieved, although where the extra manganese binds and if it is as Mn(III) is still yet to be determined. The manganese ions may form a cluster which then binds to transferrin. This may then greatly influence the growth of crystals and the necessary conditions required. Further, the Mn-hTf produced using $KMnO_4$ may not be homogenous which would again greatly affect the growth of crystals.

The crystallisation process used quite acidic conditions, in the region of pH 5.5. Results of the experiment detailed in Section 3.3.8 show that Mn(III) dissociates

from transferrin in a manner similar to that seen with Fe-hTf. It is likely that at the pH used for these crystallisation experiments, only one Mn(III) is bound to transferrin. The lack of bicarbonate in the conditions used may also contribute to dissociation of Mn(III). These factors could contribute to lack of success of crystallisation due to a heterogenous solution of Mn-hTf.

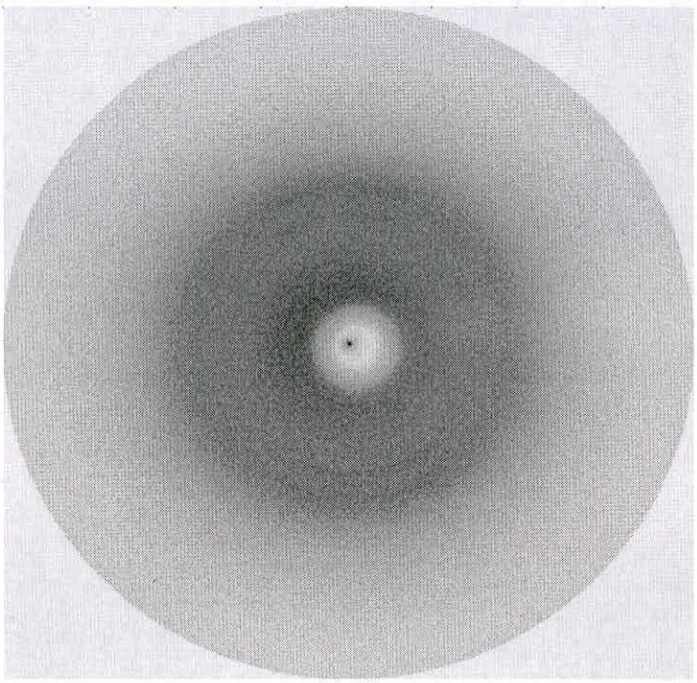

Figure 4.8 Diffraction image of Mn-hTf crystal taken at Edinburgh. There is an absence of black spots on the film showing that the crystals did not diffract.

4.3.2.1 Screening Technique

A crystal screen was set up in order to try to optimise the crystallisation conditions required for Mn-hTf. A screen containing fifty solutions was purchased (Structure Screen 1, Molecular Dimensions Ltd., UK). The composition of the solutions used are given in Appendix H. Of each solution, 1 ml was used as the reservoir solution and a hanging drop set up using 5 µl of the reservoir solution and 5 µl Mn-hTf. Two

screens were set up on 24 well plates as before using Mn-hTf that had been loaded using $KMnO_4$ to give 1 and 2 metals loaded onto the transferrin as determined by UV/Vis spectroscopy and ICP-AES. The Mn-hTf was used at a concentration of *ca.* 0.15 mM in the drop. A full list of the solutions used is shown in Appendix H with the results. Unfortunately no evidence of crystal formation was found, with only precipitate forming in some of the wells with possible aggregation seen with one of the solutions. This was the case for both Mn-hTfs used in the screening test. Again, the problems may arise from the heterogeneity of the Mn-hTf used.

4.4 Conclusions

The disordered growth phase suggested by the unusual shapes of the Fe-hTf crystals needs to be overcome before good X-ray data can be obtained. Although the transferrin used is of high purity it may be necessary to subject the protein to further purification after metal loading in order to achieve a greater homogeneity. The development of a high performance liquid chromatography (HPLC) method may prove beneficial particularly in the case of Mn-hTf where use of $KMnO_4$ may result in a mixture of Mn-hTf with varying loading and variable modification of amino acid side chains (e.g. oxidation of methionine to the sulfoxide and sulfone). This may then reduce stress in the crystals.

It may also be worthwhile to treat all transferrins with neuraminidase to remove the terminal sialic acid from the protein. Alternatively, treatment of proteins with endoglycosidase F has shown to remove all glycan chains from proteins [37]. Again, HPLC methods may be useful in then separating protein that has had all glycan chains removed or just its terminal sialic acid residues from any remaining protein

which has not to achieve a homogenous mixture. This may allow the formation of an ordered crystal lattice which should produce crystals of a higher quality. Deglycosylated transferrin has not been shown to behave differently to glycosylated protein in biological assays [38, 39] therefore the only effect would be to aid crystallisation. Refinement of conditions and seeding failed to yield better quality crystals, although it may take longer than the time available in this present study for crystals to form from seeding. Alternatively, better crystals may be grown by collecting already formed crystals, re-dissolving them and allowing to grow under refined conditions.

Mn-hTf crystals grew only in conditions similar to those required for growing Fe-hTf crystals suggesting these are the best conditions. However, the crystals were not of very good quality and took a considerable length of time to grow so these conditions may need to be refined although it is a good starting point. Further, no crystals formed in the screening solutions suggesting the current conditions are close to optimum.

The current conditions used to crystallise transferrin are acidic (pH *ca.* 5.5) which is known to result in dissociation of Fe(III) from the N-lobe. The results shown in Section 3.3.8 show that Mn(III) also dissociates from transferrin under acidic conditions, although it is not possible to say which lobe loses Mn(III) first. Therefore in these crystallisation experiments, any crystals that form are likely to have only one lobe of transferrin occupied by metal. Also, the lack of carbonate in these conditions may also contribute to loss of metal from the protein.

Within any metal-donor atom combination, the co-ordination number and its oxidation state (spin state) of the metal may affect the bond distance, the chemical

nature of the ligand, in particular its charge and also can affect other surrounding ligands around the metal atom. This may be the case with Mn-hTf with regards to the chemical and physical behavioural differences compared with Fe-hTf. The EXAFS data have shown there is a slight difference in the metal binding site of transferrin when Mn(III) is bound rather than Fe(III). However, this may not have such an effect to warrant entirely different growth conditions for crystallisation. Further, loading transferrin with Mn(III) from different sources such as $MnCl_2$ and $KMnO_4$ may also affect transferrin and its behaviour and it may not be until a crystal structure is solved that these differences become clear. From the evidence in Chapter 3 it seems likely that the addition of $KMnO_4$ to transferrin may also result in oxidation of the protein, in particular the methionine residues. This alteration of the protein structure and perhaps the chemical nature of the residues in the protein may then alter the crystallisation conditions required and make successful crystallisation much more difficult to achieve. The glycan chains may also be targets of oxidation so removal of these may be beneficial when attempting to crystallise Mn-hTf that has been produced using $KMnO_4$. Further, manganese may bind to transferrin at sites other than the two identified metal binding sites or may bind as a cluster when loaded using MnO_4^-. This may result in different crystallisation conditions being required when different sources of manganese are used to produce Mn-hTf.

All of the conditions mentioned above would contribute to the difficulty in crystallising transferrin. While some crystals have formed under the conditions used different forms of the protein, particularly in the case of Mn-hTf produced using $KMnO_4$, may pack onto the crystal resulting in stress and disorganisation. Once these problems are resolved better crystals should be obtainable.

4.5 References

1. D.E. McRee, *Practical Protein Crystallography*, Second Edition ed. Academic Press **1999**.

2. http://www-structmed.cimr.cam.ac.uk.

3. B. Magdoff-Fairchild and B.W. Low, *Arch. Biochem. Biophys.*, **1970**, 138: 703.

4. L.J. DeLucas, F.L. Suddath, R.A. Gams, and C.E. Bugg, *J. Mol. Biol.*, **1978**, 1223: 285-286.

5. H.J. Zuccola, PhD Thesis, 1992, Georgia Institute of Technology, Atlanta.

6. R.T.A. MacGillivray, S.A. Moore, J.C. Chen, B.F. Anderson, H. Baker, Y. Luo, M. Bewley, C.A. Smith, M.E.P. Murphy, Y. Wang, A.B. Mason, R.C. Woodworth, G.D. Brayer, and E.N. Baker, *Biochemistry,* **1998**, 37: 7919-7928.

7. P.D. Jeffrey, M.C. Bewley, R.T.A. MacGillivray, A.B. Mason, R.C. Woodworth, and E.N. Baker, *Biochemistry,* **1998**, 37: 13978-13986.

8. S. Bailey, R.W. Evans, R.C. Garratt, B. Gorinsky, S. Hasnain, C. Horsburgh, H. Jhoti, P.F. Lindley, A. Mydin, R. Sarra, and J.L. Watson, *Biochemistry,* **1988**, 27: 5804-5812.

9. H. Kurokawa, B. Mikami, and J. Hirose, *J. Mol. Biol.*, **1995**, 254: 196-207.

10. A. Rawas, H. Muirhead, and J. Williams, *Acta Crsytallogr.*, **1996**, D52: 631-640.

11. B. Gorinsky, C. Horsburgh, P.F. Lindley, D.S. Moss, M. Parkar, and J.L. Watson, *Nature,* **1979**, 281: 157-158.

12. B.F. Anderson, H.M. Baker, E.J. Dodson, G.E. Norris, S.V. Rumball, J.M. Waters, and E.N. Baker, *Proc. Natl. Acad. Sci. USA,* **1987**, 84: 1769-1773.

13. D.R. Hall, J.M. Hadden, G.A. Leonard, S. Bailey, M. Neu, M. Winn, and P.F. Lindley, *Acta Crsytallogr.,* **2002**, D58: 70-80.

14. R.W. Evans and A.D. Madden, *Biochem. Soc. Trans.,* **1984**, 12: 661-662.

15. D. Legrand, J. Mazurier, M.H. Metz-Boutigue, J. Jolles, P. Jolles, J. Montreuil, and G. Spik, *Biochim. Biophys. Acta,* **1984**, 787: 90-96.

16. D. Nurizzo, H.M. Baker, Q. He, R.T.A. MacGillivray, A.B. Mason, R.C. Woodworth, and E.N. Baker, *Biochemistry,* **2001**, 40: 1616-1623.

17. H.M. Baker, A.B. Mason, Q. He, R.T.A. MacGillivray, and E.N. Baker, *Biochemistry,* **2001**, 40: 11670-11675.

18. R. Sarra, R. Garratt, B. Gorinsky, H. Jhoti, and P.F. Lindley, *Acta Crsytallogr.,* **1990**, B46: 763-771.

19. M.H. Metz-Boutigue, J. Jolles, J. Mazurier, F. Schoentgen, D. Legrand, G. Spik, and P. Jolles, *Eur. J. Biochem.,* **1984**, 145: 659-676.

20. B.F. Anderson, H.M. Baker, G.E. Norris, D.W. Rice, and E.N. Baker, *J. Mol. Biol.,* **1989**, 209: 711-734.

21. T.M. Rose, G.D. Plowman, D.B. Teplow, W.J. Dreyer, K.E. Hellstrom, and J.P. Brown, *Proc. Natl. Acad. Sci. USA,* **1986**, 83: 1261-1265.

22. A. Dautry-Varsat, *Biochimie,* **1986**, 68: 375-381.

23. E.N. Baker, *Adv. Inorg. Chem.,* **1994**, 41: 389-463, and references therein.

24. H. Sun, H. Li, and P.J. Sadler, *Chem. Rev.,* **1999**, 99: 2817-2842.

25. R.T.A. MacGillivray, E. Mendez, S.K. Sinha, M.R. Sutton, J. Lineback-Zins, and K. Brew, *Proc. Natl. Acad. Sci. USA,* **1982**, 79: 2504-2508.

26. R.C. Warner and I.J. Weber, *J. Am. Chem. Soc.*, **1953**, 75: 5086-5094.

27. B.P. Gaber, V. Miskowski, and T.G. Spiro, *J. Am. Chem. Soc.*, **1974**, 96: 6868-6873.

28. J.L. Zweir and P. Aisen, *J. Biol. Chem.*, **1977**, 252: 6090-6096.

29. E.W. Ainscough, A.M. Brodie, S.J. McLachlan, and V.S. Ritchiw, *J. Inorg. Biochem.*, **1983**, 18: 103-112.

30. B.M. Alssaadi, R.J.P. Williams, and R.C. Woodworth, *J. Inorg. Biochem.*, **1981**, 15: 1-10.

31. S. Bihari, PhD Thesis, 2002, University of Edinburgh, Edinburgh.

32. M.M. Harding, *Acta Crsytallogr.*, **2001**, D57: 401-411.

33. J.M. Harp, D.E. Timm, and G.J. Bunick, *Acta Crsytallogr.*, **1998**, 54: 622-628.

34. C.A. Smith, E.W. Ainscough, H.M. Baker, A.M. Brodie, and E.N. Baker, *J. Am. Chem. Soc.*, **1994**, 116: 7889-7890.

35. Z. Otwinowski and W. Minor, *Methods Enzym.*, **1997**, 276: 307-326.

36. S. Robinson, MSc Res, 2001, University of Edinburgh, Edinburgh.

37. H.M. Baker, C.L. Day, G.E. Norris, and E.N. Baker, *Acta Crsytallogr.*, **1994**, D50: 380-384.

38. A.B. Mason, M.K. Miller, W.D. Funk, D.K. Banfield, K.L. Savage, R.W.A. Oliver, B.N. Green, R.T.A. MacGillivray, and R.C. Woodworth, *Biochemistry,* **1993**, 32: 5472-5479.

39. G. Spik, B. Coddeville, and J. Montreuil, *Biochimie,* **1988**, 70: 1459-1469.

Chapter 5 Effects of Manganese Transferrin on Hepatocytes

5.1 Introduction

Work reported in this thesis and that of Bihari [1] has shown that Mn is able to bind to the iron transport protein transferrin. Therefore, the next step is to determine if Mn-hTf can be used as a transport mechanism for Mn delivery to hepatocytes. Mn is known for its redox chemistry therefore it is of interest to observe the effects that Mn may have on hepatocytes, in particular on the mitochondria which is where Mn is found in high concentrations [2].

There is little information on the pharmacokinetics of manganese. Absorption appears to occur through the small intestine by both active transport and passive diffusion mechanisms. Mn ions are transported via the portal circulation to the liver. In what forms manganese is transported to the liver, for example bound to albumin or $alpha_2$-macroglobulin or as aqua manganese complexes., is also unclear. A fraction of Mn is taken up by hepatocytes and a fraction is transported by the systemic circulation to the various tissues of the body. Absorbed Mn is excreted *via* the billiary route with very little manganese being excreted in the urine. Tissues with high levels of mitochondria tend to have high levels of manganese, as the manganese concentration of mitochondria is higher than that found in the cytoplasm [3].

Using a homologous competition of ^{54}Mn-transferrin with Mn-transferrin and ^{65}Zn-transferrin with Zn-transferrin, it was found that there are receptors which bind Mn-

transferrin and Zn-transferrin on the plasma membrane of lactating mouse mammary gland cells confirming that the same receptor accepts all three (Fe, Mn and Zn) metals from transferrin [4].

5.1.1 ***Hepatocyte Iron Metabolism***

The liver is a major storage site for iron and is a principal site of synthesis of transferrin, the transport protein for iron. As a result the liver has a major function in the maintenance of whole body iron homeostasis. Under normal conditions, storage iron is found mainly in hepatocytes with small quantities found in Kupffer cells [5]. Hepatic iron totals *ca.* 0.4 g and is localised mainly in the hepatocytes where it can be found in the form of ferritin, haemosiderin, haem and transferrin-bound iron [5]. The hepatocyte synthesises and secretes transferrin into the plasma where it circulates and delivers iron from absorptive sites in the small intestine to storage sites in the liver and reticuloendothelial system and to sites of utilisation, principally the bone marrow, muscle and the liver [5].

Hepatocytes take up transferrin-bound iron by two mechanisms. One pathway consists in the binding of transferrin to high affinity receptor sites and uptake *via* receptor-mediated endocytosis. The other mechanism involves low affinity, non-specific and non-saturable internalisation of transferrin-bound iron, probably through pinocytosis, adsorptive endocytosis or low affinity binding sites [6].

Changes in hepatic storage are regulated by a complex series of interactions in the liver including availability of iron, storage of the protein ferritin, haem synthesis, release of iron from transferrin and circulating iron-bound transferrin [5].

The mechanisms of delivery of iron to mitochondrial membranes and uptake into mitochondria are still unclear. Within mitochondria, iron is found in three biochemical forms: approximately one third is found in haemoproteins such as the cytochromes, a third is located in iron-sulfur clusters found in enzymes within the inner and outer membrane such as succinate dehydrogenase and cytochrome *c* and the remaining third is thought to represent a mitochondrial transit pool that provides iron for incorporation into haem [7].

5.1.2 Manganese Uptake

Using kinetic studies, Bertini *et al* [8] suggested that manganese is released from transferrin in the same manner as iron. Manganese transferrin binds to the transferrin receptor on cells and is internalised by receptor mediated endocytosis [9]. The endosome vesicles probably undergo acidification as seen with the internalisation of iron transferrin whereby Mn^{3+} is released by transferrin. The Mn^{3+} generated in the endosomes is thought to be reduced to Mn^{2+} prior to its transportation across the endosomal membrane into the cell *via* the transport protein DMT1 (also referred to as Nramp2 or DCT1). A proton gradient across the endosomal membrane is thought to be the force behind metal ion/proton transport out of the endosomes by DMT1. Manganese can also be directly taken up into the cell by a transferrin-independent mechanism requiring DMT1 [9, 10]. DMT1 has a broad substrate specificity and is likely to be the transmembrane protein responsible for the uptake of many divalent cations including Mn^{2+}, Cd^{2+}, Zn^{2+}, Co^{2+}, Ni^{2+}, Pb^{2+} and Cu^{2+} [11].

Thermodynamic modelling of Mn(II) in serum suggests it exists in several forms, including an albumin-bound species (84%), as a hydrated ion (6.4%) and in 1:1

complexes with HCO_3^- (5.8%), citrate^{3-} (2.0%) and other small molecular weight ligands [12]. Similar modelling of Mn(III) in serum predicts that it is almost 100% bound to transferrin [12, 13]. Diffusion and transport of substances across membranes depend on the size, charge and shape of the molecule.

Finley [14] has shown that the hepato-carcinoma cell line Hep-G2, like isolated rat hepatocytes, has an efficient homeostatic mechanism for uptake and regulation of Mn, and that the uptake of Mn is by a facilitated mechanism. Galeotti *et al* [15] obtained evidence for three Mn uptake systems in rat liver slices incubated *in vitro*: a low affinity system suggested to be receptor-operated Ca channels, a system whereby Mn entered the cell *via* the Ca/Na exchange pump of medium affinity and a third Mn-specific high affinity system.

Chua *et al* [16] have found three manganese transport mechanisms in rabbit erythroid cells: two for Mn^{2+} (high and low affinity processes) and one for manganese bound to transferrin. Manganese metabolism has been reported to be abnormal in the Belgrade rat which is characterised by defects in transferrin metabolism [17]. Thus there appears to be evidence that the plasma and transmembrane transport of Mn and Fe share common mechanisms [17, 18].

Once manganese enters the liver it can enter one of several pools. A high percentage enters the lysosome pool, from which it is transferred to the bile canaliculus. A second pool of manganese is associated with the mitochondria; the uptake and release of manganese by mitochondria is thought to be linked to calcium flux, and manganese may move through calcium channels. A third pool is found in the nuclear fraction of the cell although its role is poorly understood. A fourth pool is

incorporated into, or associated with, newly synthesised manganese proteins. A fifth pool is free Mn^{2+} [2]. Under physiological conditions, Mn in serum would be surrounded by potential ligands and so very little would be expected to exist as the free (aqua) ion.

The rate of uptake of Mn by enterocytes within the intestinal lining and its overall hepatic elimination in bile tightly regulates systemic Mn levels [9]. A complex series of events including uptake, retention and release, regulates cellular levels of Mn. However, manganese deposition can be influenced by iron intake since both metals appear to be transported by the same protein in serum and other cellular transport systems, thus complicating the process further [9]. Manganese is supplied to the brain as Mn(II) and Mn(III) *via* both the blood-brain and the blood-cerebrospinal fluid barriers and transferrin is thought to be involved in these processes [19]. It is unclear whether there is a predominant Mn species crossing the blood-brain barrier (BBB). Crossgrove *et al* [20] show evidence for carrier mediated transport of Mn(II) by DCT1, Mn-hTf and manganese citrate across the BBB. Transporters for Mn citrate have yet to be confirmed although likely candidates include a monocarboxylate transporter (MCT) and/or members of the organic anion transporter polypeptide (OATP) or ATP-binding cassette (ABC) superfamilies [17].

The transport mechanism for Mn may depend upon the tissue itself. The liver is known to have a high number of transferrin receptors [6, 21] so transferrin may provide a favourable transport mechanism for delivery of manganese to hepatocytes. This allows delivery of manganese to hepatocytes in a bound non-toxic form where it

can then be removed using a method already established for iron and then incorporated into enzymes such as SOD. Further, work on the Belgrade rat supports this as a mode of transport.

5.1.3 Manganese Toxicity

Chronic exposure to metals such as iron, lead, manganese and chromium has been linked to the development of severe and often irreversible, neurological disorders. This neurotoxicity is most probably due to the transport of these metals across the blood-brain barrier and their uptake into targeted cells within the brain. Once inside the brain biochemical changes caused by the metals may lead to apoptosis and/or necrosis [9]. Owing to the increased use of manganese as the petrol additive, methylcyclopentadienyl manganese tricarbonyl (MMT), the metal and its potential health risks are being studied more closely. Exposure to high environmental levels of Mn produces a syndrome known as manganism which displays symptoms similar to that seen in Parkinson's disease [9]. Mn is normally eliminated in bile and anything that compromises normal liver function potentially can lead to Mn intoxication. The mechanism by which Mn exerts its cytotoxicity is still under discussion but it is likely that both apoptosis and necrosis are responsible [10].

One mechanism by which manganese is thought to exert its toxicity is by alteration of mitochondrial function. Manganese promotes calcium accumulation in mitochondria by inhibiting sodium- dependent and independent exporters thus activating the permeability transition pore (PTP), which eventually leads to disruption of mitochondrial function [22, 23]. Gavin *et al* [24] have shown that

uptake of Mn^{2+} into mitochondria leads to inhibition of oxidative phosphorylation and thus decreased cell respiration. During their studies there was no evidence of oxidative stress from the metal ion. Inhibition of oxidative phosphorylation would have the greatest effect in cells experiencing a constant high demand for ATP. Cells with high energy requirements include the central and peripheral nervous system and the liver which both contain many mitochondria.

5.1.4 Mitochondrial Transmembrane Potential

The mitochondrial transmembrane potential, which is essential for mitochondrial function, results from the asymmetric distribution of protons and other ions on both sides of the inner mitochondrial membrane. This gives rise to chemical, (pH) and electric gradients which are essential for mitochondrial function [25]. The inner side of the inner mitochondrial membrane is negatively charged. As a result, cationic lipophilic fluorochromes such as chloromethyl-X-rosamine (CMXRos) distribute to the mitochondrial matrix [25]. These dyes can then be used to measure variations in the mitochondrial membrane potential. The extent of dye uptake is dependent upon the size of the membrane potential; dissipation of the membrane potential results in a decrease in cell-associated fluorescence. This can be useful when investigating the decrease in membrane potential of mitochondria prior to apoptosis, irrespective of the stimulating factor.

5.1.5 Cell Adhesion and Divalent Cations

Cell adhesion receptors are important in maintenance and promotion of cell anchorage, migration and differentiation. Many of the known adhesion receptors

belong to the integrin family. Gailit and Rouslahti [26] have shown that Mn^{2+} increases the binding of the fibronectin receptor to fibronectin compared with Ca^{2+} and Mg^{2+}, suggesting that Mn^{2+} is able to compete with Ca^{2+} for the same cation-binding sites.

An insoluble meshwork of proteins and carbohydrates that fill most of the intercellular spaces make up the extracellular matrix (ECM). The interaction of cells with the adhesive proteins in the ECM not only supports proper attachment of the cells to maintain tissue and organ integrity, but also plays an important role in the morphological and functional development of the cells. Integrins are a superfamily of membrane receptors for a variety of ECM proteins. They are heterodimers made up of an α and β subunit. The integrin receptor for several ECM proteins including vitronectin, fibronectin and thrombospondin recognise a tripeptide sequence Arg-Gly-Asp (RGD) in the ligand molecules. This RGD-dependent binding has been shown to require the presence of divalent cations, particularly Mn^{2+} [27]. Changes in the binding characteristics of integrins are thought to be responsible for the Mn^{2+}-stimulated cell-substrate adhesion and cell spreading seen in a variety of cell culture systems [28-32]).

5.1.6 ***WRL-68 Cells***

Studies with isolated rat hepatocytes have elucidated some major events in hepatocytic uptake of Mn. However rats and swine differ in their ability to secrete Mn into the bile [33], so rat hepatocytes may be a poor model in which to study human hepatic Mn uptake and metabolism. Therefore the development of a model for hepatocyte uptake and metabolism of Mn from a human cell line would be of

great benefit. Although the human hepatic cell line WRL-68 is of foetal origin, it still exhibits many liver specific functions [34]. WRL-68 cells are not grown in human serum and therefore should not have the added complication of requiring endogenous human transferrin. However, some bovine transferrin may be present in the growth medium used to cultivate the cells and so may influence metal uptake. Hamilton *et al* [35] have shown that transferrin receptors are present on four phenotypically-distinct cell lines, supporting the theory that WRL-68 cells are capable of transferrin uptake.

The work in this Chapter is concerned with the uptake of Mn from Mn-hTf by WRL-68 cells and its subsequent effects. The comparative effect of apo- Fe- and Mn-hTf on the growth, viability and mitochondrial function of WRL-68 cells is studied. The use of Trypan blue, MTT assay and Feulgan stain was used to study the cells response to treatment. As manganese is known to alter mitochondrial function, the effect of Mn-hTf on the mitochondria of the cells was also investigated using the fluorochrome CMXRos. This allows visualisation of changes in mitochondrial membrane potential. This also served as a useful stain for observing the cells following treatment.

5.2 Materials and Methods

5.2.1 ***Cell Culture***

The human hepatocyte cell line WRL-68 was used in cell experiments. The standard cell culture conditions are described in Section 2.10.1. Cell viability and number was established prior to experiments using trypan blue exclusion. A detailed

description of this is given in Section 2.10.2.

5.2.2 *Production of Fe-hTf and Mn-hTf*

Iron-free apo-transferrin of the highest grade was purchased from Sigma (catalogue number T1147) and weighed into a sample vial. It was then fully dissolved in 0.1 M KCl and transferred to a 'Centricon 30' ultrafilter and washed three times using 0.1 M KCl to remove low-molecular-weight impurities. The Centricon tube was then inverted and the purified apo-hTf collected for further use. Concentrations of apo-hTf and other hTfs were determined by UV/Vis spectroscopy using ε_{280} 93, 000 $M^{-1}cm^{-1}$ [36]. To produce Fe_2-hTf and Mn_2-hTf (herein referred to as Fe- and Mn-hTf), apo-hTf was reacted with $Fe(NTA)_2$ or $KMnO_4$ in 20 mM Hepes buffer, pH 7.4 with 10 mM bicarbonate. The solution was kept at 310 K for approximately one hour. After this time the solutions were washed using 0.1 M KCl in Centricon tubes and then collected and concentrated. ICP-AES and UV/Vis spectroscopy were then used to determine metal and protein concentrations, respectively (a more detailed description can be found in Section 3.2). The transferrins were subsequently diluted using the same medium used to grow cells (supplemented DMEM). Prior to addition to cells all solutions were filter-sterilised (0.2 μm filters).

5.2.3 *Analysis of Cellular Metal Content*

5.2.3.1 Growth of Cells Under Standard Conditions

WRL-68 cells were grown in large (175 cm^2) tissue culture grade flasks under normal conditions with supplemented DMEM (see Section 2.10.1). Once fully confluent, cells were removed using trypsin-EDTA and washed twice with PBS

which was added to the cell suspension. Cells were then pelleted using a Mistral MSE centrifuge and counted using trypan blue (see Section 2.10.2). The cell suspension was again centrifuged and the remaining pellet was then frozen and kept at 253 K. Once removed from the freezer, 5 ml of ultrapure water was added to the pellet to ensure rupture of the cells. Metal content was then determined using ICP-AES (Section 5.2.3.3).

5.2.3.2 Growth of Cells in Transferrin

Cells were seeded into large (175 cm^2) tissue culture grade flasks at an initial concentration of *ca.* 10^6 cells/ml using 1 ml per flask and medium added. Cells were then left to equilibrate overnight and medium containing apo-hTf, Mn-hTf or Fe-hTf at a concentration of 25 μM was added to the flasks. Medium alone was added to cells to act as a control. After two days, the medium was removed and kept for analysis and fresh medium applied using the same concentration of transferrins as previously. Once the cells were confluent, the medium was removed and retained for metal analysis. Cells grown in medium, apo-hTf and Fe-hTf were confluent on the fourth day. However, those treated with Mn-hTf were not, so medium was removed and kept and fresh medium containing Mn-hTf added and the cells incubated for a further two days. The cells were then harvested as before. The medium removed from the cells treated with Mn-hTf on the final day of incubation was centrifuged and a small pellet of cells was collected for metal content analysis.

Trypsin-EDTA was used to remove the cells from the layer and washed twice with PBS. The cell suspension was then centrifuged using a MSE Mistral 1000

centrifuge. The pellet was then re-suspended and a cell and viability count made using trypan blue. The cell suspension was again centrifuged and the remaining pellet was then frozen and kept at 253 K. Once removed from the freezer, 5 ml of ultrapure water was added to the pellet to ensure rupture of the cells.

5.2.3.3 Determination of Cellular Metal Content Using ICP-AES

Metal content was determined using ICP-AES. Prior to introduction of samples the machine was calibrated to detect Mn, Fe, Cu and Zn (further details are given in Section 2.3). Aqueous standard solutions were prepared from appropriate dilutions of 1000 ppm certified standard element solutions. Samples of medium, trypsin-EDTA and the growth medium aspirated from the cells were analysed without dilution. Metal concentration was calculated as mg/ml. Samples of the cells were studied as the 5 ml solution obtained from the pellet re-suspended in ultrapure water. Cellular metal content was then calculated as mg metal in 10^{10} cells.

*5.2.4 **MTT Assay of Hepatocyte Viability Following Treatment with Transferrins***

Cells were seeded at *ca.* 3 x 10^4 cells/ml in 24 well plates at 0.5 ml/well and allowed to equilibrate overnight. Apo-hTf, Fe-hTf and Mn-hTf were added to the cells at concentrations of 25, 2.5 and 0.25 μM. Medium alone was used for controls. The medium and medium containing transferrin was changed after two days and following a further two days the cells were ready for analysis.

MTT was added to the cells to give a final concentration of 1 mg/ml in the medium and the plate incubated at 310 K for 3 hours. The medium was removed and the cells were washed twice with PBS and allowed to dry completely. DMSO was then added

and 100 µl of the cells transferred to a 96 well plate, with dilution if necessary, and absorbance read at 490 nm.

This experiment was also carried out using 96 well plates where cells were seeded at *ca.* 6 x 10^3 cells/ml at 150 µl/well. In this instance all conditions were the same except the cells were left for two days following treatment, one plate had MTT at 1 mg/ml and absorbance was read directly without transfer or dilution. A second plate had the medium and medium containing transferrin replaced after two days and was left for a further two days before the MTT was added and absorbance read as for the first plate.

5.2.5 ***Evaluation of Apoptosis and Mitosis Following Treatment with Transferrins***

Cells were seeded at *ca.* 6 x 10^3 cells/ml at 150 µl/well on 96 well plates and left to equilibrate overnight. Medium was aspirated off and the cells washed with PBS. Apo-hTf, Fe-hTf and Mn-hTf were added to the cells at concentrations of 25, 2.5 and 0.25 µM. Medium alone was used for controls. After two days, the medium was aspirated off one plate and the cells washed twice with PBS and Bouins solution added to each well. A second plate had the medium and medium containing transferrin replaced and left for a further two days after which time medium was removed, cells washed and fixed with Bouins as before. Both plates were then stained with Feulgan stain as described in section 2.10.4.

Cells were seeded at *ca.* 2.5 x 10^4 cells/ml at 0.5 ml/well onto 4 well chamber slides and allowed to equilibrate overnight. Medium was then removed and cells washed with PBS. Mn-hTf made up in medium was added to the wells to give

concentrations of 25, 2.5 and 0.25 μM. Medium alone was used as a control. After two days, the medium was removed and fresh medium and transferrin added to cells. After a further two days all medium was removed and cells were washed and fixed with Bouins solution. Cells were then stained with Feulgan stain and assessed for apoptosis and mitosis.

*5.2.6 **Assessment of Mitochondrial Effect of Transferrins on Hepatocytes***

Cells were seeded at *ca.* 2.5 x 10^4 cells/ml at 0.5 ml/well onto 4-well chamber slides and allowed to equilibrate overnight. Medium was then removed and cells washed with PBS. Apo-hTf, Fe-hTf and Mn-hTf were made up in medium and added to the wells to give concentrations of 25, 2.5 and 0.25 μM. Medium alone was used as a control. After two days the medium was removed and fresh medium and transferrin added to cells. After a further two days, CMX-Ros was added to all wells to give a concentration of 100 nM and slides incubated in the dark at 310 K for 45 minutes. Slides were then protected from light from this point onwards. The medium was then aspirated and the cells washed twice with PBS and slides fixed in 4% paraformaldehyde for 10 minutes and washed again in PBS. Slides were then allowed to dry before being cover-slipped with mowiol. Slides were then assessed for any visible mitochondrial changes including depolarisation.

5.2.6.1 Induction of Mitochondrial Depolarisation

Cells were seeded at *ca.* 4 x 10^4 cells/ml at 0.5 ml/well onto 4 well chamber slides and allowed to equilibrate overnight. Medium was then aspirated, cells washed and fresh medium applied. The mitochondrial depolariser, mClCCP, was made up in

DMSO and added to the cells to give concentrations of 30, 40 and 50 mM. CMX-Ros was also added to the cells to give a concentration of 100 nM and slides were incubated in the dark at 310 K for 45 minutes. From this stage onwards the slides were protected from light. Following incubation the medium was removed and slides fixed in 4% paraformaldehyde for 10 minutes and washed again in PBS. Once dry, slides were then cover-slipped using mowiol and assessed visually for mitochondrial depolarisation.

5.3 Results and Discussion

5.3.1 Analysis of Cellular Metal Content

Due to the high numbers of cells required to allow determination of the metal content using ICP-AES (detection limits are given in Table 2.2, Chapter 2), large flasks were used to grow cells. Preliminary work was carried out to ensure there were enough cells in a large flask to allow metal detection. Unfortunately this meant that large quantities of apo and metal-loaded transferrins were required in order to obtain transferrin concentrations similar to those found in serum, 35 μM [37]. Consequently the metal determinations on cells were carried out only once. Due to limited quantities of metal-loaded transferrin available cells were incubated with 25 μM transferrin.

First, preliminary experiments were carried out. These included growing four large flasks of cells in normal medium and analysing these for Cu, Fe, Mn and Zn content. The results of the cellular metal content grown under standard conditions are given in Table 5.1 (the data for these results can be found in Appendix F, Figure F.1 and Table F.1).

Table 5.1 Average cellular metal content of 4 flasks grown under standard conditions.

Metal	Average mg metal in 10^{10} cells	Standard Deviation (±)
Cu	1.39×10^{-1}	0.013
Fe	9.61×10^{-1}	0.036
Mn	6.88×10^{-2}	0.002
Zn	5.37	0.113

The cellular metal content of the four flasks are similar with little variation between cells cultured in parallel. WRL-68 cells were also grown as previously described and cells pelleted. When the four samples were made ready for metal analysis, internal standards were added to two of the cell suspensions at concentrations of 0.01 and 0.05 ppm for each metal analysed. This was done to confirm that small increases in metal content could be detected by ICP-AES. The results in Table 5.2 (full results are shown in Appendix F, Figure F.2 and Table F.2) show that increases in metal content can be detected at the 0.01 ppm level.

Table 5.2 Cellular metal content (ppm) detected in cells grown under standard conditions and with addition of internal standards prior to analysis

Metal	Cells (average)	+ 0.01 ppm metal std	+ 0.05 ppm metal std
Cu	0.010 ± 0.0011	0.019	0.046
Fe	0.030 ± 0.0003	0.039	0.081
Mn	0.001 ± 0.0001	0.010	0.044
Zn	0.256 ±0.0014	0.264	0.291

The growth medium used for cell culture was also analysed for metal content and

again internal standards were added. These results can be seen in Table 5.3 (results also in Appendix F, Figure F.3 and Table F.3). Trypsin-EDTA was also analysed for metal content to ensure that metal levels were low. Internal standards were again added to trypsin-EDTA and analysed. The results can be found in Table 5.3 (results also shown in Appendix F, Figure F.4 and Table F.4)

Table 5.3 Metal content (ppm) detected in DMEM and Trypsin-EDTA and with addition of metal internal standards prior to analysis

Metal	DMEM (average)	+ 0.01 ppm	+ 0.05 ppm	Trypsin-EDTA	+ 0.01 ppm	+ 0.05 ppm
Cu	0.052 ±0.0054	0.057	0.085	0.0014	0.010	0.043
Fe	0.127 ±0.0028	0.134	0.174	0.012	0.023	0.069
Mn	0.001 ±0.0001	0.010	0.047	0.000	0.010	0.051
Zn	0.076 ±0.0006	0.085	0.118	0.003	0.022	0.053

5.3.1.1 Cell Numbers Following Treatment

After four days of treatment with transferrin, all cells except those treated with Mn-hTf were confluent. Cells incubated with Mn-hTf had not grown as well as the others and the medium had turned yellow in colour. This was not the case for any of the other flasks. When medium containing 25 μM Mn-hTf only was incubated there was no colour change suggesting that the colour change of the medium in the flasks containing Mn-hTf is due to a metabolic process. The medium often changes colour from red to yellow when cells are overgrown and the medium requires changing. Phenol red has a transition range of pH 6.5 to 8. Thus, the medium is red at physiological pH levels and turns yellow in acidic conditions indicating a loss of

buffering capacity due to the metabolic activity of the cells. This supports the idea of the colour change being due to a metabolic effect. It is notable that the medium did not undergo any colour change following the first two days of the cells incubation with Mn-hTf. Although there were fewer cells grown on the layer, there did not appear to be any more dead cells floating in the medium compared with the other flasks. Further, the cells that had grown on the flask surface had a dendritic-like appearance with finger like projections protruding from the cells. No change was apparent for cells incubated with medium alone, apo-hTf or Fe-hTf. Due to the cells treated with Mn-hTf not reaching confluence simultaneously with the other flasks, they were left for an extra two days, with fresh medium and Mn-hTf, to try and ensure that enough cells were obtained to carry out ICP-AES. The medium removed on the sixth day following treatment with Mn-hTf had also changed colour. This medium was kept for analysis of cell numbers and cell viability of any non-adherent cells found in the medium. Cell numbers and viability of the cells are shown in Table 5.4. When cell numbers are compared between groups there is no obvious difference between the control cells and those treated with apo-hTf, there being a 5-fold increase in cell numbers from plating. There is a slight fall in numbers in cells treated with Fe-hTf but this is close to a 5-fold increase in cell numbers. There is a considerable drop in cell numbers from flasks treated with Mn-hTf, with only a 3.5-fold increase in numbers from initial plating values. When comparing viability, although numbers of cells in apo-hTf are still high, cell viability has decreased slightly. However, for cells treated with Fe-hTf, although cell numbers have fallen, cell viability is still high.

Table 5.4 Cell numbers and viability of cultured cells

Condition	Total cell number	% Cell viability
Medium only	51×10^6	96
Apo-hTf	51.2×10^6	86
Fe-hTf	47×10^6	96
Mn-hTf	35×10^6	82
Mn-hTf (medium)[a]	6.05×10^6	64

[a] Medium removed from flask and non-adherent cells analysed

Viability had decreased in cells treated with Mn-hTf but only to the same extent as that seen with apo-hTf. It is typical in cell culture to consider anything above 85% (B. Tura, personal communication) as a high viability indicating a healthy cell population. The medium that had been removed from the flask of cells treated with Mn-hTf, was also spun down to determine if there were many non-adherent cells floating in the medium. Some cells were present, which were found to have quite low viability, perhaps representing dead cells that had lifted off the flask surface. However, if Mn-hTf was exerting a cytotoxic effect, then cell viability would be low in the cell layer and the cells found in the medium would be expected to have extremely low cell viability consisting of mostly dead cells and not just non-adherent cells.

5.3.1.2 Iron Content

In cells treated with Fe-hTf, quite noticeably cells have a much higher content of iron (see Figure 5.1).

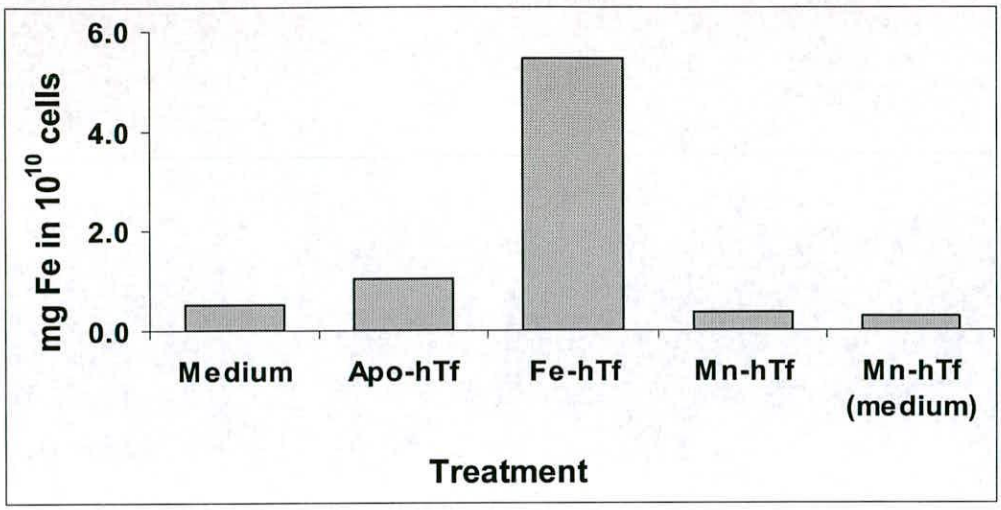

Figure 5.1 Comparison of iron content in cells treated with DMEM alone, apo-hTf, Fe-hTf and Mn-hTf. Transferrin added to give 25 μM. Cells grown in DMEM, apo-hTf and Fe-hTf confluent after 4 days and harvested. Mn-hTf treated cells left for 6 days when still not confluent. Mn-hTf (medium) represents non-adherent cells collected from the medium that had been removed from the flasks on the final day.

Cells treated with apo-hTf have a slightly elevated iron content when compared with cells grown in medium alone. This could be due to apo-hTf binding any available iron present in the medium and transporting this to the cells. From the results shown in Appendix F, Figure F.3, there is some iron present in the medium (1.27×10^{-4} mg/ml). This may explain the small increase seen in number for cells treated with apo-hTf. Cells treated with Mn-hTf showed no increase in iron content compared with those grown in medium alone. The non-adherent cells extracted from the medium after the sixth day of treatment with Mn-hTf showed no increase in iron content.

For medium removed from flasks containing the cells treated with Fe-hTf (Figure 5.2), the level of iron is higher than all other treatment groups and control group, as

expected.

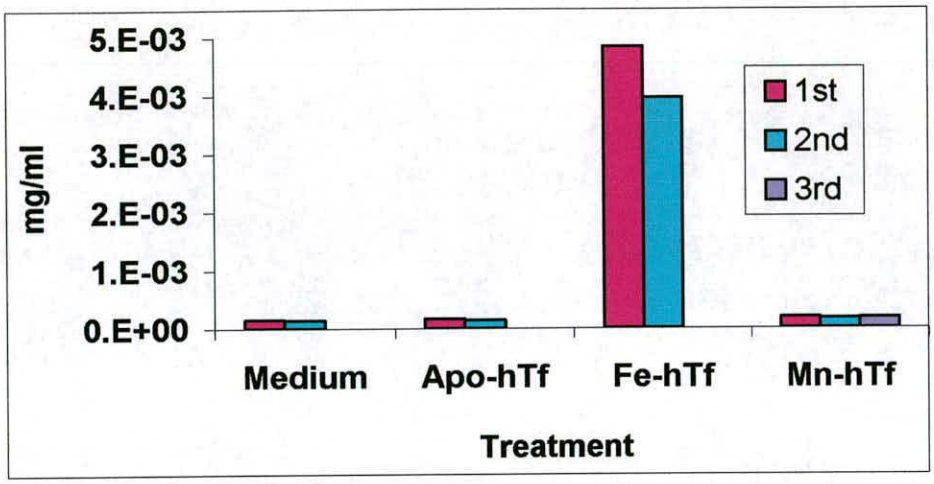

Figure 5.2 Comparison of iron content in growth medium removed from flasks containing cells. Cells grown in DMEM, apo-hTf, Fe-hTf and Mn-hTf at 25μM. Medium removed after 2, 4 and 6 (Mn-hTf treated only) days of growth of cells.

There is a slight decrease in the level of iron found in the first and second medium removed from the cells treated with Fe-hTf (days 2 and 4), which is surprising as Fe-hTf was given at the same concentration. This suggests that more iron was taken up by the cells between days 2 and 4. However, this is probably merely due to higher cell numbers from cell growth and hence more iron overall has been absorbed from the solution. There is no difference in iron content in medium removed from the other groups.

5.3.1.3 Manganese Content

In cells treated with Mn-hTf, there is a noticeable increase in manganese levels compared with the control group and other treatment groups, see Figure 5.3. The cells removed from the medium taken on the last day of incubation also show an

increase in manganese content. This suggests that manganese is being taken up from Mn-hTf by WRL-68 cells.

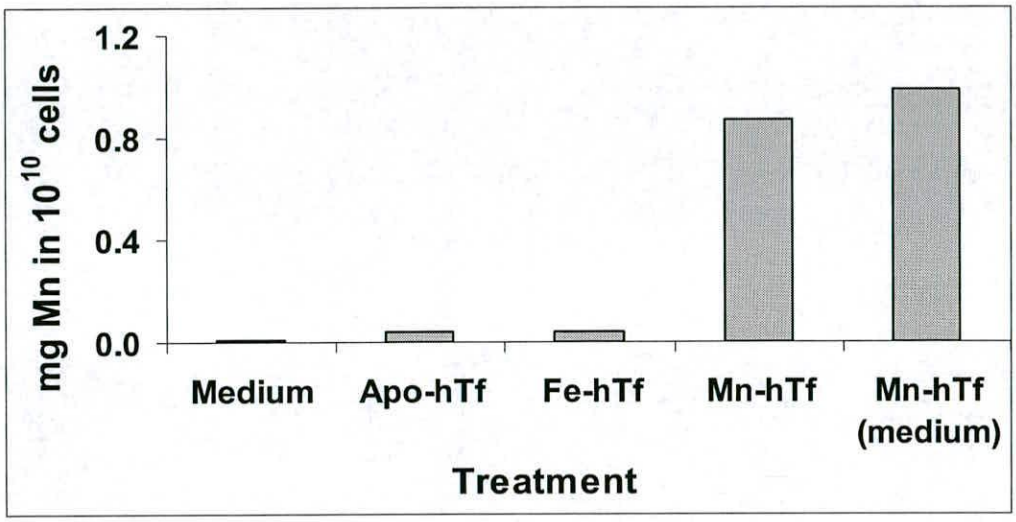

Figure 5.3 Comparison of manganese content in cells treated with DMEM alone, apo-hTf, Fe-hTf and Mn-hTf. Transferrin added to give 25μM. Cells grown in DMEM, apo-hTf and Fe-hTf confluent after 4 days and harvested. Mn-hTf treated cells left for 6 days when still not confluent. Mn-hTf (medium) represents non-adherent cells collected from the medium removed from the flask on the final day.

The cells recovered from the medium collected on day six also appear to have absorbed manganese from transferrin. The levels are slightly higher in these cells suggesting that more manganese was absorbed, possibly at toxic levels resulting in the cells detaching from the flask. However, without the experiment being repeated it is difficult to say if this is a significant increase.

The manganese content of the medium removed from the flasks containing the cells was in quite different ranges between treatment groups, so in order to see the levels more clearly the results are displayed as two graphs (Figure 5.4).

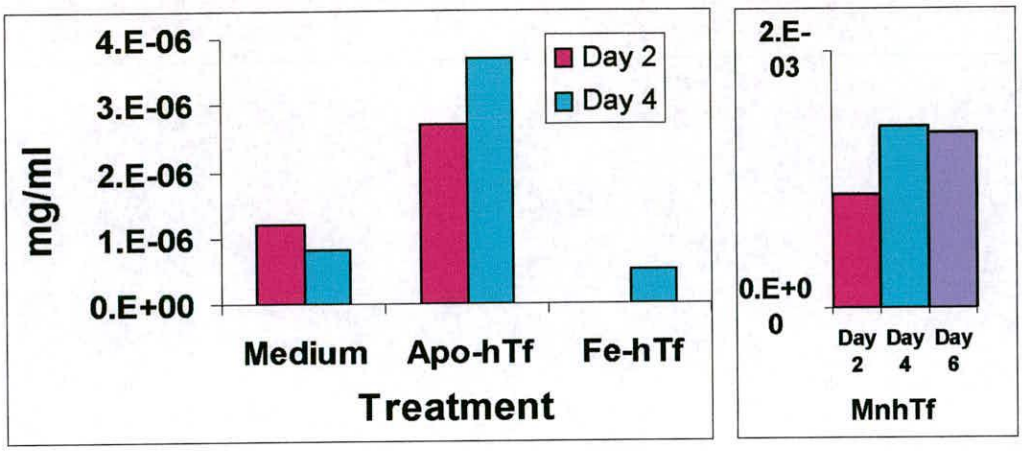

Figure 5.4 Comparison of manganese content in medium removed from cells. Cells grown in DMEM, apo-hTf, Fe-hTf and Mn-hTf at 25 μM. Medium removed from flasks containing cells after 2, 4 and 6 (Mn-hTf treated only) days. Due to a much higher level of Mn compared with other metals a different vertical scale has been used.

Medium removed from cells treated with Mn-hTf was found to have considerably higher manganese levels. The difference is probably more noticeable as there is very little base level of manganese found in the medium (approximately 0.0015 ppm Mn, Appendix F, Figure F.3). However, the levels of manganese in the medium removed from flasks containing the cells on the fourth and sixth days of treatment, are higher compared with that found in medium removed after two days. This is the opposite to that seen with iron which was found to decrease over treatment days.

Cells had not grown as well as with the other groups but cell numbers and confluence had increased in the cell layer during the six days of growth. This suggests that although there are more cells to take up manganese this does not appear to occur. The cells do seem to be taking up the manganese from transferrin, as shown by the

metal content analysis of the cells, but it may be that some level is reached whereby the cells then actively stop taking up the Mn-hTf. Alternatively, internal manganese may be under tight regulation by the cell *via* an efflux pump. The cells may be taking up manganese for the first two days, during which time the cells are behaving normally, then changes start to occur once a certain level of manganese intake is reached. It may be that normal proliferation of the cells slows or stops, as indicated by the low cell numbers compared with other groups, shown in Table 5.4. There is a very small increase in manganese content in the medium removed from cells treated with apo-hTf which may be due to apo-hTf being passively loaded with any manganese present. However, as the experiment was only carried out once we are unable to say if this is a significant increase.

5.3.1.4 Copper and Zinc Content

Cells were monitored for copper and zinc levels to see if these were altered by treatment of cells with transferrins. The results are shown in Figure 5.5.

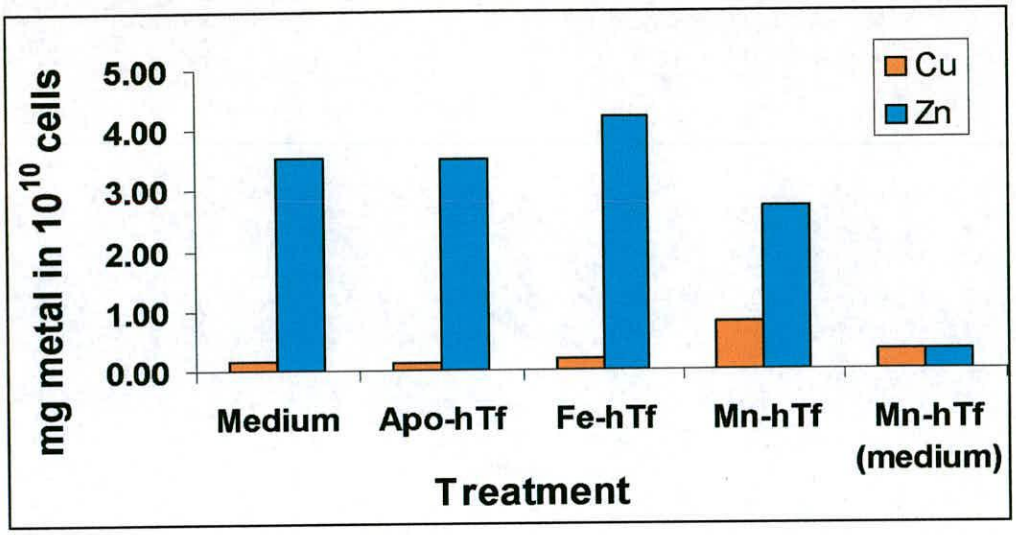

Figure 5.5 Comparison of copper and zinc content in cells treated with DMEM alone, apo-hTf, Fe-hTf and Mn-hTf. Transferrin added to give 25μ M. Cells grown in DMEM, apo-hTf and Fe-hTf harvested after 4 days, Mn-hTf after 6 days. Mn-hTf (medium) represents non-adherent cells collected from medium removed on final day.

The copper content is somewhat higher in cells treated with Mn-hTf whereas zinc is slightly lower. However, at such low levels with just a single set of results it is difficult to interpret this as an effect of treatment with Mn-hTf.

The results of the copper content found in medium removed from cells during growth are shown in Figure 5.6. There is no noticeable difference in copper levels between treatment groups.

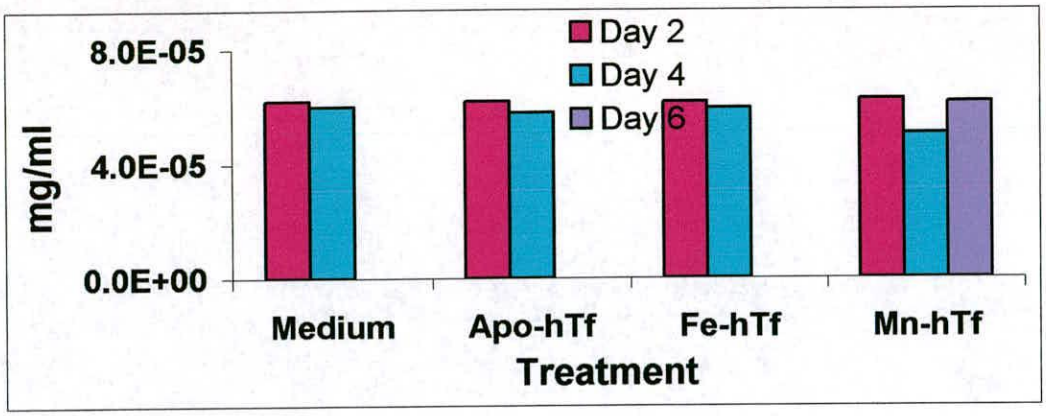

Figure 5.6 Comparison of copper content in medium removed from flasks during cell growth. Cells grown in DMEM, apo-hTf, Fe-hTf and Mn-hTf at 25 μM. Medium removed after 2, 4 and 6 (Mn-hTf treated only) days.

The zinc contents of the media removed from cells during growth are shown in Figure 5.7. There is a decrease in zinc in the medium removed from the flasks after four days of growth in cells treated with medium alone, apo-hTf and Fe-hTf, consistent with zinc uptake during cell growth.

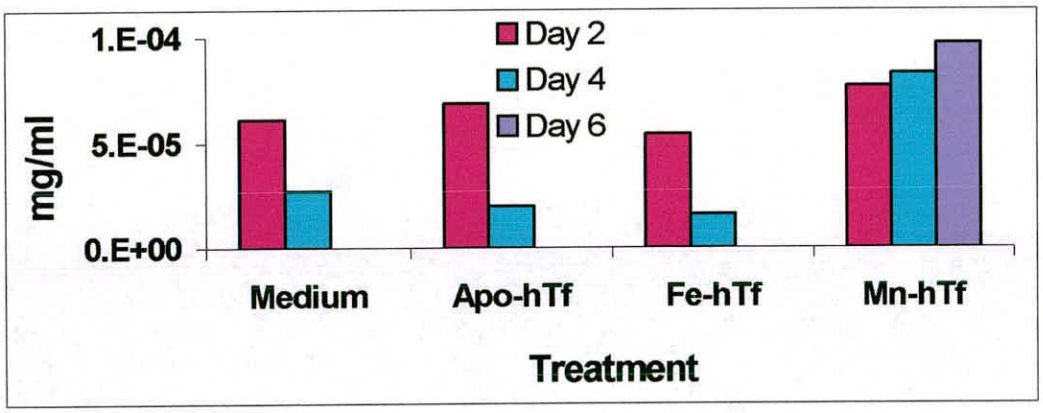

Figure 5.7 Comparison of zinc content of the media removed from flasks during cell growth. Cells grown in DMEM, apo-hTf, Fe-hTf and Mn-hTf at 25μM. Medium removed after 2, 4 and 6 days (Mn-hTf treated only).

In cells treated with Mn-hTf there is a small increase in zinc levels in the medium during growth. This could be due to efflux of zinc from WRL-68 cells treated with manganese. The medium removed from flasks containing cells treated with Mn-hTf had changed in colour from red to yellow indicating a drop in pH; this suggests a metabolic effect that may involve zinc. Furthermore, the cell morphology had changed compared to other groups (this is described in more detail later in Section 5.3.4) and this process may involve manganese and zinc. This could be due to interference with the cells cytoskeleton, and perhaps relates to the metal transporter DMT1 which is responsible for transporting a number of divalent cations including Mn(II), Cu(II) and Zn(II) [11].

*5.3.2 **Analysis of Hepatocyte Viability***

The MTT assay is used to assay cell proliferation as an alternative to ^{1}H-thymidine uptake. Active mitochondrial dehydrogenases of living cells cause the conversion of the soluble yellow dye to the insoluble purple formazan. Dead cells do not cause this change. While the assay gives information on cell proliferation, it also provides some information on mitochondrial function. This combined with other data can help to determine the state of the cells following treatment.

Plates (24 wells) were set up in which cells were treated with medium only, apo-hTf, Fe-hTf and Mn-hTf at 0.25, 2.5 and 25 μM concentrations of transferrin. All treatments were carried out in quadruplicate. Two plates were required to accommodate all experimental conditions. Therefore two sets of results are obtained for control groups of medium alone. The results of the MTT assay are displayed in

Figure 5.8. Treated cells are compared to the corresponding controls on the same plate (displayed to the left of them). As can be seen from Figure 5.8, there is a slight difference in cell numbers between the two control groups (Med). The plates were grown under the same conditions using the same number of plating cells. After four days incubation with the transferrins, the medium for the cell groups treated with 25 μM manganese transferrin had again changed colour from red to yellow. Medium in sealed tubes containing Mn-hTf at this concentration that had been placed in the incubator at the same time underwent no colour change.

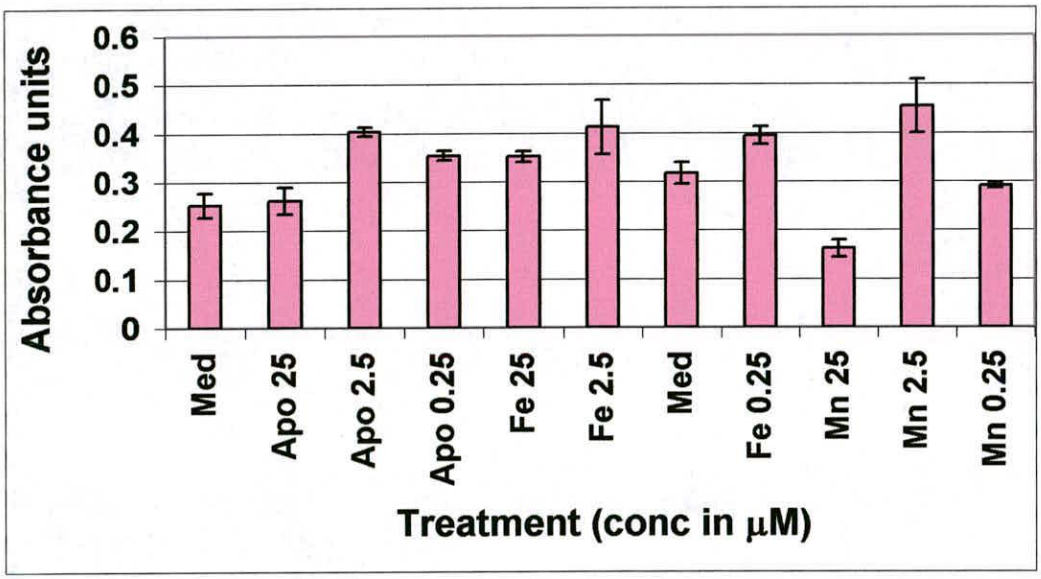

Figure 5.8 MTT assays for WRL-68 cells following treatment with transferrins. Cells grown on 24-well plates in medium alone, apo-hTf, Fe-hTf and Mn-hTf at 25, 2.5 and 0.25 μM. Standard deviation bars are shown. Medium changed after two days, MTT assay run after four days. Treatment groups can be compared to the control groups (Med) to the left of them. The absorbance of MTT (formazan) at 490 nm is indicative of viable cells.

It can be seen from Figure 5.8 that treatment of cells with transferrin, with the exception of 25 μM Mn-hTf, has either no effect compared with the control groups or results in an increase in cell growth. All transferrins added at 2.5 μM increase cell growth. Cells treat with 25 μM Mn-hTf show a decrease in cell growth.

The above experiment was repeated using the same conditions as before but the MTT assay was performed after only two days incubation instead of four days in an attempt to detect changes at an earlier time. No colour change of the medium was noted in any of the treatment groups after only two days. The results of the MTT assay can be seen in Figure 5.9.

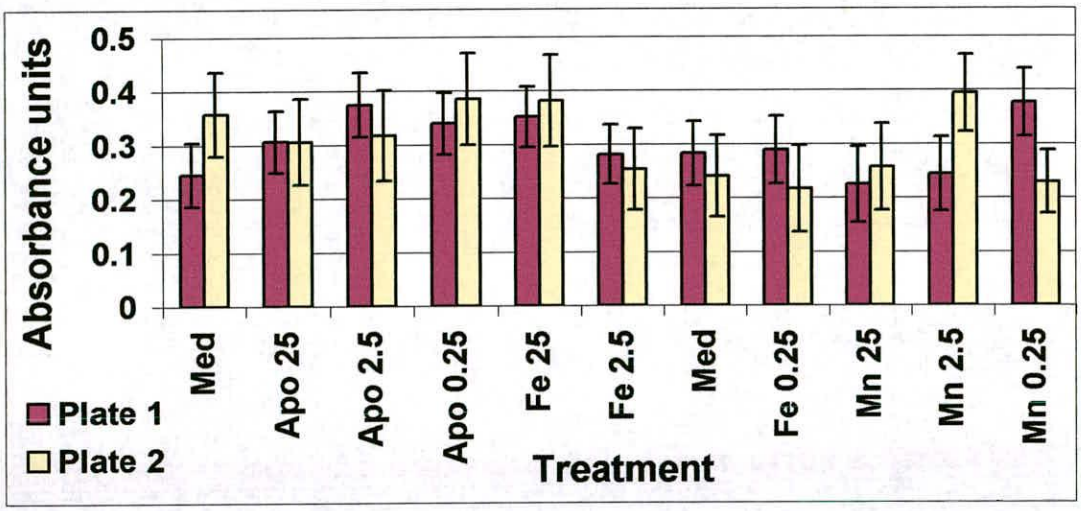

Figure 5.9 MTT assay of WRL-68 cells following treatment with transferrins. Cells grown on 24 well plates in medium alone, apo-hTf, Fe-hTf and Mn-hTf at 25, 2.5 and 0.25 μM. Standard deviation bars are shown. MTT assay run after two days. Treatment groups should be compared to control groups to the left of them.

Initially the standard deviations are rather large. This may be attributable to the fact

that the cell population may not have stabilised after only two days. Other errors arise from pipetting when cells are plated, and also the cells tend to form clumps which could lead to variations in growth patterns between wells in the first two days. In order to establish if there was any effect after two days which then became more pronounced after four days, the experiment was repeated using 96 well plates. As 96 well plates were used, this allowed treatments to be applied in duplicate (i.e. 2 sets of results obtained for each treatment group). After two days, one plate was assayed using MTT; the other plate had the medium changed and was incubated for a further two days and then assayed using MTT. Data from the plate assayed after two days are shown in Figure 5.10.

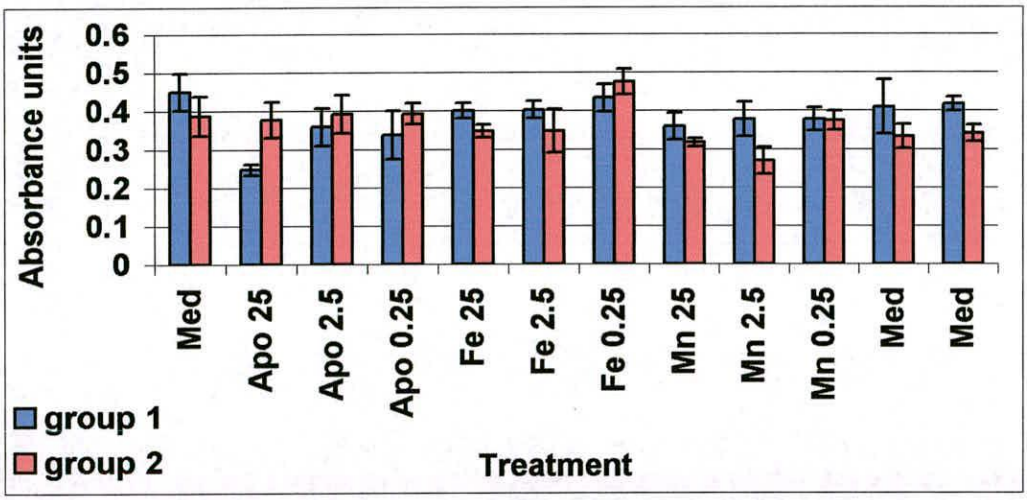

Figure 5.10 MTT assay of WRL-68 cells following treatment with transferrins. Cells grown on 96 well plates in medium alone, apo-hTf, Fe-hTf and Mn-hTf at 25, 2.5 and 0.25 μM. Two groups grown on plate. MTT assay run after two days. Standard deviation bars shown.

With the exception of treatment groups of apo-hTf at 25 μM and Mn-hTf at 2.5 μM,

the two groups gave similar results to the experiment carried out previously on 24-well plates (Figure 5.9).

The second 96-well plate was incubated for four days, having the medium changed on the second day. The results of the MTT assay for this second plate are shown in Figure 5.11. Again, the lack of cell growth in wells treated with 25 μM Mn-hTf compared with other groups is noticeable, confirming the result seen in Figure 5.8.

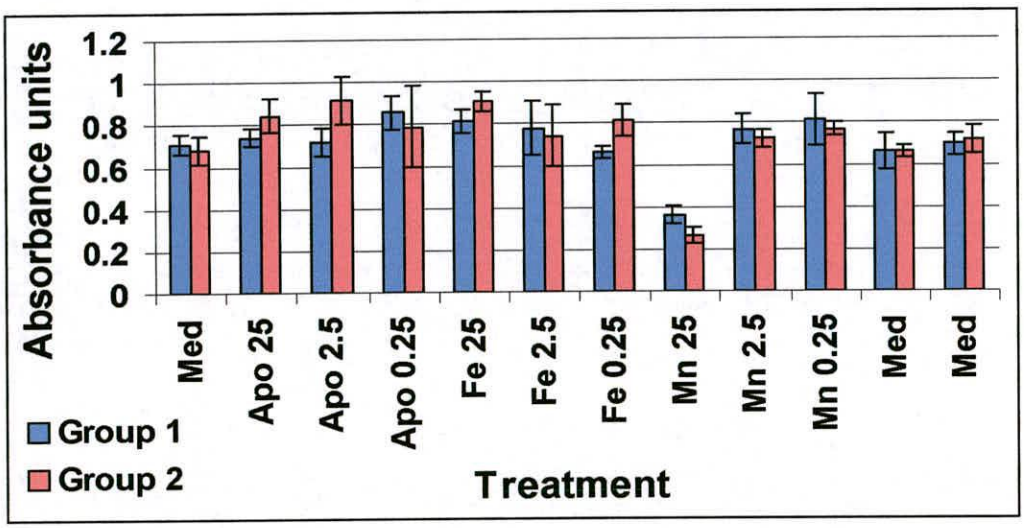

Figure 5.11 MTT assay of WRL-68 cells following treatment with transferrins. Cells grown on 96 well plates in medium alone, apo-hTf, Fe-hTf and Mn-hTf at 25, 2.5 and 0.25 μM. Medium changed after two days. Two groups grown on plate. MTT assay run after four days. Standard deviation bars shown.

The results of the experiments using the two 96 well plates being grown and treated simultaneously show that Mn-hTf gives rise to a pronounced effect after four days incubation. These results suggest that the effect of Mn-hTf is first evident between two and four days, although this may be due to the nature of growth of the cells masking any real effect that occurs during the first days of cell growth.

Although the MTT assay gives only an indication of cell numbers in the mono-layer, it does provide some information on the activity of the cell in terms of cell proliferation and rates of mitosis and cell death. To further complicate results, cells grown on 24 well plates form a better mono-layer and have greater room in which to settle following plating and growth. However, for the MTT assay these cells are then transferred to a 96-well plate in order for the absorbance to be read. When cells are grown on 96 well plates no transfer is necessary for the plate reader. However, cells do not form such a good mono-layer and conditions are somewhat more cramped for cell growth and the wells can quickly become overgrown.

*5.3.3 **Analysis of Hepatocyte Mitosis and Apoptosis***

To investigate the number of cells undergoing cell death and mitosis, a DNA stain can be used so that mitotic and apoptotic cells can be quantified in a cell population. Initially cells were seeded on 96-well plates simultaneously with cells used for the MTT assay described in Section 5.3.2. This was then used in parallel with the MTT assay to provide further information on the effect of transferrins on hepatocytes. Cells were treated with the same conditions as used in the MTT assay. Again after two days one of the plates had the medium removed and was stained using Feulgan stain as described Section 5.2.5. The second plate had fresh medium and transferrins applied. On the fourth day this plate had medium removed and was stained using Feulgan stain. Cells were then assessed for apoptosis.

It proved to be quite difficult to assess cells grown in 96-well plates due to poor visibility and due to clumps of cells forming at the bottom of the individual wells. This was particularly evident after four days of growth when, in some cases, the well

had become quite overgrown. Unlike the MTT assay, the use of Feulgan stain relies quite heavily on the formation of an even mono-layer of cells to allow reliable counting.

There appeared to be no noticeable increase in apoptosis in any of the treatment groups, including Mn-hTf where cell numbers were less than for other groups as shown by the MTT assay. The only difference between groups was in cell morphology. Unfortunately no further information could be gained from the 96 well plates.

As there was no difference between treatment groups to suggest that counting of apoptotic cells was required, attention was focused on the cells in the group showing a difference in morphology and growth, that is treatment with Mn-hTf. In order to look more closely at the effect of Mn-hTf on WRL-68 cells, cells were seeded onto 4 well chamber slides. One of the wells was incubated with medium alone. Mn-hTf was added at concentrations of 0.25, 2.5 and 25 μM. After two days, the medium was changed, and on the fourth day all medium was removed and cells stained using Feulgan stain. Slides were then examined and counted for mitotic activity. Cells were counted in the field of view until at least 100 cells in total were counted. This was repeated five times in order to obtain average counts of mitotic and non-mitotic cells. The results are shown in Figure 5.12. It became apparent during the counting of these cells that there were considerably fewer cells on the area of the slide that had been treated with 25 μM Mn-hTf. There did however appear to be slightly more cells undergoing mitosis with increasing concentrations of Mn-hTf. This seems to contradict the result of there being fewer cells which suggests that the cell cycle itself

may be altered or slowed so that there are a larger number of mitotic cells visible.

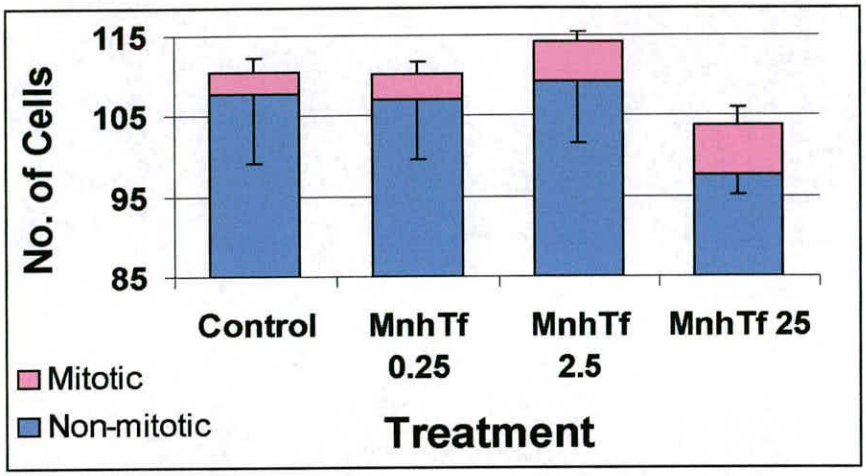

Figure 5.12 Number of mitotic cells after treatment with Mn-hTf. Cells were plated on 4-well chamber slides and left overnight then treated with Mn-hTf at 0.25, 2.5 and 25 μM with medium alone as controls. Medium changed after 2 days, then cells fixed and stained with Feulgans stain after 4 days treatment. Lower standard deviation bars for non-mitotic counts, upper bars for mitotic counts.

5.3.4 Investigation into the Effect of Mn-hTf on Hepatocytes

This work was initially carried out to investigate if treating cells with Mn-hTf could result in an increase in uptake of manganese by hepatocytes. If this was the case, there was a possibility that the manganese could be directed to the mitochondria where it could be used by Mn-SOD for protection against oxidative stress. Mn-hTf when used at doses of 25 μM, has been shown to be taken up by the WRL-68 cells resulting in increased manganese levels in the cells but there is also another effect at these concentrations. To try and determine if this is a mitochondrial effect, cells

were treated with Mn-hTf over the same range of concentrations used previously and stained using CMX-Ros. This is a fluorescent stain used to detect mitochondrial depolarisation. As manganese is redox active it may be taken up by cells *via* transferrin and could alter the redox status of the cell, possibly leading to oxidative stress and alteration of mitochondrial function.

5.3.4.1 Induction of Mitochondrial Depolarisation by mClCCP

In order to determine if a mitochondrial effect was observed following treatment with Mn-hTf, WRL-68 cells were first treated with mClCCP, a well known mitochondrial depolariser, to give a positive result. Cells were seeded on 4-well chamber slides and were treated with mClCCP at concentrations of 30, 40 and 50 μM and with medium alone to act as a control. Once cells were stained with CMX-Ros they were analysed using fluorescence microscopy with the kind help of Mrs. Linda Wilson (Pathology department, University of Edinburgh). The results of treating cells with mClCCP at 50 μM compared with control are shown in Figure 5.13.

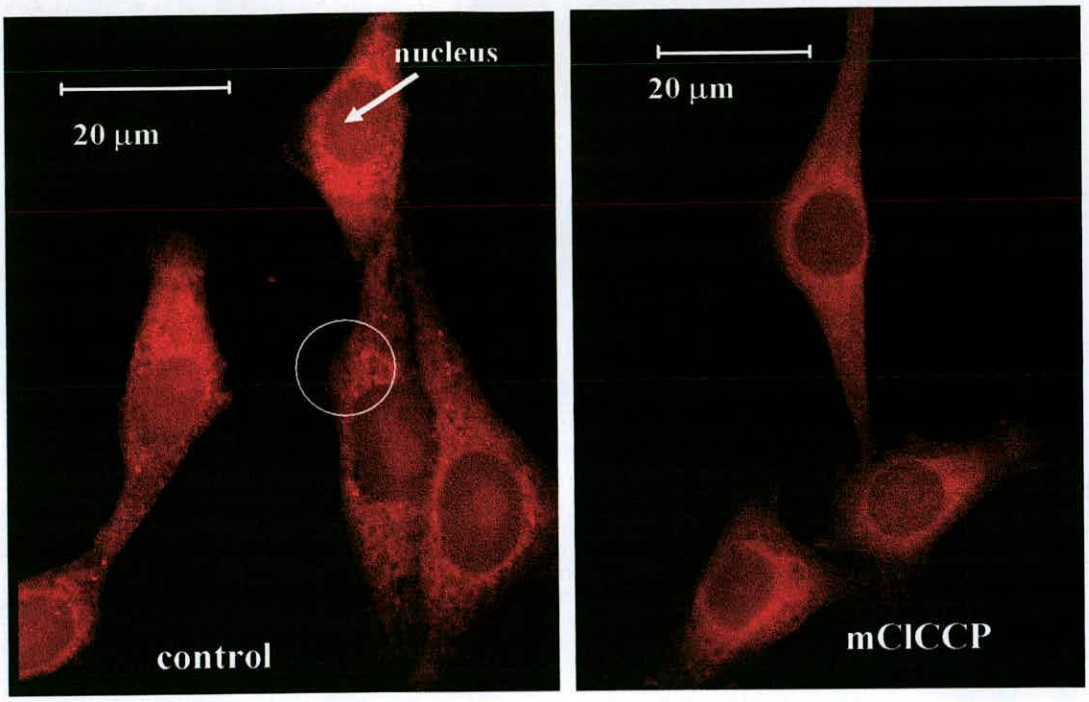

Figure 5.13 CMX-Ros stained WRL-68 cells. Cells were incubated with medium alone (control, left) or with the mitochondrial depolariser mClCCP (right). Image shown when treated with 50 μM. Cells grown in 4-well chamber slides for 2 days. Cells treated with mClCCP for 45 mins. Brightly fluorescing mitochondria are shown by a circle.

In the control image the mitochondria can be seen as fluorescing brightly as punctate staining of red. The majority of the mitochondria surround the nucleus and are highlighted in Figure 5.13 by a circle. In the cells treated with mClCCP there is a distinct lack of these brightly fluorescing pinpricks of red. The stain surrounding the nucleus is much duller, this indicates that the mitochondria have become depolarised. Depolarisation of the mitochondrial membrane can then lead to membrane permeabilisation and cell death as described in Chapter 1. Signs of mitochondrial depolarisation were then looked for after treating cells with manganese transferrin.

5.3.4.2 Effect of Mn-hTf on Hepatocytes

Cells were incubated with apo-hTf, Fe-hTf and Mn-hTF at concentrations of 0.25, 2.5 and 25 μM on 4-well chamber slides with medium alone as controls. The images taken from the slides shown in Figure 5.14 are for the highest concentration of transferrin added (25 μM).

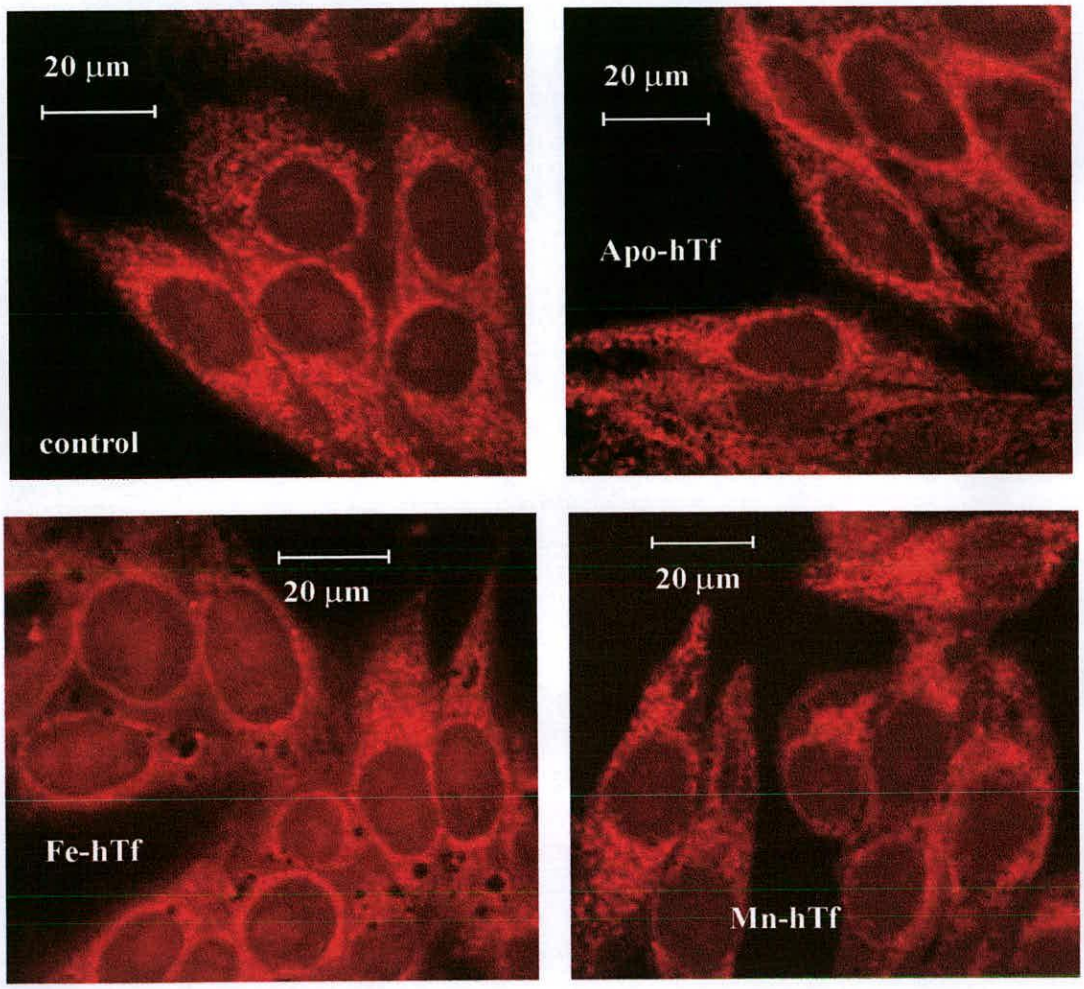

Figure 5.14 Comparison of transferrin treated cells stained with CMX-Ros. Images shown are for cells grown in the presence of 25 μM transferrin for 4 days, with the medium changed after 2 days.

As can be seen in the images, all show the brightly fluorescing punctate staining representing fully functional mitochondria. None of the treatment groups showed any signs of mitochondrial depolarisation. This result suggests that any effect of manganese on cells does not appear to include alteration of mitochondrial transmembrane potential. There is, however a definite effect on the cells which is clearly visible on the fluorescent images. An example of this is shown below in Figure 5.15.

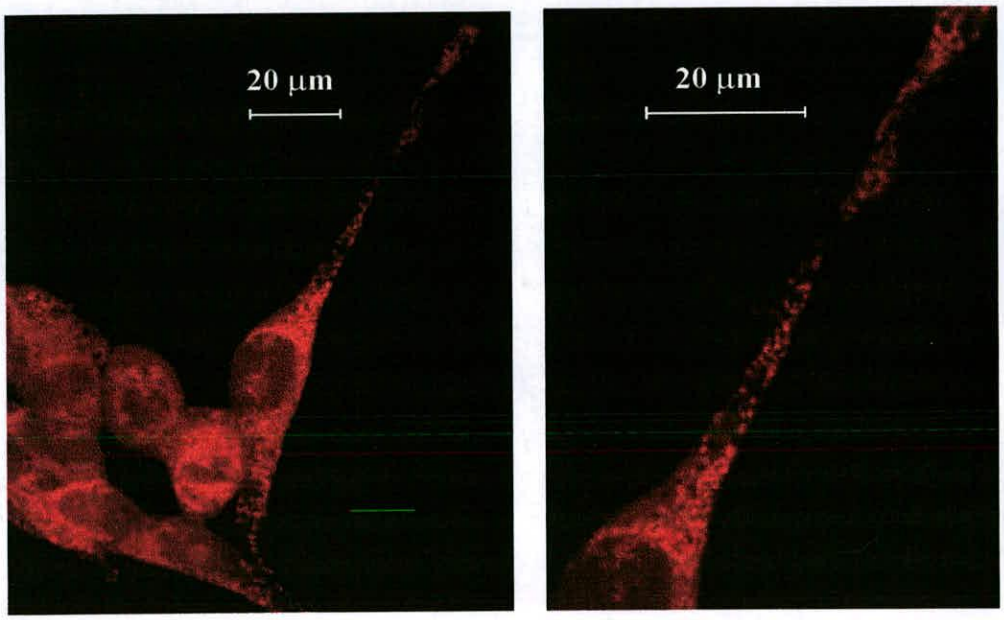

Figure 5.15 Effect of 25μM Mn-hTf on WRL-68 cells. Cells grown on 4 well chamber slides, incubated with 25 μM Mn-hTf for 4 days, medium changed on day 2. Slides stained with CMX-Ros and fluorescent images taken. Image on right is a magnification of image on left.

When the cells were treated with 25 μM Mn-hTf the morphology of the cells changed. The cells became dendritic in appearance with a stretched effect as if the

cells were spreading. As can be seen in Figure 5.15, the cell contains many mitochondria in these finger-like protrusions from the cells. Nothing like this was observed following treatment with other transferrins or at other doses.

Grinnell [28] has shown that in the presence of Mn^{2+}, baby hamster kidney cells (BHK) are able to attach and spread on substrata without the usually necessary adhesion factors. This adhesion was able to take place even in the presence of treatments that would usually inhibit cell attachment. This suggests that manganese plays an important role in cell attachment. Mn^{2+} was found to be more effective than Co^{2+}, Mg^{2+} and Ca^{2+} in adhesion and spreading of BHK21 cells in serum [38].

Interactions of extracellular matrix (ECM) molecules with integrins have been shown to either directly stimulate neurite outgrowth or facilitate neurite outgrowth induced by other factors in cultures or neurons or neuron-like cells, including rat pheochromocytoma (PC12) cells [31, 39]. Lin *et al* [31] report that Mn^{2+} causes not only cell spreading but also stimulates extension of neurite-like processes in PC12 cells through a mechanism related to its ability to enhance an RGD-dependent ECM-integrin interaction. Further, they showed that the growth required new synthesis of proteins. Lin *et al* [31] went on to show that these long processes were not due to stimulation of adenylate cyclase and were dependent on RGD receptors and ECM molecules. PC12 cells do not extend neurites in response to Mn unless grown in substrates treated with vitronectin, fibronectin or culture medium containing serum [31, 40]. Binding of ligand to integrin receptors activates intracellular signalling cascades that may alter gene transcription [40].

The results in this study are similar to those found by Lin *et al* [31] in that the

outgrowth from the cells took at least two days of growth. Unlike previous studies where cell spreading was seen immediately [28-30], cells were left overnight so that cell attachment was allowed to take place. This suggests that more complex intracellular events may be involved to promote this effect in cells that are already attached, other than integrin-mediated effects.

These results are consistent with the hypothesis that manganese is able to stimulate projection-like growths in serum containing medium on tissue culture plates. Further studies should include growth of cells treated with transferrins on uncoated tissue culture plates and with minimal medium. From these studies alone it is not possible to say whether Mn^{3+} is removed from transferrin and then reduced in the cell to Mn^{2+} which then exerts its effect, although this seems the most likely event.

The possibility that the phenotype of a clonal cell line such as WRL-68, maintained for long periods of time may drift in subtle ways cannot be ruled out. However, no obvious changes were observed in the cell behaviour, and culture conditions remained the same during standard cell culture. Further, the lack of dendritic-like processes from cells grown as controls, other transferrins and low dose Mn-hTf treatment groups, confirms the specificity of this morphological change.

5.4 Conclusions

These studies show that manganese and iron are taken up by WRL-68 cells when incubated with Mn_2-hTf and Fe_2-hTf respectively as shown by ICP-AES studies. This supports previous work using inhibition studies which has shown that addition of Fe_2-hTf, Ga_2-hTf, Bi_2-hTf and Ti_2-hTf to placental BeWo cells results in uptake of

the metals [41]. Further, at higher Mn-hTf concentrations of 25 μM, cell numbers decreased compared with controls and other treatment groups but this was not a cytotoxic effect, and the cell morphology changed. Transferrin is found in blood serum at concentrations of *ca.* 35 μM. However, human serum manganese levels are considerably lower than this at typically 0.057 μg/100 ml (9.8 nM) [42]. Therefore the results seen here at 25 μM Mn_2-hTf are under extreme conditions with much higher than normal cellular manganese levels. The Mn-hTf used in these cell studies was produced using $KMnO_4$. This suggests that although transferrin may be altered by the use of $KMnO_4$ to load Mn(III) onto the protein, the cellular receptors still recognise manganese-transferrin and actively absorb it.

The MTT assays have shown that there is a decrease in cell metabolic activity in cells treated with 25 μM Mn-hTf compared with other treatment groups and controls. Further, staining of cells treated with Mn-hTf at varying concentrations suggests an increase in mitosis or alteration of the cell cycle with increasing concentrations of Mn-hTf although this finding needs to be confirmed in future work.

Doses of 25 μM Mn-hTf result in finger-like protrusions from the cells. These protrusions contain mitochondria but there is no alteration of the mitochondrial transmembrane potential following treatment.

Manganese, when added as manganese transferrin, is capable of inducing the process of outgrowth from WRL-68 cells. These morphological changes appear to be time and dose-dependent. It is likely that new protein synthesis is required to allow these processes to occur and that they form due to an interaction of Mn(II) or Mn(III) with RGD-dependent ECM-integrin interactions. This interaction probably takes the form

of either increasing affinity of the binding or by a change in specificity. Further studies are required in order to determine the ECM molecule(s) and integrin(s) involved in this process.

It could be that Mn-hTf delivers Mn to the cell which then leads to up-regulation of expression of integrins on the plasma membranes of WRL-68 cells. The effect could also be a result of the subcellular distribution of integrins or from alteration of receptor affinity. Alterations may be due to transcription and translation and modification of various signalling pathways. Further work studying any up-regulation of gene transcription would need to be carried out in order to determine this. Also, in order to investigate the possibility of manganese being delivered to the cell by Mn-hTf to increase MnSOD activity, a model system of oxidative stress in cells needs to be established. This model would have to ensure that the reactive oxygen species were created specifically in the mitochondria in order to best test this theory.

5.5 References

1. S. Bihari, PhD Thesis, 2002, University of Edinburgh, Edinburgh.

2. A. Sigel and H. Sigel, *Manganese and its role in biological processes*, Metal Ions in Biological Systems. Marcel Dekker Inc.37 **2000**.

3. C.L. Keen, J.L. Ensunsa, and M.S. Clegg, in *Metal ions in Biological Systems: Manganese and its Role in Biological Processes*, A.S. Sigel, H. Ed, Marcel Dekker Inc, New York, **2000**, 37: 89-121

4. D. Moutafchiev, L. Sirakov, and P. Bontchev, *Biol. Trace Elem. Res.*, **1998**, 61: 181-191.

5. B.R. Bacon and A.S. Tavill, *Sem. Liv. Dis.*, **1984**, 4: 181-192.

6. R. Sciot, P. Van Eyken, and V.J. Desmet, *APMIS Suppl.*, **1991**, 23: 21-31 and refs therein.

7. A. Tangeras, T. Flatmark, D. Backstrom, and A. Ehrenberg, *Biochim. Biophys. Acta,* **1980**, 589: 162-175.

8. I. Bertini, J. Hirose, C. Luchinat, L. Messori, M. Piccioli, and A. Scozzafava, *Inorg. Chem.*, **1998**, 27: 2405-2409.

9. J.A. Roth and M.D. Garrick, *Biochem. Pharm.*, **2003**, 66: 1-13.

10. J.A. Roth, C. Horbinski, D. Higgins, P. Lein, and M.D. Garrick, *Neurotoxicol.*, **2002**, 23: 147-157.

11. H. Gunshin, B. Mackenzie, U.V. Berger, Y. Gunshin, M.F. Romero, W.F. Boron, S. Nussberger, J.L. Gollan, and M.A. Hediger, *Nature,* **1997**, 388: 482-488.

12. W.R. Harris and A. Chen, *J. Inorg. Biochem.*, **1994**, 54: 1-19.

13. P. Aisen, R. Aasa, and A.G. Redfield, *J. Biol. Chem.*, **1969**, 244: 4628-4633.

14. J.W. Finley, *Biol. Trace Elem. Res.*, **1997**, 64: 101-118.

15. T. Galeotti, G. Palombini, and G.D.V. van Rossum, *Arch. Biochem. Biophys.*, **1995**, 322: 453-459.

16. A.C.G. Chua, L.M. Stonell, D.L. Savigni, and E.H. Morgan, *J. Phys.*, **1996**, 493: 99-112.

17. A.C.G. Chua and E.H. Morgan, *J. Comp. Phys.*, **1997**, 167: 361-369.

18. L. Davidson, B. Lönnerdal, B. Sandstrom, K. Kunz, and C.L. Keen, *J. Nutr.*, **1989**, 119: 1087-1092.

19. A. Takeda, *Brain Res. Rev.*, **2003**, 41: 79-87.

20. J.S. Crossgrove, D.D. Allen, B.L. Bukaveckas, S.S. Rhineheimer, and R.A. Yokel, *Neurotoxicology,* **2003**, 24: 3-13.

21. P. Aisen, in *Metal Ions in Biological Systems*, A. Sigel and H. Sigel Ed, Marcel Dekker Inc., New York, **1998**, 35: 585-631

22. C.E. Gavin, K.K. Gunter, and T.E. Gunter, *Tox. App. Pharm.*, **1992**, 115: 1-5.

23. C.E. Gavin, K.K. Gunter, and T.E. Gunter, *Neurotoxicol.*, **1999**, 20: 445-454.

24. C.E. Gavin, K.K. Gunter, and T.E. Gunter, *Tox. App. Pharm.*, **1992**, 115: 1-5.

25. G. Kroemer, N. Zamzami, and S.A. Susin, *Immunol. Today,* **1997**, 18: 44-51.

26. J. Gailit and E. Ruoslahti, *J. Biol. Chem.*, **1988**, 263: 12927-12932.

27. M.J. Elices, L.A. Urry, and M.E. Hemler, *J. Cell. Biol.*, **1991**, 112: 169-181.

28. F. Grinnel, *J. Cell Sci.*, **1984**, 65: 61-72.

29. F. Grinnel and R. Beckman, *Exp. Cell. Res.*, **1991**, 195: 218-223.

30. M. Rabinovitch and M.J. DeStefano, *J. Cell. Biol.*, **1973**, 59: 165-176.

31. W.H. Lin, D. Higgins, M. Pacheco, J. Aletta, S. Perini, K.A. Marcucci, and J.A. Roth, *J. Neurochem. Res.*, **1993**, 34: 546-561.

32. P. Lein, P.J. Gallagher, J. Amodeo, H. Howie, and J.A. Roth, *Brain Res.*, **2000**, 885: 220-230.

33. J. Finley, J. Caton, Z. Zhou, and K. Davison, *J. Nutr.*, **1997**, 127: 2334-2341.

34. M.C. Gutierrez-Ruiz, L. Bucio, V. Souza, J.J. Gomez, C. Campos, and A. Carabez, *In Vitro Cell. Develop. Biol. Animal.*, **1994**, 30A: 366-371.

35. T.A. Hamilton, H.G. Wada, and H.H. Sussman, *Proc. Natl. Acad. Sci. USA,* **1979**, 76: 6406-6410.

36. N.D. Chasteen, *Coord. Chem. Rev.*, **1977**, 22: 1-36.

37. D.C. Harris and P. Aisen, in *Iron Carriers and Iron Proteins*, T.M. Loehr Ed, VCH Publishers, Inc., New York, **1989**, 239-351

38. J.G. Edwards, R.T. Robson, and G. Campbell, *J. Cell Sci.*, **1987**, 87: 657-665.

39. L.F. Reichardt and K.J. Tomaselli, *Ann. Rev. Neurochem.*, **1991**, 14: 531-570.

40. M.J. Humphries, *Curr. Opin. Cell Biol.*, **1996**, 8: 632-640.

41. M. Guo, H. Sun, H.J. McArdle, L. Gambling, and P.J. Sadler, *Biochemistry,* **2000**, 39: 10023-10033.

42. J. Versieck, F. Barbier, A. Speecke, and J. Hoste, *Acta Endocrinologica,* **1974**, 76: 783-788.

Chapter 6 Conclusions and Future Work

6.1 Conclusions

Transferrin is the natural transport protein for iron to cells and delivers iron by receptor mediated endocytosis [1, 2]. Other metals have been shown to bind transferrin and occupy the same metal binding site [3-6] thereby providing a specific pathway for the delivery of other metal ions into cells. The work in this thesis has investigated the binding of manganese to transferrin, and some chemical and biological characterisation of the metal loaded protein.

In vitro oxidation coupled uptake of Mn^{2+} to Mn^{3+} by transferrin is very slow and incomplete. The use of the blood serum oxidant caeruloplasmin, was shown to speed up this oxidation, however, not at rates that would be likely to occur *in vivo*. The slow rate and only partial loading of Mn^{3+} in the presence of caeruloplasmin may in fact be due to pH changes that could occur during the reaction. Carbonate may be lost to the air resulting in increased pH which may inhibit Mn^{3+} binding and the oxidative action of caeruloplasmin by inactivating the protein. The oxidant potassium permanganate was found to give much faster and more complete loading. Interestingly, it was found that more than two manganese ions were able to be bind to one transferrin molecule. This suggested either that manganese was binding as a cluster, with more than one metal binding to each site, or that the metal was binding to other areas of the protein. Ferric Binding protein (FBP), which belongs to the transferrin superfamily, was recently found to bind Hafnium as a metal cluster. Hafnium was also found to bind to transferrin in ratios exceeding 2:1 [7]. The N-

lobe of transferrin is thought in this instance to remain open and hence be capable of binding more than one metal ion. Open lobe conformations with a single Fe^{3+} bound are known supporting this notion [8-10].

The use of potassium permanganate also raised questions pertaining to oxidation. The hepes buffer used during reactions was found to be oxidised, thus contributing to the loading of Mn^{3+} onto transferrin but also it became apparent that the protein itself could be being oxidised during the reaction. NMR studies of amino acids confirmed this suggesting that the methionine residues were likely targets for oxidation. The use of ε-[^{13}C]Met-labelled recombinant transferrin allowed 2D NMR analysis of the protein following reaction with potassium permanganate. It was found that the protein underwent conformational changes similar to those seen previously with other metal binding [4]. Further, a chemical shift was seen for Met26 which could be attributable to the oxidation of the residue to the corresponding sulfoxide and sulfone as a result of the reaction.

Other characteristics of Mn-hTf were investigated. It was found that the addition of $KMnO_4$ was unable to displace Fe^{3+} from transferrin but $Fe(NTA)_3$ when added to Mn-hTf, was able to displace Mn^{3+} from the protein suggesting that Mn^{3+} is not as tightly bound to transferrin as Fe^{3+}. However, pH studies of Mn-hTf confirmed that metal dissociation at low pH occurred in a similar manner for the two metal ions supporting the theory that if Mn-hTf could be transported to the cell by receptor mediated endocytosis then dissociation in the endosomes would occur due to the acidic conditions.

The fact that metal ions dissociate from transferrin at low pH (*ca.* pH 5.0-6.0) may have impaired the attempts to crystallise transferrin. Although crystals did form for both Fe-hTf and Mn-hTf the former were of quite low quality and the latter of very poor quality. The crystallisation conditions used were of low pH (*ca* pH 5.5) so it seems likely that one of the metal ions will have dissociated which can contribute to crystal stress. So far the only crystal structure obtained for iron loaded human serum transferrin is that found in a thesis [11]. The conditions used for crystallisation in the work presented here were close to those given previously in Zuccola's thesis suggesting that these are close to optimal as crystals grew from untreated and unpurified transferrin with relative ease. It seems that the purity is of importance when attempting to grow good quality crystals.

The information gained from the experiments carried out in chapters 3 and 4 suggest that there are some similarities between Fe-hTf and Mn-hTf. Work was carried out to try and establish if the similarities between the two proteins could be used to some advantage in cell systems in terms of uptake of Mn-hTf by the same pathway in hepatocytes as Fe-hTf, to enable delivery of the metal ion to cells. Levels of cellular metal ion were found to alter following treatment with Fe- and Mn-hTf suggesting that uptake of the metals from transferrin by the human hepatocyte WRL-68 cells, had occurred. However, the method of cellular metal detection needs to be optimised to ensure accurate readings in the future. The metal may form a precipitate if released from transferrin in the medium solution which may then result in sedimentation during ICP-AES analysis of the medium removed. Sedimentation

would also be a problem when analysing cells for metal content. These problems need to be addressed in the future.

The expected changes in mitochondrial function due to excess manganese did not occur; that is mitochondrial function and membrane polarisation remained normal. Cell metabolism was found to decrease at the highest dose of Mn-hTf (25 μM), and mitosis appeared to have increased. There was no evidence of increased apoptosis compared to other treatment groups. Changes of a more morphological nature also took place; the hepatocytes became dendritic in appearance with finger-like protrusions occurring. This effect could be the result of the interference of manganese with RGD-dependent ECM-integrin interactions. Alternatively, alterations of cell signalling could be occurring. The cell line used was of foetal origin so pathways may be being induced thus changing the behaviour and morphology of the cells to that seen in other tissues *i.e.* neurons.

These results presented in this thesis support the ability of transferrin to load Mn^{3+} but the choice of the donating salt used may have an effect on the protein, this could then result in altered function of the protein in terms of binding affinity to the receptor and metal ion release. Another important factor to consider is the effect of pH on the loading of the protein and also the consequences to the cell. A decrease in cell metabolism was observed in cells treated with the highest dose of Mn-hTf coupled with a change in colour of the medium suggesting a change in pH which may or may not be related to change in metabolism. A lower pH has also been shown to result in metal ion dissociation from transferrin. Therefore, pH may be an

important contributing factor in cells systems and in vitro investigations which needs further consideration.

The cell studies suggest the possibility of using transferrin as a delivery mechanism for manganese to cells thus creating potential for its use as a therapeutic agent. However, much more further work is required in this field before this potential can be reached. Some of the interactions that have been observed in this thesis are artificial in terms of a functioning biological system, for example, how likely is it that transferrin is loaded with Mn^{3+} from Mn^{7+}? However, investigations into all aspects of the chemical and biological nature of the protein may provide us with insights into the possible transport mechanism(s) of manganese and other metals.

6.2 Future Work

Although in this thesis loading of transferrin using caeruloplasmin as an oxidant did not provide good results this method should still be explored. Optimum conditions need to be found which closely resemble those found *in vivo* and this may lead to successful and fast loading of transferrin with manganese when caeruloplasmin is present. The pH of the system plays an important part so should be investigated further. This can also be investigated when loading the protein using permanganate. Further work needs to be done in this system to investigate the theory of manganese clusters and to determine if the manganese is binding as MnO_4^-.

Reactions of manganese with transferrin need to be carried out in the absence of carbonate to investigate if this perturbs loading. This should be done using $MnCl_2$ as a source of manganese and using $KMnO_4$ to aid the investigations of altered metal binding. The results could then help confirm if carbonate is required as a synergistic anion in all cases of metal loading or if binding as MnO_4^- negates the necessity for this extra ligand. Further work on manganese binding by the different methods should also include determination of lobe-loading preference under various conditions and if there appears to be any favoured lobe. The work on manganese binding to transferrin could also be applied to the similar proteins lactoferrin and ferric binding protein (FBP). This may again provide further insights into metal binding and alteration of binding sites.

The use of 2D NMR provides an effective tool for investigating metal loading of transferrin. Unfortunately, in this study the ε-[^{13}C]Met-labelled recombinant transferrin was quite old and had been used several times. Therefore to obtain more definitive answers with respect to the action of $KMnO_4$ on transferrin it would be beneficial to use fresh samples of the protein. This could then go on to be used in further displacement studies to investigate if there has been a permanent change to the transferrin molecule as a result of the use of a strong oxidant

Ultimately a crystal structure of Mn-hTf will provide definitive answers to the many questions that arose throughout this thesis. Ideally, crystals of the protein will obtained where Mn^{3+} is bound using $MnCl_2$ and $KMnO_4$ to enable a direct comparison between the two methods of loading. This will then allow further

investigations into metal binding of the protein. To help obtain crystals of transferrin the issue of purity needs to be addressed. In this study, the transferrin used was obtained from Sigma with no further purification. Purification is an important factor in protein crystallisation. Future methods of purification could include development of a good HPLC technique in order to separate different forms of the protein *i.e.* mono- and di-metal loaded protein. Treatment of the protein to remove the glycan chains may also help facilitate crystallisation. HPLC could again then be employed to separate the de-glycosylated protein. Seeding from crystals obtained from this method may then also be more successful. Attempts could be made to load fragments of transferrin with manganese which would not include the problem of glycosylation. This may then prove easier to crystallise.

Extended X-ray Absorption Fine Structure (EXAFS) and X-ray Absorption Near Edge Structure (XANES) can provide much useful information when it is difficult to crystallise compounds such as transferrin. Although the information is not as detailed as with a crystal structure they can still give some insights into the metal binding site and the oxidation state of the metal. This may be of use again when comparing the different methods employed in this study to load transferrin with Mn^{3+} and how this compares with the binding site with Fe^{3+} loaded.

Once successful crystallisation conditions have been determined the use of mutants could be used to provide further information on Mn-hTf such as alterations to the metal binding site. Mutations could also provide information on receptor binding to transferrin and release of manganese from the binding site.

Further work is required on the release of Mn^{3+} from transferrin in terms of biological and chemical characteristics. It may be of benefit to attempt competition studies between the different transferrins and cell uptake, *i.e.* between Fe-hTf and Mn-hTf that has been loaded with Mn^{3+} using different methods. Use of radio-isotopes may prove productive in this area to allow detection of the metal loaded transferrins and metal deposition in the cell. Time-lapse microscopy may also help provide further information into the unusual effect of higher doses of Mn-hTf on cells. Also, the use of cell markers may give some insight into the mechanisms of action although various endpoints and potential altered markers would initially have to be determined.

To investigate what cell signalling may be occurring polymerase chain reaction (PCR) could provide answers on gene activation due to increased levels of manganese in cells. This may also be of use to investigate the prospect of cell adhesion molecules and the extracellular matrix being affected by Mn-hTf. Further studies on this effect could include the use of different mediums, lack of serum supplementation and cell culture wear, *e.g.* specifically coated plastics.

The use of different cell lines may also prove beneficial in this work to investigate if the effect of high dose Mn-hTf is specific to the cell line used here, which as mentioned earlier are of foetal origin. The cell lines used need not be restricted to humans or liver cells. Cancer cell lines may provide some useful information on the transferrin receptor and metal requirement and uptake. The transferrin used in cell

studies was not purified any further upon receipt. More purification steps may again be useful when investigating the effect of Mn-hTf on cells to eliminate the possibility of toxic side effects from impurities.

A model system for oxidative stress in cells would also help to provide information on the potential use as Mn-hTf as a therapeutic against oxidative stress. The model would have to ensure that it mimicked that of reperfusion injury and that the reactive oxygen species were being generated in the mitochondria. Various chemicals may provide the necessary response or alternatively some form of a hypoxic tank may more closely mimic the conditions seen during of ischaemia. This may then allow testing of Mn-hTf to see if the desired action is achieved.

6.3 References

1. A. Dautry-Varsat, *Biochimie,* **1986**, 68: 375-381.

2. A. Dautry-Varsat, A. Ciechanover, and H.F. Lodish, *Proc. Natl. Acad. Aci. USA,* **1983**, 80: 2258-2262.

3. P. Aisen, R. Aasa, and A.G. Redfield, *J. Biol. Chem.,* **1969**, 244: 4628-4633.

4. M. Guo, H. Sun, H.J. McArdle, L. Gambling, and P.J. Sadler, *Biochemistry,* **2000**, 39: 10023-10033.

5. H. Li, P.J. Sadler, and H. Sun, *Eur. J. Biochem.,* **1996**, 242: 387-393.

6. H. Sun, H. Li, and P.J. Sadler, *Chem. Rev.,* **1999**, 99: 2817-2842.

7. W. Zhong, J.A. Parkinson, M. Guo, and P.J. Sadler, *J. Biol. Inorg. Chem.,* **2002**, 7: 589-599.

8. K. Mizutani, H. Yamashita, H. Kurokawa, B. Mikami, and M. Hirose, *J. Biol. Chem.,* **1999**, 274: 10190-10194.

9. J.A. Khan, P. Kumar, A. Srinivasan, and T.P. Singh, *J. Biol. Chem.,* **2001**, 276: 36817-36823.

10. P. Kuser, D.R. Hall, M.L. Haw, M. Neu, R.W. Evans, and P.F. Lindley, *Acta*

Crsytallogr., **2002**, D58: 777-783.

11. H.J. Zuccola, PhD Thesis, 1992, Georgia Institute of Technology, Atlanta.

Appendix

Appendix A

Buffer for Caeruloplasmin

0.25 M NaCl

0.05 M Na Acetate

pH 7.0

1 mg caeruloplasmin dissolved in 1 ml of buffer and kept at 253 K in 50 µl aliquots.

1 unit of oxidative activity = 20-33 µl of caeruloplasmin

Appendix B

Schiff Reagent

2.5 g Fuschin Basic (99% pure grade, Sigma) in 500 ml boiled H_2O

Cool to 323 K, add 50 ml 10% HCl

Cool to 298 K, add 5 g metabisulphite

Incubate in dark at room temperature, 24-48 hours

Filter using a no.1 filter, solution should be clear.

Sore at 277 K in dark where the solution will remain stable for 6 weeks.

Appendix C

Mowiol Mountant

Mowiol 4-88 (Calbiochem)

Glycerol (Fisher Chemicals)

Tris (Sigma)

DABCO (Sigma)

1. Add 2.4 g Mowiol to 6 g glycerol and stir briefly with a pipette.

2. Add 12 ml H_2O and stir at room temp for several hours.

3. Add 12 ml of 0.2 M Tris (pH 8.5) and heat to 323 K for 1-2 hrs while stirring.

4. When the Mowiol has dissolved, clarify by centrifugation at 500 x g for 15 mins.

5. Add DABCO to 2.5% (0.72 g), aliquot and store at 253 C. Bubbles can be removed by centrifugation. Aliquots can be stored for up to 2 weeks at 277 K or frozen at 253 K.

Appendix D ^{1}H NMR Spectra

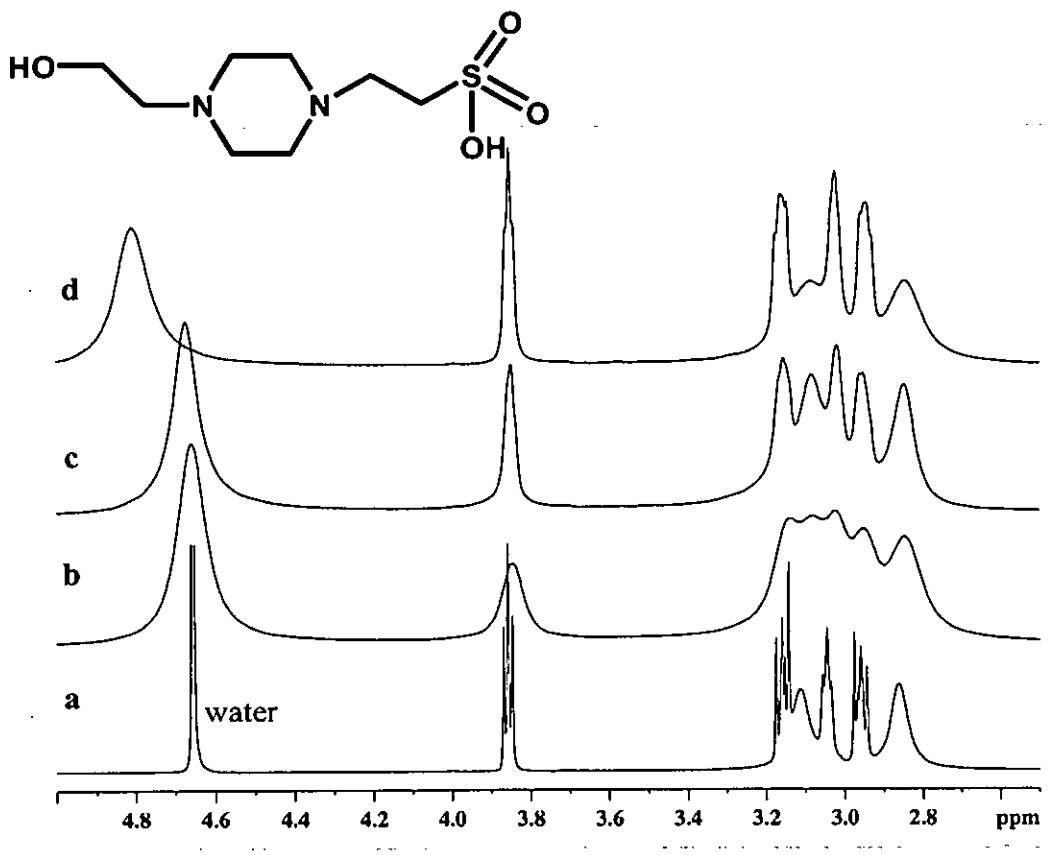

Figure D.1 ^{1}H NMR spectra for the reaction between HEPES buffer and $KMnO_4$. Spectrum a) 20 mM HEPES (pH 7.4) alone, b) HEPES buffer with 0.2 molar equivalents $KMnO_4$, c) same solution as in b after 4 hours, d) after 24 hours. All solutions were made up in D_2O and internally referenced to TSP (0 ppm). The water peak has broadened considerably and shifted by *ca.* 0.2 ppm.

Appendix E ^{13}C NMR Spectra

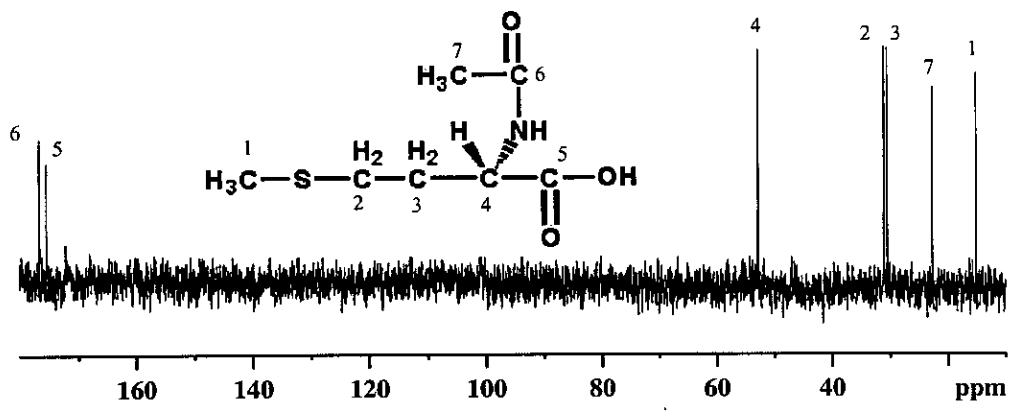

Figure E.1 ^{13}C-{^{1}H} NMR spectrum of N-acetyl-L-methionine (100 mM), referenced to TSP (0.0 ppm). The εCH_3 peak is at 15.14 ppm, labelled as 1.

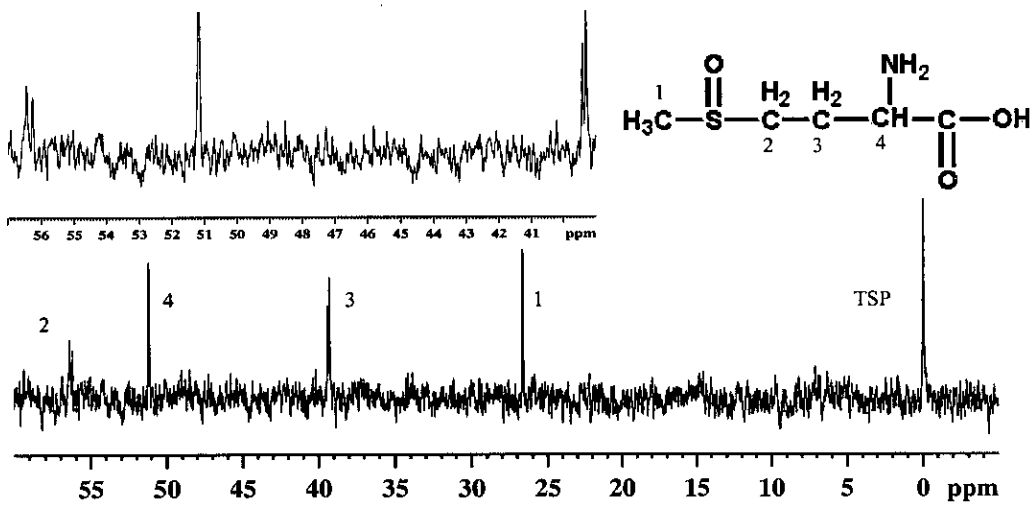

Figure E.2 ^{13}C-{^{1}H} NMR spectrum of L-methionine sulfoxide (101 mM). The εCH_3 peak is at 26.65 ppm, labelled as 1. The formation of doublets is due to the presence of diastereomers (S configuration at Cα (labelled as 4 on the spectrum), R or S at sulfur).

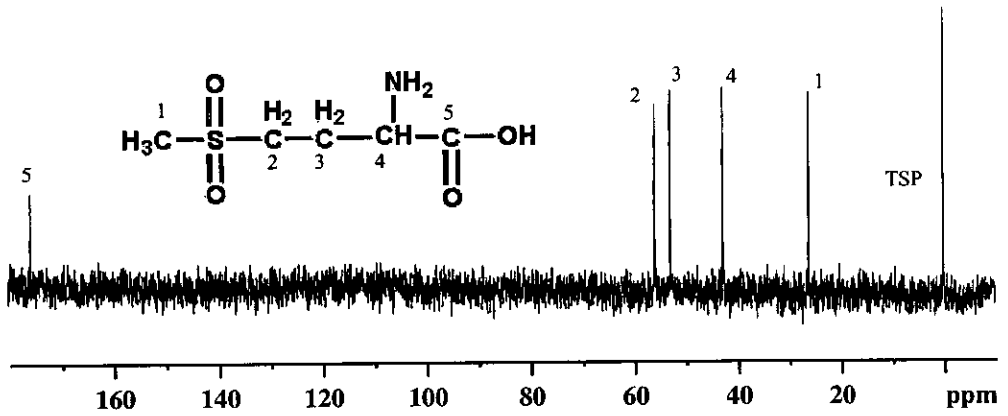

Figure E.3 ^{13}C NMR spectrum of L-methionine sulfone (102 mM). The εCH_3 peak is at 26.08 ppm, labelled as 1.

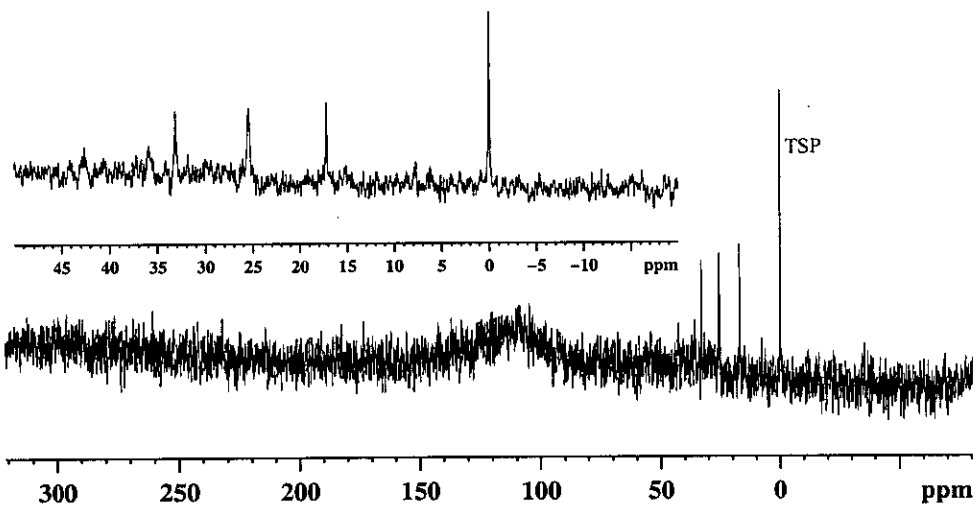

Figure E.4 ^{13}C NMR spectrum of N-acetyl-L-methionine (100 mM) following addition of 1 molar equivalent $KMnO_4$ (1.02 M). Peaks at 17.15 and 25.43 ppm most probably represent εCH_3. The paramagnetic effect causes a shift of the original εCH_3 peak to 17.15 ppm and a new peak at 25.43 ppm. This peak is probably attributable to oxidation of methionine to sulfoxide and sulfone where the εCH_3 peak is at 26.65 and 26.08 ppm respectively.

Appendix F Metal Content Analysis

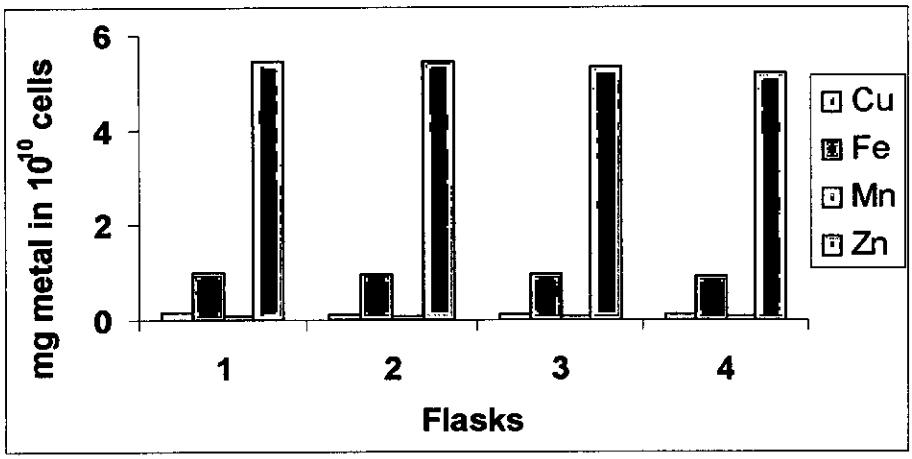

Figure F.1 Metal content of WRL-68 cells (mg metal in 10^{10} cells). Cells grown in large flasks with medium alone until confluent. Cells then harvested and pelleted. Pellet then re-suspended in ultrapure water for metal analysis by ICP-AES.

Table F.1 Metal content (ppm) of cells grown in large flasks determined by ICP-AES

Metal	Flask 1	Flask 2	Flask 3	Flask 4
Cu	0.0179	0.0172	0.017	0.0143
Fe	0.1192	0.1163	0.1133	0.1092
Mn	0.0085	0.0082	0.0081	0.008
Zn	0.6497	0.6504	0.6364	0.6218

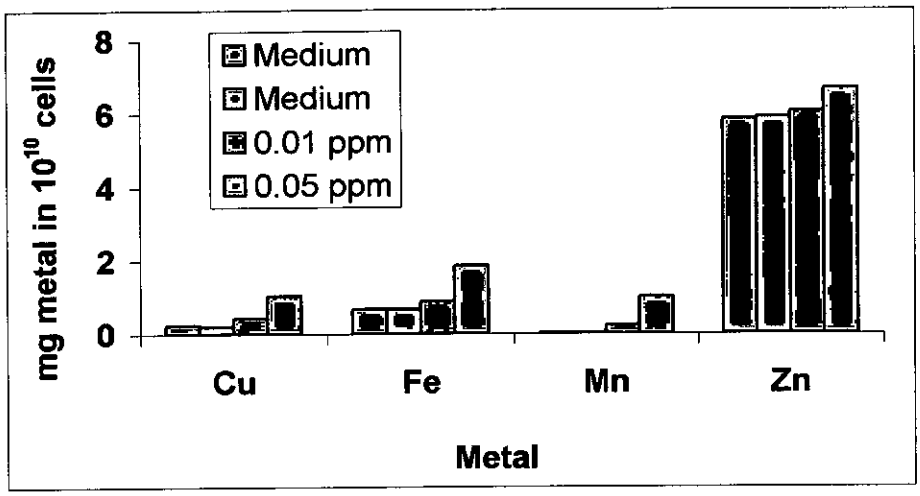

Figure F.2 Metal content of WRL-68 cells. Cells grown in large flasks with medium alone. Cells then harvested and pelleted then resuspended in ultrapure water for metal analysis by ICP-AES. Two cells suspensions run with no additions. Internal metal standards added to give 0.01 and 0.05 ppm to two separate cell suspensions.

Table F.2 Cellular metal content (ppm) in cells grown in medium alone and after addition of internal standard to the sample prior to analysis by ICP-AES

Metal	Medium[a]	Medium[a]	+ 0.01 ppm metal	+ 0.05 ppm metal
Cu	0.0104	0.0089	0.0186	0.0456
Fe	0.0297	0.0293	0.0389	0.0809
Mn	0.0006	0.0004	0.0098	0.0441
Zn	0.255	0.257	0.2908	0.2908

[a] Metal content of cells (with no addition of standard) run in duplicate

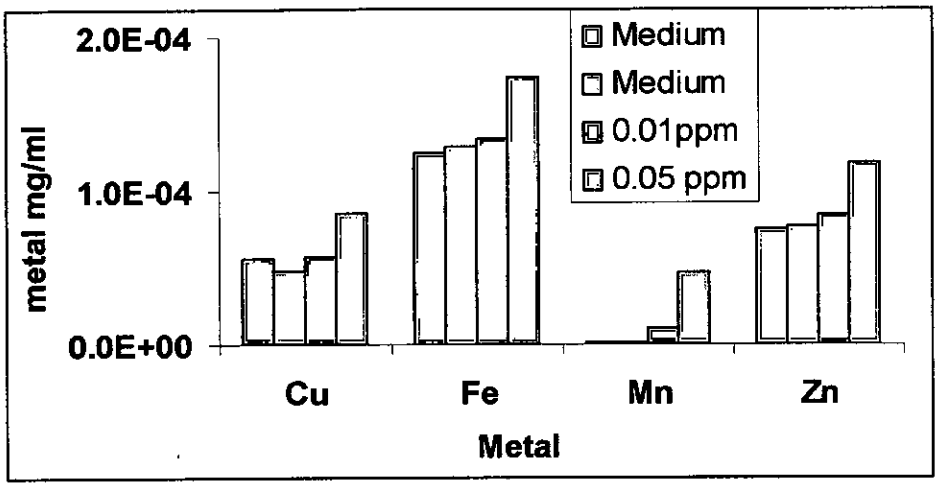

Figure F.3 Metal content of the medium DMEM (two samples used) and DMEM with added internal standards to give additional 0.01 and 0.05 ppm. DMEM was used as medium for all cell experiments.

Table F.3 Metal content (ppm) of the culture medium DMEM and after addition of internal standards determined by ICP-AES

Metal	DMEM[a]	DMEM[a]	+ 0.01 ppm metal	+ 0.05 ppm metal
Cu	0.0554	0.0478	0.0566	0.0851
Fe	0.1253	0.1292	0.1338	0.1737
Mn	0.0015	0.0013	0.0104	0.0468
Zn	0.0757	0.0765	0.085	0.1179

[a] DMEM (without the addition of standards) run in duplicate

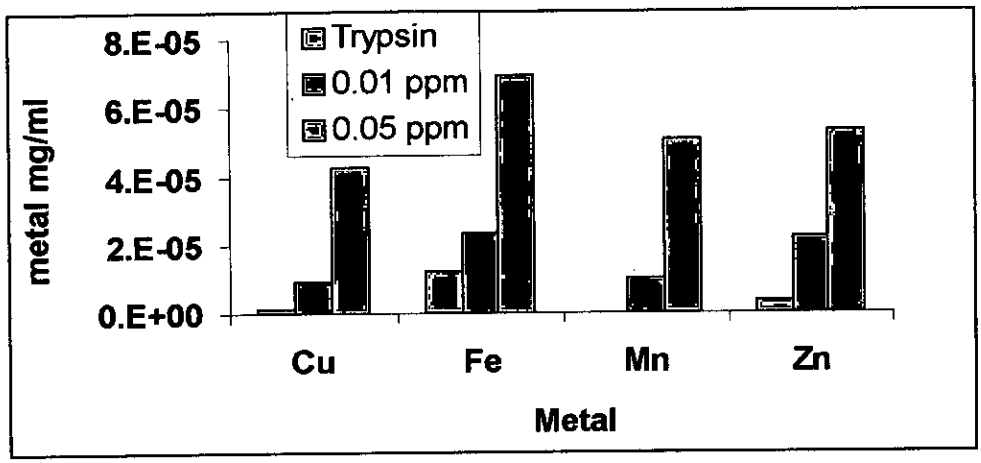

Figure F.4 Metal content of trypsin-EDTA and after addition of internal standards to give additional 0.01 and 0.05 ppm. Trypsin-EDTA was used in all cell experiments to remove the cell layer from flasks.

Table F.4 Metal content (ppm) of trypsin-EDTA and after addition of internal standards determined by ICP-AES

Metal	Trypsin-EDTA	+ 0.01 ppm metal	+ 0.05 ppm metal
Cu	0.0014	0.0095	0.0425
Fe	0.0122	0.0232	0.0692
Mn	0.0002	0.0098	0.051
Zn	0.0034	0.0222	0.0531

Appendix G Crystallisation Experiments

Plates are labelled as wells 1-6 along the horizontal from left to right and A-D along the vertical from top to bottom.

Plate G.1

20% PEG 400 pH 5.6 Fe-hTf	20% PEG 400 pH 5.6 Fe-hTf	20% PEG 400 pH 5.6 Fe-hTf	20% PEG 400 pH 5.6 Mn-hTf	20% PEG 400 pH 5.6 Mn-hTf	20% PEG 400 pH 5.6 Mn-hTf
22% PEG 400 pH 5.6 Fe-hTf	22% PEG 400 pH 5.6 Fe-hTf	22% PEG 400 pH 5.6 Fe-hTf	22% PEG 400 pH 5.6 Mn-hTf	22% PEG 400 pH 5.6 Mn-hTf	22% PEG 400 pH 5.6 Mn-hTf
24% PEG 400 pH 5.6 Fe-hTf	24% PEG 400 pH 5.6 Fe-hTf	24% PEG 400 pH 5.6 Fe-hTf	24% PEG 400 pH 5.6 Mn-hTf	24% PEG 400 pH 5.6 Mn-hTf	24% PEG 400 pH 5.6 Mn-hTf
26% PEG 400 pH 5.6 Fe-hTf	26% PEG 400 pH 5.6 Fe-hTf	26% PEG 400 pH 5.6 Fe-hTf	26% PEG 400 pH 5.6 Mn-hTf	26% PEG 400 pH 5.6 Mn-hTf	26% PEG 400 pH 5.6 Mn-hTf

All wells contained PEG 400 at 20 to 26%, 100 mM sodium cacodylate pH 5.6. Fe_2-hTf or Mn_2-hTf (produced using $MnCl_2$ with caeruloplasmin) at a concentration of *ca.* 0.5 mM in the drop. Plate kept at 277 K. Crystals were found in wells A1, B1-3, C2, D2 and D3.

Plate G.2

22% PEG 400 pH 5.43	22% PEG 400 pH 5.43	22% PEG 400 pH 5.43	22% PEG 400 pH 5.43	22% PEG 400 pH 5.43	22% PEG 400 pH 5.43
22% PEG 400 pH 5.43	22% PEG 400 pH 5.43	22% PEG 400 pH 5.43	22% PEG 400 pH 5.43	22% PEG 400 pH 5.43	22% PEG 400 pH 5.43
24% PEG 400 pH 5.43	24% PEG 400 pH 5.43	24% PEG 400 pH 5.43	24% PEG 400 pH 5.43	24% PEG 400 pH 5.43	24% PEG 400 pH 5.43
24% PEG 400 pH 5.43	24% PEG 400 pH 5.43	24% PEG 400 pH 5.43	24% PEG 400 pH 5.43	24% PEG 400 pH 5.43	24% PEG 400 pH 5.43

All wells contained PEG 400 at 22 or 24%, 100 mM sodium cacodylate pH 5.43. Fe_2-hTf in the drop. Plate kept at 277 K. Ellipsoidal red crystals found in wells D1 and D2 after approx. 6 weeks. More crystals formed in other wells later.

Plate G.3

20% PEG 400 pH 5.43 Fe-hTf	20% PEG 400 pH 5.43 Fe-hTf	20% PEG 400 pH 5.43 Fe-hTf	20% PEG 400 pH 5.43 Fe-hTf	20% PEG 400 pH 5.43 Fe-hTf	20% PEG 400 pH 5.43 Fe-hTf
22% PEG 400 pH 5.43 Fe-hTf	22% PEG 400 pH 5.43 Fe-hTf	22% PEG 400 pH 5.43 Fe-hTf	22% PEG 400 pH 5.43 Fe-hTf	22% PEG 400 pH 5.43 Fe-hTf	22% PEG 400 pH 5.43 Fe-hTf
24% PEG 400 pH 5.43 Fe-hTf	24% PEG 400 pH 5.43 Fe-hTf	24% PEG 400 pH 5.43 Fe-hTf	24% PEG 400 pH 5.43 Fe-hTf	24% PEG 400 pH 5.43 Fe-hTf	24% PEG 400 pH 5.43 Fe-hTf
26% PEG 400 pH 5.43 Fe-hTf	26% PEG 400 pH 5.43 Fe-hTf	26% PEG 400 pH 5.43 Fe-hTf	26% PEG 400 pH 5.43 Fe-hTf	26% PEG 400 pH 5.43 Fe-hTf	26% PEG 400 pH 5.43 Fe-hTf

All wells contained PEG 400 at 20 to 26%, 100 mM sodium cacodylate pH 5.43. Fe_2-hTf in the drop at *ca.* 0.6 mM. Plate kept at 277 K. First crystal found in well D6 after 2 weeks. Others formed later.

Plate G.4

20% PEG 400 pH 5.6 Fe-hTf	20% PEG 400 pH 5.6 Fe-hTf	20% PEG 400 pH 5.5 Fe-hTf	20% PEG 400 pH 5.5 Fe-hTf	20% PEG 400 pH 5.4 Fe-hTf f	20% PEG 400 pH 5.4 Fe-hTf
22% PEG 400 pH 5.6 Fe-hTf	22% PEG 400 pH 5.6 Fe-hTf	22% PEG 400 pH 5.5 Fe-hTf	22% PEG 400 pH 5.5 Fe-hTf	22% PEG 400 pH 5.4 Fe-hTf	22% PEG 400 pH 5.4 Fe-hTf
24% PEG 400 pH 5.6 Fe-hTf	24% PEG 400 pH 5.6 Fe-hTf	24% PEG 400 pH 5.5 Fe-hTf	24% PEG 400 pH 5.5 Fe-hTf	24% PEG 400 pH 5.4 Fe-hTf	24% PEG 400 pH 5.4 Fe-hTf
26% PEG 400 pH 5.6 Fe-hTf	26% PEG 400 pH 5.6 Fe-hTf	26% PEG 400 pH 5.5 Fe-hTf	26% PEG 400 pH 5.5 Fe-hTf	26% PEG 400 pH 5.4 Fe-hTf	26% PEG 400 pH 5.4 Fe-hTf

All wells contained PEG 400 at 20 to 26%, 100 mM sodium cacodylate pH 5.4 – 5.6. Fe_2-hTf in the drop at *ca.* 0.6 mM. Plate kept at 277 K. Crystals found in wells A2, A5, B1, B4-6, C3, C5, C6, D1, D3-6.

Plate G.5

20% PEG 400 pH 5.4 Fe-hTf 0.26 mM	20% PEG 400 pH 5.4 Fe-hTf 0.128 mM	20% PEG 400 pH 5.6 Fe-hTf 0.26 mM	20% PEG 400 pH 5.6 Fe-hTf 0.128 mM	20% PEG 400 pH 5.5 Fe-hTf 0.26 mM	20% PEG 400 pH 5.5 Fe-hTf 0.128 mM
22% PEG 400 pH 5.4 Fe-hTf 0.26 mM	22% PEG 400 pH 5.4 Fe-hTf 0.128 mM	22% PEG 400 pH 5.6 Fe-hTf 0.26 mM	22% PEG 400 pH 5.6 Fe-hTf 0.128 mM	22% PEG 400 pH 5.5 Fe-hTf 0.26 mM	22% PEG 400 pH 5.5 Fe-hTf 0.128 mM
24% PEG 400 pH 5.4 Fe-hTf 0.26 mM	24% PEG 400 pH 5.4 Fe–hTf 0.128 mM	24% PEG 400 pH 5.6 Fe-hTf 0.26 mM	24% PEG 400 pH 5.6 Fe-hTf 0.128 mM	24% PEG 400 pH 5.5 Fe-hTf 0.26 mM	24% PEG 400 pH 5.5 Fe-hTf 0.128 mM
26% PEG 400 pH 5.4 Fe-hTf 0.26 mM	26% PEG 400 pH 5.4 Fe-hTf 0.128 mM	26% PEG 400 pH 5.6 Fe-hTf 0.26 mM	26% PEG 400 pH 5.6 Fe-hTf 0.128 mM	26% PEG 400 pH 5.5 Fe-hTf 0.26 mM	26% PEG 400 pH 5.5 Fe-hTf 0.128 mM

All wells contained PEG 400 at 20 to 26%, 100 mM sodium cacodylate pH 5.4 – 5.6.

All wells contained Fe_2-hTf at the concentrations shown, i.e. 0.26 mM or 0.128 mM.

Plate kept at 277 K.

Plate G.6

20% PEG 400 pH 5.6 Mn-hTf	20% PEG 400 pH 5.6 Mn-hTf	20% PEG 400 pH 5.5 Mn-hTf	20% PEG 400 pH 5.5 Mn-hTf	20% PEG 400 pH 5.4 Mn-hTf	20% PEG 400 pH 5.4 Mn-hTf
22% PEG 400 pH 5.6 Mn-hTf	22% PEG 400 pH 5.6 Mn-hTf	22% PEG 400 pH 5.5 Mn-hTf	22% PEG 400 pH 5.5 Mn-hTf	22% PEG 400 pH 5.4 Mn-hTf	22% PEG 400 pH 5.4 Mn-hTf
24% PEG 400 pH 5.6 Mn-hTf	24% PEG 400 pH 5.6 Mn-hTf	24% PEG 400 pH 5.5 Mn-hTf	24% PEG 400 pH 5.5 Mn-hTf	24% PEG 400 pH 5.4 Mn-hTf	24% PEG 400 pH 5.4 Mn-hTf
26% PEG 400 pH 5.6 Mn-hTf	26% PEG 400 pH 5.6 Mn-hTf	26% PEG 400 pH 5.5 Mn-hTf	26% PEG 400 pH 5.5 Mn-hTf	26% PEG 400 pH 5.4 Mn-hTf	26% PEG 400 pH 5.4 Mn-hTf

All wells contained PEG 400 at 20 to 26%, 100 mM sodium cacodylate pH 5.4 – 5.6. Mn-hTf (produced using $KMnO_4$ and found to have ratio of 1 hTf : 3 Mn determined by UV/Vis spectroscopy and ICP-AES as described in Chapter 2) in the drop at *ca.* 0.5 mM protein. Crystals found in wells D1 and D3.

Appendix H Crystallisation Screening Technique

Solution No.	Buffer	Precipitant	Additional component	Result 1Mn:1Tf	Result 2Mn:1Tf
1	0.1 M Na acetate trihydrate pH 4.6	30% 2-methyl-2,4 pentanediol	0.02 M calcium chloride dihydrate	P/A	P
2	0.1 M Na acetate trihydrate pH 4.6	30% PEG 4000	0.2 M ammonium acetate	P	P
3	0.1 M Na acetate trihydrate pH 4.6	25% PEG 4000	0.2 M ammonium sulphate	P	P
4	0.1 M Na acetate trihydrate pH 4.6	2.0 M sodium formate	None		
5	0.1 M Na acetate trihydrate pH 4.6	2.0 M ammonium sulfate	None	P	P
6	0.1 M Na acetate trihydrate pH 4.6	8% PEG 4000	None		
7	0.1 M tri-sodium citrate dihydrate pH 5.6	30% PEG 4000	0.2 M ammonium acetate	P	
8	0.1 M tri-sodium citrate dihydrate pH 5.6	30% 2-methyl-2,4-pentanediol	0.2 M ammonium acetate		
9	0.1 M tri-sodium citrate dihydrate pH 5.6	20% 2-propanol, 20% PEG 4000	None		
10	0.1 M Na citrate pH 5.6	1.0 M ammonium dihydrogen phosphate	None		
11	0.1 M Na acetate trihydrate pH 4.6	20% 2-propanol	0.2 M calcium chloride dihydrate		
12	0.1 M Na cacodylate pH 6.5	1.4 M Na acetate trihydrate	None		
13	0.1 M Na cacodylate pH 6.5	30% 2-propanol	0.2 M tri-sodium citrate dihydrate		
14	0.1 M Na cacodylate pH 6.5	30% PEG 8000	0.2 M ammonium sulphate		
15	0.1 M Na cacodylate pH 6.5	20% PEG 8000	0.2 M magnesium acetate tetrahydrate		

16	0.1 M Na cacodylate pH 6.5	30% 2-methyl-2,4-pentanediol	0.2 M magnesium acetate tetrahydrate		
17	0.1 M imidazole pH 6.5	1.0 M sodium acetate trihydrate	None		
18	0.1 M Na cacodylate pH 6.5	30% PEG 8000	0.2 M sodium acetate trihydrate	P	P
19	0.1 M Na cacodylate pH 6.5	18% PEG 8000	0.2 M zinc acetate dihydrate	P	P
20	0.1 M Na cacodylate pH 6.5	18% PEG 8000	0.2 M calcium acetate hydrate		
21	0.1 M Na hepes pH 7.5	30% 2-methyl-2,4-pentanediol	0.2 M tri-sodium citrate dihydrate		
22	0.1 M Na hepes pH 7.5	30% 2-propanol	0.2 M magnesium chloride hexahydrate		
23	0.1 M Na hepes pH 7.5	28% PEG 400	0.2 M calcium chloride dihydrate	P	P
24	0.1 M Na hepes pH 7.5	30% PEG 400	0.2 M magnesium chloride hexahydrate	P	P
25	0.1 M Na hepes pH 7.5	20% 2-propanol	0.2 M tri-sodium citrate dihydrate		
26	0.1 M Na hepes pH 7.5	0.8 M K, Na tartrate tetrahydrate	None		
27	0.1 M Na hepes pH 7.5	1.5 M lithium sulphate monohydrate	None		
28	0.1 M Na hepes pH 7.5 and 0.8M K dihydrogen phosphate monohyd.	0.8 M Na dihydrogen phosphate	None		
29	0.1 M Na hepes pH 7.5	1.4 M tri-sodium citrate dihydrate	None		
30	0.1 M Na hepes pH 7.5	2% PEG 400, 2.0 M amm sulfate	None		
31	0.1 M Na hepes pH 7.5	10% 2-propanol, 20% PEG 4000	None	P	P
32	0.1 M tris HCl pH 8.5	2.0 M ammonium sulphate	None		

33	0.1 M tris HCl pH 8.5	30% PEG 4000	0.2 M magnesium chloride hexahydrate	P	P
34	0.1 M tris HCl pH 8.5	30% PEG 400	0.2 M tri-sodum citrate dihydrate		
35	0.1 M tris HCl pH 8.5	30% PEG 4000	0.2 M lithium sulphate monohydrate	P	P
36	0.1 M tris HCl pH 8.5	30% 2-propanol	0.2 M ammonium acetate		
37	0.1 M tris HCl pH 8.5	30% PEG 4000	0.2 M sodium acetate trihydrate	P	P
38	0.1 M tris HCl pH 8.5	8% PEG 8000	None		
39	0.1 M tris HCl pH 8.5	2.0 M ammonium dihydrogen phosphate	None		
40	None	0.4 M K, Na tartrate tetrahydrate	None		
41	None	0.4 M ammonium dihydrogen phosphate	None		
42	None	30% PEG 8000	0.2 M ammonium sulfate	P	P
43	None	30% PEG 4000	0.2 M ammonium sulfate	P	P
44	None	2.0 M ammonium sulfate	None		P
45	None	20% PEG 8000	0.05 M potassium dihydrogen phosphate	A	A
46	None	30% PEG 1500	None	P	
47	None	2% PEG 8000	1.0 M lithium sulfate monohydrate	P	P
48	None	15% PEG 8000	0.5 M lithium sulfate monohydrate	P	P

P = Precipitate formed. A = Aggregation

Plates were set up using Mn-hTf to give concentrations of 175 μM in the drop.

Conditions 1 – 24 used Mn-hTf with 1 Mn bound to the protein, as determined by UV/Vis and ICP-AES. Conditions 25-48 used Mn-hTf where 2 Mn were bound to the protein. Mn-hTf used had been prepared from apo-hTf using $KMnO_4$.